Application of neuroanatomical and immunocytochemical techniques for the detection of neurotransmitters in identified neurons in vertebrate And invertebrate tissues.

Richardson, Anne Christine

Application Of Neuroanatomical And Immunocytochemical Techniques For The Detection Of Neurotransmitters In Identified Neurons In Vertebrate And Invertebrate Tissues.

Anne Christine Richardson

Submitted for the degree of Master of Science

School of Biological and Biomedical Sciences
Durham University

2007

Table Of Contents.

Abstract.

The techniques that have become available to the neurobiologist have over the past 35 years transformed the ways in which the nervous system can be investigated both in terms of connectivity and chemical make up. When given a specific neurobiological question concerning the synaptic interactions or the neurochemistry of the neuronal populations, careful consideration has to made of the techniques that are applied to obtain meaningful results.

Two specific biological questions are addressed and the techniques that were applied are discussed. Firstly, to investigate whether the reduction of brain-derived neurotrophic factor (BDNF) in the granule cells of the stargazer mutant mouse compromises the phenotype of the cerebellar neurons. The levels of γ-aminobutyric acid (GABA) and glutamate neurotransmitter expressed in cerebellar neurons and the phenotype of the synaptic contacts were compared in stargazer and wild-type controls using electron microscopy (EM) and quantitative post-embedding EM immunogold labelling.

Secondly, the flight motor system of the locust represents a model preparation for the investigation of neuromodulation. The monosynaptic connections between the locust forewing stretch receptor (fSR) and the first basal motorneuron (BA1) is part of a sensory pathway involved in flight and by combining *in vivo* horseradish peroxidase (HRP) backfills of the fSR with post-

embedding EM immunogold labelling the proportion and location of inputs to the fSR were analysed. This and other data show the majority of inputs to the fSR are from either glutamatergic or GABAergic neurons, but not all. Electrophysiological studies have shown that the fSR/BA1 synapse is also modulated by biogenic amines. ICC fluorescent methods have established that the neuropile region is octopamine immunoreactive (IR). To identify these octopamine-IR processes at the EM level two different techniques were used; an immunogold cryosectioning method and a pre-embedding immunogold silver intensification technique.

Declaration

The work presented in this thesis was carried out by me and is an accurate account of the experimental work undertaken by me. This work, under the supervision of Dr. Beulah Leitch, has been carried out in the School of Biological and Biomedical Sciences, at Durham University, and has not been previously submitted for a higher degree.

Copyright

In Press

The majority of the work from Chapter 2 has been published in,

Richardson CA, Leitch B. CEREBELLAR GOLGI, PURKINJE AND BASKET CELLS HAVE REDUCED GAMMA – AMINOBUTYRIC ACID IMMUNOREACTIVITY IN STARGAZER MUTANT MICE. J.Comp.Neurol. 453:85-99., 2002.

The majority of the work from Chapter 3 has been published in ;

Christine A. Richardson and Beulah Leitch. THE PHENOTYPE OF CEREBELLAR GLUTAMATERGIC NEURONS IS ALTERED IN STARGAZER MUTANT MICE LACKING BDNF MRNA EXPRESSION. J. Comp. Neurol. 481:145-159, 2005.

The majority of the work from Chapter 4 has been accepted for publication in

Christine A. Richardson and Beulah Leitch. IDENTIFICATION OF THE NEUROTRANSMITTERS INVOLVED IN MODULATION OF TRANSMITTER RELEASE FROM THE CENTRAL TERMINALS OF THE LOCUST WING HINGE STRETCH RECEPTOR. J. Comp. Neurol. (IN PRESS).

List Of Figures.

Figure 4.18. A neuronal profile showing distinctive 'elongate' shaped granules.

Figure 4.19. An octopaminergic neuronal profile with two output synapses.

Figure 4.20. A profile with the same distinctive granules lies very close to the fSR.

Figure 4.21. A profile with the same distinctive granules lies very close to the fSR.

List Of Tables.

Acknowledgments.

I wish to express my deepest gratitude to my supervisor, Dr Beulah Leitch for giving me the confidence and support to begin my Master's degree. She has provided me with unfailing guidance, support and encouragement during some difficult times.

I am indebted to Dr. R.W. Banks who as my internal advisor provided constructive comments on this thesis.

I also wish to thank the School of Biological and Biomedical Sciences and Durham University for supporting me and allowing me to complete my research.

A special thank you to my parents, David and Vera, for always giving me warm encouragement and love.

Finally, I owe my loving thanks to my husband Ian and my son Andrew. They have lost a lot due to my research. Without their unwavering encouragement and understanding it would have been impossible for me to complete this work.

Glossary.

Ach	acetylcholine
AMPA	a-amino-3-hydroxyl-5-methyl-4-isoxazolepropionate
AMPAR	a-amino-3-hydroxyl-5-methyl-4-isoxazolepropionate receptors
aLAC	anterior lateral association centre
BDNF	brain - derived neurotrophic factor
BSA	bovine serum albumin.
$Ca^{2}+$	calcium
CNS	central nervous system
DAB	diaminobenzidine
DUM	dorsal unpaired neurons
EM	electron microscope/ electron microscopical
EPSP	excitatory postsynaptic potential
fSR	forewing stretch receptor
GABA	gamma amino butyric acid.
GABAergic	gamma amino butyric acid containing
GAD	glutamic acid decarboxylase
GC	granule cell
HRP	horseradish peroxidase
ICC	immunohistochemistry
IR	immunoreactive
LM	light microscope

MF	mossy fibre
ml	millilitre
μl	microlitre
μm	micrometre
mRNA	messenger ribonucleic acid.
NGF	nerve growth factor.
NT-3	neurotrophin – 3.
NT-4	neurotrophin – 4.
PSD	postsynaptic density
PC	purkinje cell
RRP	ready releasable pool
RT	room temperature
TrkB.	tyrosine kinase receptor B.
TrkC	tyrosine kinase receptor C.
Stg	stargazer
WT	wild-type

Chapter 1. General Introduction.

Since Charles Sherrington, in 1897, first proposed the existence of the synapse as a special connection between one nerve cell and another, and later the first electron micrographs showed the presence of presynaptic vesicles, neuroanatomists have utilised and developed many techniques for the identification of synaptic connectivity and chemical make up of neuronal processes.

Early neuroanatomists used reconstructions from serial sections to demonstrate the 3- dimensional relationship between neurons. Advances in digital photography, computer technology, confocal microscopy and electron tomography have all aid the modern neuroanatomist towards this goal.

It was the work of T.R. Elliot, H.H. Dale and Otto Loewi in the first part of the twentieth century that first introduced the concept of chemical neurotransmission (Elliot 1904; Loewi. O 1921; H.H. Dale 1935). Using the techniques of electrophysiology and neuropharmacology it is possible to monitor the release of neurotransmitters at synapses. But it was not until advances were made in the preparation of antibodies for small molecule transmitter substances (Storm-Mathisen 1983; Seguela 1984) that neuroanatomists were able to visually demonstrate, with convincing evidence, the presence of neurotransmitters in axon terminals using immunogold labelling.

When it was shown that immunogold labelling could, at the very least, be semi- quantitative, (Somogyi 1986; Ottersen 1989; Bramham *et al.*, 1990;

Lucocq 1992) it became possible to show the effects that physiological, pathological or genetic differences had on neuronal neurotransmitter content. Using neuronal tracing to mark where neurons send their axons, in combination with immunogold labelling to mark pre- or postsynaptic input or output, it is also possible to map synaptic connectivity and neurochemistry.

Skepper, 2000 and Kobbert *et al* 2000 describe many of the major techniques employed today. However to achieve successful labelling with acceptable ultrastructure a careful planning of protocol is necessary. (Totterdell *et al* 1992).

Immunocytochemistry.

Immunocytochemistry (ICC) is now a major tool used in electron microscopy (EM) and allows the localisation of proteins in tissues and cells with antibodies. It has been developed to such a degree that qualitative and quantitative analysis of the chemistry of the nervous system is possible but choices have to be made on the particular method to use (Kellenberger and Hayat 1991).

It is dependant on the basic principle of any immunochemical technique in that a specific antibody will combine with its specific antigen to give an exclusive antibody –antigen complex, this is then visualised with either a coloured, fluorescent or in the case of EM an electron dense marker.

Antibodies.

Antibodies are proteins produced in the spleen by B lymphocytes of the immune system in response to, and capable of binding to the foreign substance (antigen) that caused their production. Antibodies exist as a Y-shaped molecule. Each has two matching heavy chains, and two matching light chains. Below is a diagrammatic representation of the basic antibody structure taken from http://www.cat.cc.md.us/courses/bio141/lecguide/unit3/humoral/antibodies/abydiversity/abydiversity.html.

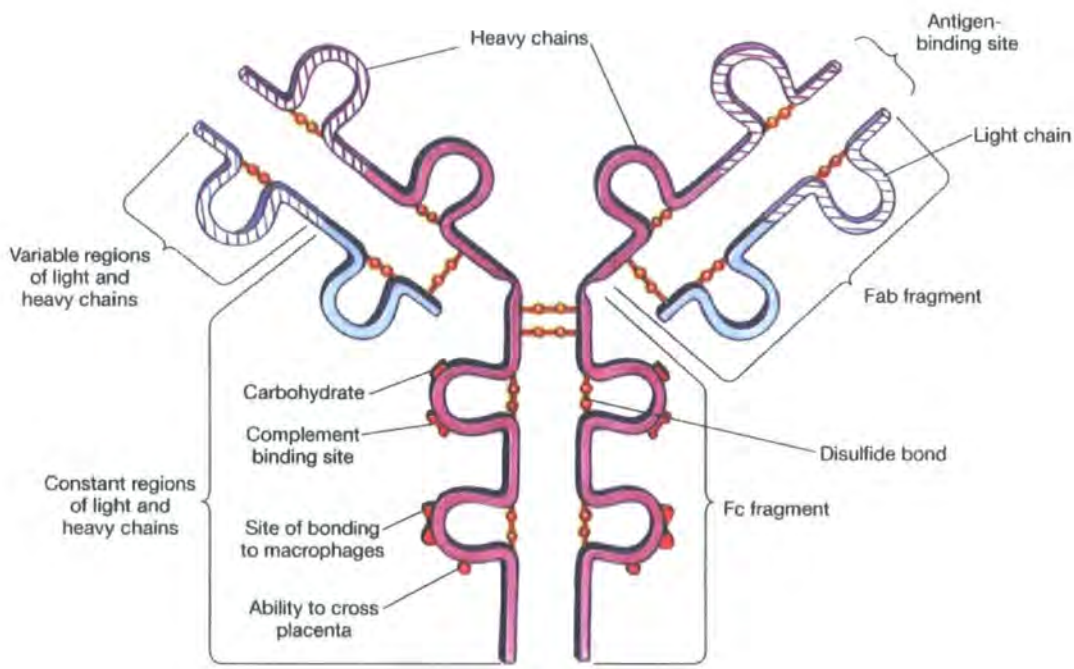

Antibodies are bi-functional, the constant region, the Fc region (Fragment , crystallisable) is the area used to destroy antigens, and is composed of two

heavy chains that each contribute two to three constant domains. By binding to different cell receptors or compliment proteins it can cause, for instance, cell lysis and opsonisation.

The variable region, called the Fab (Fragment, antigen binding) region gives the antibody its specificity for binding antigen. There are two Fab regions per antibody molecule, one from each half of the forked end of the "Y," these are composed of one constant and one variable domain of each of the heavy and the light chain. The end of the Fab region, the N- terminal, has a constant and a variable region that together shape the antigen binding site. There are five classes of antibody IgG, IgM, IgA, IgD, and IgE, named by the type of heavy chain, gamma, mu, alpha, delta and epsilon that they contain. There are two classes of light chains, kappa (κ) or lambda (λ). The most commonly used antibodies in immunochemical procedures are of the IgG class because they are the major immunoglobulins (Ig) released in serum.

Purified antibodies are often produced by injecting the antigen into a mammal or bird, including; mouse, rabbit, horse, goat, and chicken. B-lymphocytes in the spleen respond to the immunogen to produce one kind of antibody, but different B-cells will produce structurally different antibodies that bind to different parts (epitopes) of the antigen. This mixture of antibodies is known as polyclonal antibodies. They can be isolated from the blood serum of the animals and, if necessary, purified further by antigen affinity chromatography or by Protein A/G purification.

Monoclonal antibody production was developed by Köhler and Milstein (1976). The purified immunogen is injected into mice and the B lymphocytes are

isolated from the spleen after allowing time for an immune response. As isolated B cells have a finite life span, they are fused with mouse myeloma cells that can grow perpetually in culture. Myeloma's consist of B lymphocyte tumour cells that have lost the ability produce their own antibodies and therefore do not contaminate the antibody of interest. The fused cells divide to produce hybridomas that are then selected for specificity. The hybridoma is formed from the prodigy off an immortal cell-line that produces Igs specific for a single epitope.

The manner in which polyclonal and monoclonal antibodies are produced gives rise to advantages and disadvantages for using one over the other. Polyclonal antibodies have higher affinity and wide reactivity but lower specificity when compared with monoclonal antibodies (Hayat .2005). Polyclonal antisera contain different antibodies that bind to different parts (epitopes) of the antigen but, if not affinity purified, also contain a high concentration (up to 10 mg/ml) of unrelated antibodies. (Mighell, *et al* 1998). Polyclonal antibodies are much cheaper to produce than monoclonal antibodies but do suffer from batch to batch variation and hence reproducibility (Nelson *et al*; 2000). This must be taken into account whenever a new batch of polyclonal is used. Monoclonal antibodies do not suffer from batch variation, are highly specific and have reduced cross reactivity compared to polyclonal antibodies, background staining is also reduced but they do suffer from a higher sensitivity to fixation which can be a problem when good ultrastructure, requiring better fixation, combined with high labelling is required.

The enzyme pepsin can be used to cleave an immunoglobulin molecule into two Fab fragments and an Fc fragment. The enzyme cleaves near the hinge region, just below the disulphide bonds, the two Fab regions stay together and form an F(ab')2 fragment and contains two antibody binding sites (bivalent for antigen binding). The remaining Fc fragment is digested into small peptides. If papain is used instead of pepsin the cleavage of the whole molecule takes place above the disulphide bridges which hold the two heavy chains together but below the bonds holding the light and heavy chains together. (Porter 1959). This results in two Fab fragments each with a single antibody binding site (monovalent for antigen binding), and a complete Fc fragment. The fragments can then be purified by affinity chromatography. Fab and F (ab')2 antibody fragments are useful when the tissue may contain Fc receptors and capable of binding the Fc region of intact antibodies and causing background staining in areas that do not contain the antigen of interest. Using F(ab')2 or Fab fragments rather than whole IgG molecules ensures that the antibodies are binding to the antigen and not to Fc receptors. Especially in electron microscopy F(ab)2 and Fab fragments give increased antigen localisation and with the Fab fragment it is possible to perform immunolabelling at the molecular level (Harris *et al* . 2006). Fab fragments of secondary antibodies can be used to sterically cover the surface of immunoglobulins for double labelling primary antibodies from the same host species, or to block endogenous immunoglobulins on cells or tissue sections (Stratech Scientific Ltd).

Antigens.

An antigen is a substance which on entering the body is perceived as foreign, produces an immune response and is capable of combining with the specific antibodies formed. Common antigens are high molecular weight proteins or polysaccharides. Substances with low molecular weights, which include small amino acid neurotransmitters such as GABA glutamate and octopamine, are generally not immunogenic and require the aid of carrier proteins to stimulate an immune response. However when coupled to a larger protein carrier they can then act as an antigen (Storm-Mathisen *et. al.* 1983; Seguela *et.al.* 1984; Ottersen and Storm-Mathisen 1987).These low-molecular-weight immunogens, or haptens, are chemically conjugated to the carrier protein using a suitable cross-linking agent. Carrier proteins have relatively high molecular weights and carry many epitopes to which T lymphocytes can respond and subsequently provide the necessary help for antibody-producing B cells. An immune response to a hapten-carrier conjugate results in antibodies that are specific to the antigen –carrier –conjugate complex, the final antigenic structure must be identical to the antigens fixed to the tissue for antibodies to be used in immunocytochemical studies. Geffard *et al.* (1985) and Campistron *et al.* (1986) have shown that the linkage region of glutaraldehyde-conjugated amino acids is an important part of the epitope and good immunolabeling with antibodies produced in this way is only possible on glutaraldehyde-fixed tissues. This advance was particularly valuable in the

detection and visualisation of GABA (Storm-Mathisen *et. al.* 1983) as until then it was only possible to demonstrate its presence using the synthesizing enzyme glutamic acid decarboxylase(GAD), an enzyme that catalyzes the decarboxylation of glutamate to GABA and CO_2.

Conjugating either GABA or octopamine to the carrier bovine serum albumin with glutaraldehyde produced the anti-GABA and anti-octopamine antibodies used in this study. The anti-glutamate was developed in rabbit using purified glutamate conjugated to Keyhole Limpet Haemocyanin (KLH) as the immunogen. Keyhole Limpet Haemocyanin (KLH) is generally a very efficient coupling agent. It is another common carrier protein used in the preparation of hapten conjugates. Glutaraldehyde was chosen as the conjugate for its high yield of coupling with the E-amino group of lysyl residues in proteins. (Seguela *et.al.* 1984). The specific site to which the antibody binds is called an epitope. This is usually one to six monosaccharides (linear epitopes) or 5–8 amino acid residues (conformational epitopes) on the surface of the antigen. Most epitopes can be thought of as three-dimensional surface features of an antigen molecule, these features fit precisely and bind to antibodies. The part of an antibody that recognizes the epitope is called a paratope.

Fixation.

The aims of fixation for ICC are a) to maintain the structural integrity of tissues or cells so that they can be studied in the EM; b) the antigens must remain recognisable for their antibody; c) the antigens must be immobilised in their natural state; and d) the antigens must be accessible for the immuno-reagents used.

Double fixation is universally used for neuroanatomical EM. Primary fixation in a solution of buffered paraformaldeyhde and glutaraldehyde is followed by post-fixation in osmium tetroxide. Paraformaldehyde is the highly polymerised powdered form of formaldehyde. Formaldehyde is a gas that dissolves rapidly in water. Its small molecules (HCHO, of which the -CHO is the aldehyde group, combine chemically with water to form methylene hydrate, $HO\text{-}CH_2\text{-}OH$. This is the form in which formaldehyde exists in aqueous solutions; its chemical reactivity is the same as that of formaldehyde. Methylene hydrate molecules react with one another, combining to form polymers. A solution of formaldehyde prepared from paraformaldeyhde is commonly used in fixatives for electron microscopy. The polymers in paraformaldeyhde are hydrolysed by heating to 60^{o}c and this aided by the addition of hydroxyl ions (from sodium hydroxide). It is thought that the aldehydes retain cellular constituents in their in vivo relationships to each other by forming cross-links between proteins, creating a gel. Soluble proteins are fixed to structural proteins and rendered insoluble, giving some mechanical strength to the entire structure, which

enables it to withstand subsequent processing. With the formaldehyde, cross-links are formed with or between protein molecules by forming methylene bridges, the most frequent reaction being cross-linking of a lysine side-chain to a peptide nitrogen atom (Gustavson, 1956, Kiernan 2000). Although it penetrates the tissue quickly its reactions are slow.

Glutaraldehyde has also been used extensively for fixation. In aqueous solution it is a mixture of monomers and larger oligomers (Monsan *et al.*, 1975). These penetrate the tissue more slowly than the formaldehyde molecules but because they have free aldehyde groups at both ends of the molecule as well as on the side chains the rate at which cross-linking may occur obviously increases.

Karnovsky introduced a mixture of paraformaldeyhde and glutaraldehyde in 1956 to combine the fast actions of formaldehyde and the slower but more stabilising actions of glutaraldehyde. (Karnovsky 1956). A modification of this, buffered 2% paraformaldehyde mixed with 2.5% glutaraldehyde is still used today for many standard EM fixation protocols. (Appendix 7)

Johnson 1987 and Hardy *et al.*, 1976 have shown that perfusion fixation with glutaraldehyde is necessary to prevent the loss of small molecule amino acids and peptides (neurotransmitters) from tissue sections during washing and embedding. To obtain antibodies that are immunoreactive to glutaraldehyde fixed tissue it is necessary that glutaraldehyde be used to conjugate the hapten and the carrier, just as described earlier under antigens. It is advisable

to consult the original paper describing the production of the specific antibody before embarking on ICC work to check if and how the antigen was conjugated to the carrier.

However, the methods that are best for the preservation of tissue structure do so by altering proteins, masking some epitopes, and even prohibit the recognition of the target protein by intensifying matrix compactness due to cross linking of cellular components. Antigens all behave differently with regard their sensitivity to fixation and subsequent processing and so it is important to experiment with different fixatives to optimise ultrastructure and labelling efficiency.

Buffers.

Buffers are aqueous systems that resist changes in pH when small amounts of acid or base are added. Buffer solutions are composed of a weak acid (the proton donor) and its conjugate base (the proton acceptor). Buffering results from two reversible reaction equilibria in a solution in which the concentration of proton donor and its conjugate proton acceptor are equal. For example, in a buffer system when the concentrations of acetic acid and acetate ions are equal, addition of small amounts of acid or base do not have any detectable influence on the pH. This point is commonly known as the isoelectric point. At this point there is no net charge and pH at this point is equal to pKa.

$$pH = pKa + \log \frac{[CH3COO^-]}{}$$

[CH3COOH]

At isoelectric point [CH_3COO^-] = [CH3COOH] hence, pH = pKa

Buffer capacity is a term used to describe the ability of a given buffer to resist changes in pH on addition of acid or base. A buffer capacity of 1 is when 1 mol of acid or alkali is added to 1 liter of buffer and pH changes by 1 unit. The buffer capacity of a mixed weak acid-base buffer is much greater when the individual pKa values are in close proximity with each other.

Buffers play an extremely important yet complex role during fixation. When formaldehyde or glutaraldehyde is added to tissue large amounts of acid are produced (Johnson 1985). Cells have naturally occurring buffering systems but they cannot cope with the changes of pH that the addition of an unbuffered fixative would cause and structural artifacts occur. Conventionally in electron microscopy fixatives are buffered at a pH in the range of 6.8- 7.4, as for most cells the intracellular pH is about 7.0- 7.4 (Roos and Boron 1983; Griffiths 1993.). However it is thought that the effects of the buffer charged ions is predominantly extracellular as they can not pass into the cell, at least in the initial stages of fixation.(Griffiths 1985). The two most common buffers used in EM are phosphate and cacodylate and their effects on ultrastructure are well documented (Bullock, 1984; Hayat, 1981).

Phosphate buffer is considered to be the most physiological of all used for EM, because it is thought to have no toxic effects. Phosphates in the form of inorganic phosphates and phosphate esters are also abundant in living tissue (Glauert 1975; Hayat 2000). However, Good (1966), pointed out that

phosphate buffer is not an ideal buffer for biological purposes as it tends to precipitate most polyvalent cations and often acts a metabolite or an inhibitor in many biochemical processes (Griffiths 1993). For preparation of 0.2M Sorensen's sodium phosphate buffer see Appendix 4.

Cacodylate buffer (Appendix 5.), on the other hand, proposed for EM by Sabatini (1963), is easily prepared and far more robust and results in less extraction. It contains no additional phosphates and therefore is thought to be more compatible with cytochemical studies. However it has been found to redistribute cellular materials along an osmotic gradient and also cause changes in membrane permeability. (Hayat, 2000). Cacodylate is an arsenate based compound and it is thought it may increase the amount of oxygen available for crosslinking reactions by quickly shutting down respiration (Griffith 1993). This effect could be beneficial for ultrastructural preservation but may be detrimental to antigenicity.

Conflicting evidence exits regarding the advantages of each of these two buffers as vehicles for fixation: Reith *et al* (1984) favoured phosphate buffer: conversely, Hulstaert and Blaauw (1986) preferred cacodylate buffer for animal tissue as a vehicle for normal fixation for EM. A direct comparison of their effects on antigenicity has been never made between the two. (Stirling 1990).

Buffering is also important during immuno-labelling techniques; it must provide the optimal environment for antibody-antigen interactions while preventing non-specific reactions taking place. The buffer should therefore contain a balanced salt solution at an optimal physiological concentration and contain

additives that counter reactions from hydrophobic charge, aldehyde and non-specific receptor binding. Phosphate buffered saline (PBS) or Tris buffered saline (TBS) + 1% BSA + 0.1% Tween 20 + 1% normal serum (of the second antibody species) adjusted with HCl / NaOH, either to pH7.4 or pH8-8.5 is a typical incubation and blocking buffer. The PBS or TBS provides the physiological salt solution. 1% BSA prevents non-specific antibody binding. The BSA molecules bind to the reactive sites on the sections and occupy them, preventing the antibodies from binding to them. Reactive sites on the empty resin are similarly blocked (Brorson 1997b). Hydrophobic attraction of gold or proteins to the section is prevented by the addition of the non-ionic surfactant polyoxyethylene sorbitan monolaurate (Tween 20) (Craig & Goodchild 1982). Gelatin-containing buffers (Moeremans *et al.* 1984) are also used to reduce non-specific background labelling.

The 1% Normal serum should be from the second antibody species (e.g. normal goat serums if goat anti-mouse gold conjugates are used). This prevents gold labelled goat antibodies binding to receptors for goat antibodies in the section. Adjusting the pH to pH8 - 8.5 for the secondary incubation step produces a net negative charge on the tissue section proteins and prevents non specific binding of negative gold particles. Raising the pH even further to pH9 may also help if there are many positively charged components such as collagen and elastin containing many lysine groups. Formvar and epoxy resin contains high levels of sulphur and this can also produce non-specific attraction of gold particles. The charge from the formvar may also be reduced

by evaporating a thin layer of carbon on the grids before picking up the sections.

Tissue preparation.

Accessibility of the antibody to the antigen is one of the major factors governing successful immunocytochemistry. If the antigens are intracellular then the antibodies may not even reach the antigen. Cutting sections through the tissue allows access. To prepare ultra thin sections through biological material the tissue has to be made hard enough for sections as thin as 60-100nm to be cut. Either the water within the material is replaced with a synthetic resin that can be hardened or it is frozen as vitreous ice.

Pre or Post Embedding.

EM ICC resin techniques can be divided into two groups: Those where the immunolabelling is undertaken after resin embedding are known as post-embedding. Those methods where the immunostaining takes place prior to resin embedding are referred to as pre-embedding.

The choice of whether to apply a pre- or post-embedding method to the detection of an antigen in any particular tissue depends on the properties of primary antibody and accessibility of the antigen.

Post-embedding ICC.

Post embedding ICC combined with colloidal gold conjugates for electron microscopy enables the visualisation of antigenic sites on thin sections of tissue that has been fixed and dehydrated followed by infiltration and embedding in a resin. Great care must be taken when selecting an embedding medium for EM ICC so as not to prevent immunostaining occurring by directly interacting with antigens or excluding immunoreagents. (Bendayan 1987) There are many resins available to the electron microscopist only some of which have proved useful for EM ICC (Causton 1984).They can be broadly categorised as water immiscible and water miscible (Hayat 2000) each having advantages and disadvantages when used for ICC. (Stirling 1990, Skepper 2000).

Water immiscible resins include the epoxy resins Epon, Araldite, Spurr and Durcupan ACM. (Glauert 1975; Hayat 2000). Only some variations of epoxy resin have been successful in EM ICC, Durcupan ACM (an araldite based resin) and Epon 812 are widely and successfully used (Kann *et al* 1989; Ji *et al* I 1991; Bozóky *et al* 1992; Shupliakov 1992; Tömböl *et al* 2000; Watson *et al* 2000; Watson *et al* 2001). Spurr resin is much less successful for ICC and is mainly used with botanical samples as its low viscosity increases infiltration through tough cell walls, but it has also been used by some workers in an Epon / Spurr mixture (Hand 1989; Naisbitt 1997). Epoxy resins have aromatic structures which co-polymerise, form covalent bonds with the tissue, especially the proteins, binding the antigens tightly to the polymer network. As

a result they produce the best ultrastructural preservation and stability under the electron beam. Specimens to be embedded in this type of resin need to undergo long dehydrations and high temperatures are required for polymerisation of the resin, both of which could have deleterious affects on antigenicity. Some small peptide hormones and amino acid neurotransmitters such as glutamate and GABA are known to survive this treatment (Storm-Mathisen & Ottersen, 1990). Some workers have also found reducing the temperature of polymerisation of the epoxy resin improves labelling without affecting ultrastructure and section cutting qualities (Kann 1989).

Tissue to be embedded in epoxy resins can be dehydrated, infiltrated and embedded with ethanol alone but as epoxy resins, particularly the Araldites can be viscous, propylene oxide is used to help infiltrate the tissue and complete the dehydration. Propylene oxide may extract lipids from the tissue (Hayat, 1989a) and it may therefore be damaging to delicate antigens. However Brorson (1996) has shown that the immunogold labelling of epoxy sections can be improved by the use of propylene oxide as an additional agent in dehydration, infiltration and embedding.

These resins also require the addition of accelerators, hardeners and sometimes plasticisers, which recipe is used dictates the final hardness of the block and section cutting qualities and ultimately the labelling properties. Increased amounts of accelerator and heat retrieval have also proved useful for increased labelling with epoxy resin. (Hayat, 1970; Mark et al. 1986; Brorson 1998a; Rocken & Roessner, 1999;.Brorson & Nguyen 2001) It is thought that the increased accelerator and the addition of propylene oxide to

the resin have similar affects, in that there is a reduction in co-polymerisation. During sectioning, co-polymerisation, in epoxy resins, tends to cause the proteins themselves to cleave, the epitopes remaining covered and protected by thin layers of resin. If this co-polymerisation is reduced then cleavage might follow the interface between resin and proteins during the cutting process. (Brorson and Skjorten, 1996a, b).

Additionally, epoxy resins are hydrophobic and the penetration of aqueous reagents, such as antibodies, is hindered. Bendayan and Zollinger (1983) and Stirling and Graff, (1995) showed that it was possible, using saturated sodium metaperiodate, to unmask the hidden antigens by de-osmicating the section surface, and obtain better immunolabelling while retaining ultrastructure with epoxy resins. (Brorson and Skjørten 1995; 1996c). Numerous methods have been offered for increasing immunolabelling in epoxy resin, oxidising agents such as hydrogen peroxide, potassium permanganate, and periodic acid, or with sodium alkoxide (sodium ethoxide, sodium methoxide (Brorson and Skjørten 1995; 1996c, Stirling and Graff, 1995 ; Brorson 1997a).These more vigorous means of antigen retrieval are though to etch the surface of the section and reveal hidden antigens. For a few antigens better labelling is obtained using epoxy resins without etching. (Holm *et al.* 1988; Linke *et al.* 1989).

The most commonly used resins for EM ICC are the water miscible acrylic resins, LR White, LR Gold and the Lowicryls. They are said to be better for immunoelectron microscopy than epoxy resins (Causton 1984, Newman,

1987, 1989; Newman and Hobart, 1987; 2001: Brorson & Skjorten, 1996b, 1996c, Rawdon 1997).Their hydrophilic nature allows the passage of aqueous solutions such as antibodies into sections and also means they are compatible with small amounts of water, so that complete dehydration of the tissue is not necessary, although some protocols now include an absolute alcohol step. Acrylic resins do not co-polymerise, they surround tissue but do not bind to them. (Kellenberger *et al*, 1987). When a knife cuts acrylic resins, the cleavage will follow the interfaces between the resin and the proteins, exposing the epitopes at the surface so they become available to the antibodies, leading to higher immunolabelling (Kellenberger *et al*, 1987), This increased surface corrugation is, however, detrimental to high resolution EM (Kellenberger *et al*, 1986, Kellenberger 1998).

They also polymerise at relatively low temperatures and therefore cause less protein denaturation. L.R.White (with added initiator) will polymerise, at about 50°C in the absence of oxygen, by chemical catalysis at temperatures as low as -20 °C or by UV- light. However, only very small blocks of unosmicated tissue are recommended for UV polymerisation. LR Gold is less viscous at lower temperatures and penetrates tissue better than L.R. White and can be polymerised at temperatures as low as -25 °C. Lowicryls are the least viscous of the acrylic resins can be polymerised at temperatures as low as -35 °C for Lowicryl K4M or to -20 °C in HM20, -60 °C for K11M and -80 °C for HM23.with U.V Light (again in the absence of oxygen). This makes them extremely useful for low temperature techniques, such as freeze substitution and progressive lowering of temperature (PLT), which are though to give the best

immunolabelling (Skepper 2000). Freeze-substitution involves the replacement of ice in a frozen specimen with an organic solvent at a higher temperature than that at which the specimen was frozen. Fixation continues to occur at a low temperature during the substitution process, resulting in less extraction. The solvent is then replaced by a resin for specimen embedding. In general, ultrastructure preservation is improved by slow dehydration and the low temperature embedding. Depending upon the choice of resin, the sample can then be sectioned for morphology in epoxy resin, or immunolabeled after embedding in Lowicryl or L.R. White. The specimen is frozen by cold metal mirror freezing (freeze slamming).This involves rapidly bringing flat thin specimens into contact with a polished copper surface that has been cooled to -190°C with liquid nitrogen. This produces a better depth of freezing than plunge freezing because higher freezing rates are obtained. This technique has been used very successfully for neurotransmitter receptors (Baude *et al* 1993: Nusser *et al* 1996; Nyíri *et al* 2001). Even though the tissue may have been previously chemically fixed by perfusion, the subsequent freeze substitution reduces the harmful affects that the dehydration and embedding reagents have on antigenicity.

PLT involves the sample being chemically fixed using aldehydes; dehydration is begun usually with an organic solvent. To reduce extraction and loss of antigenicity during dehydration, the temperature is decreased stepwise while simultaneously increasing the concentration of the dehydrating agent. The sample must not be allowed to freeze at any time so temperature of the

dehydration mixture must be above its freezing-point. Also the dehydrating agent must be miscible with the resin used for subsequent embedding. Lowicryls are usually the resin of choice for low temperature methods but even though they give improved immunolocalisation, the quality of the ultrastructure is inferior to that of the epoxy resins (Hayat 2000)

Pre-embedding ICC.

Many antigens will not withstand the post-embedding treatment and the epitopes are damaged or accessibility of the antibody is severely reduced. (Humbel *et al* 1998). In pre-embedding the ICC technique is applied after fixation but before embedding in the resin of choice. The structures of interest are made accessible in three dimensions, whereas on sections only the section surface is exposed to the antibodies (Stierhof *et al.*, 1986). The tissue requires permeabilisation in some way to allow the reagents access to the antigens. (Humbel *et al* 1998). Cryosections are a mechanical way of permeabilising cells; ice crystals formed during freezing disrupt the cell membranes, enough to allow reagents to pass in and out. (Matsuno *et al.*, 1994; Yazama *et al.*, 1997). Detergents such as Triton –X 100 (De Graaf *et al.*,1992; Langanger *et al.*, 1984; Martone *et al.*, 1996; Satijn *et al.*,1997).and Saponin (Heuser, 1981; Macville *et al.*, 1995; Tanner *et al.*,1996) have been used to chemically disrupt the bilayer by removing lipid and membrane proteins. (Helenius and Simons, 1975). Lipid removal from the bilayer can be prevented by permeabilisation with sodium borohydride (Van Lookeren

Campagne *et al.*, 1992; Young and Furness, 1995). In an evaluation of five different methods for permeabilisation Humbel *et al* 1996 found the method of choice is prefixation with formaldehyde/glutaraldehyde and permeabilisation with Triton X-100. Similarly dehydrating in an alcohol series and then re-hydrating perforates the plasma membrane and allows access to the antigen.

Colloidal Gold.

Since the first demonstration of immunofluorescent labelling of the antigen – antibody complex to localise tissue substances (Coons *et al.* 1941) many new markers have been attached to antisera in both the LM and the EM. Faulk and Taylor (1971) introduced colloidal gold as an EM ICC marker. They showed that antigenicity was not affected when antibodies are absorbed onto gold particles. Because of its ease of manufacture, versatility and electron density it is now the preferred marker. (Faulk & Taylor, 1971; Romano *et al.*, 1974; Bauer *et al.*, 1975; Horisberger, 1981). Gold conjugates may be used directly or indirectly to label antigens. Direct labelling involves using gold that is conjugated to the primary antibody. This is the simplest detection method and involves a single incubation. For indirect labelling the primary antibody is applied to the specimen to interact with its antigen. A gold-labelled secondary antibody then detects the primary antibody. The indirect method, although requiring more incubation steps, is the most commonly used. The choice of gold particle size depends on the magnification to be used and also the

sensitivity required. Smaller gold particles tend to produce higher labelling intensity as they present a lower steric hindrance than larger gold particles. Colloidal gold particles can be thought of as particles coated with protein, whereas ultrasmall gold particles are proteins coated with one or more gold particles. The main advantage of ultra-small gold particles over larger ones is increased detection efficiency whether they are used for pre or post embedding immunolabelling. There are more gold particles per secondary antibody, so as particle size decreases, the number of gold particles attaching to each antigen increases, giving increased signal (more gold particles per surface area in the specimen).The reduction in particle size means there is less steric hindrances and more antigen binding sites will be accessible to the ultra small secondary antibody giving an increased signal. Ultra small gold particles carry less negative charge and so they have less charge determined repulsion to the section surface.

It is common to use ultra small immunogold probes for pre-embedded tissue and the labelling efficiency is even more pronounced that that on post embedded immunolabelled sections because the matrix density is lowered by permeabilisation and they can penetrate further into the tissue (Humbel *et al.* 1995).

Robinson *et al* 1998 reported that there is increased penetration of these probes into specimens and increased labelling efficiency compared to colloidal gold. Small colloidal gold particles in the range of 1–3 nm and gold clusters that are in the 0.8–1.4 nm range have all been used for immunocytochemical applications (Baschong *et al.*, 1985; Slot and Geuze, 1985; Hainfeld,

1987,1988; Baschong and Wrigley, 1990; Chan *et al.*, 1990; De Valck, 1991; Hainfeld and Furuya, 1992; Van de Plas and Leunissen, 1993; Robinson *et al* 1998). Once the antigen –antibody complex has formed it can then be silver enhanced for greater visibility for LM or EM. Ultra small gold particles are too small to resolved in the electron microscope and so their size is enhanced by the deposition of silver. Treatment with a silver developer adds another brief step to the specimen preparation enables the benefits of this small and stable probe to be visualised, either on labelled sections or once they have penetrated the tissue (Burry *et al* 1992).

Quantitation of Gold Probes.

To be sure of positive immunolabelling and specificity on a particular organelle or cell type the gold particle density must be significantly above the background particle density and have significantly higher densities in the structure when compared with other structures that are known to be negative for the particular antigen. (Ingham 1992: Griffith 1993). The structures must be examined in serial sections to see if labelling is consistent. In the case of a metabolic substance such as glutamate, a potential neurotransmitter role can be demonstrated by showing significantly higher labelling in that structure when compared to another structure. Because of the particulate nature of the gold label, quantitation in the electron microscope is relatively simple. Many methods have been used (Somogyi 1986, Ottersen 1989; Bramham *et al.*, 1990, Lucocq 1992; Mayhew *et al* 2002)., the most useful being direct particle counting.The density of immunogold labelling is calculated by counting gold

particles in a measured area or length of membrane and is expressed as gold / μm^2 or as gold/μm. Statistically the signal needs to exceed that considered to be background to be considered 'real' (Mayhew *et al* 2002)

Counting of gold particles can give an impression of changes in antigen concentrations in tissues. Ottersen 1989 has shown a roughly linear relationship between the concentration of fixed glutamate and gold particle density. With the necessary precautions, absolute measurement of antigen concentrations is possible. (Posthuma *et al.* 1987; Slot *et al* 1989). Any attempt to determine the actual content of a secretory protein within a granule (or other structure) by immunogold labeling would require knowledge of the labeling efficiency (Slot et al., 1989) and /or verification by independent measurements of protein concentration

Because the number of gold particles and the number of antigen molecules may not relate directly, the labelling efficiency must be carefully calculated. (Howell *et al.*,1987). Antigen related, tissue related and experiment related factors can all affect the labelling efficiency. These include particle size, (Yokota, 1988) three-dimensional particle distribution, fixation, embedding, extraction and tissue density (Posthuma *et al.*, 1987),

Cryosectioning.

Since Bernhard *et al* (Bernhard and Leduc, 1967; Leduc *et al.*, 1967; Bernhard and Viron, 1971) introduced the use of ultrathin thawed cryosections for immuno-EM in the sixties, many have gone on to develop the technique.

(Tokuyasu 1973, 1976, 1986; Tokuyasu and Singer 1976; Griffiths 1984, 1993; Griffiths *et al* 1983: Keller *et al.*, 1984) and it is now a very valuable technique for subcellular immunocytochemistry and for some antigens it appears to be the most sensitive detection method available (Griffiths and Hoppeler, 1986). This technique also avoids dehydration; solvent and resin embedding steps that can affect antigenicity. Briefly, it involves cutting ultrathin frozen sections from lightly fixed, sucrose infused, and gelatine encapsulated blocks of tissue. The sections are collected onto grids and immunolabelling is carried out in a similar way as for plastic sections. The sections are then stained and embedded in a methylcellulose matrix to prevent collapse of the sections as they dry. This technique tends to be used for sparse and labile antigens or for antigens that are very fixative sensitive.This technique is similar to a pre-embedding technique as the sample is sectioned at low temperature and the thawed sections are collected onto grids immunolabelled and stained. The sections are then embedded *in situ* on the grid. The 'Tokuyasu' technique is particularly good for membrane bound proteins such as receptors, but can also be used for other antigens particularly when some gluteraldehyde as been added to the fixative.

The Synapse.

Sherrington's studies during the 1890's of spinal cord reflexes, combined with the anatomical studies of Cajal, led him to the conclusion that the way in which neurons communicated with each other at the "synapse" was different from the way the signal is conducted in the fibres themselves (Shepherd 1994). He

suggested that synapses behaved as one-way valves consistent with the 'Law of dynamic polarisation' of Gehuchten and Cajal. These ideas provided the conceptual basis for the flow of information in neurons and how they communicated with each other. Dendrites and cell bodies received the signal, acting as the receptor part of the neuron and the axon emitted the signal acting as an effector. Although it was shown later that functional communication is also effected by axon interacting with axon (axo-axonic), dendrite with dendrite (dendro-dendritic), axon with dendrite (axo-dendritic), and even axo-somatic, somata –dendritic and somata-axonic interaction. (Bodian 1972, Shepherd 1972). Axon terminals are also commonly seen to make synaptic contact on the axon hillock (the part of a neuron that connects the soma (cell body) to the axon).These complex input/output relationships form the basis of neural circuits.

Dale, Elliot and Loewi introduced the idea of chemical neurotransmission and the physiologists del Castillo and Katz suggested a quantal release of this neurotransmitter. When the first electron micrographs showed the presence of vesicles in axon terminals this fitted with Sherrington's model of the synapse as a specialised area of functional contact. However, the high resolution micrographs of Palay of central synapses showed that the vesicles were not uniformly distributed within the axon terminal or along the whole of the presynaptic membrane but crowded together at regions of membrane thickening between the neurons: the region now called the 'active zone'. This is the modern day concept of the vertebrate chemical synapse (Fig.1.1). A

Fig.1.1 A typical mammalian chemical Synapse

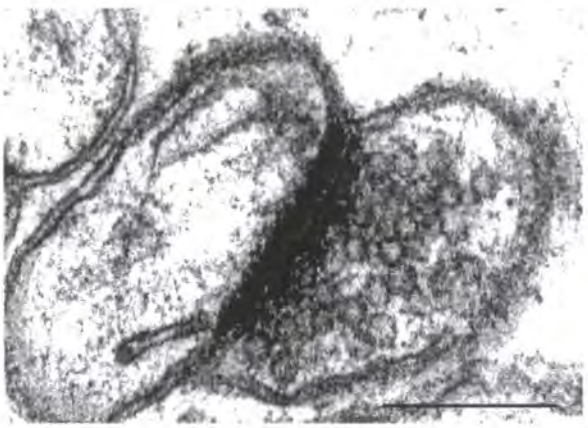

A presynaptic element, an axon, and a postsynaptic element are in close apposition at the synapse but not in direct contact. The pre- and postsynaptic membranes are separated by a gap, the synaptic cleft.Within the presynaptic axonal bouton, clouds of synaptic vesicles are evident. A characteristic feature of the synapse is the opaque material on the cytoplasmic face of the postsynaptic membrane. This material is referred to as the postsynaptic density. Scale Bar = 0.25µm.

presynaptic element, typically an axon, and a postsynaptic element, for example a dendritic spine, are in close apposition at the synapse but not in direct contact. The pre- and postsynaptic membranes are separated by a gap, the synaptic cleft. Chemical transmitters bridge this gap by diffusing from release sites on the presynaptic side to receptors on the postsynaptic side. A variety of ultrastructural specializations occur at the synapse enabling recognizable identification of the pre- and postsynaptic elements. A characteristic feature of the synapse is the opaque material on the cytoplasmic face of the postsynaptic membrane. This material is referred to as the postsynaptic density (PSD). The density represents the accumulation of neurotransmitter receptors and signalling proteins essential for chemical synaptic transmission. Post synaptic densities are contained within dendritic spines, specialized structures that protrude from dendritic shafts. Most excitatory synapses in the mature mammalian brain occur on spines. Many of the major neurons, glutamate or GABA releasing types have dendritic spines, but many do not, e.g. most GABA-releasing interneurons. Invertebrates rarely have spiny neurons suggesting that spines are involved in the more complex functions of 'advanced' nervous systems, such as the mammalian brain. Within the presynaptic axonal bouton, clusters of synaptic vesicles are evident There are estimated to be 200-300 synaptic vesicles in a typical vertebrate presynaptic terminal. Only about fifty percent are actively involved in synaptic transmission at any one time and of those only about 10 of these are within 100nm of 'the active zone' and are termed 'docked vesicles' (morphologically) or a 'readily releasable pool' RRP) of vesicles (physiologically). (Tyler and

Murthy 2004). It has been shown (Hanse and Gustafsson 2001a 2001b , 2002) that only about two of the RRP are actually released per active zone during stimulation and that this takes about a millisecond. A synaptic vesicle may fuse with the presynaptic membrane and release its contents into the synapse; the vesicle membrane is then recycled (Heuser and Reese 1973, Heuser 1989). Alternately, a synaptic vesicle can form a transient fusion pore in the presynaptic membrane and release only part of its contents; in such 'kiss-and-run' exocytosis, the vesicle is then reused. (Ceccarelli *et al* 1973, Fesce *et al.* 1994).

Gray (1959) using osmium tetroxide fixed tissue, classified two types of synapses within the brain, based on the ultrastructural characteristics of the presynaptic and postsynaptic elements. For Type I the cleft is widened to 30nm, the active zone being 1-2μm^2 with dense protrusion and the vesicles tend to be round. The postsynaptic density is broad and dense material appears in the synaptic cleft. Type I synapses are often excitatory. Type II are classified as having a 20nm synaptic cleft, less obvious presynaptic projections and postsynaptic density and no material in the cleft. Their vesicles are likely to be more oval and flattened and these synapses are mainly inhibitory in action. Similar nomenclatures are the terms asymmetric synapse and symmetric synapse described by Colonnier (1968). Colonnier extended the observations of Gray using aldehyde-fixed brain. In aldehyde-fixed tissue, asymmetric synapses include axons that contain predominantly round or spherical vesicles and form synapses that are distinguished by a thickened, postsynaptic density. In contrast, symmetric synapses involve axons that

contain clusters of vesicles that are predominantly flattened or elongate in their appearance. The pre-and postsynaptic membranes are more parallel than the non-synaptic membrane, and the synapse does not contain a prominent postsynaptic density.

In insects, electron-lucent vesicles in the presynaptic terminal are typically associated with presynaptic bars (Fig1.2) or rows of electron-dense particles (Watson & Schürmann, 2000) and are round with a diameter of 35-50nm. Neurons with this type of vesicle have been shown to be immunoreactive for the excitatory neurotransmitter glutamate (Watson 1988). Neurons containing predominantly small pleomorphic vesicles diameter 20-30nm are immunopositive for the inhibitory neurotransmitter γ-amino-butyric acid (GABA). (Watson, 1988; Watson & Schürmann, 2002).The presynaptic bars are often only associated with one postsynaptic process, monodic contact, but can also be found associated with two, dyadic contact (Fig. 4.20) or more polyadic. (Watson and Burrows, 1982; Watson & Schürmann, 2002). Similar specialisations 'ribbon synapses' are found in the terminals of vertebrate photoreceptors, bipolar cells, auditory and vestibular hair cells and in electrosensory receptors (Sterling and Matthews 2005).

Neurons communicate with each other in other, non-synaptic or extrasynaptic transmission, ways. Today it is common to describe the different modes of communication as either 'wiring' transmission or 'volume' transmission classified as such by Agnati *et al* .1995,

Fig.1.2. Electron micrograph showing the different shaped vesicles

A. A presynaptic inhibitory neuron labelled with anti-GABA antibody, contains predominantly small, pleomorphic,agranular vesicles.Two output synapse (arrows) are easily recognised by the presence of presynaptic bars.Scale bar = 500nm.

B.Glutamate immunoreactive neuron containing morphologically distinct larger clear round vesicles. Scale bar = 500nm.

Fig.1.2. Electron micrographs showing the different shaped vesicles in **A.** a presynaptic inhibitory neuron and **B**. an excitatory neuron from a locust mesothorsacic ganglion.Scalebars = 500nm

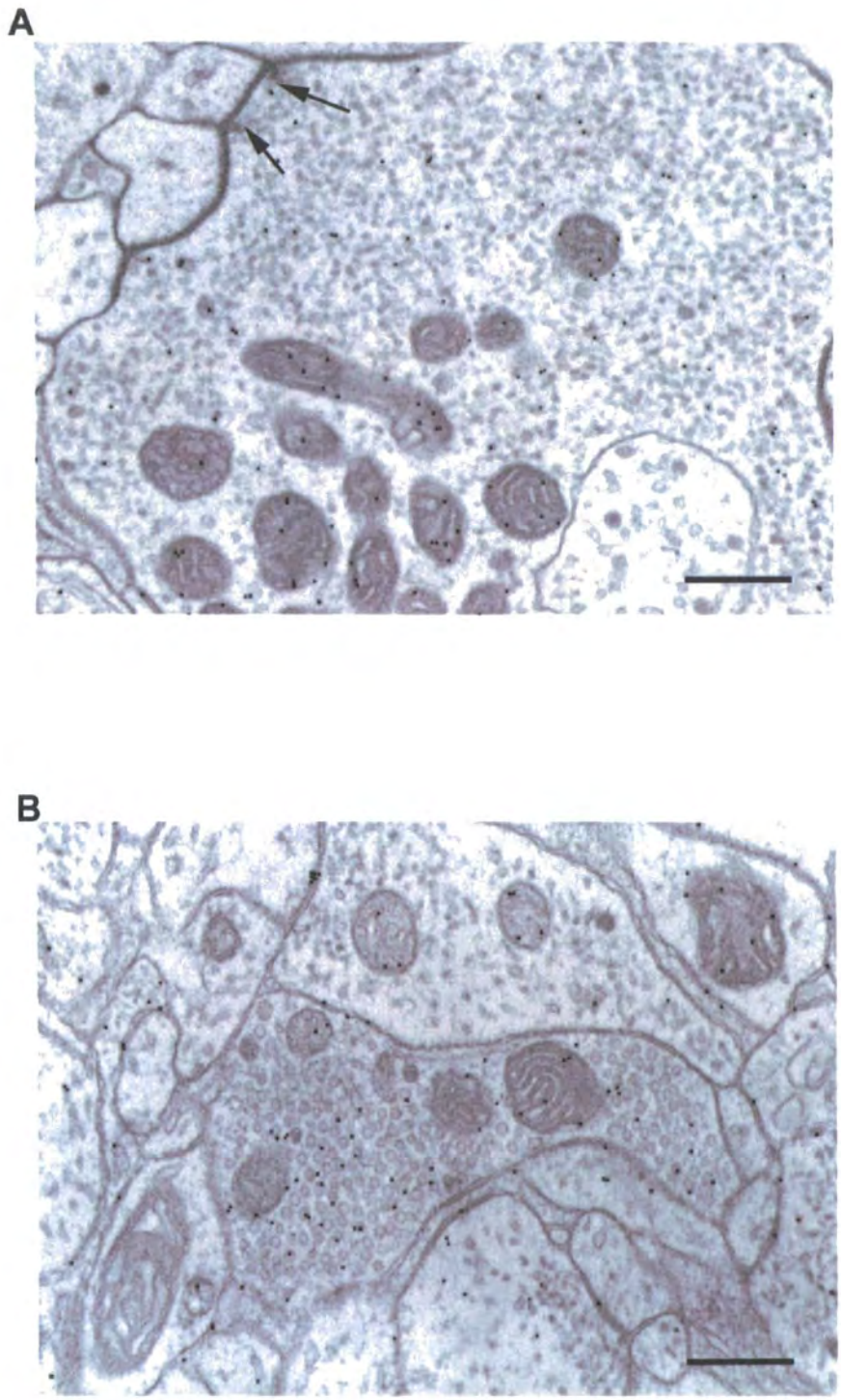

"Wiring" transmission (WT) is defined as intercellular communication occurring through a well-defined connecting structure. Wiring transmission has a physically defined pathway. It includes synaptic transmission but also other types of intercellular communication through a connecting structure e.g., gap junctions). (Agnati *et al* .1995).

The chemical synapse already described is one example of WT, electrical synapses or gap junctions are another. They are intercellular channels approximately 1.5–2 nm in diameter. These permit the free passage between the cells of ions and small molecules. They are cylinders constructed from 6 copies of transmembrane proteins called connexins. Because ions can flow through them, gap junctions permit changes in membrane potential to pass from cell to cell. At some synapses in the brain, gap junctions permit the arrival of an action potential at the synaptic terminals to be transmitted across to the postsynaptic cell without the delay needed for release of a neurotransmitter. The action potential in heart (cardiac) muscle flows from cell to cell through the heart providing the rhythmic contraction of the heartbeat. Juxtaposed neurones (in very close contact) are also sites at which wiring transmission can take place and the nature of the nervous system dictates that many neurones are closely apposed. Examples being, the parallel fibers of the cerebellum, the terminals of axons and dendrites, and between axons and glial cells. They mainly allow the exchange of ions and transmitters but are also thought to be sites of electrical interaction called "ephapses" (Shepherd 1994)

WT is a fast, one-to-one communication whereas "Volume" transmission (VT) is characterized by signal diffusion in a three-dimensional fashion within the brain extracellular fluid and is a one to many form of communication. (Agnati *et al* 1995). VT is a non-synaptic diffuse mode of neurotransmission including both short- (but larger than synaptic cleft, i.e. about 20 nm) and long-distance diffusion of signals through the extracellular and cerebrospinal fluid. (Agnati *et al* 1995, Ridet and Privat. 2000). In rat it has been shown that the monoaminergic (Ridet *et al* 1993, Marlie et.al. 1991) and cholinergic systems (Descarries et.al 1997) are organized in a non-synaptic manner. In insects, Buma and Roubos, 1986, Golding, 1994; Schürmann *et al.*, 1991, have all suggested that large dense cored vesicles could be released at sites other than conventional synapse by VT. Exocytotic omega profiles that are of similar size and shape to the large dense cored vesicles have been reported under certain fixation conditions. (Kerwien and Schürmann 1990; Watson and Schürmann 2002).

Neurotransmitters.

Neurotransmitters are chemicals released by a presynaptic neuron into the synaptic cleft, causing a change in the postsynaptic membrane potential. They are synthesised in the cell body and transported to the synaptic bouton and stored in vesicles. When an action potential occurs an influx of calcium ions causes the vesicles to fuse with the presynaptic membrane and their contents are released into the synaptic cleft. The neurotransmitter diffuses across the

synaptic cleft and binds to receptors on the postsynaptic neuron. This causes a change in the postsynaptic membrane potential of the postsynaptic neuron and the signal moves towards the cell body. The neurotransmitter is now released back into the synaptic space where it is either degraded by enzymes or absorbed by the presynaptic neuron for recycling. Excitotoxicity can occur when there is toxic build up of certain neurotransmitters such as glutamate in the synaptic cleft. This is regulated by active, ATP-dependent transporters in glial cells.

There are more than 300 known or putatative neurotransmitters. These can be divided into three main classes of neurotransmitter: (1) amino acids (primarily glutamic acid , GABA, aspartic acid and glycine; (2) peptides (vasopressin, somatostatin, neurotensin, etc.); and (3) monoamines (noradrenaline, dopamine & serotonin). Others include the ester acetylcholine, the purines, (Adenosine, ATP, GTP and their derivatives, the endorphins, and gases, such as nitric oxide. The action of neurotransmitters can be inhibitory or excitatory, causing either hyperpolarisation or depolarisation of the postsynaptic membrane. Some can function as both depending on the receptor they bind with on the postsynaptic neuron.

Chemical neurotransmission at central synapses was established in the 1950s with evidence collected from electrophysiological and biochemical experiments. But not until significant advances were made in the 1980s in the production of neurotransmitter antibodies could it be visually shown that central synapses had significant levels of the amino acid neurotransmitters

GABA and glutamate. On their own, these small amino acids are too small to produce an immune response but can be conjugated to a carrier protein such as bovine serum albumin (BSA) or keyhole limpet haemocyanin (KLH). (Storm-Mathisen 1983; Seguela 1984.)

GABA is the predominant inhibitory neurotransmitter in the CNS of vertebrates (Seguela, 1985; Gabbott *et al*, 1986; Somogyi *et al* 1986; Ottersen *et al*, 1988; Ottersen and Laake.1992) and invertebrates. (Watson, 1986, 1988; Watson and Pflüger, 1987 O'Dell and Watkins 1988; Schäfer and Bicker, 1986; Homberg *et al*, 1987). GABA- immunoreactive neurons contain morphologically distinct vesicles (Ottersen 1988; Watson, 1988) that are predominantly small, pleomorphic, and agranular. Glutamate is the main excitatory neurotransmitter in the CNS of vertebrates (Ottersen and Storm-Mathisen, 1984; Somogyi *et al* 1986;Ottersen *et al*, 1990; Ottersen *et al*, 1992; Ottersen and Laake.1992.) and invertebrates (Watson *et al*, 1991; Bicker *et al*, 1988; Watson 1988; Watson and Seymour-Laurent, 1993). Glutamate-immunoreactive neurons also contain morphologically distinct larger clear round vesicles (Ottersen 1988; Watson, 1988 ; Watson *et al* 2001 , Watson *et al* 2003).

It would be wrong to attempt to identify excitatory and inhibitory terminals by synaptic morphology and vesicle shape alone as Acetylcholinergic terminals contain agranular vesicles and make asymmetrical synapses, whilst glycinergic terminals contain pleomorphic vesicles and make symmetrical contacts. In fact taurine and GABA are co-localised in Purkinje cell terminals of

the cerebellum as is GABA and glycine. (Ottersen *et al* 1988; Ottersen *et al* 1992). Also the shape of the vesicles has been shown to change with certain fixation regimes (Tisdale and Nakajima, 1976) and become rounded in hyperosmotic solutions. This demonstrates the significance of using primary antibodies to identify the neurotransmitter content of a neuron and not on the basis of vesicle morphology alone.

Octopamine is a biogenic amine. Biogenic amines are a group of amines found in both vertebrate and invertebrates. They can act either as neurotransmitters or neuromodulators. Unlike neurotransmitters, neuromodulators may not excite or inhibit the neuron that they act upon, but may alter the cellular properties of the neuron to modify the transmission of the neurotransmitter. Octopamine is the most important biogenic amine in invertebrates (Evans *et al*, 1985; Orchard *et al*, 1993; Roeder, 1999), and has been reported to act as both a neurotransmitter and neuromodulator (Orchard *et al*, 1993; Roeder, 1999.). Octopamine has been shown to modulate many of the neurons and muscles involved in locust walking (Evans 1981; Sombati and Hoyle ,1984 a,b; Ramirez *et al.*,1993).

Octopamine is an analogue of the vertebrate monamine, noradrenaline, and physiological experiments suggest it plays a similar role to adrenaline and noradrenaline in vertebrates (Orchard *et al*, 1993; Roeder, 1999.). It has been demonstrated in many LM preparations. (Lee and Wyse, 1992; Stevenson *et al.*, 1992; Eckert *et al*, 1993; Stevenson and Spörhase -Eichmann, 1995). Neuronal profiles containing abundant large, polymorphic, electron-dense

granules as being octopamine-IR have been identified at the EM level (Lee & Wyse, 1991;Schürmann *et al.*, 1995, Watson and Schürmann 2002)

Retrograde Tracing With Horseradish Peroxidase.

The use of neuronal tracers can be a powerful technique in demonstrating anatomical relationships between groups of cells. Neuronal tracing allows us to identify where neurons send their axons and then determine, by using subsequent ICC methods, the neurochemical identity of synaptic inputs onto them.

Retrograde tracing was introduced over twenty years ago (Kristensson and Olsson 1971, LaVail and LaVail 1972). The plant enzyme horseradish peroxidase (HRP) was the first of many tracers now available to the neuroanatomist and is still used today for retrograde tracing of nerve trunks by direct application to the cut end. Pinocytotic vesicles take up the HRP and the enzyme is transported back through the axon to the cell bodies. (Llewellyn-Smith *et al* 1992; Kobbert *et al* 2000). Diaminobenzidine (DAB) was the first chromogen used for visualising retrogradely transported HRP (Kristensson and Olsson 1971, LaVail and LaVail 1972) and is still widely used today. DAB is oxidized to a detectable reaction product through the enzymatic activity of HRP on its substrate, hydrogen peroxide. One of the primary problems associated with the use of HRP is nonspecific staining that results from endogenous peroxide activity in certain tissues. A better signal to noise ratio is attained by using glucose oxidase to generate hydrogen peroxide (Itoh *et.al*

1979). Glucose oxidase is an enzyme isolated from Aspergillus niger. This enzyme catalyzes the oxidation of β-D-glucose, producing hydrogen peroxide and gluconic acid. Glucose oxidase is often the label of choice when the presence of endogenous peroxidase activity in mammalian tissue can lead to misinterpretation of staining patterns. There is no endogenous glucose oxidase activity in mammalian tissues, making this enzyme an excellent choice for detection of antigens in tissue. It is important to choose a glucose oxidase with low catalase activity because catalase destroys the hydrogen peroxide end product in the reaction. The peroxidase reaction generates a brown-coloured polymeric oxidation product localized at HRP-labelled sites. The DAB reaction product, which is electron dense, can be visualized, following osmication, by electron microscopy. It is unaffected by exposure to any of the fixatives, buffers or solvents used in subsequent resin embedding procedures. This makes it ideal for determining the neurotransmitter content of inputs onto the retrogradely labelled neurons by subsequent immunogold labelling. (Smith and Bolam 1992).

Aims.

The aims of this study were to consider the strategies available for the immunocytochemical identification of neurotransmitters and to apply them to identified neurons in vertebrate and invertebrate preparations with the purpose of maximising ultrastructural preservation whilst retaining antigenicity.
For the vertebrate system the cerebellum of the mutant mouse Stargazer (*stg*), which has a disruption in the gene encoding the brain-specific protein

stargazin (Letts *et al.*, 1998) was studied. The granule cells in the cerebellum of the *stg* mouse exhibit a pronounced deficit of BDNF mRNA expression and subsequent defect in tyrosine kinase B (TrkB) receptor signalling (Qiao *et al.*, 1998). To investigate whether the levels of neurotransmitter and phenotype of the cerebellar neurons were affected, post–embedding immunolabelling procedures were employed and optimised for high quality ultrastructure in addition to high immunolabelling levels. Embedding media, buffering conditions and etching times were examined.

Identification of the neurotransmitters involved in the modulation of transmitter release from the central terminals of the locust wing-hinge stretch receptor was used for the invertebrate system. This involves using the neuronal tracer HRP to define the fSR neural pathway and then subsequent post embedding immunolabelling identifies the synaptic inputs onto it. Confocal microscopy confirmed the presence of octopamine in the neuropile. To identify the octopaminerigic neurons at the EM level a cryo-immunolabelling and pre-embedding immunogold silver intensification techniques were used.

Chapter 2. GABA-Immunoreactivity In The Cerebellar Golgi, Purkinje And Basket Cells Of The Stargazer Mutant Mouse.

Introduction.

The stargazer (*stg)* mutant mouse has characteristic ataxia and head tossing traits coupled with spike-wave seizures that appear at approximately postnatal day 14 (Noebels *et al.*, 1990; Qiao *et al.*, 1996). Adult *stg* also displays a severe impairment in the acquisition of classical eye-blink conditioning (Qiao *et al.*, 1998). These phenotypes are a consequence of disruption in the gene encoding the brain-specific protein stargazin (Letts *et al.*, 1998). It is thought that this gene mutation is responsible for inappropriate Ca^{2+} entry that could cause functional changes in cortical neurons and thus account for the seizures evident in the *stg* mutant mouse (Di Pasquale *et al.*, 1997; Letts *et al.*, 1998).

The ataxia and impairment in acquisition of classical eye-blink conditioning however, are thought to be cerebellar mediated and have been attributed to the specific reduction in brain-derived neurotrophic factor (BDNF). The granule cells (GC) in the cerebellum of the *stg* mouse exhibit a near total and exclusive ablation of BDNF mRNA expression and subsequent defect in tyrosine kinase B (TrkB) receptor signalling (Qiao *et al.*, 1998) which is temporally related to the onset of ataxia at postnatal day 14. The GCs of the *stg* mouse also display an abnormality in the $GABA_A$ receptor subunit expression profile. Decreased expression of the $\alpha 6$ subunit, which is specific to these neurons, and also the

β3 subunit have been reported by Thompson *et al.*, (1998). Other workers (Hashimoto *et al.*, 1999; Chen *et al.*, 2000) have demonstrated that postsynaptic AMPA (a-amino-3-hydroxyl-5-methyl-4-isoxazolepropionate) receptor function is also impaired in the *stg* mutant GCs, but this does not appear to result from reduced BDNF-TrkB signalling (Hashimoto *et al.*, 1999) despite the fact that BDNF has been shown to affect AMPA receptor function in cultured hippocampal neurons (Bolton *et al.*, 2000).

BDNF has been shown to promote the formation and maturation of synapses in neurons of many brain regions, including inhibitory synapses (Vicario-Abejón *et al.*, 1998; Seil *et al.*, 1994; Seil & Drake-Baumann, 1994; Seil, 1999; Huang *et al.*, 1999; Bao *et al.*, 1999, Marty *et al.*, 2000). Results from studies by Bao *et al.*, (1999) suggest BDNF may modulate GABAergic synapse maturation in the cerebellum. Furthermore BDNF has been shown to increase the GABA content and GAD activity in cultured striatal neurons (Mizuno *et al.*, 1994; Ventimiglia *et al.* 1995) and neocortical neurons (Rutherford *et al.* 1997).

In the intact cerebellum, excitatory mossy inputs to the granule cells could release BDNF onto the Golgi interneurons and may be critical for their differentiation and maturation. Blockade of BDNF signalling in GABAergic cortical interneurons mimics the effects of activity blockade on GABA expression (Rutherford *et al.*, 1997). In *stg* mutant mouse, ablation of cerebellar granule cell BDNF expression may consequently affect development of the Golgi interneuron phenotype resulting in changes in the

GABAergic inputs onto granule cell dendrites in the glomerulus, and altered levels of GABA expression. Similarly, lack of granule cell BDNF could affect development of Purkinje and basket cell phenotypes. In the intact cerebellum, these inhibitory cells receive excitatory inputs from the parallel fibres (granule cell axons).

The aim of the present study was to determine whether the GABA immunoreactivity of the Golgi interneurons, Purkinje and basket cells is compromised by the lack of availability of BDNF in the GCs of the *stg* mouse. There were two objectives: first to investigate whether the levels of GABA neurotransmitter expressed in Golgi, Purkinje and basket cells are altered in *stg,* using semi-quantitative immunogold labelling EM ICC; and second to determine whether the number of inhibitory synaptic contacts between the Golgi interneurons and the GCs and also between basket cell terminals and Purkinje cell somata are changed in *stg* compared to wild-type controls.

To determine the optimal conditions for immunolabelling, while preserving maximal ultrastructural definition of glomerular and synaptic morphology, initially two different buffering solutions (cacodylate or phosphate buffer) and embedding media (Araldite or L.R. White resin) were tested on cerebellar tissue sections from wild-type mouse brains.

Materials And Methods.

WT (C57BL/6J; +/+) and stargazer mutant (C3B6Fe+; *stg/stg*) mice were raised from breeding stock obtained from the Jackson Laboratory (Bar Harbor, ME). Heterozygous males (+/*stg*) and homozygous females (*stg*/*stg*) were mated to produce *stg*/*stg* mutants. Adult mice (2 months) were used in all experiments. Animals were deeply anaesthetized with pentobarbitone sodium (Sagatal, 60mg/kg i.p.) and perfused transcardially with 0.9% saline followed by fixative (details given below). Rabbit anti-GABA antiserum was obtained from Sigma (Poole, United Kingdom). Gold-labelled goat anti-rabbit antibody was obtained from Biocell U.K. All animal protocols used were approved by The Ethical Review Committee of the University of Durham.

Post-embedding ICC.

Sections were cut from perfusion-fixed *stg* and wild-type brains and processed for GABA immunoreactivity using an immunogold labelling method. In total, 8 mice brains (4WT and 4 *stg*) were prepared and examined. Brains were first fixed *in situ* by transcardial perfusion with 2% paraformaldehyde and 2.5% glutaraldehyde in either 0.1M Sorensen's phosphate buffer or 0.1 M cacodylate buffer (CB). (pH 7.4).They were then removed from the skull and transferred to fresh fixative to be processed simultaneously. The cerebellum of each mouse brain was dissected out, sliced into 100-150 □m sections using a

vibrating blade tissue slicer (Campden) and fixed for a further 2 hours at RT. Tissue slices were then washed thoroughly in either PB or CB and then post-fixed in 1% osmium tetroxide (Agar Scientific, Stansted, U.K.) for 1 hour. After post –fixation, and following a brief distilled water wash, the tissue slices from each mouse were processed either into Araldite CY212 or L.R.White resin Slices to be processed into Araldite CY212 were dehydrated through an ascending series of ethanols , 50%, 70% and 95% ethanol, three 10 minute rinses in each respectively. This was followed by two 30 minute rinses in 100% ethanol and then a 30 minute rinse in a 50:50 100% ethanol/ propylene oxide mixture. Infiltration with Araldite CY212 was begun by first making a 50:50 mixture of Araldite CY212 and propylene oxide. The tissue was left in this overnight with the lids off the glass vials to allow the propylene oxide to evaporate slowly and concentrate the Araldite into the tissue. The following morning the tissue slices were given two changes of fresh Araldite CY212 (1 hr each) and then placed in their final embedding moulds. Polymerisation was carried out in an oven at 50°C for 48 hrs. The Aradite CY212 recipe used was as follows ; 10ml DDSA (Dodecenyl Succinic Anhydride), 10ml Araldite CY212 0.4ml BDSA (Benzyldimethylamine).Tissue slices being processed into L.R.White were dehydrated through an ascending series of ethanol 50%-70%, three 10 minute rinses in each. The slices were then transferred to an L.R. White Medium grade resin and 70% ethanol (2:1) mixture for 30 minutes. (Agar Scientific, Stansted, UK). The L.R. White from this supplier already has an initiator added so no further additions are necessary for heat polymerisation. This mixture is made by slowly adding one part of 70% ethanol

(drop by drop) to two parts of L.R. White, and shake gently (otherwise the mixture will become milky). The 70 % alcohol should be freshly made from absolute alcohol (Ours is routinely stored over a molecular sieve in a tightly sealed bottle to keep it 'dry'.).Two fresh changes of LR White resin were followed by an overnight infiltration. Next morning the slices were placed in a fresh change of LR White resin for 30mins before being positioned in gelatin capsules. The specimen was placed at the bottom of the capsule which was then filled up with L.R. White to the brim, and the other half of the capsule was inverted onto it to exclude air. The resin was then polymerised by placing in an oven overnight at 50°C to preserve antigenticity (Newman and Hobot., 2001). Ultrathin sections (70nm) were cut on a Reichert-Ultracut ultra-microtome and mounted on carbon coated /Formvar nickel grids. Inert nickel grids are used in preference to the normal copper grids for immunogold labelling as they do not react adversely with the buffer solutions. Copper grids can be etched by the buffer solutions and introduce contamination on the sections.

Immunocytochemistry.

For all immunocytochemical labelling experiments statistical comparisons were only made between brains that had been fixed and processed at the same time using the same batch of resin and then immunolabelled in parallel. This avoided any differences that might occur in different batches of resin and ensured equal incubation times for etching, antibody labelling and washing. Sections for immunocytochemistry were etched with a saturated solution of

sodium metaperiodate (Bendayan and Zollinger, 1983) for either 1-3 minutes if embedded in L.R.White resin or 10-20 minutes if embedded in Araldite (CY212) resin and then thoroughly washed with distilled water. The grids were then floated face down on droplets of 5% normal goat serum in bovine serum albumin (BSA/Tris buffer (pH 7.4) for 30 minutes. Sections were incubated in the primary antibody by floating the grids on droplets of rabbit anti-GABA antiserum (Sigma, UK) in BSA/Tris buffer (pH 7.4) for 2-3 hours at room temperature. The antibody had been obtained from rabbits after immunisation with a GABA-glutaraldehyde-BSA conjugate (Seguela *et al.,* 1984). It was initially tested in a dilution series from 1:50 to 1:32,000; optimal staining was achieved with 1:500 and this dilution was then used in all experiments. Following incubation in the primary antibody, sections were thoroughly washed in BSA/Tris buffer and transferred to droplets of 10nm gold-labelled goat anti-rabbit antibody (Biocell, UK) diluted 1:20 in BSA/Tris buffer (pH 8.2) for 1 hour at room temperature. Adjusting the pH to pH8.2 for the secondary incubation step produces a net negative charge on the tissue section proteins and prevents non specific binding of negative gold particles. The grids were finally washed in a series of distilled water droplets to remove unbound gold conjugate then stained for 10 mins. in 1% ethanolic uranyl acetate, rinsed in distilled water and then stained for a futher 10 mins. in Reynolds Lead citrate (Reynolds 1963) before a final rinse in distilled water. Once dry the sections were examined in a Philips EM 400T electron microscope.

A number of positive and negative controls were performed to test the specificity of labelling. The anti-GABA antibody was applied to sections containing known gamma amino butyric acid –immunoreactive (GABA-IR) axons (see Leitch and Laurent, 1993). The antibody bound specifically to the axons known to be GABA-IR; this staining was absent in all negative controls. The following negative controls were performed on test and control sections: (a) omission of the primary antibody and replacement with incubation buffer only; (b) pre-absorption of the GABA antibody overnight with BSA/GABA conjugate, prepared according to the method of Seguela *et* al 1984; and (c) replacement of the primary antibody with non-immune serum. None of these negative controls showed significant immunolabelling.

Statistics.

The significance of the density of gold particles distributed over labelled profiles as against background levels was assessed using a paired Student's t-test (Table 2.1) according to the method of Watson (1988). The paired t-test was used in preference to an unpaired t-test to avoid any effects of differences in labelling density due to variable access of antibody to different parts of a section (e.g. caused by uneven etching) and differences between grids. Randomly selected labelled profiles were delineated and their areas calculated using the computer program Scion Image (Scion Corporation http:// www.scioncorp.com). The number of gold particles within each profile was counted and the density of gold particles per μm^2 calculated. This was then

compared to the density within the nearest adjacent profile that was not clearly labelled (background levels). A total of 40 pairs of measurements were used for each comparison. To compare the density of gold particles distributed over labelled Golgi interneuron profiles in *stg* and wild-type cerebellar sections an unpaired Student's t-test was used. A total of 40 pairs of measurements for each mouse brain examined, taken from different sections throughout the cerebellum, was used for each comparison. To assess the level of GABA-IR in Purkinje cell soma and basket cell terminals, the following sampling protocol was adopted. Purkinje cells were selected for analysis provided the section was through the Purkinje cell nucleus. All of the Purkinje cells present in a selected ultra-thin section were analysed. Only one ultra-thin section from each sample block of cerebellum was examined. In this way each Purkinje cell soma analysed for GABA-IR was different. Gold beads were counted over the cytoplasm but not the nucleus of each Purkinje cell and the density of gold particles distributed over labelled Purkinje cell soma profiles in *stg* cerebellar sections compared to wild-type controls. An equal number of sections was sampled from each animal to ensure unbiased sampling. All of the basket cell terminals in synaptic contact with these Purkinje cell soma profiles were examined and analysed. The density of gold particles distributed over labelled basket cell profiles in *stg* and wild-type cerebellar sections were calculated as described above and compared using an unpaired Student's t-test. The number of basket cell-Purkinje cell synapses was also counted for each Purkinje cell profile analysed.

Table 2.1. Density of gold (particles /μm^2) over GABA – IR processes in Wild-type controls compared to background levels following labelling with an anti-GABA antibody.

Treatment	Label density (particles/μm^2)		Ratio
WT1. Araldite Phosphate 10 mins etch			
Labelled profiles	31.04 ± 13.22	$P < 0.001$	1 : 17.64
Unlabelled profiles	1.76 ± 1.65		
WT2. Araldite Phosphate 20 mins etch			
Labelled profiles	50.28 ± 15.81	$P < 0.001$	1 : 17.64
Unlabelled profiles	2.85 ± 3.07		
WT1. Araldite Cacodylate 10 mins etch			
Labelled profiles	9.97 ± 3.69	$P < 0.001$	1 :18.81
Unlabelled profiles	0.53 ± 1.15		
WT1. Araldite Cacodylate 20 mins etch			
Labelled profiles	27.7 ± 13.37	$P< 0.001$	1 :18.34
Unlabelled profiles	1.51 ± 2.41		
WT1. L.R.White Cacodylate 1 mins etch			
Labelled profiles	41.23 ± 16.30	$P < 0.001$	1 : 21.81
Unlabelled profiles	1.89 ± 2.28		
WT2. L.R.White Cacodylate 3 mins etch			
Labelled profiles	54.98 ± 31.06	$P< 0.001$	1 : 24.88
Unlabelled profiles	2.21 ± 3.19		

For analysis of the number of synapses per Golgi interneuron profile, a total of 100 GABA-IR profiles from both wild-type and *stg* were randomly selected. Synapses made by GABA immunoreactive terminals (and so assumed to be inhibitory) were symmetrical, while those made by terminals that were not immunoreactive for GABA (assumed to be excitatory), were asymmetrical. Golgi axon-granule cell dendrite synapses were identified as inhibitory and those between mossy fibres and Golgi cell dendrites were identified as excitatory. For the purpose of quantification in this study, the following criteria were used to classify the contact as a synapse: (1) consistent apposition of presynaptic and postsynaptic membranes, (2) widening of the extracellular space in the synaptic cleft, and (3) clustering of small synaptic vesicles at the release site .The mean density of all synapses per Golgi interneuron profile and also the mean density of only inhibitory synapses per Golgi axonal profile were calculated for both wild-type and *stg* mice. To compare the mean density of synapses in wild-type and *stg* mice a Student's t-test was used. The total numbers of synapses on each Golgi profile were also plotted as frequency distribution histograms. To compare the frequency distribution of synapse number per Golgi profile, in *stg* and wild-type mice, a Chi-Squared test was used.

Data Analysis.

Electron micrographs at a magnification of x 10,000 were taken on a Philips 400T (Philips Electron Optics, Eindhoven, The Netherlands) using Kodak 4489 Electron microscope film (Eastman Kodak Company Rochester NY USA).

These were scanned with an Epson GT 7000 Negative scanner (Epson UK Ltd) at a resolution of 600 d.p.i. For analysis of gold labelling density greyscale TIFF files were imported via a microcomputer system (Roldec Computers UK) into Scion Image v.4.0.2 (Scion Corporation www.scioncorp.com). Cell profiles were delineated and the cross sectional areas measured .All gold particles within the outlined area were counted and the particles/μm^2 calculated.

Results.

Morphology Of The Cerebellar Cortex.

To provide a background for the analysis of GABA immunoreactive (GABA-IR) and later the analysis of glutamate immunoreactive (Glut-IR) synapses in the cerebellar cortex, a description of the gross morphology, cell types and their interconnections is given. Light- or electron-micrographs were obtained through a Nikon Coolpix 900 digital camera attached to a Nikon Optiphot (Nikon,U.K.) or a Philips 400T electron microscope.(Philips Electron Optics, Eindhoven, The Netherlands), respectively. Sections used were, a) paraffin wax sections of 10 μm thickness that had been stained with cresyl fast violet for Nissl granules; b) semi- thin sections of 1 μm thickness that had been stained with 1% toluidine blue from material that had been prepared for EM and; c) ultrathin sections from material that had been prepared for EM.

The Cerebellum.

The human cerebellum is located towards the back of the brain, underneath the occipital lobe of the cerebrum. It is only 10% of the total brain volume yet has a surface area of almost 75% of the cerebral hemispheres and has more than half of all the neurons in the central nervous system (CNS). It is connected to the brain stem by three symmetrical pairs of tracts called the cerebellar peduncles that provide the input and output connections from the periphery and all levels of the CNS. Its main function is to co-ordinate voluntary movement, posture and equilibrium by ultimately modifying the output of the major descending motor systems of the brain.
The cerebellum plays an important role in the learning of motor tasks, and patients with damage to the cerebellum may be clumsy, have a staggering gait, hand tremors and slurred speech.

Organization Of The Cerebellum.

The cerebellum consists of an external cerebellar cortex and four internal deep cerebellar nuclei, separated by a layer of white matter. There are two primary afferent inputs into the cerebellum, the mossy fibres and the climbing fibres. Each sends collateral axons to the deep nuclei (primary cerebellar circuitry). These same afferent inputs activate the inhibitory action of the cerebellar cortex that modulates the primary circuit.

Cerebellar Cortex.

The cerebellar cortex is a convoluted sheet of grey matter that lies beneath the surface of the cerebellum, each convolution is called a folium (Fig. 2.1a). The cortex consists of three distinct layers (Fig. 2.1b). The outermost layer, the molecular layer (Fig.2.1b & Fig. 2.2a), is characterized by parallel fibres, the bifurcated axons of the granule cells, lying parallel to the long axis of the folium. Stellate cells, basket cells and the dendrites of the Purkinje cells, from the layer below, are also within the molecular layer and have all been shown to be immunopositive for the inhibitory neurotransmitter GABA. (Seguela *et al* 1985; Gabbott *et al*, 1986; Somogyi *et al* 1986; Ottersen *et al*, 1988; Ottersen and Laake.1992;)

The Purkinje layer (Figs. 2.2a & b.) is immediately below the molecular layer this contains Purkinje cell bodies. Purkinje cells are inhibitory neurons that send their axons into the white matter, below the cortex; and their dendritic tree into the molecular layer. The Purkinje cell dendrites are arranged perpendicular to the parallel fibres of the molecular layer and form tens of millions of synapses in total. Purkinje cells are the only output from the cerebellar cortex and have been shown to be GABAergic. (Seguela *et al* 1985; Gabbott *et al*, 1986; Somogyi *et al* 1986; Ottersen *et al*, 1988; Ottersen and Laake.1992)

The deepest layer is the granule cell layer (Figs. 2.1b & 2.2a & b.) containing large numbers of densely packed granule cells and much fewer, but larger, Golgi cells. Golgi cells contain pleomorphic agranular vesicles and are

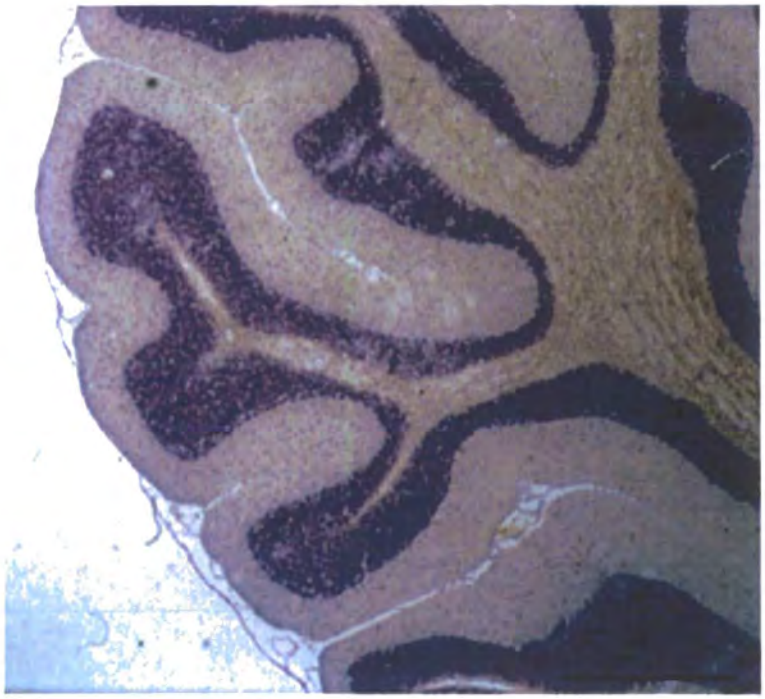

Fig. 2.1a. Light Micrograph showing a folium from adult mouse cerebellum. Stain is Cresyl fast violet. Scale bar =100um

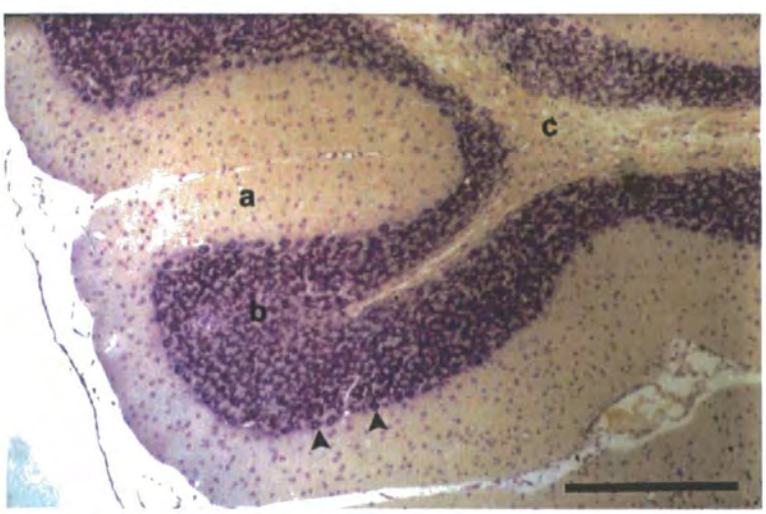

Fig.2.1b. Higher magnification of **Fig2.1a** showing the three layers of the cerebellar cortex of adult mouse. **a.** The molecular cell layer. **b.** The granule cell layer. **c.** The white matter. ▲ The Purkinje cell layer. Scale bar = 50μm

Fig. 2.2. Light micrographs from 1μm toluidine blue stained sections of the mouse cerebellar cortex. **A.** The arrowheads point out a line of Purkinje cell bodies separating the molecular layer (**a**) from the the granule cell layer (**b**). Scale bar = 50μm. **B.** Arrowheads again point out a line of distinct Purkinje cell bodies. The darkly stained nuclei of the granule cell dendrites (**b**) are interspaced with clear areas which contain the cerebellar glomeruli (see **Fig.2.3A**). Scale bar = 1μm.

Fig.2.2. Semi- thin sections of mouse cerebellar cortex.

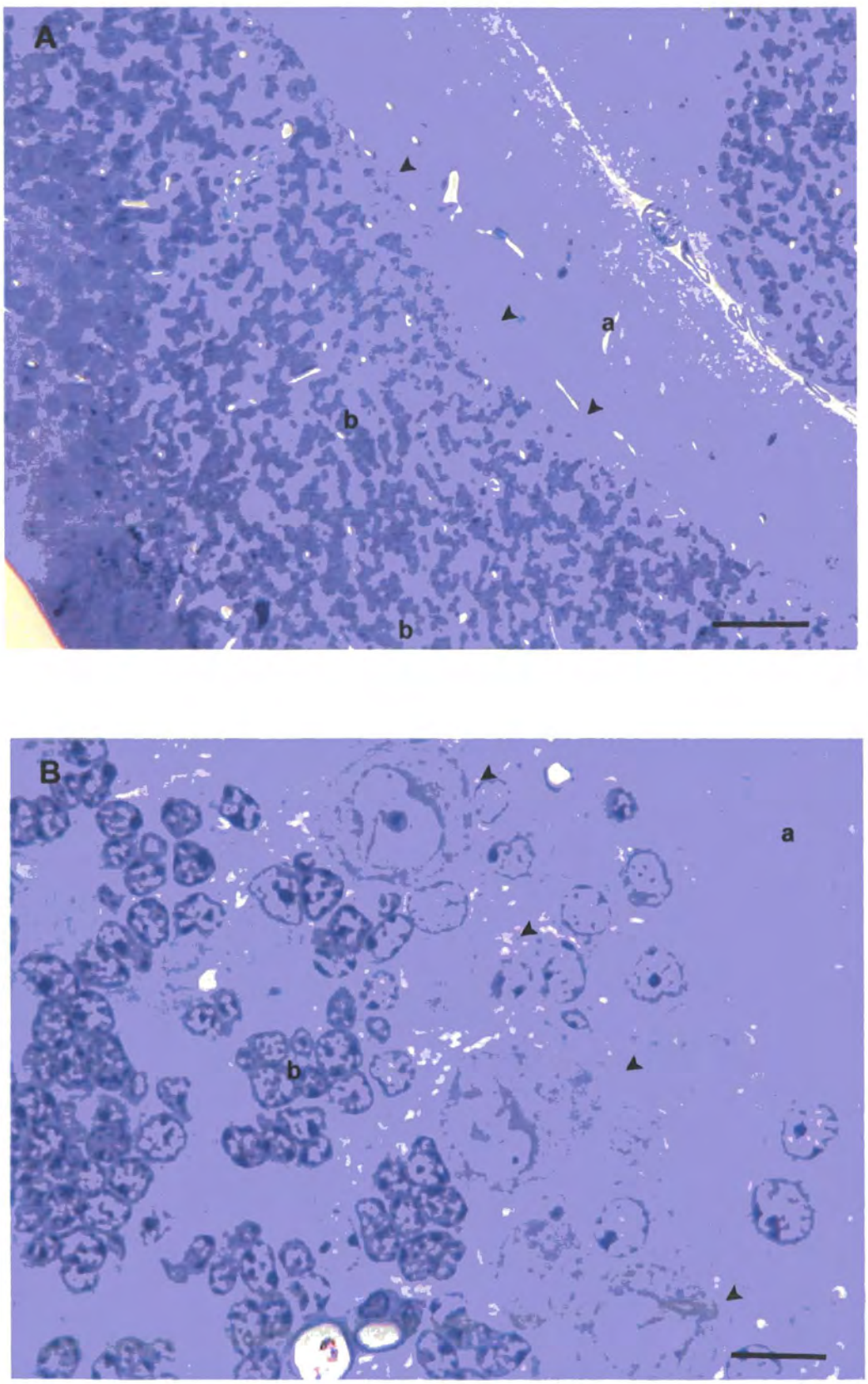

immunopositive for GABA. (Seguela, 1985; Gabbott *et al*, 1986; Somogyi *et al* 1986; Ottersen *et al*, 1988; Ottersen and Laake.1992). Also within this layer are small clear spaces known as cerebellar glomeruli (Fig. 2.3a & 2.3b). These are the complex synaptic contacts between granule cells and the expansions of the afferent mossy fibre. Granule cells and mossy fibres are both immunopositive for the excitatory neurotransmitter glutamate (Otterson and Storm- Mathisen, 1984; Somogyi *et al* 1986;Ottersen *et al*, 1990; Ottersen *et al*, 1992; Ottersen and Laake.1992.).

Circuitry Of The Cerebellar Cortex.

The activity of the Purkinje neurons, their axons being the only output from the cerebellum (Eccles 1967), is affected by two excitatory afferent inputs (Cajal, 1911) the climbing and mossy fibres and by the local inhibitory interneurons (basket, Golgi and stellate neurons) (Fig. 2.4). Each Purkinje cell receives input from only one climbing fibre, but each climbing fibre can synapse with many Purkinje cells. (Cajal 1911; Hamori and Szentagothai,1966 ; Eccles 1967; Eccles *et al* , 1967). Climbing fibre /Purkinje synapses have a powerful excitatory effect and produce what is called a complex spike (Eccles, 1966). Mossy fibres are one of the major inputs coming from the spinocerebellar and cerebro-cerebellar tracts (Fig 2.3c), each has up to 50 swellings (rosettes) containing clear round vesicles and synaptic thickenings. They influence the Purkinje cell indirectly through excitatory synapses with the granule cells. Dendrites of up to 15 granule cells can contribute to one glomerulus. Sectioned profiles of granule cell dendrites (Fig. 2.3b) are ovoid or spherical in

Fig. 2.3. Electron micrographs of ultrathin sections through,

A. A typical glomerulus in the granule cell layer of the cerebellar cortex. The mossy fibre terminal (**MF**) is packed with round clear synaptic vesicles and makes asymmetrical excitatory synapses onto the numerous granule cell dendrites (**GC**) surrounding it. Scale bar = 1μm.

B. Shows a typical Golgi cell (**GO**) in the granule cell layer of the cerebellar cortex. . These tend to be found at the periphery of the glomerulus and make symmetrical inhibitory synapses onto granule cell dendrites. Note it has smaller pleomorphic vesicles, compared to the larger and rounder vesicles of the mossy fibre terminal (**MF**). Scale bar = 0.5μm.

Fig 2.3. Electron micrographs of ultrathin section through a typical glomerulus.

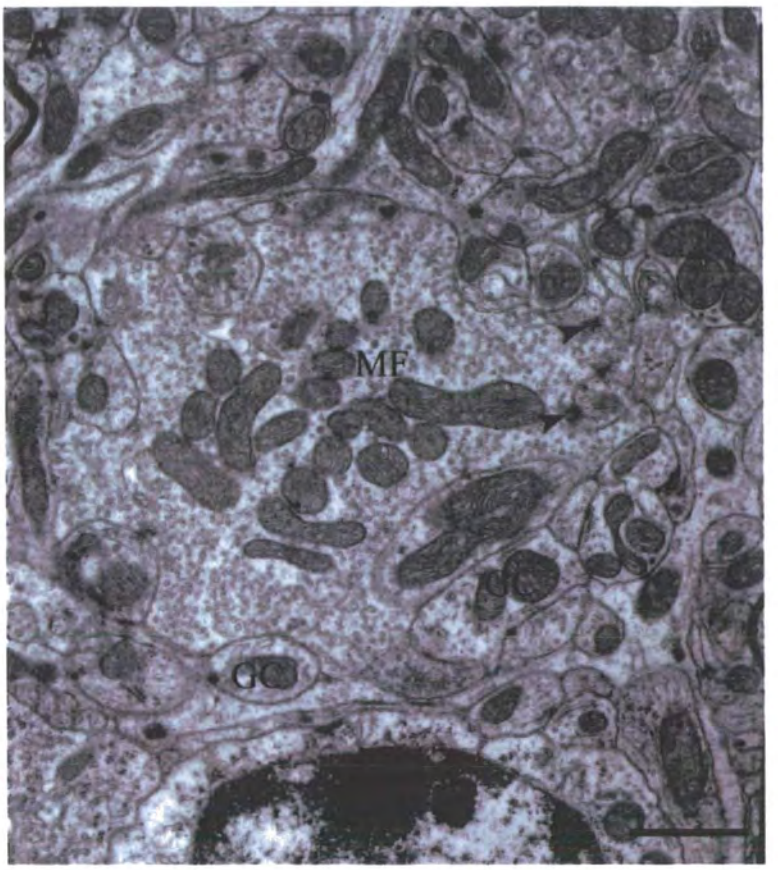

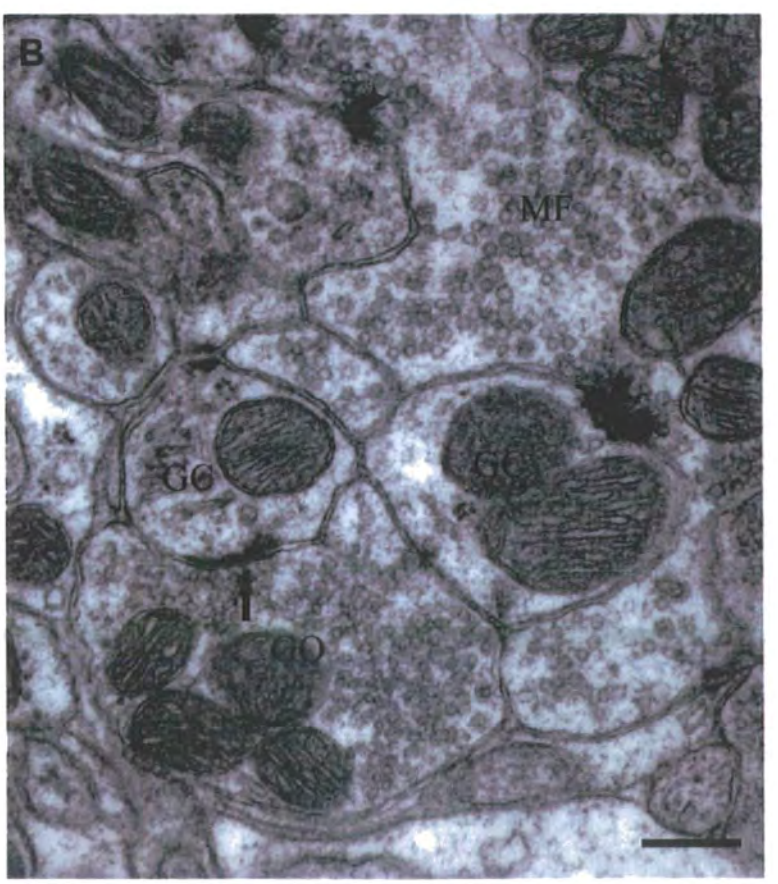

Fig. 2.3.c. Schematic showing the organisation of the cerebellar cortex, the different cell types and the two afferent inputs and their connections.

Inset. Schematic showing the detailed structure of a glomeruli within the granule cell layer of the cerebellar cortex.

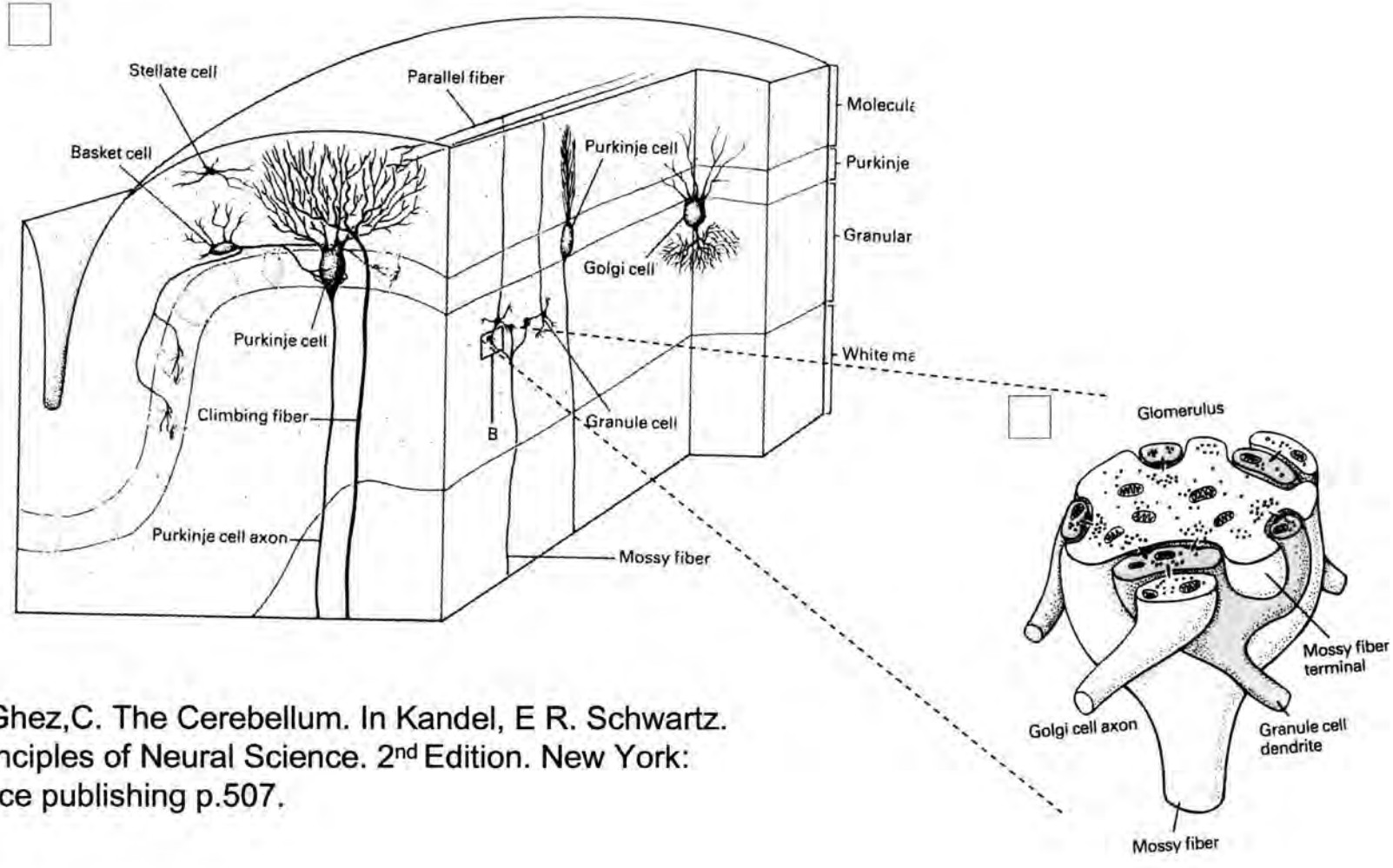

Taken from: Ghez,C. The Cerebellum. In Kandel, E R. Schwartz. J. H.(ed): Principles of Neural Science. 2nd Edition. New York: Elsivier Science publishing p.507.

Fig 2.4. Electron micrograph of an ultrathin section through a Purkinje cell body (PC). Numerous basket cell boutons★, surround the Purkinje cell and make inhibitory synaptic contacts onto it.The nuclei of several granule cells (GC) can also be seen.Scale bar = 5.0μm

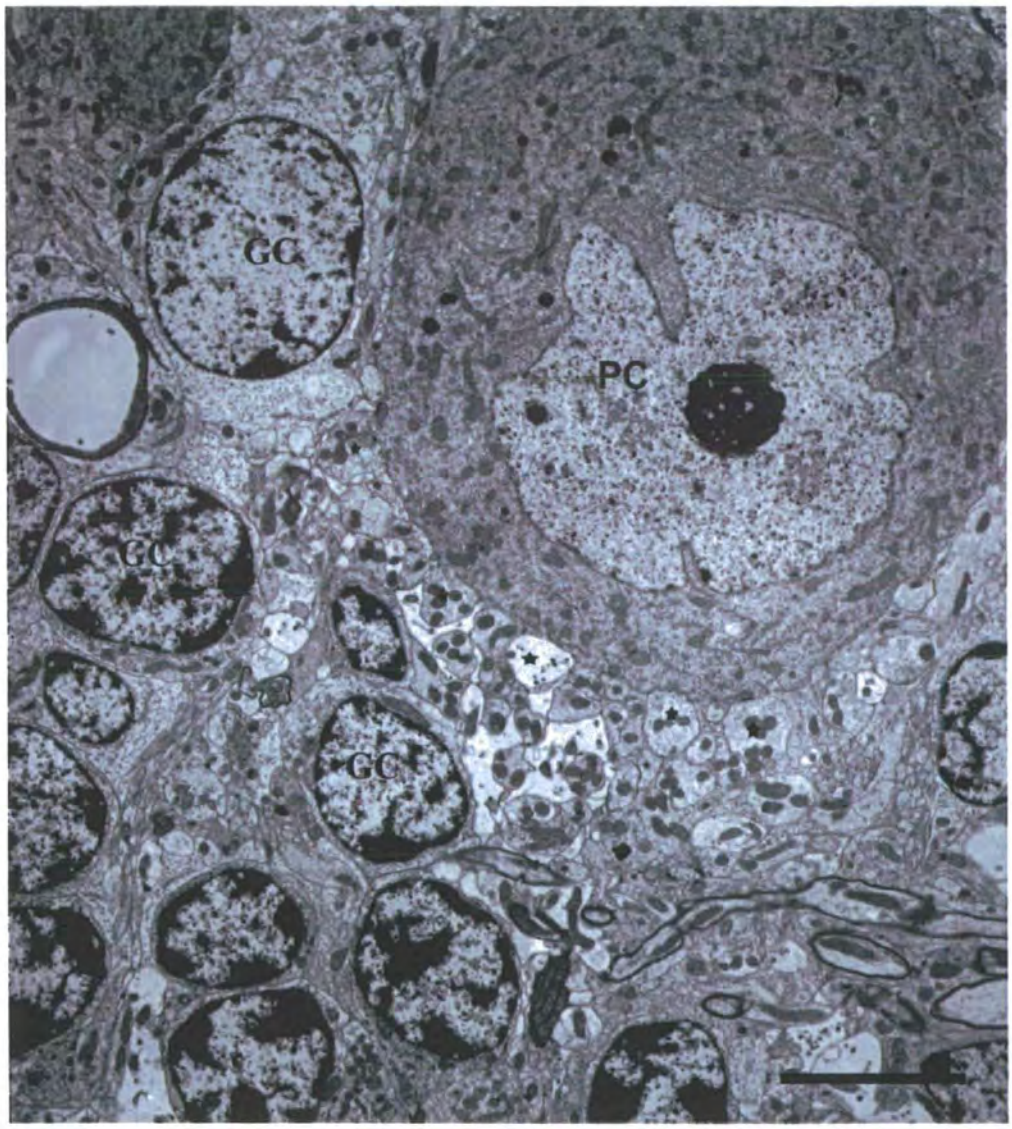

shape have no synaptic vesicles. The axons of granular cells extend through the Purkinje cell layer, where they branch into two axons called parallel fibres. When a peripheral stimulus activates the mossy fibre, groups of granule cells are activated. If enough granule cells fire simultaneously this will, via parallel fibres, activate enough spines of the Purkinje cell to cause an action potential. When this happens, the Purkinje cell generates what is called a simple spike. Golgi cell axonal terminals (Fig. 2.3b 2.3c.) lie at the periphery of the glomeruli and make synaptic contact with the granule cell dendrites. The axon of the Golgi cell has a complicated interaction with the mossy fibre terminal –granule cell dendrite and prevents information coming into the cerebellar circuitry by inhibiting the mossy fibre terminal –granule cell relay. Stellate and basket cells receive excitatory inputs from parallel fibre bundles. The short axons of the stellate cells contact nearby Purkinje cell dendrites whereas the much longer axons of the basket cells contact Purkinje neurons some distance away from the active parallel fibre bundle. This system is designed to inhibit the Purkinje neurons around the active parallel fibre bundle. Golgi cells, with their large dendritic trees in the molecular layer also receive input from parallel fibres, and shorten the duration of bursts in the parallel fibre system by innervating the granule cell dendrites directly at the mossy fibre glomeruli, an effect called feed back inhibition. (Ghez and Thach, 2000).

Optimum Resin Media And Buffering Conditions For Immunolabelling.

To determine the optimum conditions for immunolabelling, while preserving maximal ultrastructural definition of glomerular and synaptic morphology,

initially two different buffers solutions (cacodylate and phosphate buffer) and embedding media (Araldite CY212 or L.R.White resin) were tested on cerebellar tissue sections from wild type mouse brain.

Figure 2.5 shows the relative density of gold labelling over immunopositive Golgi profiles against background levels over non-GABA immunoreactive (non-GABA-IR) processes from tissue processed in the different ways outlined above. Irrespective of the buffer or embedding media used or the time taken for etching, gold-labelling densities over GABA-IR Golgi profiles were significantly ($P<0.001$) higher than over non-GABA-IR profiles (Fig. 2.5 A-C, Table 1.). In figure 2.5A the cerebellar tissue used in the analysis of gold labelling densities was from the brain of a wild-type mouse (WT1) that had been perfused with cacodylate buffered fixative and embedded in Araldite resin. Tissue from the same mouse cerebellum fixed in cacodylate buffer but embedded in L.R. White resin was used in the analysis shown in figure 2.5B. Although the average density of particles (pcles/μm^2) over Golgi profiles, in tissue embedded in Araldite and buffered with cacodylate, was less than that over Golgi profiles in tissue from the same mouse but embedded in L.R. White resin, (9.97 $\pm$ 3.69 pcles /μm^2, n = 40; 41.23 $\pm$ 16.30 pcles/ um^2, n = 40 respectively), the ratio of pcles/μm^2 over positive profiles compared to background levels was similar (18.8: 1 for Araldite embedded tissue and 21.8: 1 for matched L.R. White embedded tissue; Table 1). In all animals tested, cerebellar tissue embedded in Araldite resin showed superior ultrastructural definition of glomeruli and synaptic contacts compared to tissue embedded in

Fig. 2.5. Histograms showing the relative density of gold labelling over GABA-IR Golgi profiles compared to non-GABA-IR profiles. Tissues are from wild-type (WT) mice processed in different buffering solutions and embedding media. (**A**) WT mouse 1 processed in cacodylate buffer and embedded in Araldite. (**B**) WT mouse 1 processed in cacodylate buffer and embedded in L.R.White. (**C**) WT mouse 2 processed in phosphate buffer and embedded in Araldite. (**D**) Comparison of WT1 (**FIG.1A**) and WT2 (FIG.1C) showing effect of different buffering solutions and etching times. Values represent surface density of gold particles expressed as the Mean ± S.E.M. (n = 40 for each animal). Significance was found using a Students t-test. **, $P < 0.001$.

Fig. 2.5. Histograms showing the relative density of gold labelling over GABA-IR Golgi profiles compared to non-GABA-IR profiles.

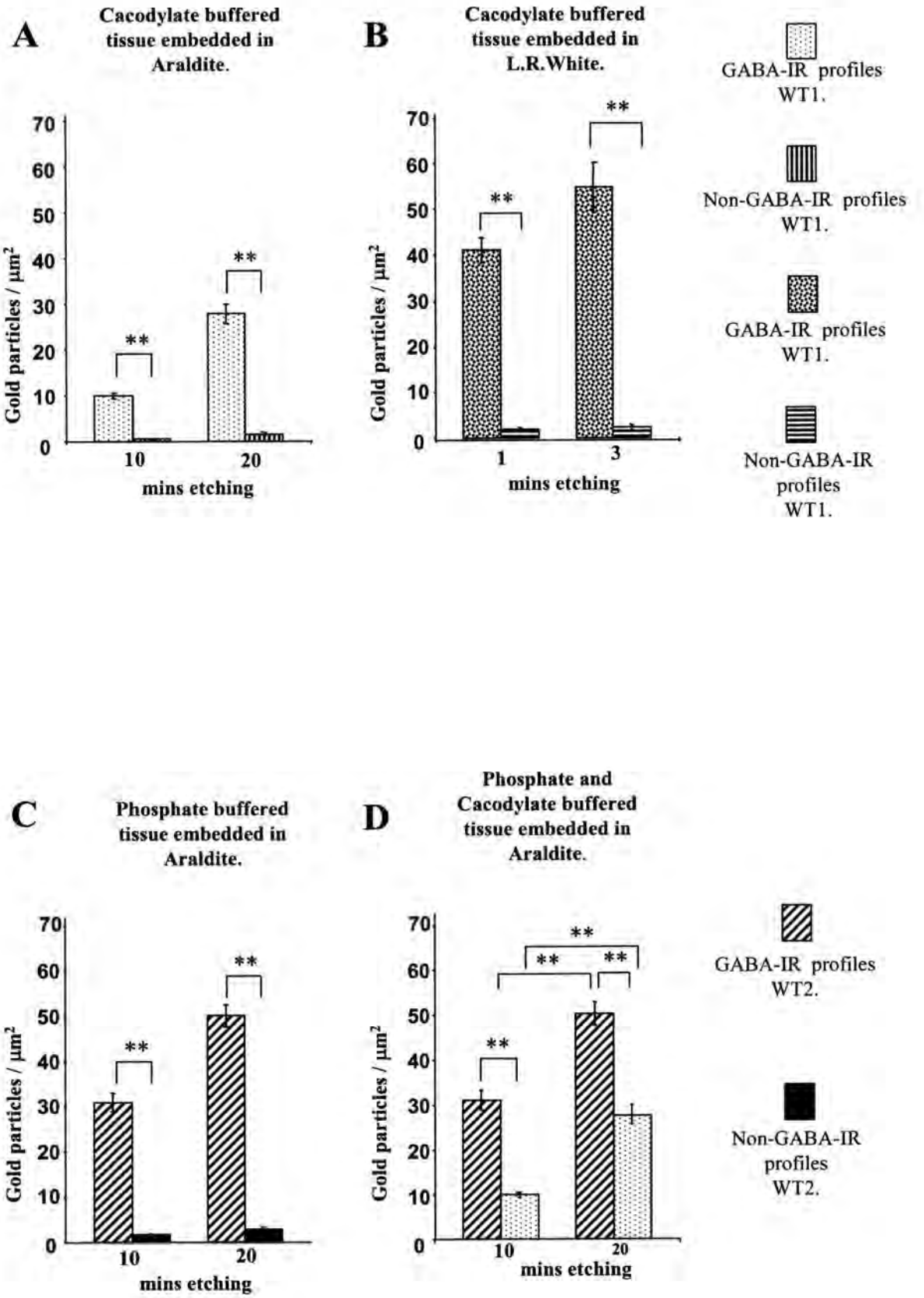

L.R. White, despite requiring longer etching times (10-20 mins) to achieve similar gold labelling densities to that achieved on L.R. White embedded sections (1-3 mins etch).

Tissue from mouse brains fixed in phosphate buffered solutions and embedded in Araldite resin (Fig. 2.5C) showed consistently higher levels of gold immunolabelling than cacodylate buffered brains embedded in Araldite resin (see Fig. 2.5D) whilst still retaining superior ultrastructural detail. Immunolabelled sections taken from brains fixed in phosphate buffered solutions but embedded in L.R. White were judged too ultrastructurally compromised to analyse (Fig. 2.6A.B).Tissue embedded in Araldite resin(Fig. 26.B) showed superior ultrastructural definition of glomeruli and synaptic contacts. For LR White embedded tissue (Fig. 26A). It was sometimes difficult to be absolutely sure of the boundaries of a cell when delineating for area measurements. Similarly accurate measurements of synaptic contacts were difficult with L.R White embedded tissue, even without the effects of etching. Hence the subsequent measurements and analysis of immunogold labelling over Golgi terminals, Purkinje soma, and basket cell terminals in *stg* mice concentrates on tissue samples from Araldite embedded specimens and in particular those fixed in phosphate buffered solutions.

Fig. 2.6. A, B. Electron micrographs showing gold labelling over GABA-IR profiles in the granule cell layer of cerebella from L.R. White embedded tissue(**A**) and Araldite embedded tissue(**B**). Scale bars = 500nm.

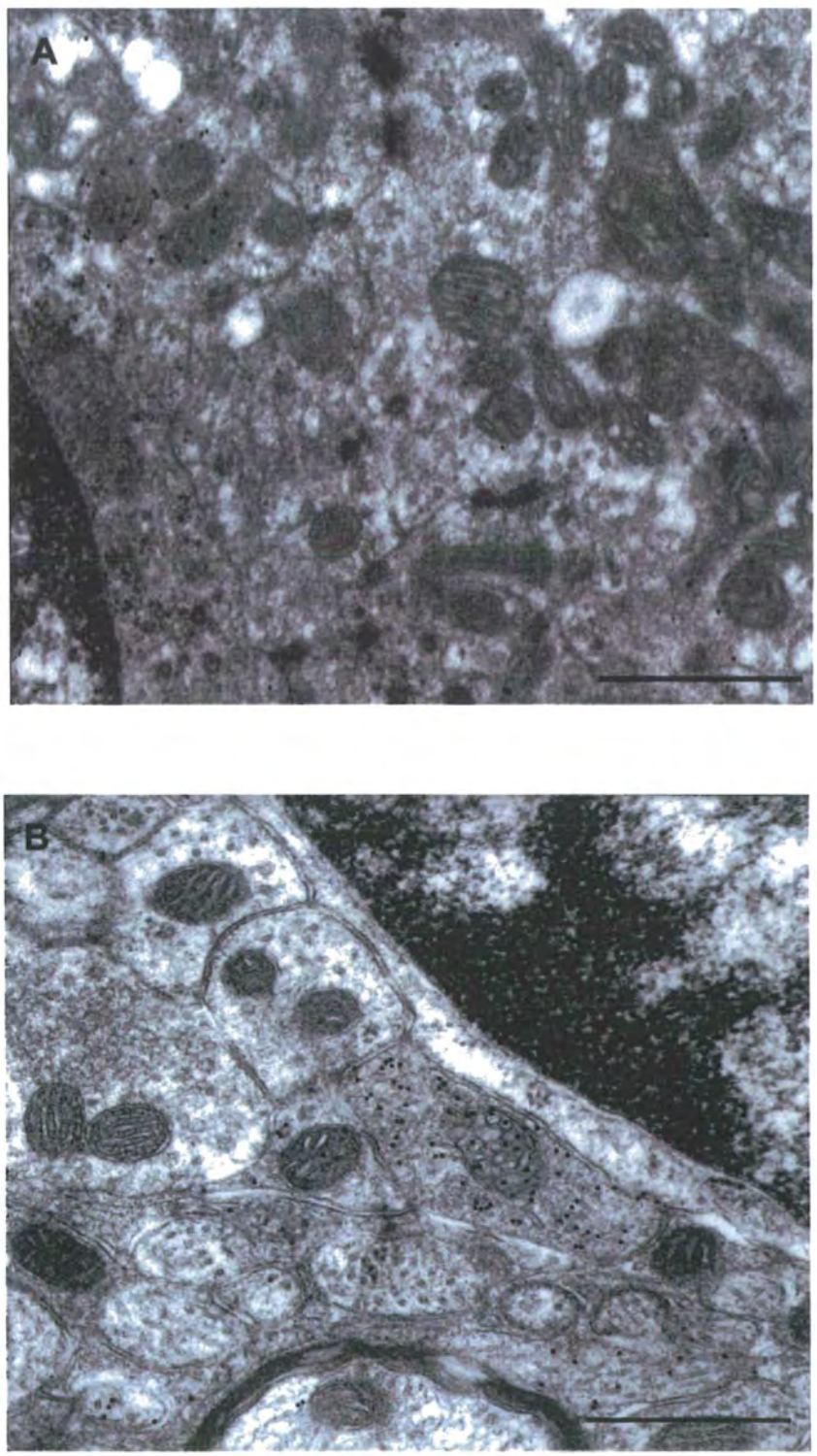

Analysis Of The Levels Of GABA In Golgi Interneurons In Stg Mutants.

In all *stg* mutants examined, the cerebellar Golgi interneurons had significantly less GABA neurotransmitter as assessed by immunogold labelling compared to wild-type controls irrespective of the buffer medium or embedding resin used. Figure 2.7B shows an ultrathin section through a glomerulus in the granule cell layer of a *stg* mutant compared to a similar section (Fig. 2.7A) from a matched wild-type control fixed in phosphate buffered fixative and embedded in Araldite resin. Gold particles are concentrated over Golgi terminals whereas granule cells and mossy fibres are only weakly labelled (equivalent to background levels over empty resin) in both *stg* mutant and WT control sections. The density of gold labelling over Golgi profiles in WT control, however, is notably higher than that over Golgi terminals in the *stg*. Figure 2.8A shows the relative density of gold labelling over Golgi profiles in cerebellar sections from a *stg* mutant (*stg1)* compared to a matched wild-type control fixed in phosphate buffered fixative and embedded in Araldite resin. The density of gold particles and hence the levels of GABA-IR are significantly reduced (P <0.001) in the *stg* Golgi interneurons (13.06 ± 1.04 pcles/μm^2, n=40) compared to similarly processed wild-type control sections (30.47 ± 2.64 pcles/μm^2, n=40) immunolabelled in the same experiment (10 min etch). The levels of GABA-IR in Golgi profiles as assessed by density of gold labelling in the *stg* mutant (*stg1)* were 43% of control values (tissue etched for 10 min) (Fig. 2.9A.).

Fig. 2.7. Electron micrographs showing the distribution of gold labelling over GABA-IR profiles in the granule cell layer of cerebella from a wild-type (WT) control (**A**) and a stargazer (*stg*) mutant (**B**) perfused with phosphate buffered fixative and embedded in Araldite resin. Gold particles are concentrated over Golgi terminals (**Go**) in the WT control but are less numerous over Golgi terminals in the *stg*. Granule cells (**Gr**) and mossy fibres (**MF**) are only weakly labelled (equivalent to background levels over empty resin).The *stg* Golgi terminals have relatively fewer gold particles than WT control Golgi profiles. Scale Bar =1μm.

Fig. 2.7 . Electron micrographs showing the distribution of gold labelling over GABA-IR profiles in the granule cell layer of cerebella from a wild-type control **(A)** and a stargazer mutant **(B).**

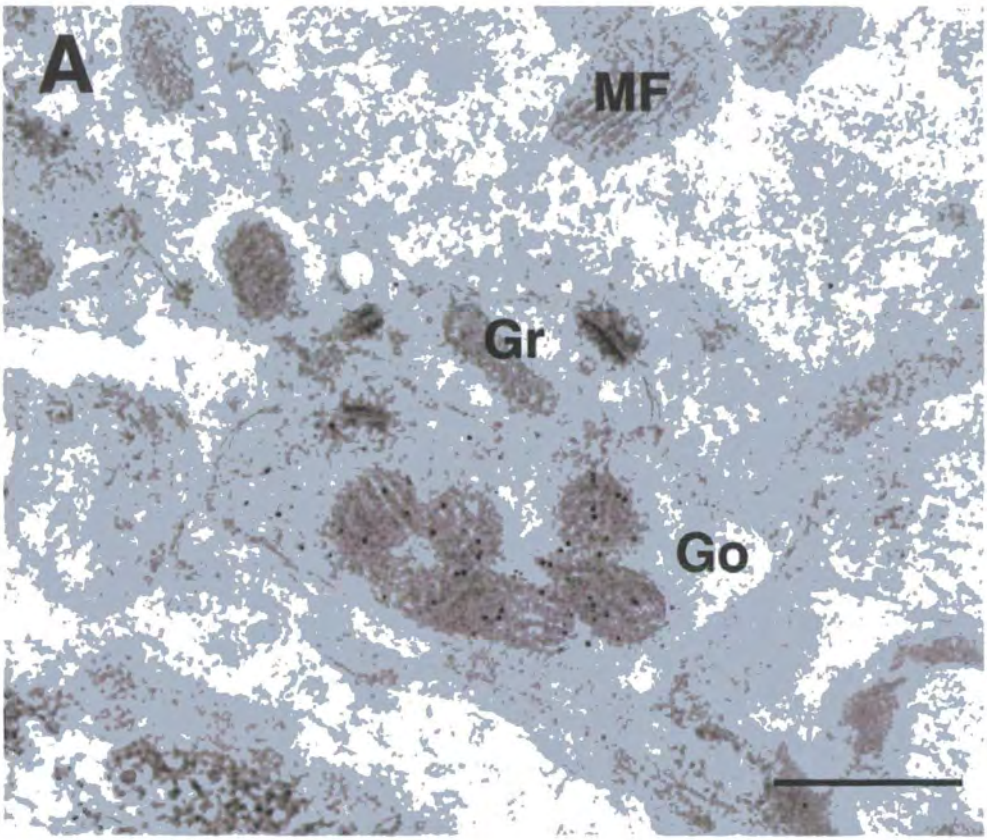

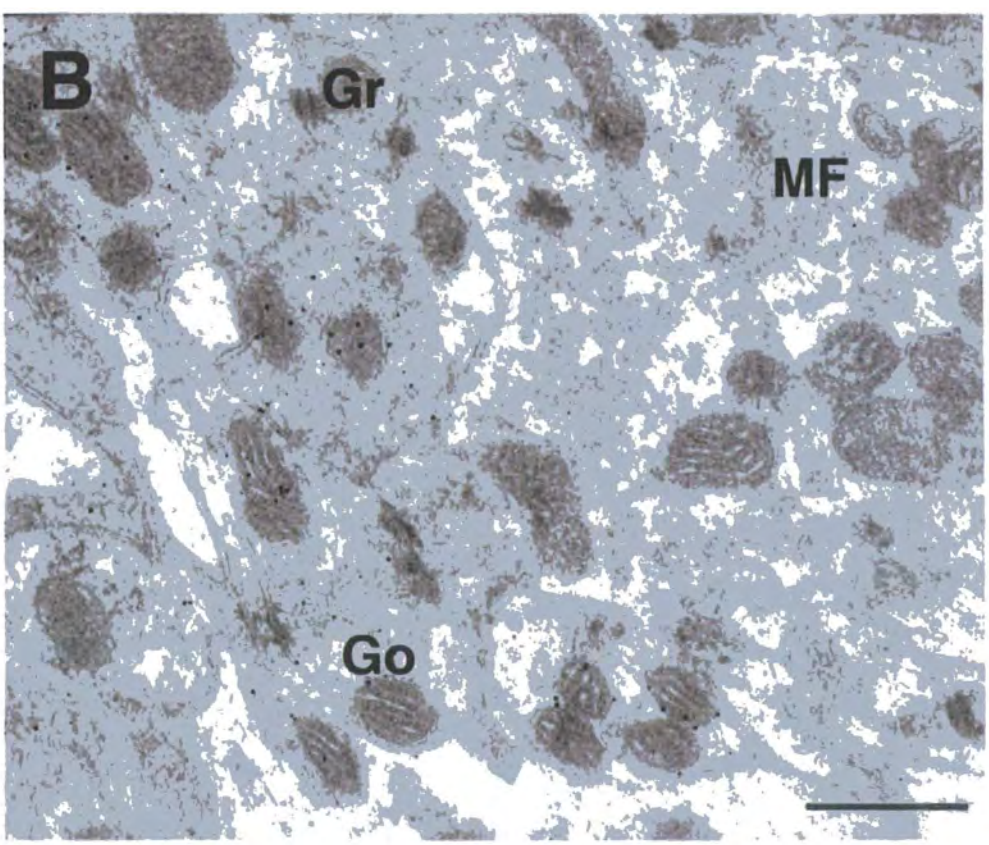

Fig. 2.8. Histograms showing the relative density of gold labelling over GABA-IR Golgi profiles in wild-type (WT) mice compared to stargazers (*stg*) mice from three separate immunolabelling experiments. All tissue was processed in phosphate buffer and embedded in Araldite. (**A**) WT mouse 2 and *stg* mouse 1. (**B**) WT mouse 3 and *stg* mice 2 and 3. (**C**) WT mouse 4 and *stg* 4. Values represent the surface density of gold particles expressed as the mean $\pm$ S.E.M. (n= 40 for each animal). Significance was found using a Students *t*-test. **, $P < 0.001$.

Fig 2.8. Histograms showing the relative density of gold labelling over GABA-IR Golgi profiles in wild-type (WT) mice compared to stargazers (*stg*) mice from three separate immunolabelling experiments.

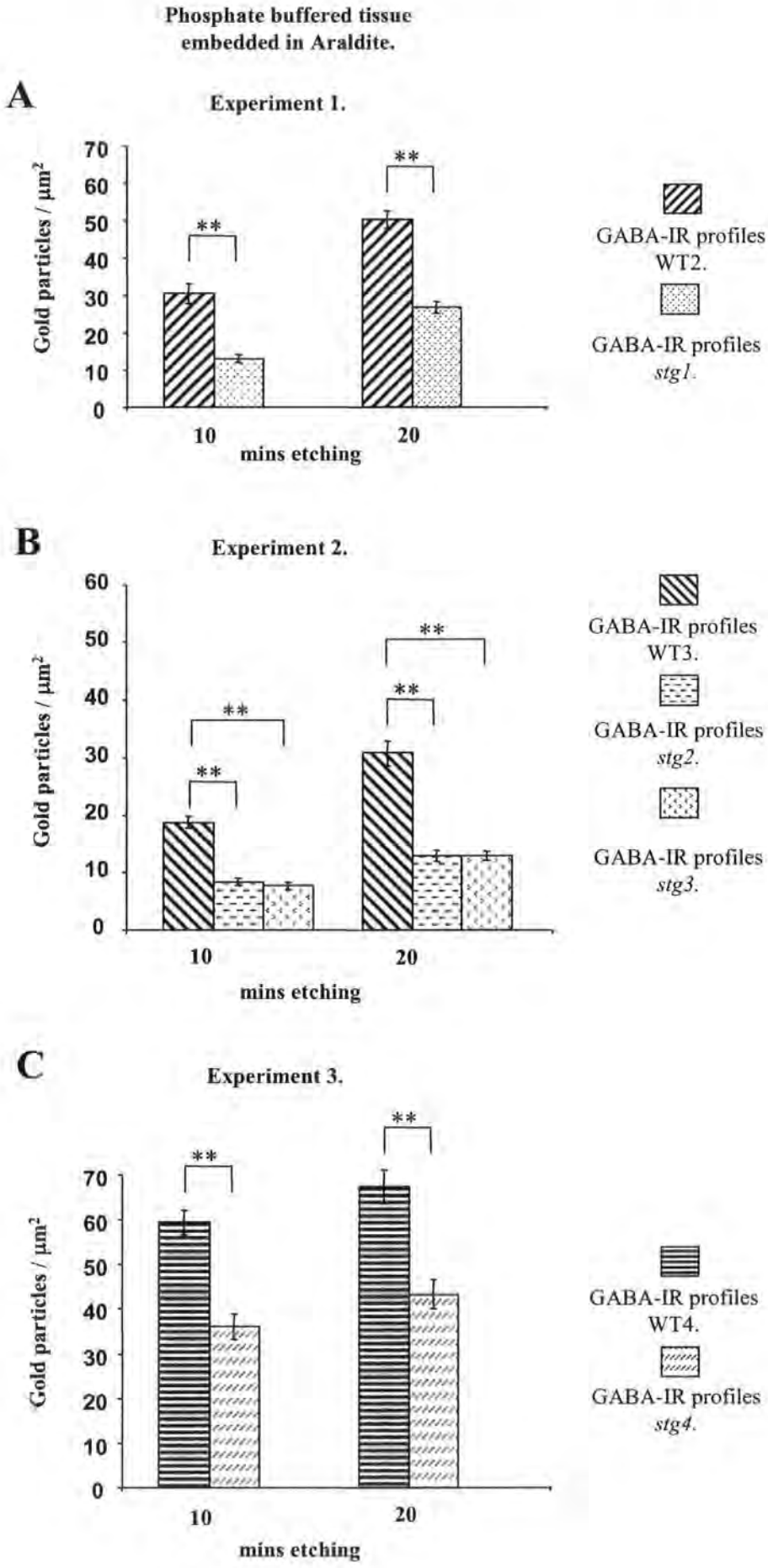

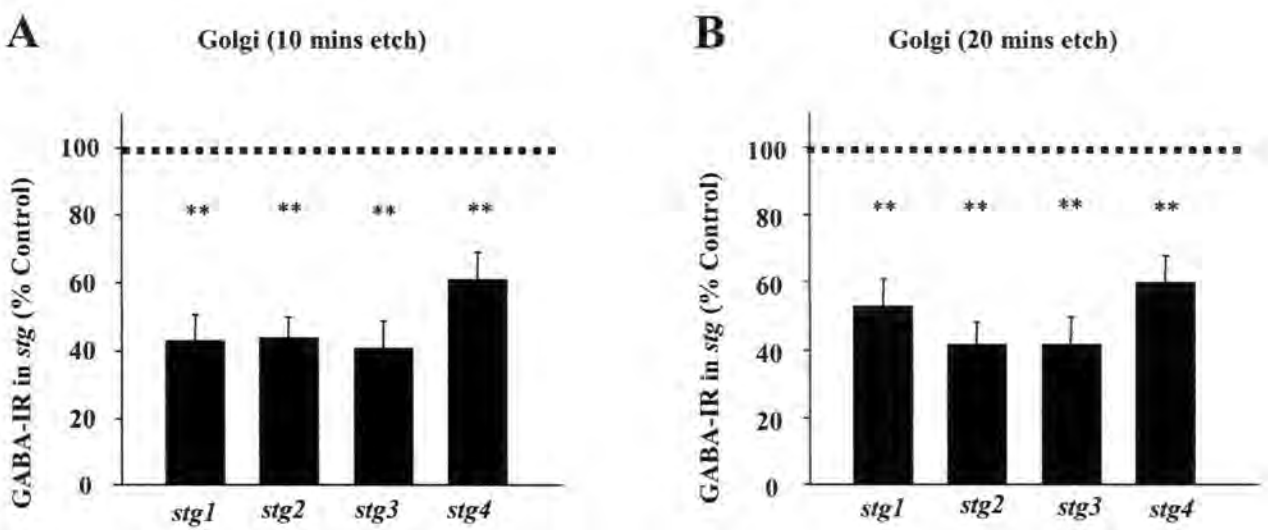

FIG.2.9. Histograms showing the density of gold particles in GABA-IR Golgi II interneurons in *stgs* expressed as a percentage of the WT control (100%, dashed line). All tissue was processed in phosphate buffer and embedded in Araldite. (**A**) Etched for 10 minutes. (**B**) Etched for 20 minutes. ** significantly different from 100% control value, $P < 0.001$.(n = 40 for each animal).

In further experiments using tissue from different animals treated with phosphate buffer and embedded in Araldite resin and etched for 10min, the overall % reduction in the levels of GABA compared to wild-type controls was similar. Figure 2.8B shows the relative densities of gold over cerebellar tissue from two different stargazers (*stg 2 & 3)* compared to control sections from a matched wild-type cerebellum. In both *stg* mutants, the density of gold particles over Golgi interneurons was significantly less (P <0.001) than over Golgi profiles in the wild-type control sections (8.35 ± 0.64 pcles/μm^2, n = 40 for *stg 2 ;* 7.76 ± 0.67 pcles/μm^2, n = 40 for *stg 3,* after 10 min etch compared to 18.79 ± 1.08 pcles/μm^2, n = 40 for WT3). There was no significant difference between *stg,* in the density of gold labelling over Golgi interneurons. For each *stg,* the levels of GABA-IR were 44% and 41% respectively of control values.

In a third experiment shown in Figure 2.8C, the relative densities of gold over cerebellar tissue from a fourth stargazer (*stg 4)* are compared to control sections from a matched wild-type cerebellum. Again the density of gold particles over Golgi interneurons was significantly less (P <0.001) than over Golgi profiles in the wild-type control sections. The level of GABA-IR in *stg* 4 was 61% of the value in the matched control WT 4.

Figure 2.9 shows the overall percentage reduction in gold particle density over Golgi interneurons in the different *stg* compared to their matched WT controls. GABA-IR levels were reduced by approximately 41-61% of control values

(tissue etched for 10 min.). A similar reduction in the levels of GABA-IR (approximately 42- 62 %) was obtained for tissue etched for 20 min (Fig.2.9B). Overall the mean level of GABA-IR in all stargazers tested was 47% of control values indicating that mean reduction in GABA content in all stargazer mutants tested compared to wild-type control cerebella was 53%.

Analysis Of The Levels Of GABA In Basket And Purkinje Cells In *Stg* Mutants.

The levels of GABA-IR in basket cell terminals and Purkinje cell somata were examined in the same *stg* samples analysed above for the Golgi labelling densities. Figure 2.10B shows ultra-thin sections through the Purkinje cell layer of *stg* mutant (*stg)* compared to a section (Fig. 2.10A) from the same region in its matched wild-type control (WT) fixed in phosphate buffered fixative and embedded in Araldite resin. Gold particles are concentrated over basket cell terminals and Purkinje cell somata in both *stg* mutant and WT control sections indicating the presence of GABA-IR in these cerebellar neurons. In each cerebellum examined the relative density of gold labelling over the different inhibitory neurons was such that Golgi profiles had more gold immunolabelling for GABA than basket cell terminals, which had more than Purkinje cell somata (Fig. 2.11). Comparison of the density of gold labelling over basket and Purkinje cell profiles in the *stg* mutants with WT controls, however, showed that in all cases the *stg* inhibitory neurons had

Fig. 2.10. Electron micrographs showing the distribution of GABA-IR in the Purkinje cell layer of the cerebellum from a wild-type control (**A**) and stargazers (*stg*) mouse (**B**) perfused with phosphate buffered fixative and embedded in Araldite resin. Gold particles are evident over the basket cell terminals (b) and, to a lesser extent, the Purkinje cell soma (P). The *stg* basket cell terminals and Purkinje cell soma have relatively fewer gold particles than WT control cells. Scale Bar = 0.5μm.

Fig.2.10. A and B. Electron micrographs showing the distribution of GABA-IR in the Purkinje cell layer of the cerebellum from a wild-type control (A) and stargazers mouse (B).

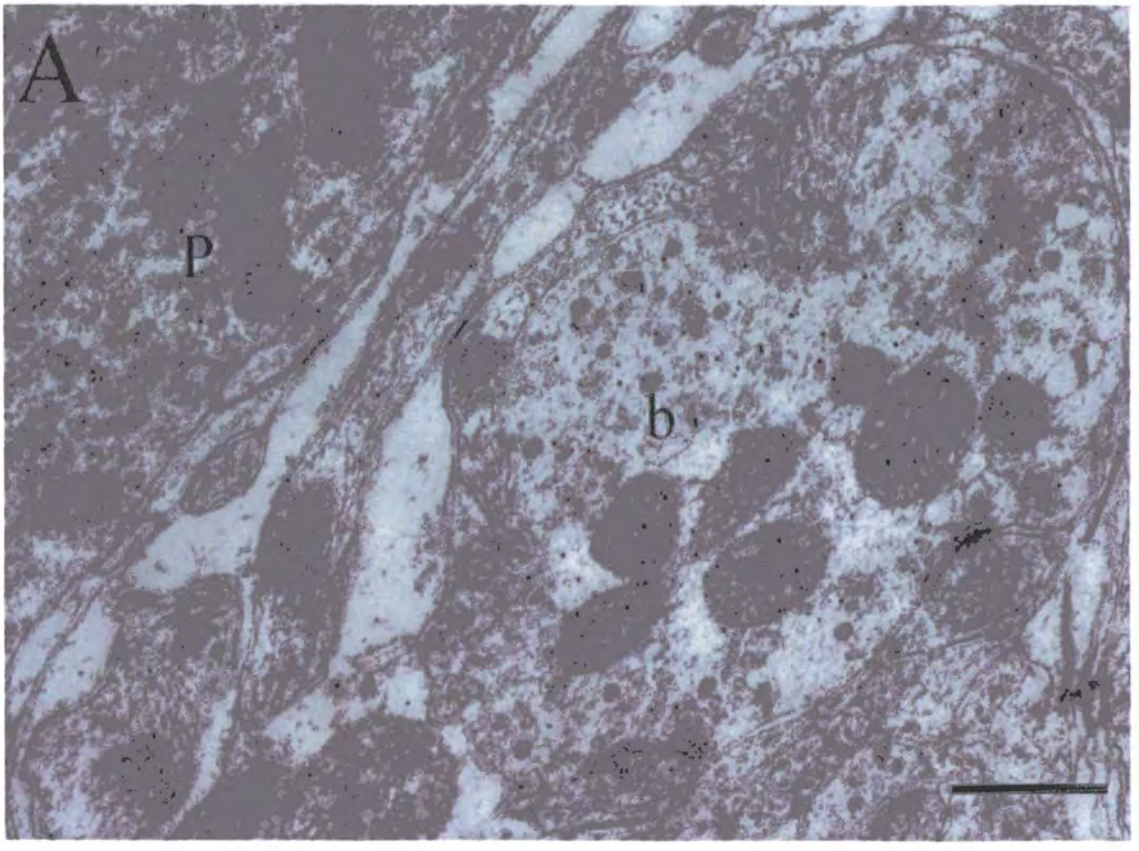

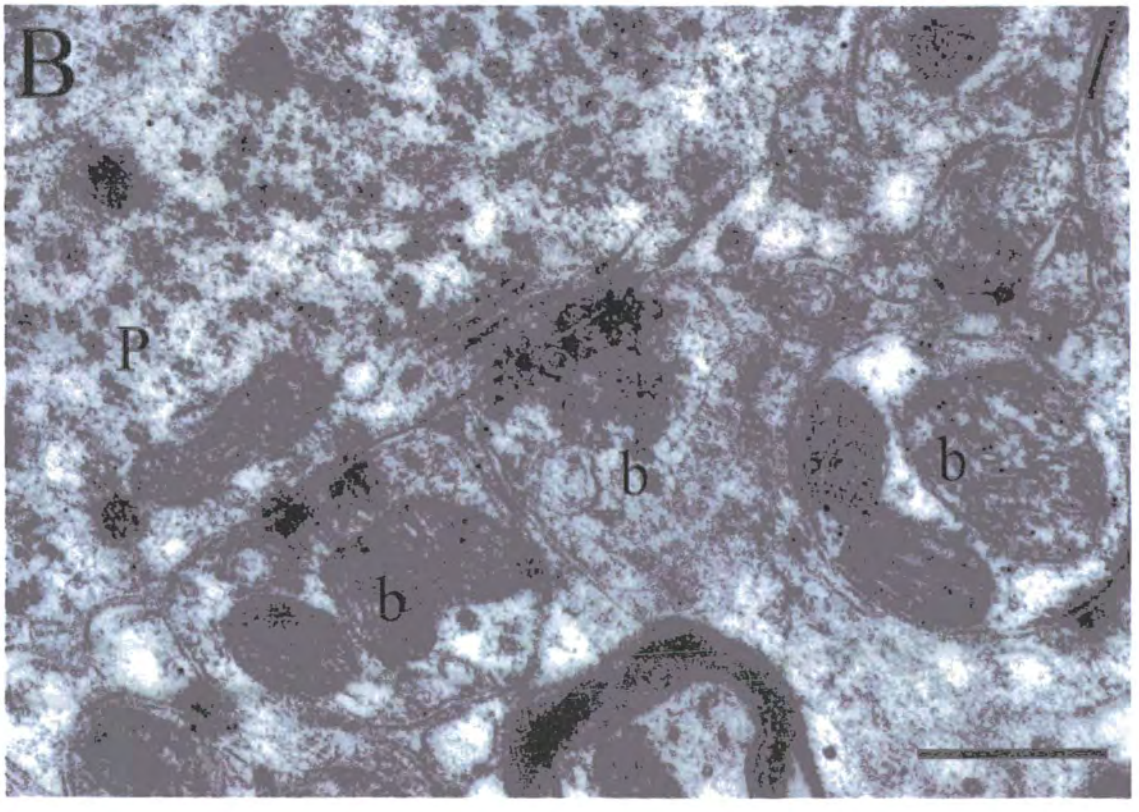

Fig. 2.11. Histograms showing the relative densities of gold labelling over Golgi, Purkinje, and basket cells profiles in cerebellar sections from *stg* mutants (*stg1-4)* compared to their matched wild-type controls fixed in phosphate buffered fixative and embedded in Araldite resin. (**A-C**) Etched for 10 minutes. (**D- F**) Etched for 20 minutes. Values represent surface density of gold particles expressed as the Mean ± S.E.M. (n = 40 for each animal). Significance was found using a Students t-test. **, $P< 0.001$.

Fig. 2.11. Histograms showing the relative densities of gold labelling over Golgi, Purkinje, and basket cells profiles in cerebellar sections from *stg* mutants compared to their matched wild-type controls.

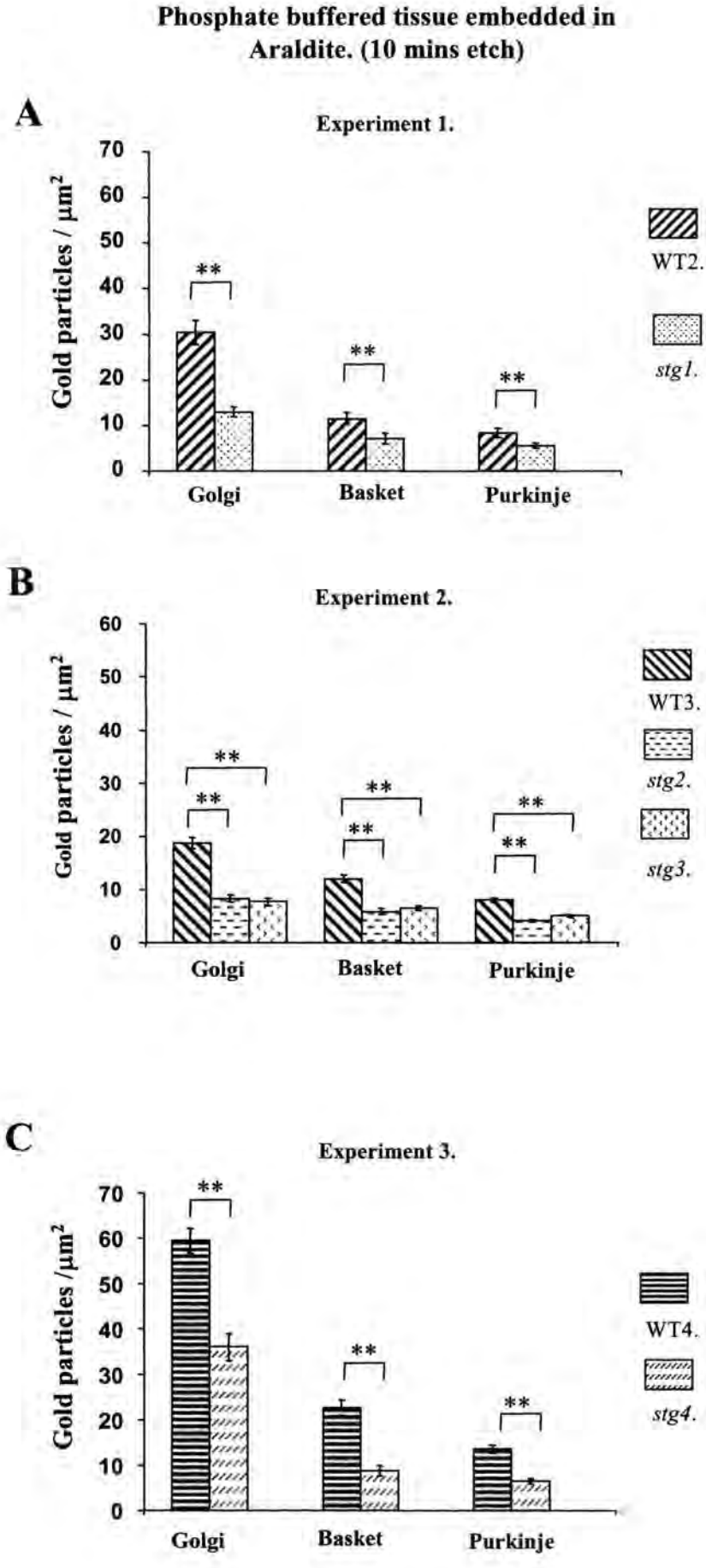

Fig. 2.11. Histograms showing the relative densities of gold labelling over Golgi, Purkinje, and basket cells profiles in cerebellar sections from *stg* mutants compared to their matched wild-type controls.

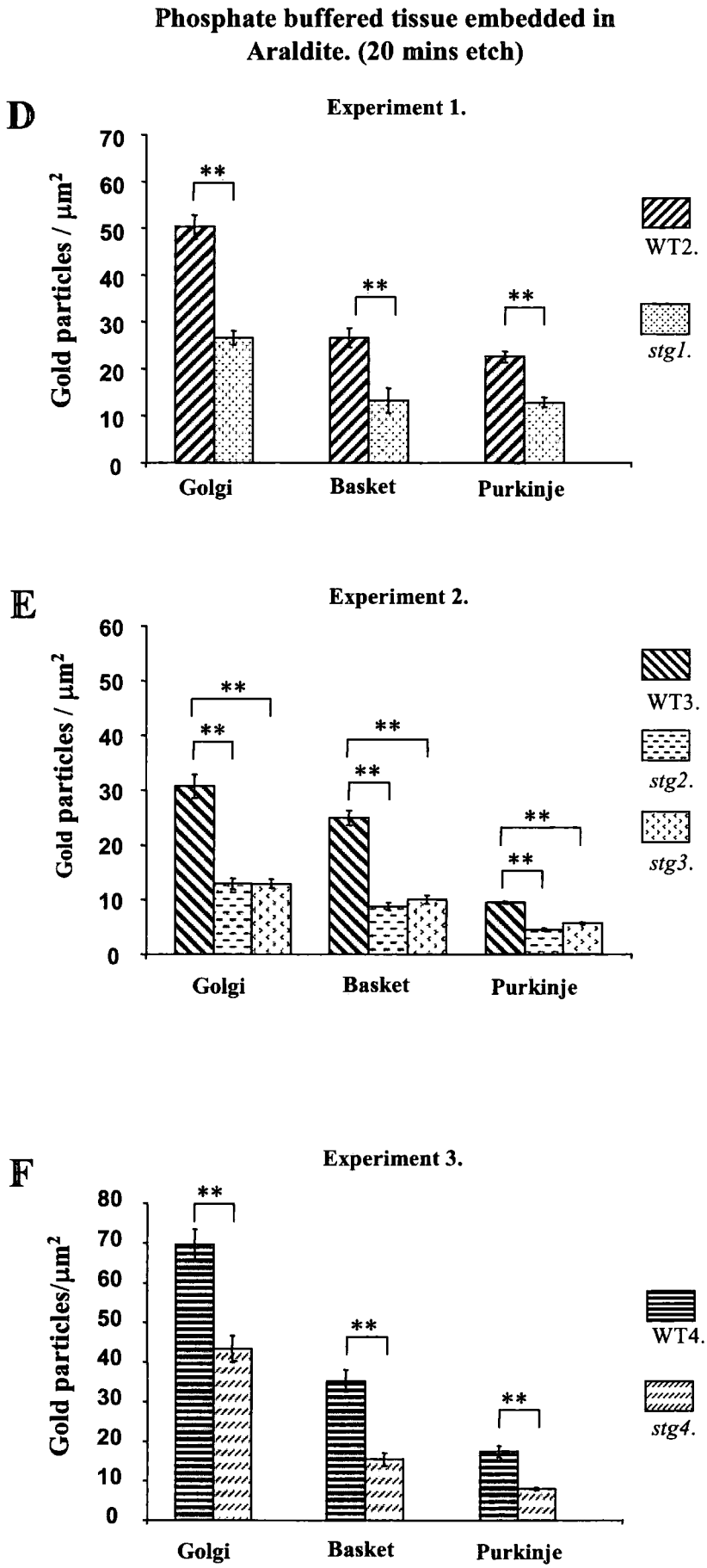

significantly less GABA neurotransmitter compared to the same cell types in wild-type controls.

Figure 2.11 shows the relative densities of gold labelling over the Purkinje, basket cells, and Golgi profiles in cerebellar sections from *stg* mutants (*stg1-4)* compared to their matched wild-type controls fixed in phosphate buffered fixative and embedded in Araldite resin. The density of gold particles and hence the levels of GABA-IR are significantly reduced (P <0.001) in the *stg* basket cell terminals compared to similarly processed wild-type control sections immunolabelled in the same experiment (Fig. 2.11 A-C, 10 min. etch; Fig.2.11 D-F, 20 min. etch). The mean level of GABA-IR in basket cell profiles as assessed by density of gold labelling in the *stg* mutants was 53% of control values (tissue etched for 10 min) (Fig. 2.12A.).

The density of gold particles over *stg* Purkinje cell somata was also significantly reduced (P <0.001) compared to similarly processed wild-type control sections. The mean level of GABA-IR over Purkinje cell somata as assessed by density of gold-labelling in the *stg* mutants was approximately 58% of control values (tissue etched for 10 min) (Fig. 2.12B.).

Analysis Of The Number And Length Of Synaptic Contacts Between Golgi Terminals And Granule Cells In Stg Mutants.

Examinations of electron microscopic sections through glomeruli in the granule cell layer of wild-type controls and *stg* mutants revealed no differences in the ultrastructural characteristics of the synapses between the Golgi terminals and

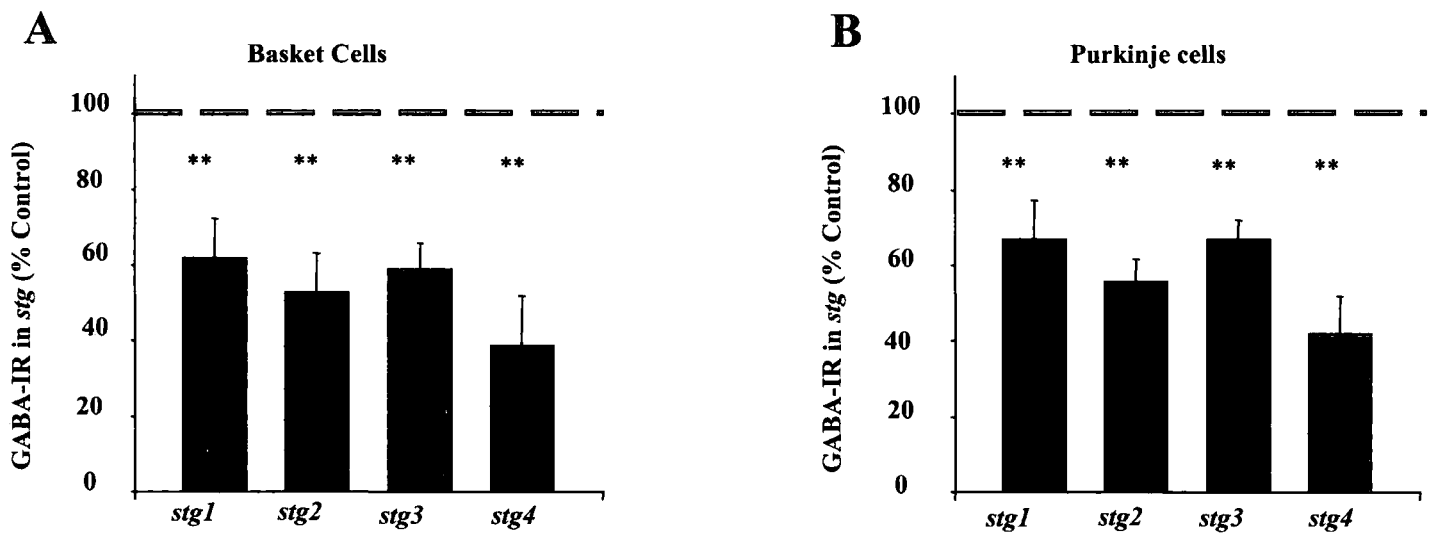

FIG.2.12. Histograms showing the density of gold particles in GABA-IR basket cell terminals (**A**) and Purkinje cell soma (**B**) in *stgs* expressed as a percentage of the WT control (100%, dashed line). All tissue was processed in phosphate buffer and embedded in Araldite. ** significantly different from 100% control value, $P < 0.001$. (n = 40 for each animal).

granule cell dendrites. Figures 2.13 & 2.14 show the ultrastructure of a typical glomerulus in the granule cell layer of the cerebellum from a wild-type mouse and a *stg* mutant. Qualitative examination of synapses between Golgi terminals and granule cell dendrites and also of synapses between granule cells and mossy fibres revealed normal synaptic structures in adult *stg* mutants (Fig. 2.14 B, C). Mossy fibres, recognisable as synaptic rosettes packed with numerous clear synaptic vesicles and some dense-cored vesicles, make asymmetrical output synapses onto smaller diameter granule cell dendrites and a few onto Golgi interneurons. The granule cell profiles in turn receive symmetrical input synapses from GABA-IR Golgi terminals which contain pleiomorphic vesicles. Ultrastructurally, these synaptic contacts appear similar in wild-type (Fig. 2.13 B, C) and mutants (Fig. 2.14 B, C). However, analysis of the number of synapses on Golgi terminal profiles within glomeruli (i.e. synaptic contacts or active zones between Golgi terminals and granule cell dendrites within glomeruli) revealed significantly fewer synapses per profile in *stg* mutants compared to wild-type controls (Table 2.2A.). The mean density of synapses per Golgi profile in wild-type controls was 2.14 ± 0.12 (n=100) compared to 0.99 ± 0.08 (n=100) in *stg* i.e. wild type controls had approximately twice as many synapses/ Golgi profile (Table 2.2A). Analysis of the density of inhibitory synapses per Golgi terminal profile indicated a mean density of 1.94 ± 0.12 inhibitory synapses/ profile in wild-type controls compared to 0.95 ± 0.07 in *stg* (Table2.2B), i.e. *stg* mutants had approximately half the number of inhibitory (Golgi-granule cell) synapses of wild-type controls. Analysis of the density of synapses between basket cell terminals

Fig. 2.13 A. Electron micrograph showing the ultrastructure of a typical glomerulus in the granule cell layer of the cerebellum from a wild-type control. The mossy fibre (**MF**) is packed with numerous clear synaptic vesicles and makes asymmetrical output synapses onto smaller diameter granule cell (**Gr**) dendrites. Granule cell profiles also receive symmetrical input synapses (arrow) from Golgi terminals (**Go**) which contain pleomorphic vesicles. Scale Bar =1μm

B. High power view of the Golgi-granule cell synapse (arrow) shown in **A**. Scale Bar = 0.5μm

C. High power view of the mossy fibre-granule cell synapse (arrowhead) shown in **A**. Scale Bar = 0.25μm

Fig. 2.14. A. Electron micrograph showing the ultrastructure of a typical glomerulus in the granule cell layer of the cerebellum from a stargazer mutant. Synapses between a Golgi terminal (**Go**) and granule cell dendrite (arrow) and between a mossy fibres (**MF**) and granule cell (**Gr**) (arrowhead) have a similar ultrastructural appearance to wild-type controls. Scale Bar =1μm

B. High power view of the Golgi-granule cell synapse (arrow) shown in **A**. Note the symmetrical appearance of the synaptic densities.Scale Bar = 0.5μm

C. High power view of the granule cell-mossy fibre synapse (arrowhead) shown in **A**. Scale Bar = 0.25μm

Fig. 2.13. Electron micrographs showing the ultrastructure of a typical glomerulus in the granule cell layer of the cerebellum from a wild-type control.

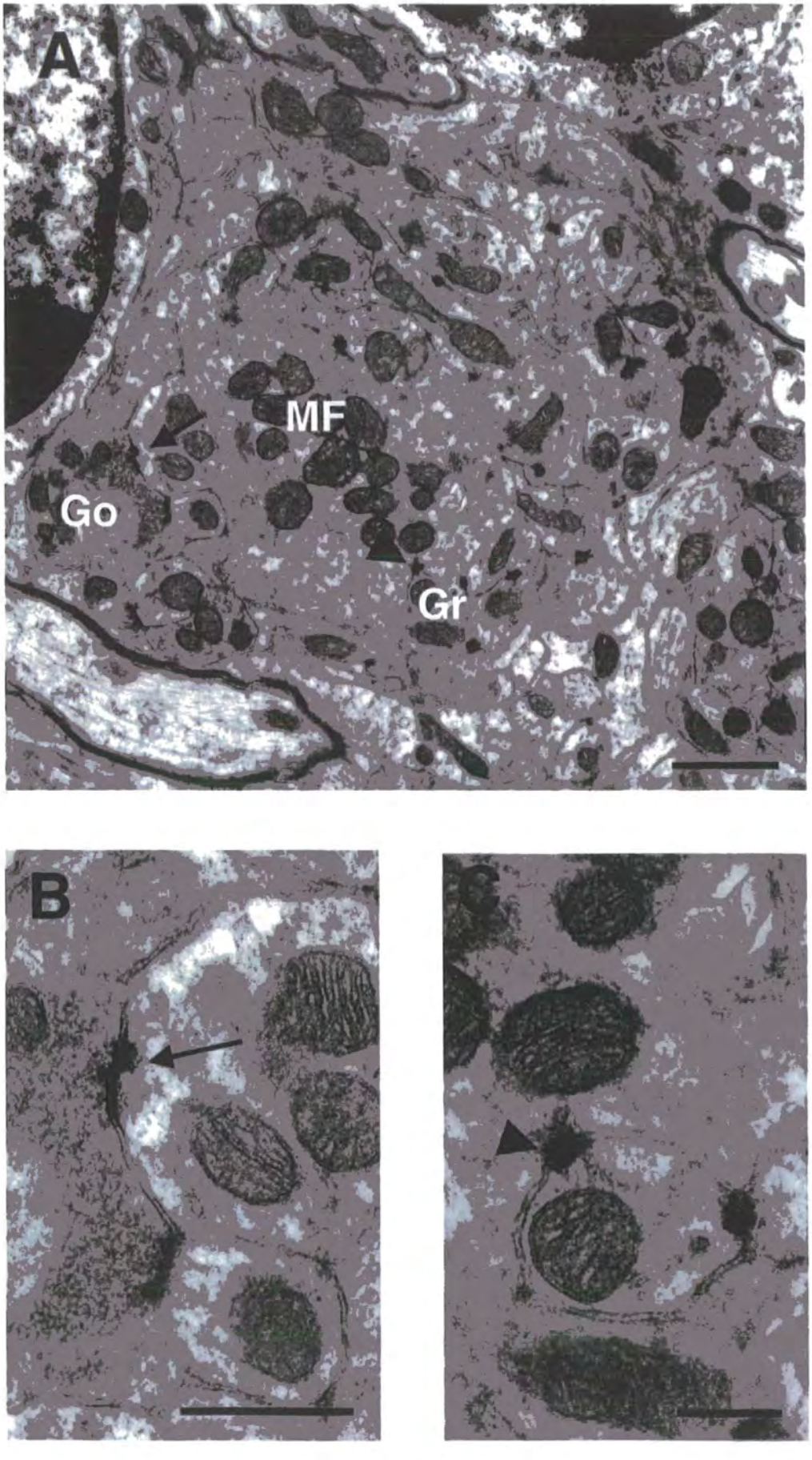

Fig. 2.14. Electron micrographs showing the ultrastructure of a typical glomerulus in the granule cell layer of the cerebellum from a stargazer mutant.

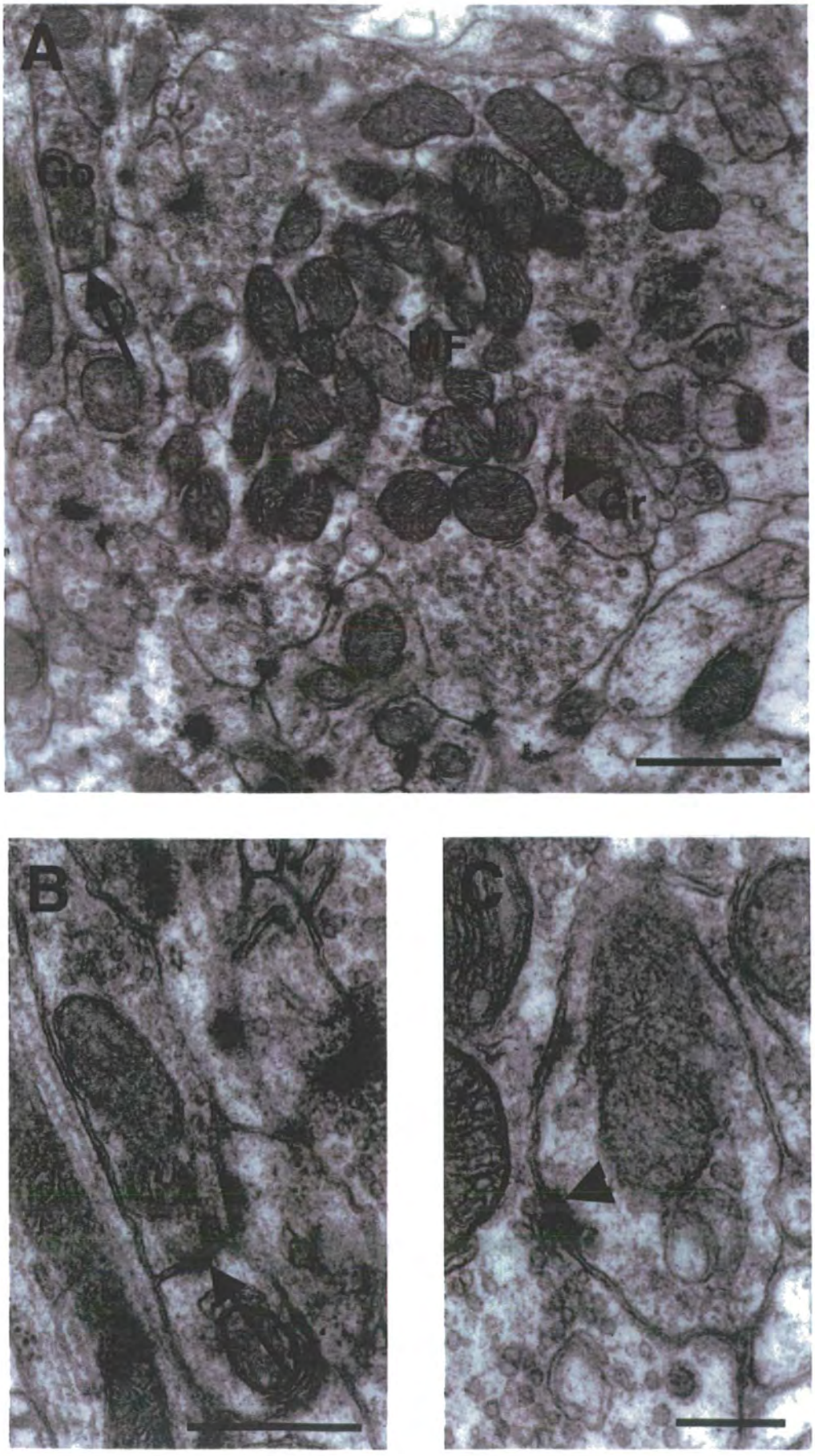

Table.2.2 A. Density of synapses per Golgi II terminal profile in Wildtype and Stargazer.

	Total no. Golgi II terminal profiles	Total no of synapses	Mean ± SEM Synapses per Golgi II terminal profile	
Wild- type	100	204	2.14 ± 0.12	($P < 0.001$).
Stargazer	100	99	0.99 ± 0.08	

Significance was found using a Students *t*-test.

2.2 B. Density of inhibitory synapses per Golgi II terminal profile in Wildtype and Stargazer.

	Total no. Golgi II terminal profiles	No. of inhibitory synapses	Mean ± SEM Inhibitory synapses per Golgi II terminal profile	
Wild- type	100	194	1.94 ± 0.12	($P < 0.001$).
Stargazer	100	95	0.95 ± 0.07	

Significance was found using a Students *t*-test.

and Purkinje cell somata also showed that these inhibitory synapses were also significantly reduced (P <0.001) in *stg* mutants compared to wild-type controls. The mean number of basket-Purkinje synapses per Purkinje cell profile in WT controls was 9.96 ± 0.89 compared to 4.68 ± 0.45 in *stg* mutants indicating that in *stg* basket-Purkinje synapses were reduced by approximately 50% compared to WT controls.

The mean length of the active zone of the inhibitory synapses between Golgi and granule cells in wild-type controls was 166 ± 6nm (n=100) compared to 137 ± 6nm (n=100) in *stg* (Table2.3A), i.e. the mean length of each synaptic contact between Golgi and granule cells in *stg* mutants was significantly (P < 0.001) less than that in WT controls (Fig. 2.15A). Analysis of the mean length of the active zone of excitatory synapses (granule cell-mossy fibre) in wild-type controls compared to *stg* revealed no significant difference (Fig. 2.15B). The mean length of the active zone was 160 ± 6nm (n=100) in WT compared to 166 ± 6nm (n=100) in *stg* (Table 2.3B), There was thus a selective reduction in length of inhibitory synapse active zones in *stg* mutants.

Analysis of the frequency distribution of synaptic contacts per Golgi profile revealed that the majority (65% of wild-type Golgi terminals had more than one synapses/profile whereas only 22% of *stg* Golgi terminals had more than one synapses/profile. The majority (78%) of Golgi terminal profiles in *stg* mutants had either one or no synapses (Fig. 2.16A). Chi-squared tests showed that the frequency distribution of synaptic contacts per Golgi profile was significantly

Table. 2.3A. Mean length of inhibitory synapses in Wildtype and Stargazer.

	Number of Golgi – granule (inhibitory) synapses	Golgi – granule (inhibitory) synapse Mean length ± SEM (nm)	
Wild- type	100	166 ± 6	} ($P < 0.001$).
Stargazer	100	137 ± 6	

Significance was found using a Students *t*-test.

Table. 2.3B. Mean length of excitatory synapses in Wildtype and Stargazer.

	Number of granule – mossy fibre (excitatory) synapses	Granule – mossy fibre (excitatory) synapse Mean length ± SEM (nm)	
Wild- type	100	160 ± 6	} ($P = 0.367$).
Stargazer	100	166 ± 6	

Significance was found using a Students *t*-test.

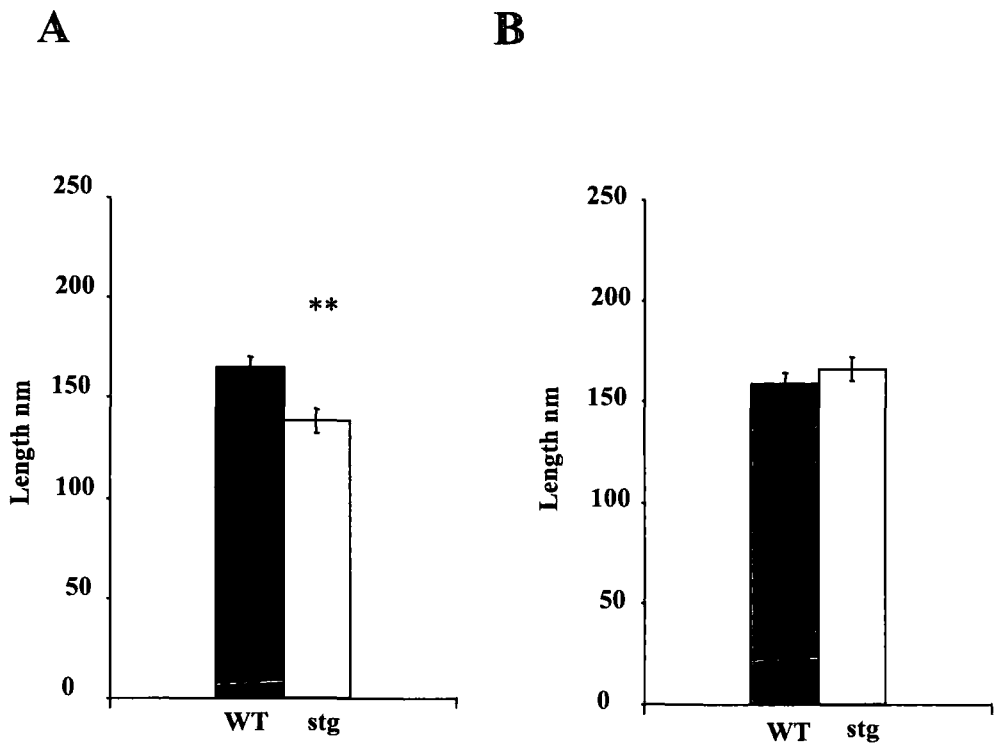

Fig. 2.15. Histograms showing the mean length of the active zone in Golgi-granule synapses (A) and granule cell-mossy fiber synapses (B) for wild-type and stargazer mice. Values are expressed as nm. (n = 100 for each animal). Significance was found using a Students t-test. **, $P < 0.001$.

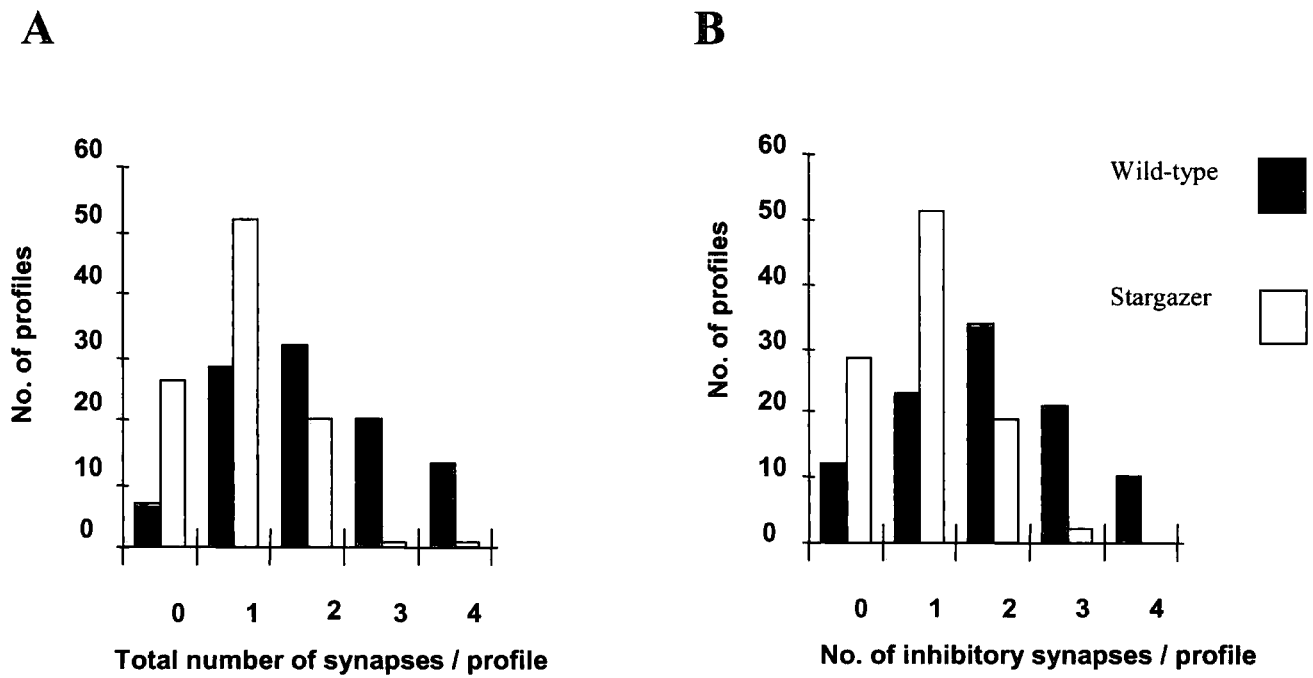

FIG.2.16. Histograms showing the frequency distribution of synapses occurring on Golgi II terminals in wild-type and stargazer mice. (**A**) Total number of synapses per profile. A Chi squared test (χ^2) revealed a significant difference in the frequency distribution of the total synapse populations in wild-type and stargazer (χ^2=105.77, P <0.001). (**B**) Inhibitory synapses per profile. A Chi squared test (χ^2) revealed a significant difference in the frequency distribution of the inhibitory synapse populations in wild-type and stargazer (χ^2=89.23, P < 0.001).

different (P <0.001) in wild-type controls compared to *stg* mutants. Only 21% of the *stg* mutants had more than 1 inhibitory synapses/profile (the majority 79% had either 1 or no synapses) whereas 65% of wild-type controls had more than 1 synapses/profile (Fig. 2.16B). The reduction in the density of synaptic contacts per Golgi profile did not appear to be related to changes in inhibitory terminal size. There was no significant difference in the mean cross sectional area of Golgi terminal profiles in *stg* compared to wild-type control mice (Fig. 2.17).

Discussion.

The data presented in this study clearly show that in the spontaneous ataxic mutant mouse stargazer, the cerebellar Golgi interneurons have significantly reduced levels of GABA immunoreactivity indicative of a significant decrease in their GABA content, compared to wild-type controls. Furthermore the density and length of inhibitory synaptic contacts between Golgi interneurons and granule cells are reduced in *stg* mutants compared to wild-type controls. Conversely, the number of excitatory (granule-mossy fibre) synapses is unaffected. Purkinje and basket cells also have significantly reduced levels of GABA immunoreactivity and the number of synaptic contacts between basket cell terminals and Purkinje cell somata in the Purkinje cell layer (i.e. inhibitory synapses) is also markedly reduced.

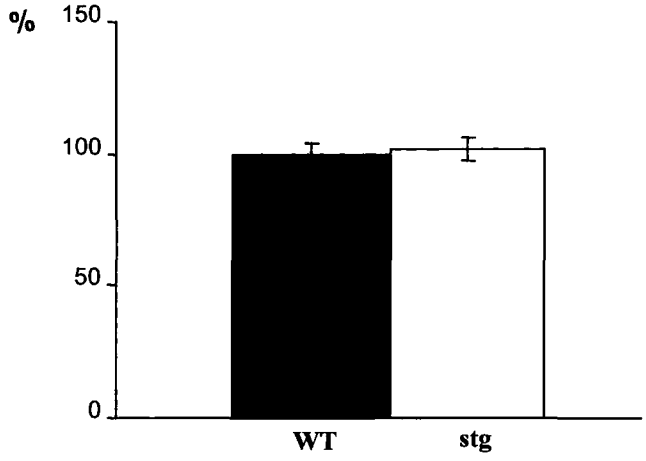

Fig. 2.17. Histogram showing the relative cross sectional area of GABA-IR terminals for wild-type and stargazer mice. Values are expressed as a percentage of the WT control value (100%). No significant difference was found. Students *t*-test, $P > 0.5$ (n = 120 for each animal).

The cerebellum of the *stg* mutant has previously been shown to have a specific and pronounced deficit in BDNF mRNA expression. BDNF protein levels in the cerebellum as a whole are reduced by 70% whereas in the granule cell layer there is a selective and near total reduction in BDNF mRNA expression (Qiao *et al.*, 1996; 1998). Other brain regions in the *stg* mutant however, express normal levels of BDNF; mRNA levels for NGF and NT-3 are normal throughout the brain including the cerebellum (Qiao *et al.*, 1996; 1998). Golgi interneurons, Purkinje, basket and stellate cells have all been reported to have TrkB receptors and to be direct targets of BDNF (Yan *et al.*, 1997; Mertz *et al.*, 2000; Schwartz 1997; Sato *et al.*, 2001). Since BDNF has been shown to promote the formation and maturation of synapses in neurons of many brain regions, including inhibitory synapses (Marty *et al.*, 1996, 1997, 2000; Vicario-Abejón *et al.*, 1998; Bao *et al.*, 1999; Huang *et al.*, 1999; Seil, 1999; Seil & Drake-Baumann, 2000;) and has also been reported to increase the GABA content and GAD activity in cultured neostriatal neurons (Mizuno *et al.*, 1994; Ventimiglia *et al.* 1995), and neocortical neurons (Rutherford *et al.* 1997), it is possible that in the *stg* mutant mouse lack of cerebellar granule cell BDNF affects development of Golgi interneuron, Purkinje and basket cell phenotype resulting in altered levels of GABA expression and synaptic density. In the intact cerebellum, all of these inhibitory cells receive excitatory inputs from the parallel fibres (granule cell axons). Excitatory mossy inputs to the granule cells could release BDNF onto the Golgi interneurons, which by analogy with GABAergic cortical interneurons, may be critical for their differentiation and maturation (blockade of BDNF signalling in cortical

interneurons mimics the effects of activity blockade on GABA expression (Rutherford *et al.*, 1997)). Expression of GABA-IR in Purkinje and basket cells could similarly be influenced by BDNF released from granule cells. Evidence from a number of recent studies (Shimada *et al.*, 1998; Mertz *et al.*, 2000; Light *et al.*, 2001,2002) suggests that differentiation, maturation and survival of cerebellar Purkinje, basket and Golgi cells involve an intimate relationship with BDNF acting via TrkB receptors.

Effect Of BDNF On GABA Content GAD Activity.

BDNF has been shown to specifically elevate cellular GABA content in rat striatal cultures without altering neuronal survival (Mizuno *et al.*, 1994) and to enhance the GABAergic phenotype in cortical neurons (Widmer & Hefti, 1994). Increase in GABA content mainly results from an increase in the GABA synthetic enzyme (GAD) and elevation of GABA uptake activity. Similarly, *in vivo* intracerebroventricular injection of BDNF into neonatal rats induces an increase in GABA content in the striatum (Mizuno *et al.*, 1994). Results from this and other studies imply that different neurotrophins may control development of different neurotransmitter phenotypes in the brain. BDNF (a trkB receptor ligand) specifically affects the expression of GABA and neuropeptide Y in striatal cultures (Mizuno *et al.*, 1994) whereas nerve growth factor (NGF), the trkA receptor ligand, promotes cholinergic development in the striatum both *in vivo* and *in vitro* (Martinez *et al.*, 1987; Mobley *et al.*, 1985). Carmona *et al* (2003) using TrkB (-/-) mice reported a decrease in K^+-evoked glutamate and GABA release from forebrain mutant synaptosomes.

In hippocampal cultures (derived from postnatal day 0 rats), chronic treatment with BDNF enhances inhibition by increasing the average size of GABAergic synaptic terminals by 50% without changing the number of synapses and by increasing the frequency of mIPSCs (Bolton *et al.*, 2000). In these cultures, fluorescence labelling intensity of puncta with an anti-GAD antibody is also concomitantly increased, presumably reflecting an increase in the level of GAD expression. The finding that BDNF increases the size of inhibitory terminals and intensity of GAD immunostaining, without affecting the number of GABAergic terminals (Bolton *et al.*, 2000), suggests that BDNF is likely to enhance the probability of transmitter release presynaptically in the hippocampus. Other studies also indicate that BDNF, induced by neuronal excitation, might be responsible for the upregulation of GAD expression in the hippocampus. GAD $_{67\,kD}$ [1]mRNA is increased in the hippocampus following brain seizures (Feldblum *et al.*, 1990) and concomitantly, BDNF mRNA is induced in the same brain region (Zafra *et al.*, 1991; Isackson *et al.*, 1991; DugichDjordevic *et al.*, 1992).

In the present study, stargazer mutants had significantly reduced levels of GABA-IR in cerebellar inhibitory neurons. The levels of GABA-IR in Golgi terminals, basket cell terminals and Purkinje cell somata of *stg* mutants were decreased by approximately 53%, 47% and 42% respectively, compared to wild-type controls. The number of inhibitory synapses between Golgi and

[1] (In mammals, GAD exists in two isoforms encoded by two different genes - *Gad1* and *Gad2*. These isoforms are GAD_{67} and GAD_{65} with molecular weights of 67 and 65 kDa, respectively, GAD1 and GAD2 are expressed in the brain where GABA is used as a neurotransmitter).

granule cells and between basket and Purkinje cells was also significantly decreased in *stg* mutants compared to wild-type controls. Changes in synapse density on Golgi terminals, however, were not accompanied by changes in average GABAergic terminal size. In the cerebellum of the *stg* mutant mouse then, where BDNF protein levels in the cerebellum as a whole are reduced by 70% and in the granule cell layer a near total reduction in BDNF mRNA expression exists (Qiao *et al.*, 1996; 1998), there is a concurrent significant depletion in both the amount of GABA neurotransmitter and in the number GABAergic synaptic contacts in inhibitory neurons.

Effect Of BDNF On Number And Size Of Synaptic Contacts, Dendrites And Axonal Branches In GABAergic Neurons.

The effect of BDNF specifically on synapse number and size and on dendritic and axonal morphology has been examined in many brain regions (Causing *et al.*, 1997; Vicario-Abejon *et al.*, 1998; Marty *et al.*, 2000). In the hippocampus, neurotrophins have been shown to potently influence the complexity of axonal arbors and to play a central role in sculpting and modifying dendrites in the CNS both in vitro and in vivo (Vicario-Abejon *et al.*, 1998). Conversely injection of specific antibodies against neurotrophins reduces axonal and dendritic complexity (see review by McAllister *et al.*, 1999). Similarly, neurons in trkB (-/-) and trkC (-/-) knockout mice show reduced axonal arborisation, lowered densities of synaptic contacts and a decreased density of synaptic vesicles (Martinez *et al.*, 1998).

Previous studies have linked specific neurotrophins in activity-dependent plastic changes in the cerebellum (Larkfors *et al.*, 1996; Shimada *et al.*, 1998; Bao *et al.*, 1999; Seil, 1999; Seil & Drake-Baumann, 2000; Mertz *et al.*, 2000). Shimada *et al.*, (1998) have shown that in co-cultures of granule and Purkinje cells, BDNF treatment increased the density of Purkinje cell dendritic spines relative to controls via TrkB signalling mechanisms. Seil (1999) has reported that the development of the full complement of Purkinje cell inhibitory synapses in cerebellar cultures requires the presence of neuronal activity but that the neurotrophins BDNF and NT-4 (TrkB receptor ligands) though not the neurotrophin NT-3 (a TrkC receptor ligand) promoted the development of inhibitory synapses in cerebellar cultures in the absence of neuronal activity suggesting that BDNF and NT-4 have a role in the promotion of activity-dependent inhibitory synaptogenesis. Conversely, exposure of the cultures to a combination of antibodies to BDNF and NT-4 resulted in reduced inhibitory synapse formation, similar to the effects of activity blockade (Seil & Drake-Baumann, 2000). These results indicate that that endogenous neurotrophins are necessary for development of the full complement of inhibitory synapses in the presence of neuronal activity and are therefore consistent with the concept that TrkB receptor ligands promote inhibitory synaptogenesis.

In the present study, the density of GABAergic synapses in cerebellar Golgi interneurons in *stg* mutants was reduced to approximately half that in wild-type control mice cerebella without a concomitant change in terminal size.

Likewise, the density of inhibitory synapses between the basket cell terminals and Purkinje cell somata was also significantly reduced.

Whether this reduction in inhibitory synapse number is directly attributable to the lack of BDNF in the cerebellum of the *stg* mutant is yet to be proven. However, it is interesting to note that the density of excitatory synapses between the mossy fibres and the granule cells was unaffected. A similar observation was made by Marty *et al.*, (2000) working on organotypic slice cultures of postnatal hippocampus; BDNF coupled with neuronal activity regulated the density of inhibitory synapses but not excitatory synapses. Rico *et al.*, (2002) demonstrated that trkB is essential to the development of γ-aminobutyric-acid-containing (GABAergic) neurons in the cerebellum and that in addition to its role in the development of axon terminals it regulates synapse formation. Recently Carmano *et al* (2006) have also shown an impairment of GABAergic function in the hippocampus of mice lacking TrkB.

Data from this study and others cited in this paper are clearly suggestive of a strong role for BDNF in synaptic plasticity within the developing cerebellum. The conclusions that may be drawn from all these studies are, although neuronal activity regulates the density of inhibitory synapses made in the developing CNS, BDNF (acting as either an anterograde or autocrine-paracrine factor) could mediate part of this regulation. Regulation of the density of inhibitory synapses could thus represent a feedback mechanism maintaining an appropriate level of activity in developing CNS networks including those in the cerebellum. In the stargazer mutant, the reduction of

BDNF in the cerebellum as a whole and its near total specific ablation in the granule cells could thus account for the selective alteration in synaptic innervation density and GABA content in cerebellar inhibitory (Golgi, basket and Purkinje) neurons.

Chapter 3. Glutamatergic Characteristics of The Granule Cell And Mossy Fibre Neurons Of The Stargazer Mutant Mouse.

Introduction.

Brain derived neurotrophic factor (BDNF) is known to influence neuronal survival, differentiation and maturation (for reviews see McAllister 2001; Huang & Reichardt, 2001). Recently, its role in synapse formation and plasticity has also emerged (see reviews by McAllister *et al.*, 1999; Lu & Gottschalk, 2000; Schinder & Poo, 2000; Lu 2001; Poo, 2001; Abejón *et al.*, 2002; Lessmann *et al.*, 2003). A role for neurotrophins in the regulation of synapse number in the CNS was first indicated by work on knockout mice by Martinez *et al.*, (1998) which demonstrated that tyrosine kinase B (TrkB) and tyrosine kinase C (TrkC) receptor signalling are required for maturation and synaptogenesis of hippocampal connections. *In vivo* visualisation of BDNFs dynamic role in synapse promotion and formation was recently demonstrated in the *Xenopus* visual system using green fluorescent protein (GTP)- tagged clusters of synaptobrevin 2 and presynaptic markers for synaptosome-associated protein (Alsina *et al.*, 2001). Evidence that BDNF enhances quantal neurotransmitter release and increases the number of docked vesicles at the active zones of hippocampal excitatory synapses has been provided by Tyler & Pozzo-Miller (2001); Tyler *et al.*, (2002); and Tyler & Pozzo-Miller (2003). Long-term treatment of hippocampal slice cultures with BDNF has been shown to increase the number of docked vesicles but not that of reserve pool

vesicles, at CA1 excitatory synapses (Tartaglia *et al.*, 2001). Likewise, Collin *et al.*, (2001) have produced results that are consistent with a presynaptic locus of action of neurotrophins to increase both the number of docked synaptic vesicles and total synaptic vesicle density in cultured hippocampal neurons.

In the developing cerebellum, BDNF has also been shown to be critical in basket and stellate cell morphogenesis and to enhance synaptic connections by concerting the formation of pre and postsynaptic structures (Mertz *et al.*, 2000). Further evidence that BDNF modulates cerebellar plasticity and synaptic ultrastructure has come from work on mutant mice with a targeted deletion of the BDNF gene (Carter *et al.*, 2002). In the cerebellum of these mutant mice there is only a slight reduction in the number of excitatory synapses between parallel fibres (PF) and Purkinje cell (PC) dendrites. Detailed ultrastructural analysis of the presynaptic terminal has also demonstrated that, although there is an increase in the total number of synaptic vesicles in these mutant mice, there is a decrease in the proportion of vesicles that are docked. Rico *et al.*, (2002) have recently demonstrated that TrkB is essential to the development of γ-aminobutyric-acid-containing (GABAergic) neurons in the cerebellum and that in addition to its role in the development of axon terminals it regulates synapse formation. Thus for the first time, this work provides evidence for an *in vivo* role for TrkB receptor signalling in the regulation of synapse number in the cerebellum.

The previous chapter (published data Richardson and Leitch, 2002) demonstrated that inhibitory neurons in the cerebella of stargazer (*stg)* mutants have significantly reduced levels of GABA (approximately 50%) and fewer, smaller inhibitory synapses compared to WT controls. The cerebellum of the spontaneous recessive mutant mouse stargazer has a pronounced deficit in BDNF mRNA expression. BDNF protein levels in the cerebellum as a whole are reduced by 70% and in the granule cells (GC) of the granule cell layer there is a selective and near total reduction in BDNF mRNA expression and subsequent defect in TrkB receptor signalling (Qiao *et al.*, 1998). The *stg* mutant exhibits characteristic ataxia, head tossing and impairment in acquisition of classical eye-blink conditioning. These phenotypes are thought to be cerebellar mediated and have been attributed to the specific reduction in BDNF, which is temporally related to the onset of ataxia at postnatal day 14. Ablation of cerebellar granule cell BDNF expression in the *stg* mutant mouse, may thus be responsible for altered development of Golgi interneuron phenotype resulting in changes in the GABAergic inputs onto GC dendrites in the glomerulus and altered levels of GABA expression.

This chapter centres on the effect of the stargazin mutation and the lack of BDNF in GC on the phenotype of glutamatergic neurons in the cerebellum, primarily the GC and their synaptic contacts, but also the mossy fibres (MF). To date, other than the paper by Carter *et al.*, (2002) there have been no quantitative analyses of excitatory synapses *in vivo* in either the hippocampus

or the cerebellum of BDNF-knockout mice, or mice with reduced BDNF or TrkB receptor levels.

The aim of the present study was therefore to determine whether glutamatergic characteristics of the GC and MF neurons are compromised by the lack of availability of BDNF in the GCs of the *stg* mouse. There were three main objectives:

- first to investigate whether the levels of glutamate neurotransmitter expressed in GC and MF neurons are altered in *stg* using semi-quantitative immunogold labelling EM cytochemistry;
- second to determine whether the number and size of synaptic contacts between the MF terminals and GC dendrites (in the GC layer) and also between PF terminals and PC dendrites (in the molecular cell layer) are altered in *stg* compared to WT controls;
- and third to analyse the distribution profile of synaptic vesicles and the proportion of docked vesicles at these synapses in *stg* compared to WT controls.

Materials And Methods.

Wild-type (C57BL/6J; +/+) and stargazer mutant (C3B6Fe+; *stg/stg*) mice were raised from breeding stock obtained from the Jackson Laboratory (Bar Harbor, ME USA). Heterozygous males (+/*stg*) and homozygous females (*stg/stg*) were mated to produce *stg/stg* mutants. Adult mice (2 months) were used in all

experiments. Animals were deeply anaesthetized with pentobarbitone sodium (Sagatal, 60mg/kg i.p.) and perfused transcardially with 0.9% saline followed by fixative (details given below). Rabbit anti-glutamate and anti-GABA antisera were obtained from Sigma, UK. Gold-labelled goat anti-rabbit antibody was obtained from Biocell, UK. The Ethical Review Committee of the University of Durham approved all animal protocols `used.

EM Immunocytochemistry.

Perfusion-fixed stg and control brains were sectioned and processed for glutamate immunoreactivity (glut-IR) and GABA-immunoreactivity (GABA-IR) using an immunogold labelling method (Richardson & Leitch 2002). In total, 10 mice brains were prepared and examined. Brains were first fixed in situ by transcardial perfusion with 2% paraformaldehyde and 2.5% glutaraldehyde in 0.1M Sorensen's phosphate buffer (pH 7.4). They were then removed from the skull and transferred to fresh fixative to be processed individually. The cerebellum of each mouse brain was dissected out, sliced into 100-150μm sections using a Vibroslice 725M tissue slicer (Campden Instruments Ltd, U.K.) and fixed for a further 2 hours at room temperature (RT). Tissue slices were then washed thoroughly in 0.1M Sorensen's phosphate buffer (pH 7.4) and osmicated for 1 hour. After osmication, tissue slices from each mouse were dehydrated, bisected and embedded in Araldite CY212 (Agar,UK) resin to be cured overnight at 50°C. Ultrathin sections (70nm) were cut on a

Reichert-Ultracut ultra-microtome and mounted on carbon coated/ Formvar nickel grids.

For all immunocytochemical labelling experiments statistical comparisons were only made between brains that had been fixed and processed at the same time using the same batch of resin and then immunolabelled in parallel. This ensured equal incubation times in etching, antibody labelling and washing. Sections were etched with a saturated solution of sodium metaperiodate (Bendayan and Zollinger, 1983) for 10 minutes and then thoroughly washed with distilled water. Sections were then floated face down on droplets of 5% normal goat serum in bovine serum albumin (BSA/Tris buffer (pH 7.4) for 30 minutes. Incubation in the primary antibody was performed by floating the grids on droplets of either rabbit anti-glutamate or rabbit anti-GABA antiserum (Sigma, UK) in BSA/Tris buffer (pH 7.4) for 2-3 hours at room temperature. Both of the primary antibodies (anti- glutamate and anti-GABA antisera) were obtained from rabbits after immunisation with an antigen-glutaraldehyde-carrier conjugate. Anti-glutamate was developed in rabbit using purified glutamate conjugated to KLH as the immunogen. The antiserum had been treated to remove lipoproteins. The anti-GABA was developed in rabbit using GABA-BSA as the immunogen. The antibody was isolated from the antiserum by immunospecific methods of purification (antigen specific affinity isolation removes essentially all rabbit serum proteins, including immunoglobulins which do not specifically bind to GABA). The rabbit anti-glutamate reacted with L-glutamate Glu-KLH, Glu-BSA, and KLH, but not with BSA using a dot blot immunobinding assay. Rabbit anti-GABA showed

positive binding with GABA, and GABA-KLH in a dot blot assay, and negative binding with BSA (Sigma, UK product information).

For immunocytochemical labelling experiments each antibody was tested using serial dilutions up to 1:32,000; optimal staining was achieved with 1:1000 for the glutamate antibody and 1:500 for GABA antibody. Following incubation in the primary antibody, sections were thoroughly washed in BSA/Tris buffer and transferred to droplets of 10nm gold-labelled goat anti-rabbit antibody (Biocell, UK) diluted 1:20 in BSA/Tris buffer (pH 8.2) for 1 hour at room temperature. The grids were finally washed in a series of distilled water droplets to remove unbound gold conjugate then stained for 10 mins. in 1% ethanolic uranyl acetate, rinsed in distilled water and then stained for a futher 10 mins. in Reynolds Lead citrate (Reynolds 1963) before a final rinse in distilled water. Once dry the sections were examined in a Philips EM 400T electron microscope.

Controls And Specificity Tests.

Positive and negative controls were performed to test specificity of labelling with each antibody. The following positive controls were performed. (a) The specificity of the anti-GABA antibody was tested by applying it to tissue sections containing known GABA-IR axons (see Leitch and Laurent, 1993; Watson *et al.*, 2000). The antibody bound specifically to axons known to be GABA-IR; this staining was absent in all negative controls. The specificity of the Sigma anti-glutamate was similarly tested and had also been tested in

other systems (Pearlstein *et al.*, 1998; Watson *et al.*, 2000). (b) Tissue from control mouse cerebellum was also serially sectioned. Serial sections were stained alternatively with anti-glutamate and anti-GABA antibodies (Fig. 3.1.) to confirm that known GABA-ergic neurons in the cerebellum (Golgi neurons (Go) and Purkinje cells (PC)) labelled specifically with GABA while known glutamatergic neurons (MF, GC and PF) showed specific, heavy labelling for glutamate. The pattern and density of labelling with anti-glutamate antiserum over cerebellar neurons in the mouse (see Table 3.1.) was comparable to that in cat cerebellum as reported by Somogyi *et al.*, (1986). Statistical comparison of the immunoreactivity (based on the density of gold particles) in different neuronal processes and non-neuronal glial profiles is shown in Table 3.1 for mouse cerebellum labelled with anti-glutamate antibody. The density of labelling over neuronal profiles compared to background glial processes (as determined by image analysis and expressed as a ratio) was 1:6:2:5:2:4 for glial cell processes: MF terminals: Go terminals: PF terminals: PC dendrites and spines: GC dendrites respectively. This was comparable to levels found in cat cerebellum (1:5:2:4:2:3) by Somogyi *et al.*, (1986); i.e. among the neuronal profiles levels of glut-IR were highest over mossy and parallel fibre terminals and lowest over known GABAergic neurons. i.e. Golgi cell terminals and Purkinje cell dendrites. So nerve terminals that are known to exert an excitatory action in both cat and mouse. i.e. mossy and parallel fibre terminals have significantly higher levels of glutamate-like immunoreactivity than putative GABAergic Golgi cell terminals and Purkinje cell dendrites. In addition to the above positive controls, the following negative controls were performed:

Fig. 3.1. A, B. Two adjacent sections labelled with antibodies against glutamate (**A**) and GABA (**B**).
The mossy fibre (**MF**) and granule cell (**GC**) profiles are heavily labelled with gold beads in (**A**) but not in (**B**) indicating that they are immunoreactive for glutamate but not for GABA. Conversely, the Golgi (**Go**) cell terminals in (**B**) are heavily labelled for GABA but show only very weak labelling for glutamate (**A**) equivalent to background levels. Scale Bar =1μm.

Fig. 3.1. A, B. Two adjacent mossy sections labelled with antibodies against glutamate **(A)** and GABA **(B).**

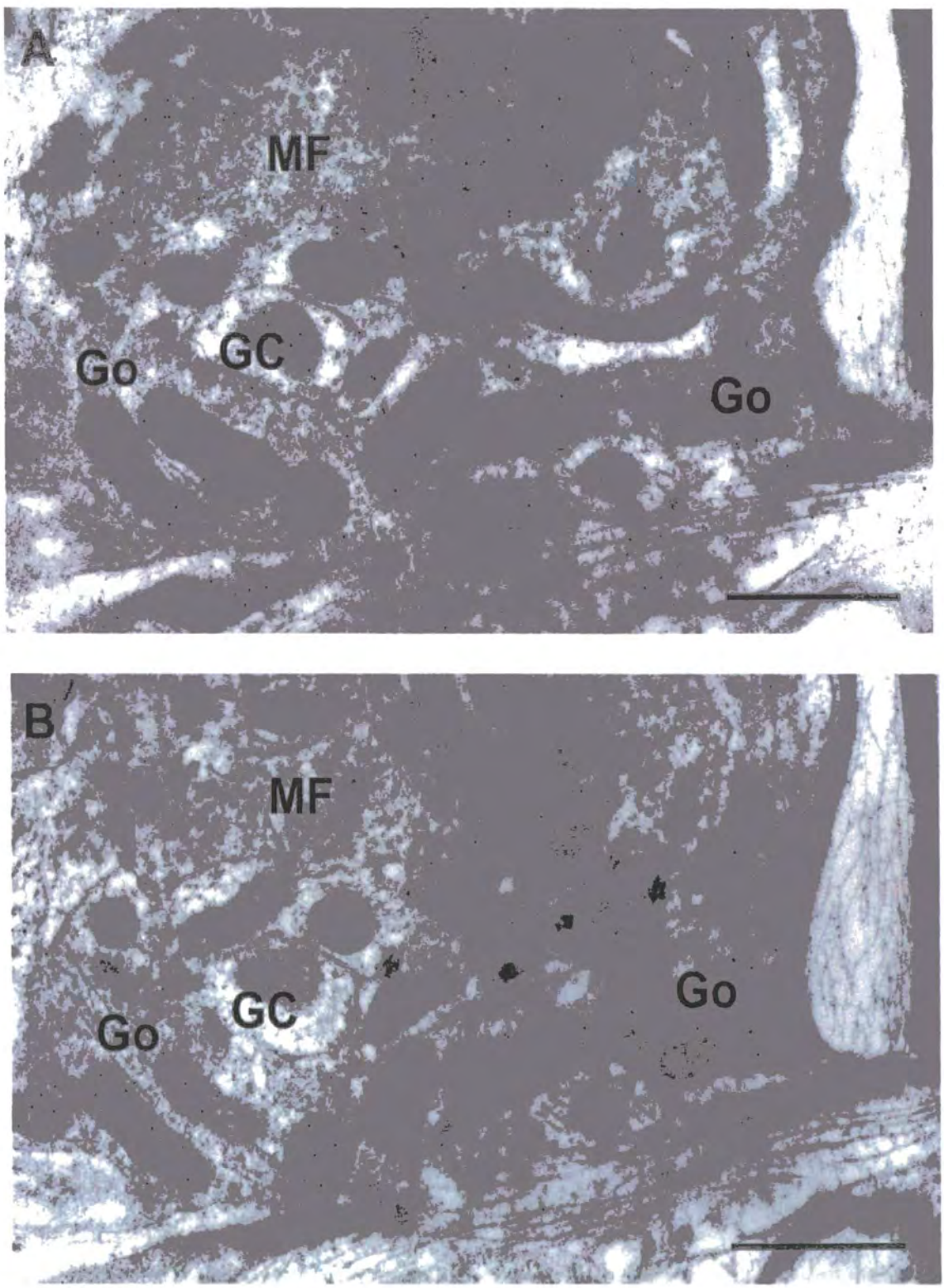

Table 3.1. Statistical comparison of glutamate immunoreactivity of different cellular elements in the cerebellar cortex.

Cell process	Mean surface density +/- SEM (n)	Statistical comparison				
Glial c.p.	7.40+/-0.91 (40)	Glial c.p				
Mossy f.t	44.43+/-2.56(40)	*P < 0.005*	Mossy f.t.			
Golgi c.t.	12.53+/-1.27(40)	*P < 0.005*	*P < 0.005*	Golgi c.t.		
Parallel f.t.	38.25+/-2.25(40)	*P < 0.005*	*P < 0.05*	*P < 0.005*	Parallel f.t.	
Purkinje c.d.	14.86+/-1.68(40)	*P < 0.005*	*P < 0.005*	*P < 0.3*	*P < 0.005*	Purkinje c.d.
Granule c.d.	29.55+/-1.43(40)	*P < 0.005*	*P < 0.005*	*P < 0.005*	*P < 0.005*	*P < 0.005*

Values represent the surface density of gold particles expressed as the mean number/ μm^2 $\pm$ standard error of the mean (SEM). Significance was determined by Student *t*-test. Glial c.p. = glial cell processes in the molecular layer; Mossy f.t = mossy fibre terminals; Golgi c.t. = Golgi cell terminals; Parallel f.t. = parallel fibre terminals; Purkinje c.d. = Purkinje cell dendrites; Granule c.d.= granule cell dendrites.

(a) omission of the primary antibody and replacement with buffer only, (b) replacement of the primary antibody with non-immune serum. None of these negative controls showed immunolabelling.

Statistical Analysis.

To compare the density of gold particles distributed over labelled profiles of MF terminals, GC dendrites, and PF terminals in *stg* and control (WT and heterozygote) cerebellar sections randomly selected labelled profiles were delineated and their areas calculated using the computer program Image J 1.28 U (Wayne Rasband. N.I.H. U.S.A. http://rsb.info.nih.gov/ij). The number of gold particles within each profile was counted and the density of gold particles per μm^2 calculated. For MF terminals and PF terminals a total of 40 pairs of measurements for each mouse brain examined, taken from different sections throughout the cerebellum, were used for each comparison. Similarly for GC dendrites 130 pairs of measurements were taken. Statistical analysis was done using an unpaired Student's t-test.

For analysis of the total number of synapses per MF profile, 100 MF profiles from both WT and *stg* were randomly identified. The number of excitatory synapses between MF terminals and GC dendrites in the glomeruli of both *stg* and WT mice was counted. For analysis of the number of excitatory synapses between PF terminals and PC dendrites in the molecular layer, all of the PF/PC synapses in a total of 30 electron micrographs (x10, 000 magnification)

were counted. The area of each micrograph was measured and the mean density of synapses per μm^2 was then calculated. The total area measured was approximately 2000 μm^2 per animal. To compare the mean density of synapses in WT and *stg* an unpaired Student's t-test was used.

For each PF synaptic terminal the number of synaptic vesicles, the length and the width of the postsynaptic density (PSD) were quantified. To prevent bias only terminals that had similar size, synaptic cleft width (WT 18.35 ± 0.26 n=123, *stg* 17.77 ± 0.22, n = 90. *P= 0.08*) and cross- sectional orientation were measured. The number of docked vesicles at each synapse was also counted and compared to the total number of vesicles at the synapse. Docked vesicles were defined as those located within 50nm (one vesicle diameter) of the active zone; vesicle distribution was quantified by measuring the distance from the centre of the vesicle to the nearest point on the active zone according to the method of Carter *et al.*, (2002). Vesicle number per 25nm bin was plotted as a function of distance from the synaptic cleft. A Kolmogorov-Smirnov test was used to determine if the two populations differed significantly.

Image Analysis.

Electron micrographs were taken on a Philips 400T (Philips Electron Optics, Eindhoven, The Netherlands) using Kodak 4489 Electron microscope film (Eastman Kodak Company Rochester NY USA). These were scanned with an

Epson GT 7000 Negative scanner (Epson UK Ltd) at a resolution of 600 d.p.i. For analysis of gold labelling density, greyscale TIFF files were imported via a microcomputer system (Roldec Computers UK) into Image J 1.28 U (Wayne Rasband. N.I.H. U.S.A. http://rsb.info.nih.gov/ij). Cell profiles were delineated and the cross sectional areas measured. All gold particles within the outlined area were counted and the particles /μm^2 calculated. PSD lengths, widths and vesicle distances were measured using the same image analysis package as above.

Figure Preparation.

Images were digitised as described above in Image Analysis and final figures prepared in Adobe Photoshop (v.5.0; Adobe Systems, Mountain View, CA). No adjustments were made other than contrast, brightness and enlargement. Images were printed on an Epson Stylus Photo R800.

Results.

Analysis Of The Levels Of Glutamate In Cerebellar Neurons.

The MF terminals, GC dendrites and PF terminals, in all *stg* mutants examined, had significantly less glutamate neurotransmitter as assessed by immunogold labelling compared to WT controls (Fig. 3.2-3.4) and stargazin heterozygotes (Fig. 3.3C). The immunogold technique used at the ultrastructural level makes it possible not only to precisely localize glutamate within neurons but also to semi-quantify the amounts present. (Ottersen, 1989:

Fig. 3.2. A, B. Electron micrographs showing the distribution of gold labelling over glut-IR profiles in the granule cell layer of cerebella from a WT (**A**) and a *stg* (**B**). Gold particles are concentrated over mossy fibre (**MF**) terminals and granule cell (**GC**) dendrites in the WT but are much less numerous in the *stg*. Scale Bar =0.5µm.

Fig. 3.2. A, B. Electron micrographs showing the distribution of gold labelling over glut-IR profiles in the granule cell layer of cerebella from a WT (**A**) and a stg (**B**).

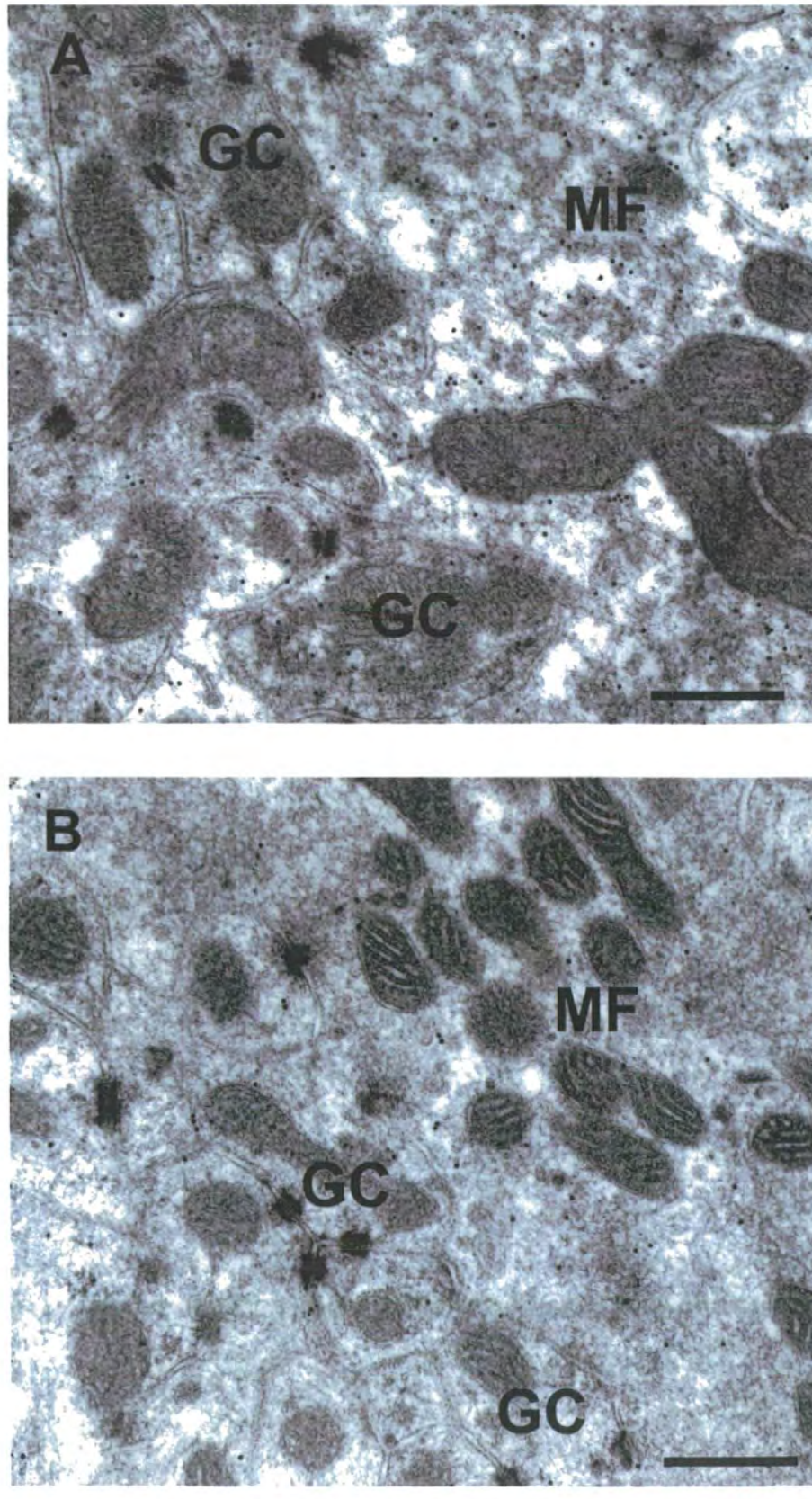

Fig. 3.3. A, B. Electron micrographs showing the distribution of gold labelling over glut-IR profiles in the molecular cell layer of cerebella from a WT (**A**) and a *stg* (**B**). Gold particles are concentrated over parallel fibre (**PF**) terminals in the WT but are much less numerous in the *stg.* Purkinje cell (**PC**) dendrites are only weakly labelled (equivalent to background levels over empty resin). Scale Bar =0.25μm.

Fig. 3.3. A, B. Electron micrographs showing the distribution of gold labelling over glut-IR profiles in the molecular cell layer of cerebella from a WT (**A**) and a stg (**B**).

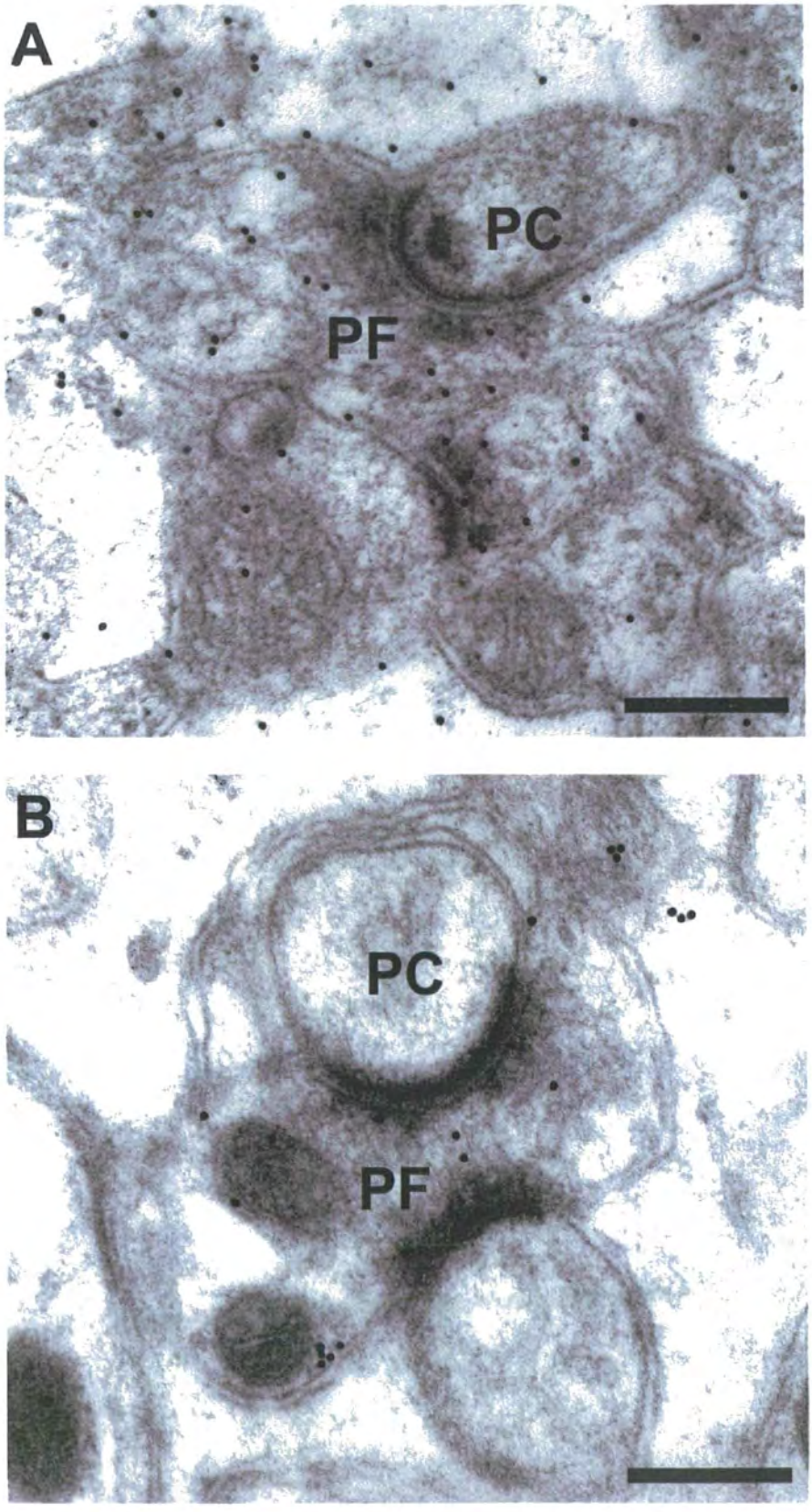

Fig. 3.4. Histograms showing the relative density of gold labelling over glut-IR profiles of MFs, GCs and PFs in sections from *stg* mice compared with their matched controls from three different glutamate immunolabelling experiments.

A. WT mouse 1 and *stg* mice 1 & 2.

B. WT mouse 2 and *stg* mice 3 & 4.

C. Control mice (WT mouse 3 and heterozygote (+/*stg*)) and *stg* mice 5 & 6.Values represent the surface density of gold particles expressed as the mean ± S.E.M. (MF and PF terminals n= 40, GC dendrites n =130 for each animal).

Significance was determined by Student *t*-test. **, $P < 0.001$.

Fig. 3.4. Histograms showing the relative density of gold labelling over glut-IR profiles of MFs, GCs and PFs in sections from *stg* mice compared with their matched controls from three different glutamate immunolabelling experiments.

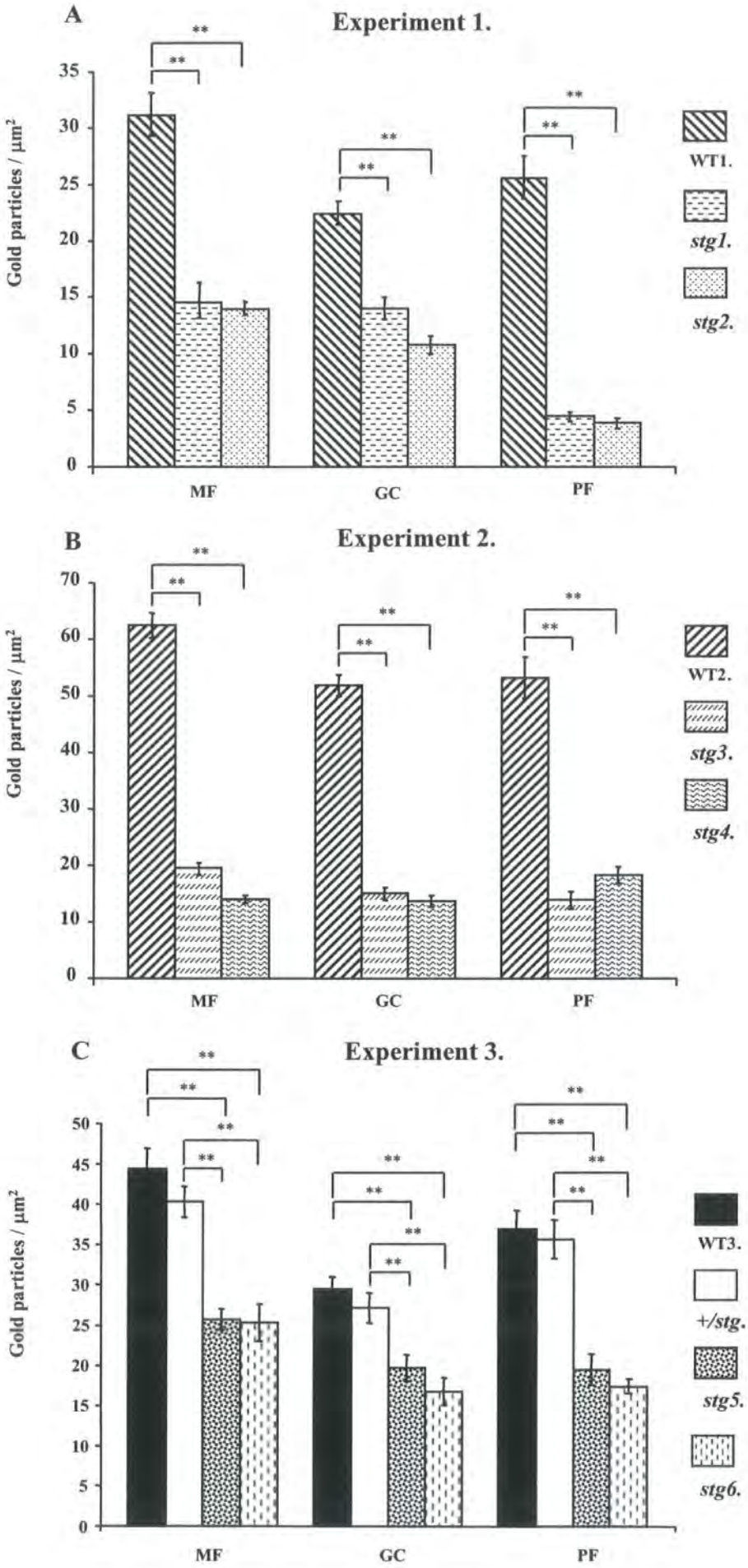

Bramham *et al.*, 1990). Ottersen, 1989 showed there is a roughly linear relationship between the concentration of fixed glutamate and gold particle density .To prevent any differences between samples arising as a result of variations in processing, the wild-type and stargazin brains used in each experiment were processed in parallel to ensure equal incubation times for etching, antibody labelling and washing. Figure 3.2A shows the density of immunogold labelling over a MF terminal and surrounding GC dendrites in the glomerulus of a WT control (Fig. 3.2A) compared to a similar region in a *stg* mutant (Fig. 2B). Likewise Figure 3.3 shows an immunogold labelled section through PF terminals and PC dendrites in the molecular layer of a WT control (Fig. 3.3A) compared to the same region in a *stg* mutant (Fig. 3.3B). The density of gold label over glutamatergic neuronal profiles in the *stg* is reduced compared to that over similar neurons in WT controls.

The histogram in Figure 3.4A shows the relative density of gold labelling over MF, GC and PF profiles in cerebellar sections from two different *stg* mutants (*stg1 & stg2)* compared to their matched WT control (WT1) processed in parallel (experiment 1). The density of gold particles and hence the levels of glut-IR are significantly reduced ($P < 0.001$) in the *stg* neurons compared to similarly processed WT control sections immunolabelled in the same experiment. In further experiments using tissue from different animals a similar reduction in the levels of glutamate compared to WT controls was found. Figure 3.4B shows the relative densities of gold over cerebellar tissue from two different stargazers (*stg* 3 *& 4)* compared to control sections from a

wild-type (WT2) cerebellum processed in parallel (experiment 2). In both *stg* mutants, the density of gold particles over MF, GC and PF profiles was significantly less (P <0.001) than over the same neuronal profiles in the WT control sections.

A third experiment was conducted to check that the differences observed in stargazer mutant cerebella compared to WT (C57BL/6J; +/+) controls were not due to strain differences. Figure 3.4C shows the relative densities of gold over cerebellar tissue from stargazers (*stg 5&6)* compared to control sections from their matched wild-type (WT3) and a stargazin heterozygote (+/*stg*) from the same litter, processed in parallel (experiment 3). This clearly demonstrates that the density of gold particles over MF, GC and PF profiles, and hence glut-IR, was significantly reduced (P <0.001) in the *stg* compared to the same profiles in both the WT and stargazin heterozygote (+/*stg)* controls. No significant difference was observed in the densities of gold labelling over WT and heterozygote control sections confirming that the relatively higher levels of glut-IR in control tissues was not due to strain differences.

Figure 3.5 shows the mean percentage reduction in gold particle density over MF, GC and PF profiles in all *stg* examined compared to their matched WT controls. Overall the mean levels of glut-IR in MF, GC and PF for all stargazers tested was 36%, 42%, and 23% respectively of control values indicating that glutamate content was reduced by approximately 64% in MF, 58% in GC, and 77% in PF in all *stg* mutants compared to the same neuronal profiles in WT control cerebella.

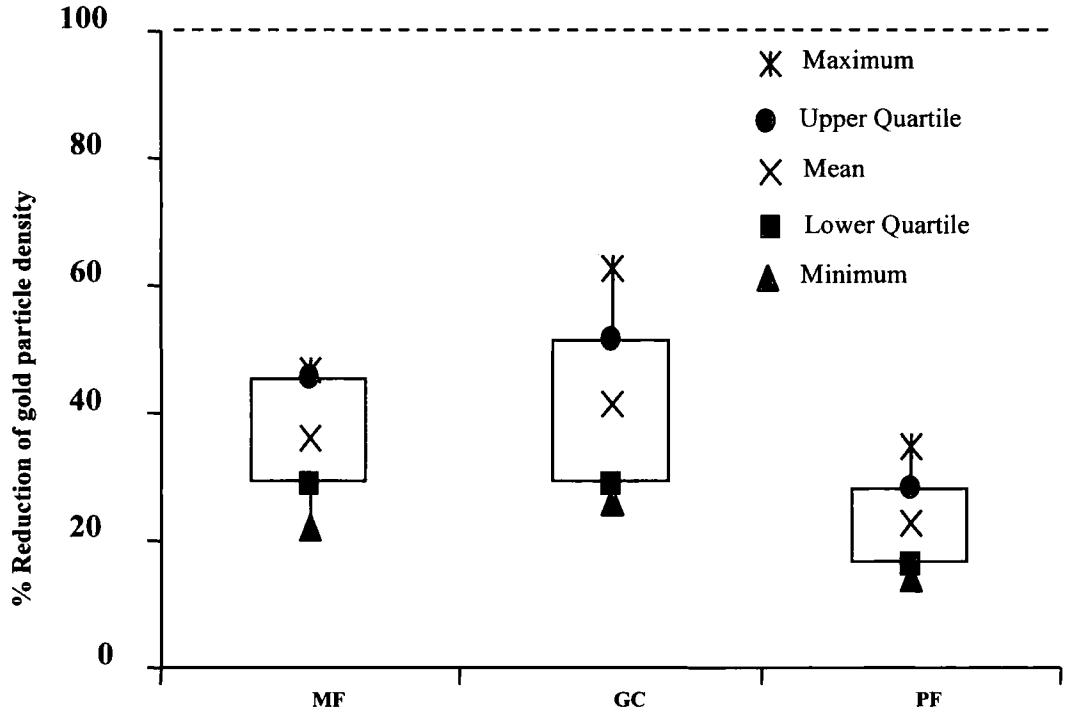

Fig. 3.5. Box plots (defined by mean and upper and lower quartile values) showing the mean percentage reduction in gold particle density over glut-IR profiles of MF, GC and PF in all *stgs* examined compared to their matched WT controls. (Dashed line represents 100% controls).

Analysis Of The Number And Size Of MF-GC Synapses and PF-PC Synapses.

Examinations of EM sections through glomeruli in the GC layer (Fig. 3.6) and through the molecular layer (Fig. 3.7) of the cerebellum of WT controls and *stg* mutants revealed no differences in the ultrastructural characteristics of the synapses between the MF terminals and GC dendrites or between PF terminals and PC dendrites. Figure 3.6 shows the ultrastructure of a typical glomerulus in the GC layer of cerebella from a WT mouse (Fig. 3.6A-B) and a *stg* mutant (Fig. 3.6C-E). Qualitative examination of MF-GC synapses and also synapses between Golgi cell terminals and GC dendrites revealed normal synaptic structures in adult *stg* mutants. MF terminals, recognisable as synaptic rosettes packed with numerous clear synaptic vesicles (Fig. 3.6A), make asymmetrical output synapses onto smaller diameter GC dendrites (Fig. 3.6B) and a few onto Golgi interneurons. The GC profiles in turn receive input synapses from Golgi terminals (Fig.3.6B) which contain pleiomorphic vesicles. Ultrastructurally, these synaptic contacts appear similar in WT (Fig. 3.6A-B) and *stg* mutants (Fig. 3.6C-E). Likewise in the molecular cell layer (Fig. 3.7), electron microscopy reveals that PF-PC synapses in WT (Fig. 3.7A-B) and *stg* (Fig. 3.7C-D) mice share the same basic ultrastructural features. PF terminals demonstrate a presynaptic swelling containing numerous spherical loosely packed synaptic vesicles and make asymmetrical output synapses, typical of excitatory synapses, onto PC dendritic spines.

Fig. 3.7. Electron micrographs showing the ultrastructure of the molecular cell layer in the cerebellum of a WT (A,B) and *stg* (C,D).

A. PF-PC synapse in WT mouse. Scale Bar =1µm.

B. High power micrograph of the PF-PC synapse shown in (A). Scale Bar = 0.25µm.

C. PF-PC synapse in a *stg* mouse. Scale Bar =1µm.

D. High power micrograph of the PF-PC synapse shown in (C). Scale Bar = 0.25µm.

Fig. 3.6. Electron micrographs through the cerebella of WT (**A,B**) and stg (**C,D**) mice.

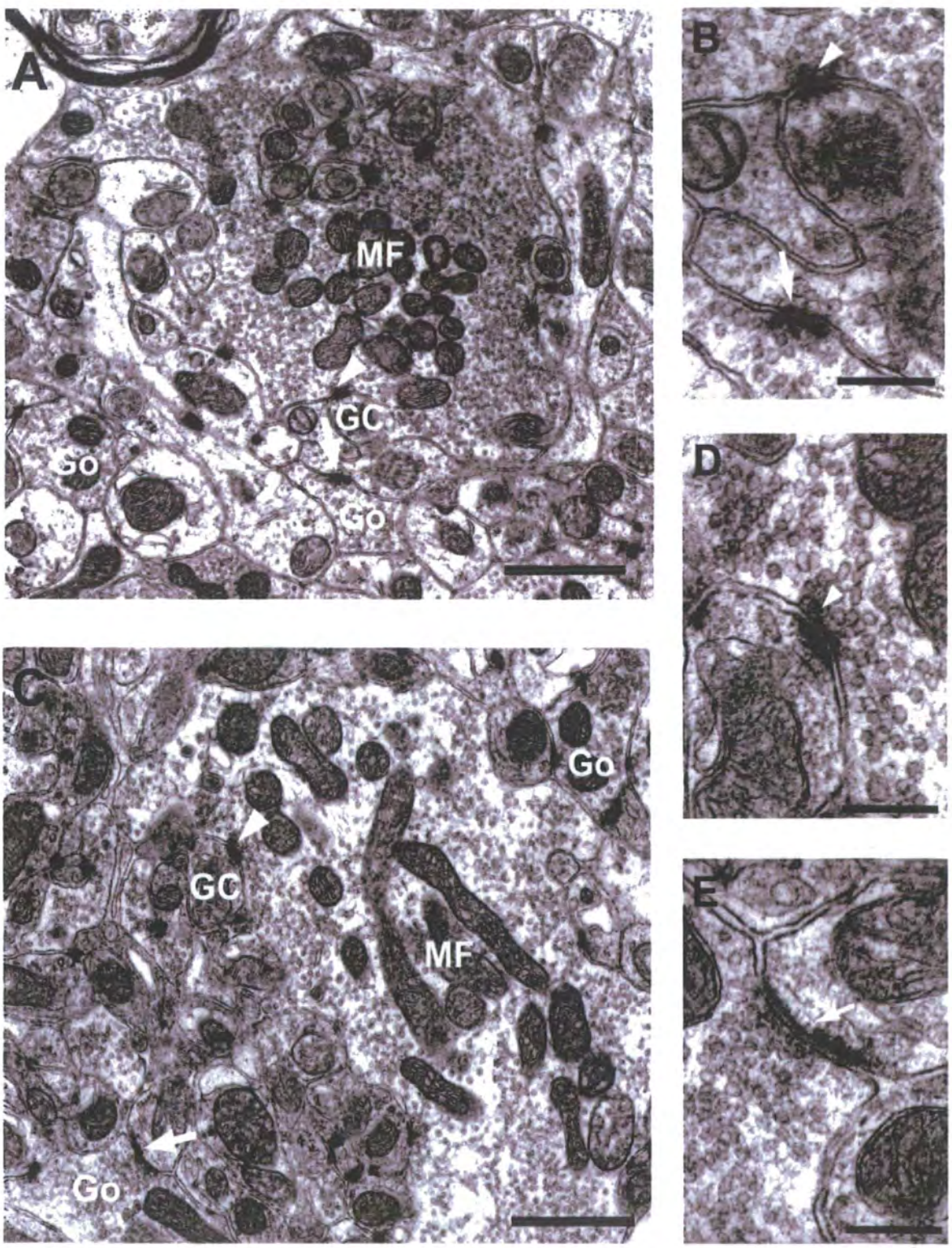

Fig. 3.6. Electron micrographs through the cerebella of WT (**A,B**) and *stg* (**C,D**) mice.

A. Typical glomerulus in the granule cell layer of the cerebellum from a WT mouse. Synapses between a mossy fibre (**MF**) terminal and granule cell (**GC**) dendrite (white arrowhead) and between a Golgi terminal (**Go**) and GC dendrite (white arrow) have a similar ultrastructural appearance to *stg* mutant synapses shown in (**C**). Scale Bar =1µm.

B. High power view of the MF-GC synapse (white arrowhead) and the Go-GC synapse (white arrow) in the WT mouse shown in **A**. Scale Bar = 0.25µm.

C. Typical glomerulus in the granule cell layer of the cerebellum from a *stg* mouse. MF-GC synapses (white arrowhead) and Go-GC synapses (white arrow) have a similar ultrastructural appearance to WT control synapses shown in (**A,B**). Scale Bar =1µm.

D. High power view of the synapse between the MF and GC (white arrowhead) in the *stg* mouse shown in **C**. Scale Bar = 0.25µm.

E. High power view of the Go-GC synapse (white arrow) in the *stg* mouse shown in **C**. Scale Bar = 0.25µm.

FIG. 3.7. Electron micrographs showing the ultrastructure of the molecular cell layer in the cerebellum of a WT (**A,B**) and stg (**C,D**).

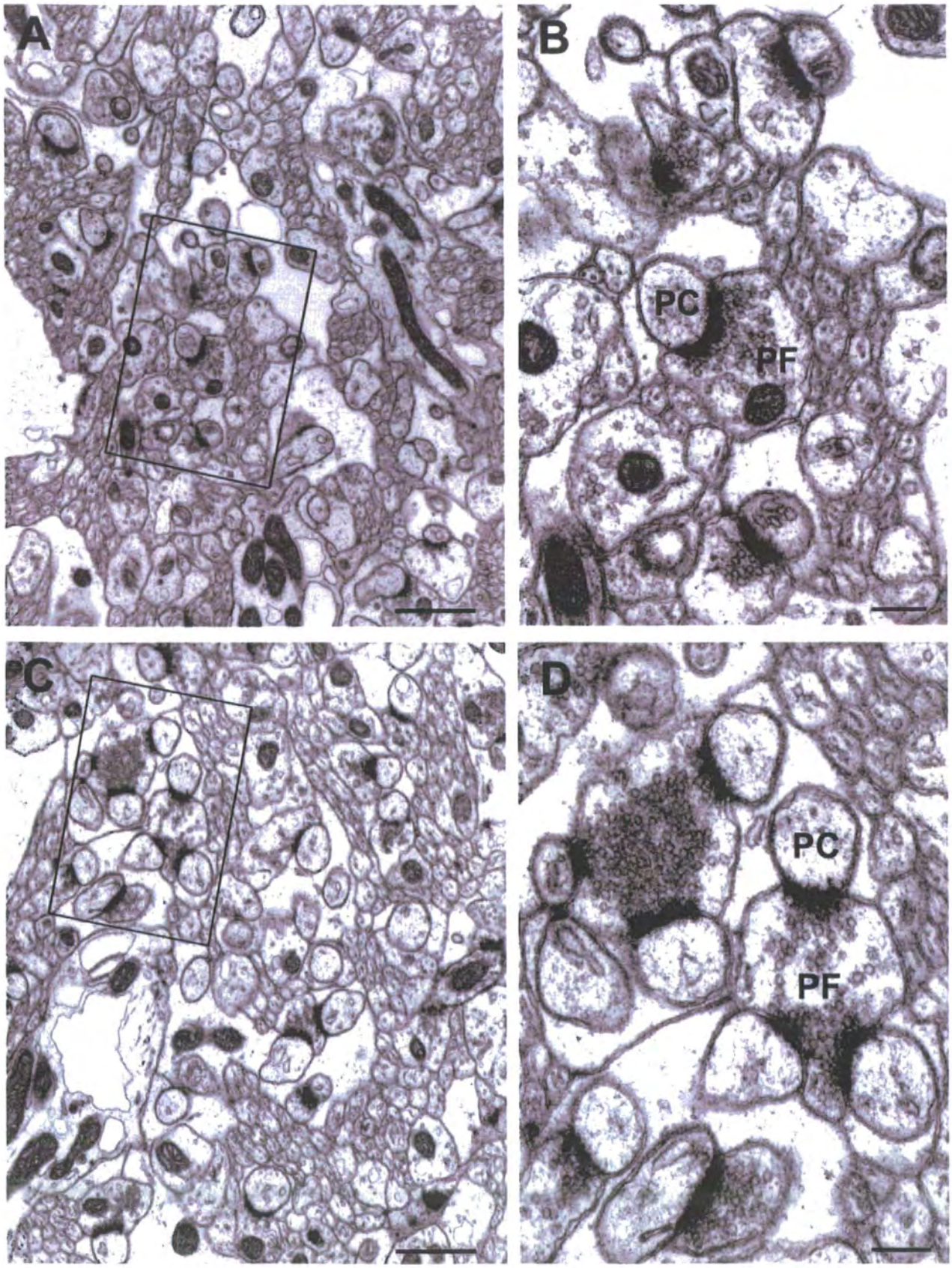

Analysis of MF-GC synapses within glomeruli (Fig. 3.8A-C) and PF-PC synapses in the molecular layer (Fig. 3.8D-F) revealed no significant differences in the number of these synapses in *stg* mutants compared to WT controls (cp. Figs. 3.8A & D). The number of MF-GC synapses per MF terminal (Fig. 3.8A) and the length (Fig. 3.8B) of the post-synaptic density (PSD) were similar in both mutants and controls. This correlates with the findings of Chen *et al* (2000) who also found no difference in the length of the PSD at MF/GC synapses in *stg*. Likewise, the density of PF-PC synapses in the molecular cell layer was not significantly different in *stg* mutants compared to WT controls (Fig. 3.8 D), however, the length of the active zone was slightly but significantly reduced in *stg* mutants compared to WT controls (Fig. 3.8 E). The most significant difference, however, in synapse morphology in *stg* compared to WTs was in PSD width. The width of the PSD at both MF-GC (Fig. 3.8 C) and PF-PC synapses (Fig. 3.8F) was significantly reduced ($P < 0.001$) in *stg*. The width of the PSD at these excitatory synapses in the cerebellum of *stg* was reduced by approximately one third (33% and 28% respectively).

Analysis Of The Number And Distribution Of Synaptic Vesicles In PF Terminals.

Quantitative analysis of synaptic vesicles in PF terminals in both mutant and WT control mice revealed no significant difference in the number of vesicles

Fig. 3.8. Histograms showing analysis of the number and size of MF-GC and PF-PC synapses in WT and *stg* mice.

A. Number of MF–GC synapses per MF terminal. No significance difference (NSD) was found. $P > 0.1$ (n =100 MF terminals for each animal).

B. Length of the PSD (nm) at MF–GC synapses. NSD was found. $P > 0.1$ (n = 120 for each animal).

C. Width of the PSD (nm) at MF–GC synapses. **, $P < 0.001$. (n = 120 for each animal).

D. Number of PF–PC synapses per μm^2 of molecular layer. NSD was found. $P > 0.1$ (area approx 2000 μm^2 per animal).

E. Length of the PSD (nm) at PF–PC synapses. *, $P < 0.05$. (n = 90 WT, n = 120 *stg*).

F. Width of the PSD (nm) at PF–PC synapses. **, $P < 0.001$. (n = 90 WT, n = 120 *stg*).

Significance was determined by Student *t*-test. Values represent the means $\pm$ S.E.M.

Fig. 3.8. Histograms showing analysis of the number and size of MF-GC and PF-PC synapses in WT and *stg* mice.

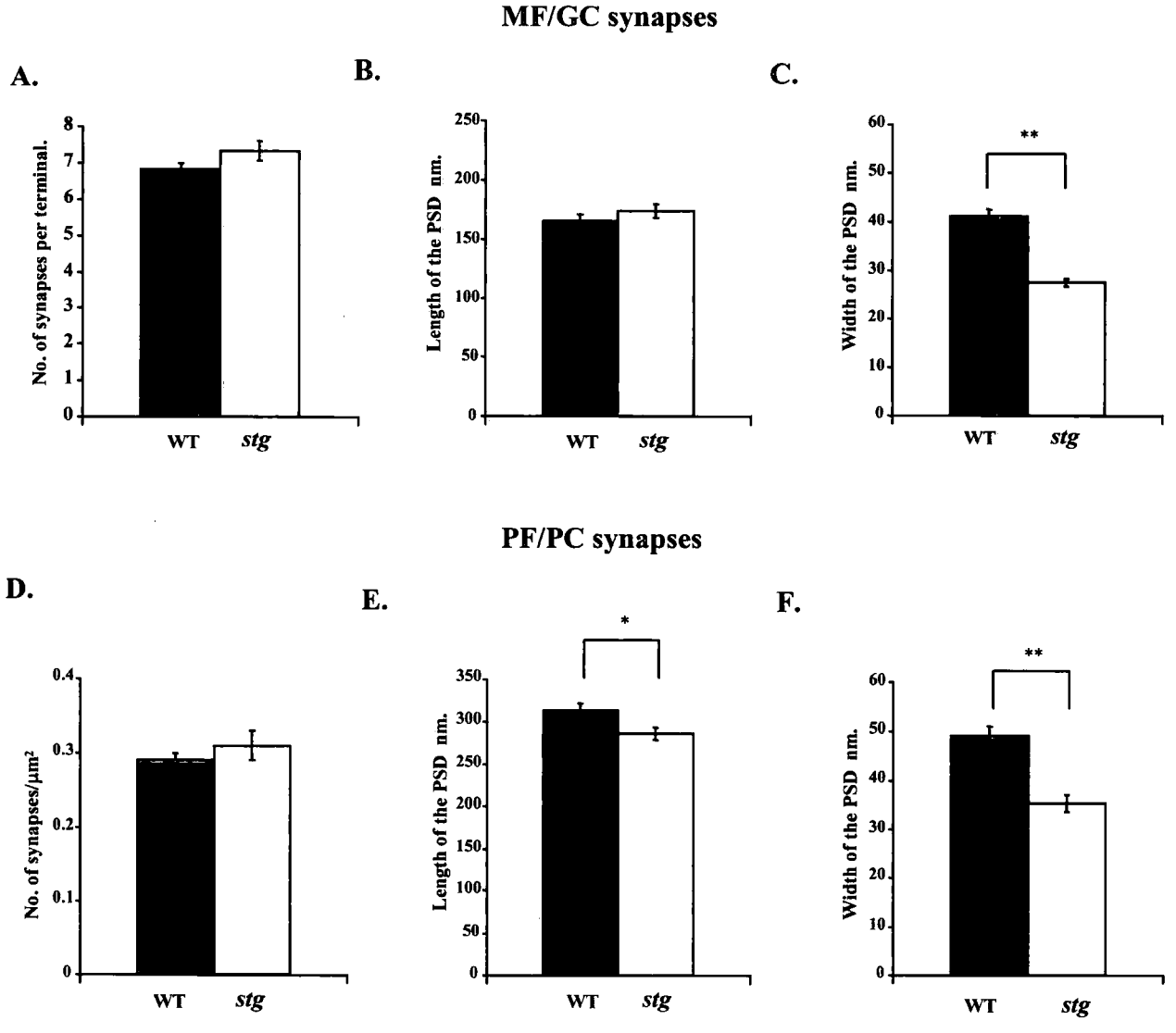

per synapse (Fig. 3.9A). However, vesicle density may change as a function of terminal size. When the density of synaptic vesicles in PF terminals was calculated, that is the number of vesicles per μm^2, a significant decrease in the density of vesicles in the PF terminals of *stg* mutants compared to WT controls was found (Fig. 3.9B). The density of vesicles in PF terminals of mutant mice was reduced by approximately 25% as a result of an increase in PF terminal size in mutant mice (Fig. 3.9C). This concurs with the findings of Carter *et al* (2002) who also found a significant difference in vesicles/ μm^2 at PF-PC synapses in the cerebella of BDNF (-/-) knockout mice.

Analysis of the number of docked vesicles in each PF terminal (Fig. 3.10) indicated that *stg* mutants had significantly (P <0.005) fewer docked vesicles per synapse (Fig. 3.10A) and that their packing density (i.e. the number of vesicles per μm^2 of PF terminal) was also markedly reduced (Fig. 3.10B), compared to WT controls. The proportion of docked vesicles out of the total vesicle pool was significantly (P<0.05) reduced in *stg* mutants compared to the WT controls (Fig. 3.10C). However, when the density of vesicles at the active zone (i.e. number of docked vesicles per µm length of PSD) was analysed, no significant difference was found (Fig. 3.10D). So although there were fewer docked vesicles at each synapse, because each synapse was slightly smaller in the *stg* mutants (see Fig 3.8E), the density of vesicles per µm length of synapse was not significantly different in *stg* mutants compared to WT controls. A similar finding was reported by Carter *et al.*, (2002) in BDNF (-/-) mutant mice. They found that the density of docked vesicles was not

Fig. 3.9. Histograms showing analysis of synaptic vesicles in PF terminals in WT and *stg* mice.

A. Number of synaptic vesicles per PF terminal. NSD was found. $P > 0.1$.

B. Vesicle packing density (vesicles/ μm^2) in PF terminals. **, $P < 0.001$.

C. Area of the PF terminal (μm^2). *, $P < 0.05$.

Significance was determined by Student *t*-test. Values represent the means $\pm$ S.E.M. (n = 90 WT, n = 120 *stg*).

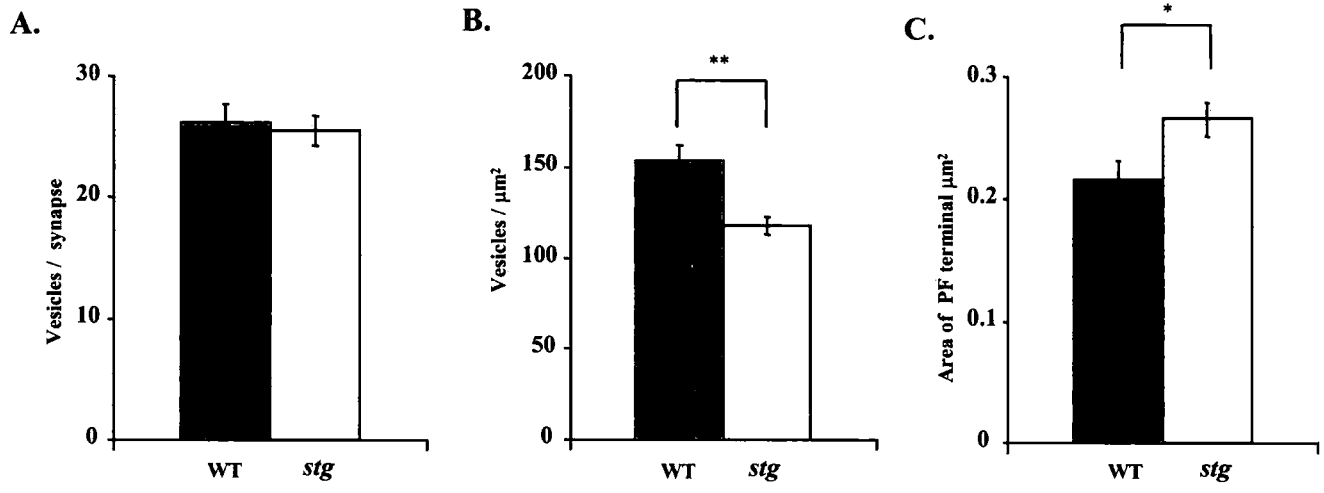

Fig. 3.9. Histograms showing analysis of synaptic vesicles in PF terminals in WT and *stg* mice.

A. Number of synaptic vesicles per PF terminal. NSD was found. $P > 0.1$.

B. Vesicle packing density (vesicles/ μm^2) in PF terminals. **, $P < 0.001$.

C. Area of the PF terminal (μm^2). *, $P < 0.05$.

Significance was determined by Student *t*-test. Values represent the means $\pm$ S.E.M. (n = 90 WT, n = 120 *stg*).

Fig. 3.10. Histograms showing analysis of docked vesicles in presynaptic PF terminals in WT and *stg* mice.

A. Number of docked vesicles in PF terminals. **, $P < 0.005$.

B. Docked vesicle packing density (docked vesicles / μm^2) in PF terminals. **, $P < 0.005$.

C. Ratio of docked / total vesicles in PF terminals. *, $P < 0.05$.

D. Number of docked vesicles per µm of PSD in PF terminals. NSD was found. $P > 0.05$.

Significance was determined by Student *t*-test.
(n = 90 WT, n = 123 *stg*).

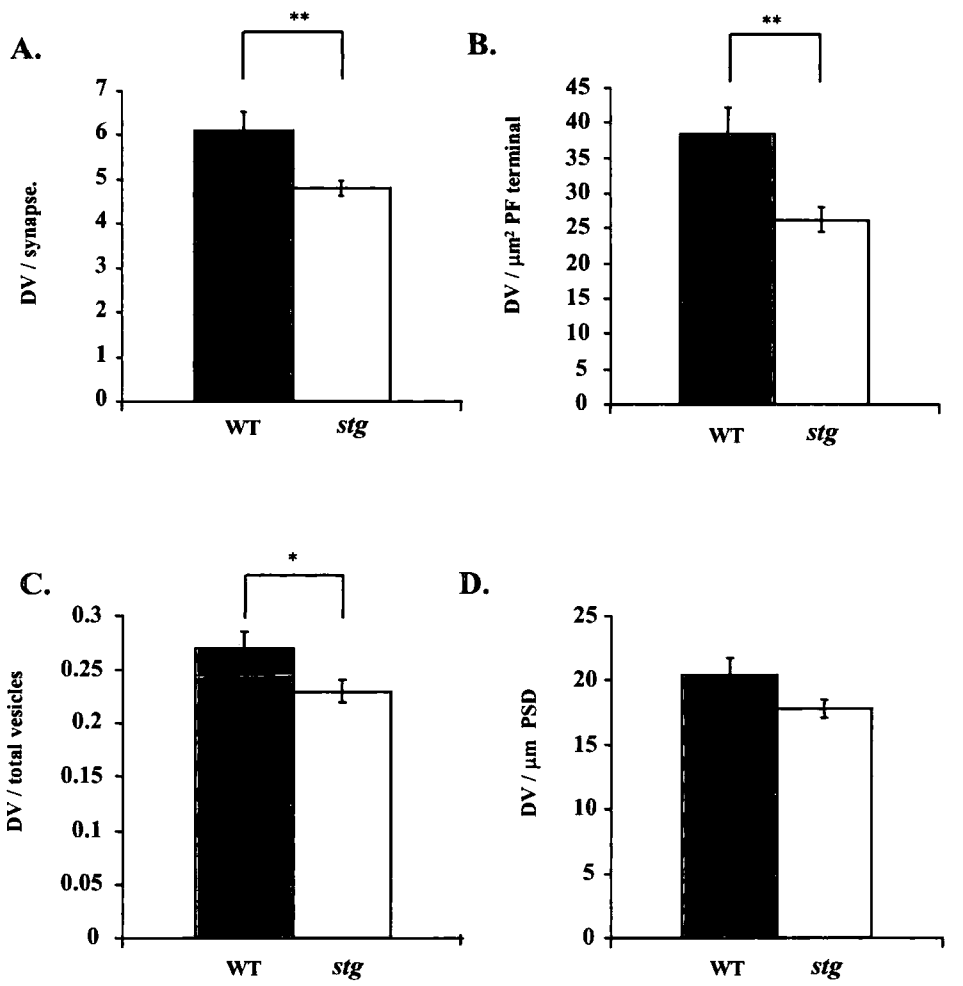

Fig. 3.10. Histograms showing analysis of docked vesicles in presynaptic PF terminals in WT and *stg* mice.

A. Number of docked vesicles in PF terminals. **, $P < 0.005$.

B. Docked vesicle packing density (docked vesicles / µm^2) in PF terminals. **, $P < 0.005$.

C. Ratio of docked / total vesicles in PF terminals. *, $P < 0.05$.

D. Number of docked vesicles per µm of PSD in PF terminals. NSD was found. $P > 0.05$.

Significance was determined by Student *t*-test. (n = 90 WT, n = 123 *stg*).

significantly different between BDNF +/+ and BDNF -/- terminals. In contrast the overall packing density of vesicles was significantly decreased in the terminals of BDNF -/- mice. PF terminals in BDNF -/- mice were larger and had abnormal distribution of vesicles.

Studies into the structure and dynamics of the vesicle pool (Li and Schwarz, 1999) have indicated that different functional pools exist in a steady relationship (i.e. an equilibrium exists between the releasable pool of vesicles in the terminal and the docked vesicles that are available for release by a given action potential). Therefore, analysis of vesicle distribution was undertaken (Fig. 3.11). Vesicle number per 25nm bin was plotted as a function of distance from the synaptic cleft. A highly significant reduction in number of vesicles proximal to the synapse i.e. the docked vesicles (within the first 50nm) and the pool of vesicles adjacent to docked vesicles (50-100nm) was evident. In the region between 125 and 250nm distal to the synapse there were relatively more synaptic vesicles in the *stg* terminals compared to WT controls. However, no significant difference was found in the numbers of reserve vesicles further than 250nm from the PSD. Clearly the distribution of vesicles within PF terminals of *stg* mutants is markedly different from that of WT controls. Although there are no differences in the total number of vesicles their distribution profile is markedly different in *stg* mutants compared to WT controls with *stg* having significantly fewer docked vesicles and fewer adjacent vesicles ready to dock.

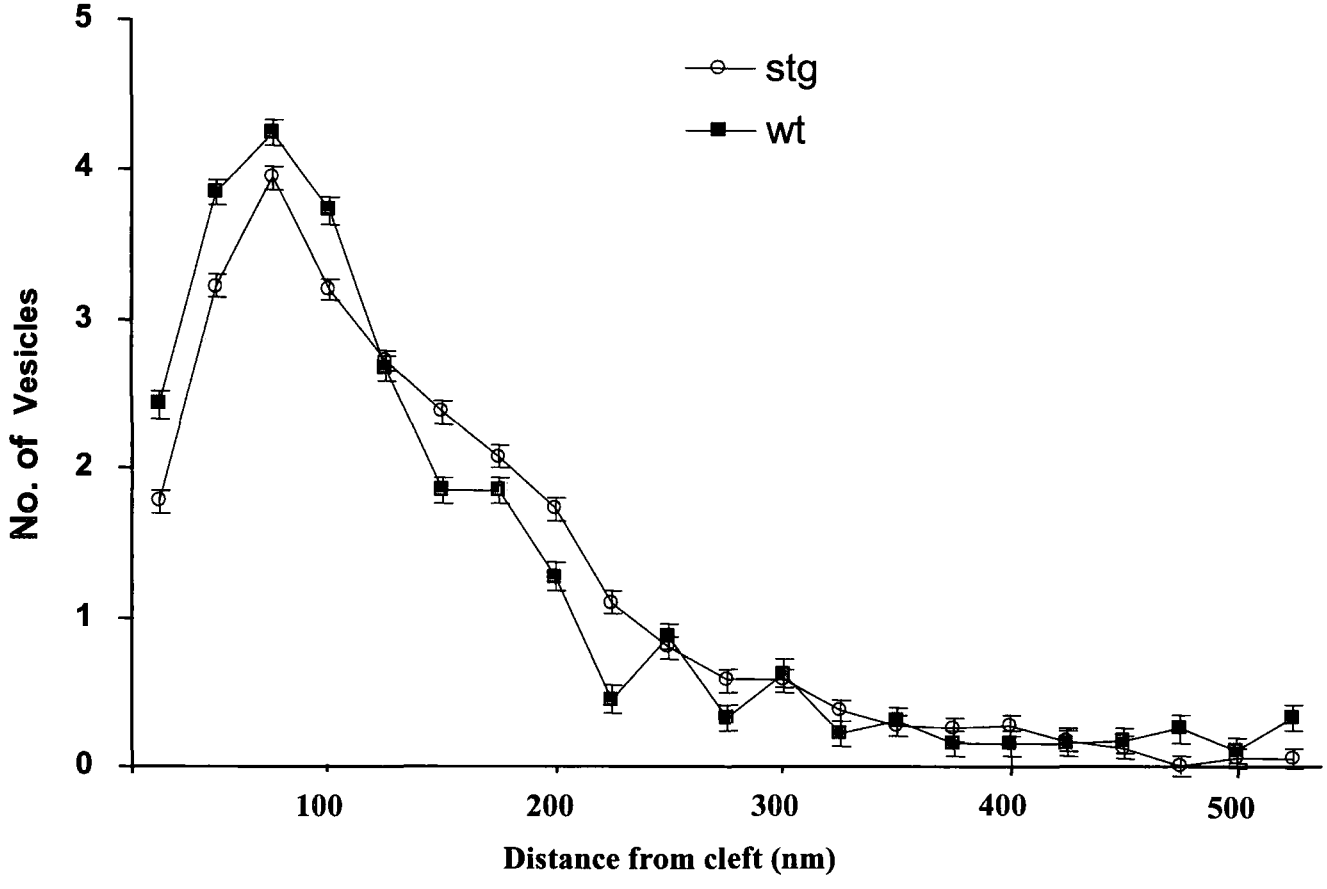

Fig. 3.11. Analysis of the vesicle distribution profile in PF terminals in WT and *stg* mice. Vesicle number per 25nm bin was plotted as a function of distance from the synaptic cleft. By Kolmogorov-Smirnov test *D*, is: 0.0787 with a corresponding *P* of 0.005 indicating a significant difference in the two populations.

Discussion.

The data presented in this study clearly show that in the mutant mouse stargazer, the cerebellar MF terminals and GC dendrites in the glomeruli, and PF terminals in the outer molecular layer have significantly reduced levels of glut-IR indicative of a significant decrease in their glutamate content, compared to WT controls.

Glut-IR was reduced by up to 64% in MF terminals; 58% in GC dendrites and 77% in PF terminals. Although the levels of immunoreactivity do not relate to the actual tissue concentrations of antigen it has been shown that there is roughly linear relationship between the concentration of fixed glutamate and gold particle density (Ottersen 1989) and so any reduction in antibody binding can be viewed as a reduction in antigen content.

Whether this reduction in Glutamate –IR reflects a change in the vesicular pool (ie the pool most directly relevant to synaptic release) or in the extravesicular pool (metabolic pool) could be investigated further by adopting a method designed by Ji *et al* 1991. They showed that there is a strong positive correlation between glutamate immunolabelling intensity and the packing density of synaptic vesicles in a population of putative glutamatergic nerve terminals. They suggested subcellular distribution of glutamate may serve as a guide to distinguish terminals in which glutamate acts as a transmitter, from terminals in which glutamate is merely engaged in metabolic functions, e.g., as a GABA precursor. By re-analysing the distribution of immunogold labelling within the glutamate –IR terminals of the cerebellar cells it should be possible

to distinguish whether the reduction in immunoreactivity is due to changes in metabolic glutamate or the transmitter content of the terminals.

Furthermore the thickness of the postsynaptic density at MF-GC and PF-PC synapses is severely reduced (up to 33% less than WT controls). The distribution profile of presynaptic vesicles is also markedly different in *stg* mutants compared to WT controls; *stg* have proportionally fewer docked vesicles and fewer vesicles located adjacent to the active zone ready to dock than WT controls. As *stg* mutants have a pronounced reduction in BDNF in their cerebella and a near total depletion in their GC it is possible that altered phenotype displayed by glutamatergic cells in the cerebellum is related to the reduction of BDNF and BDNF-TrkB signalling in this region of the mutant brain. BDNF is known to play a crucial role in neuronal differentiation and plasticity, in synaptogenesis and synapse plasticity, and in neurotransmitter release (Gottschalk *et al.*, 1998; Tyler & Pozzo-Miller 2001; Tyler *et al.*, 2002; Tyler & Pozzo-Miller 2003). Nevertheless, little is known about its role in the development of excitatory glutamatergic synapses *in vivo*.

Effects Of BDNF On Neurotransmitter Synthesis And Release.

The effects of neurotrophins, including BDNF, on neurotransmitter expression and on transmitter-synthesising enzymes levels in neurons have been reported in a number of recent studies. Ito *et al.*, (2003) recently examined BDNF, NGF and NT-3 on the expression of four neurotransmitter-synthesising enzymes (choline acetyltransferase, tyrosine hydroxylase, dopamine beta hydroxylase and glutamate decarboxylase 65 kDa) in cultured mouse stem

cells. All of the neurotrophins enhanced mRNA expression of choline acetyltransferase, tyrosine hydroxylase, and dopamine beta hydroxylase. These results suggest that neurotrophins may influence specific neurotransmitter phenotypes. BDNF has been shown to enhance the GABAergic phenotype in cortical neurons (Widmer & Hefti, 1994) and to specifically elevate cellular GABA content in rat striatal cultures (Mizuno *et al.*, 1994) mainly as a result of an increase in the GABA synthetic enzyme (GAD) and elevation of GABA uptake activity. Chronic treatment of hippocampal cultures with BDNF enhances the fluorescence labelling intensity of punctae with an anti-GAD antibody (Bolton *et al.*, 2000) presumably reflecting an increase in the level of GAD expression. Other studies also indicate that BDNF, induced by neuronal excitation, might be responsible for the upregulation of GAD expression in the hippocampus. GAD $_{67}$ mRNA is increased in the hippocampus following brain seizures (Feldblum *et al.*, 1990) and concomitantly, BDNF mRNA is induced in the same brain region (Zafra *et al.*, 1991; Isackson *et al.*, 1991; Dugich-Djordevic *et al.*, 1992). BDNF also specifically affects the expression of neuropeptide Y in striatal cultures (Mizuno *et al.*, 1994) and in the hippocampus (Reibel *et al.*, 2003) whereas NGF promotes cholinergic development in the striatum both *in vivo* and *in vitro* (Martinez *et al.*, 1987; Mobley *et al.*, 1985). Collectively these results imply that different neurotrophins may control development of different neurotransmitter phenotypes in the brain.

Conversely, depleted levels of neurotrophin in knockout and mutant mice may result in reduced levels of neurotransmitter expression. Studies on BDNF knockout mice indicate that homozygous BDNF mutations produce severe depletions within the nigrostriatal dopaminergic system and substantial reductions of noradrenaline within the hypothalamus and olfactory bulb (Dluzen *et al.*, 1999). Dopamine concentrations within the corpus striatum were found to be 54% of WT controls while hypothalamic noradrenaline concentrations were 62% of control values. In *stg* mutants, which have severely depleted levels of cerebellar BDNF, GABA-IR in cerebellar Golgi interneurons was decreased by approximately 50% compared to WT control levels (Richardson & Leitch 2002). In the present study there is a marked reduction in the levels of glut-IR in cerebellar glutamatergic neurons in *stg* mutants. Whether alterations in glutamate levels in the *stg* are attributable to reduced levels of BDNF in the cerebellum of these mutant mice, or alternatively glutamate levels affect BDNF expression, remains to be elucidated. Previous studies have indicated that subtle changes in the balance between glutamatergic and GABAergic systems significantly alter expression of BDNF in hippocampal neurons (Zafra *et al* 1991) and a recent paper has shown that GABA interacts with glutamate in the regulation of BDNF gene expression in fetal hypothalamic neurons (Marmigere *et al.*, 2003).

Effects Of BDNF On PSD Length And Thickness At Excitatory Synapses.

Collectively, data from many different reports indicates that BDNF acts on both pre- and postsynaptic mechanisms although changes in postsynaptic

membrane may be secondary to changes in presynaptic vesicle pools and neurotransmitter release. Using immunoelectron microscopic analysis, Aoki *et al* (2000) have demonstrated that BDNF and TrkB localise discretely to the PSD of axo-spinous asymmetric synaptic junctions that are morphological correlates of excitatory glutamatergic synapses. The PSD localisation of BDNF and TrkB supports the contention that this receptor/ligand pair participates in postsynaptic plasticity. Ultrastructural analysis of the postsynaptic effects of BDNF and NT-3 by Collin *et al.*, (2001) on hippocampal E16 neurons in cultures revealed that, although there was no difference in the length of the PSD at excitatory synapses, there was a marked augmentation in the thickness of the postsynaptic membrane by neurotrophin treatment. BDNF produced a dramatic 81% increase in PSD thickness, while NT-3 produced a 31% thickening of the PSD. The PSD is known to increase in thickness but not length during development (Vaughn, 1989). Other studies have also shown that there is direct correlation between the thickness of the PSD, observed *in vivo* by electron microscopy, and changes in PSD proteins composition (e.g. BDNF receptor TrkB and protein kinases), as determined by protein microsequencing (Hu *et al.*, 1998). In the present study, the lack of BDNF in the *stg* mutant GC could account for the marked decrease in thickness of the PSD at both MF-GC synapses in the GC layer and at GC-PF synapses in the molecular layer.

Chen *et al* (2000) have reported that *stg* mutant mice lack functional AMPA receptors on their cerebellar GCs. Stargazin (the protein absent in the *stg*

mutant) is restricted to excitatory synapses and regulates synaptic targeting of AMPA receptors (AMPARs). It interacts with both AMPA receptor subunits (GluR1, 2, 4) and synaptic PDZ proteins such as PSD-95. Stargazin, through its interaction with AMPA receptor subunits, is essential for delivering functional receptors to the surface membrane of GC and for targeting AMPARs to synapses via its binding with PSD-95 and other PDZ proteins. The study by Chen *et al.*, (2000) defines an essential role for stargazin in synaptic expression of glutamate receptors in the CNS. Several other studies have since implicated BDNF as having a role in AMPAR trafficking into synaptic sites (Narisawa-Saito *et al.*, 2002; Itami *et al.*, 2003; Jourdi *et al.*, 2003). Jourdi *et al* (2003) has indicated that BDNF signalling enhances and maintains the expression of AMPA receptor-associated PDZ proteins in developing cortical neurons. BDNF treatment in neocortical cultures triggered increases in PDZ proteins and resulted in elevation of their total association with AMPA receptors Glu1 and Glu2/3, which led to an increase in AMPA receptor protein. These findings reveal a novel function of BDNF in postsynaptic development by regulating PDZ protein expression. The reduction in the thickness of the PSD at excitatory glutamatergic synapses in *stg* mutant mice in the present study may thus reflect the lack of functional AMPA receptors and PDZ proteins at MF-GC and PF-PC synapses in the cerebellum of *stg* mice due to a lack of stargazin protein. Since AMPA receptors function not only as ion channels but also generate intracellular signals from the cell surface to the nucleus through the Lyn-MAPK (mitogen-activated protein kinase) pathway, it is thought that they may also contribute to synaptic plasticity by regulating the expression of

BDNF (Hayashi *et al.*, 1999). An alternative, or related, factor which could influence the thickness of the PSD is the reduced levels of glutamate in the MF and GC neurons. Direct application of glutamate to rat hippocampal neurons in culture has been shown to induce thickening of PSD and accumulation of CaMKII on PSD. Whereas removal of glutamate and Ca^2+ causes a reversal within 5 min indicating that PSDs are dynamic structures whose thickness and composition are capable of rapid and transient changes during synaptic activity (Dosemeci *et al.*, 2001).

Effect Of BDNF On Number And Distribution Of Synaptic Vesicles.

Several recent papers have reported a link between BDNF levels and an increase in the number of docked vesicles at the active zones of excitatory synapses. Collin *et al.*, (2001) demonstrated in E16 hippocampal neurons grown in culture that both the total number of vesicles and the number of docked synaptic vesicles (per terminal) were increased by neurotrophin treatment. They also found that activation of synaptic responses by neurotrophins occurred even when postsynaptic glutamate receptors and action potential discharges were pharmacologically blocked. They suggest that these data are consistent with neurotrophins having a presynaptic locus of action to increase synaptic vesicle density, which is critical for rapid synaptic transmission, and with neurotrophins being able to activate synapses in the absence of pre- and post-synaptic neuronal activity.

Tyler & Pozzo-Miller (2001) also found that BDNF specifically increases the number of docked vesicles at the active zone of excitatory synapses on CA1 dendritic spines in organotypic slice cultures of postnatal rat hippocampus with only a small increase in active zone size. Consistent with their hypothesis that BDNF enhances quantal neurotransmitter release by increasing docked vesicle density at the active zone of individual synapses, was the finding that BDNF increased frequency but not amplitude of AMPA-receptor mediated miniature EPSCs. They also found an increase in synapse number after BDNF treatment. These effects were shown to be mediated by TrkB receptor activation. They concluded that these data provided additional evidence for a fundamental role of the BDNF-TrkB signalling cascade in synaptic transmission.

Conversely, in knockouts that lack the *bdnf* gene (Pozzo-Miller *et al.*, 1999) there are significantly fewer docked vesicles at presynaptic active zones of hippocampal CA1 synapses. Furthermore, expression levels of synaptophysin and synaptobrevin (a protein known to be involved in vesicle docking and fusion) are also markedly reduced. The results reported by Pozzo-Miller *et al.*, (1999) suggested a novel role for BDNF in the mobilization and/or docking of synaptic vesicles to presynaptic zones. Earlier work by Martinez *et al.*, (1998) had also indicated a decrease in the density of synaptic vesicles in TrkB knock-out mice hippocampal neurons.

More recently, Carter *et al.*, (2002) demonstrated that paired-pulse facilitation, at PF/PC synapses in the cerebellum of mice with a targeted deletion of the BDNF gene, was significantly decreased. This was accompanied by an increase in total vesicle number but a decrease in the proportion of docked vesicles. They also reported that the vesicle distribution profile was altered in these BDNF-/- mice; there was a selective increase in the vesicle pool distal (beyond 100nm) to the active zone. They concluded that BDNF regulates synaptic ultrastructure and short-term synaptic plasticity.

The cerebella of *stg* mutant, which have severely depleted BDNF, also showed a significant decrease in the number of docked vesicles at both MF-GC synapses and PF-PC synapses. A marked difference in the vesicle distribution profile in mutants compared to WT mice was also found. However, in contrast to Carter *et al.*, (2002), the vesicles proximal to the active zone (within the first 100nm), that is docked vesicles and those ready to dock, were significantly reduced in *stg* mutants. This agrees with the findings of Tyler and Pozzo-Miller (2001) and others that BDNF, or lack of it, affects the number of docked vesicles per active zone.

It seems then from these various studies that BDNF facilitates docking of vesicles via modulation of presynaptic vesicle proteins and that lack of it in mutant or knockout mice causes a corresponding decrease in the number or the proportion of docked vesicles. It has been proposed that the release probability of evoked EPSCs at single synapses is linearly related to the readily releasable pool (RRP) of vesicles, which is thought to correspond with

the pool of docked vesicles (Dobrunz *et al*, 1997; Dobrunz, 2002; Schikorski & Stevens 2001; Murthy. 2001). Modulation of the pool of RRP vesicles is of importance as a mechanism for regulating synaptic strength.

BDNF And Modulation Of Glutamatergic Transmission.

There is clear evidence in the literature supporting a role for BDNF in glutamatergic transmission. BDNF causes enhancement of unitary glutamatergic synaptic transmission in hippocampal cultures predominantly by presynaptic modulation of transmitter release (Lessmann and Heumann, 1998). Likewise BDNF enhances depolarisation-evoked glutamate release in cultured cortical neurons (Matsumoto *et al.*, 2001). Nevertheless, the mechanism(s) by which BDNF enhances glutamatergic synaptic transmission is still highly controversial. Evidence exists to support both presynaptic and postsynaptic mechanisms. From these studies on *stg* mutants it is clear that the presynaptic docking of vesicles and postsynaptic membrane ultrastructure are altered at excitatory synapses in the cerebellum which also exhibits a marked reduction in BDNF. It would seem plausible that these factors are causally related.

Chapter 4. Identification Of Neuromodulators Involved In Modulation Of Transmitter Release From The Central Terminals Of The Locust Wing Hinge Stretch Receptor.

Introduction.

Neuromodulation is a fundamental feature of the nervous system that enables animals to switch between different behavioural sets and to act appropriately under changing environmental conditions. Neuromodulators can alter the excitable properties of neurons or the strength of synaptic connections and thereby reconfigure the functional properties of neuronal networks (Katz & Frost 1996). One invertebrate preparation which represents a model for the investigation of neuromodulation is the flight motor system of the locust. At the hinges of the wings are stretch receptors (SR) which are important elements in generating and controlling the flight motor pattern. Each wing hinge has a single SR which acts as a tonic proprioceptor signalling wing position. Information about the angle of each wing is therefore provided by its single SR neuron rather than a population of sensory neurones. As the wing is elevated the SR is stretched initiating spikes which are conducted to the central nervous system (CNS). Alterations in wing position are signalled by changes in the number of spikes fired, the instantaneous spike frequency, the duration of the spike burst and its phase during wing beat cycle. When stimulated at the correct phase of the wing beat, the combined input from the SRs of two wings

can raise the frequency of the flight motor pattern, entrain it to the frequency of stimulation, and reset the rhythm (Pearson *et al.*, 1983; Reye and Pearson, 1988).

The SR of each wing makes direct, excitatory monosynaptic contacts with most of the depressor motoneurons (MNs) controlling that wing (Burrows, 1975). Connections are only made with the depressor MNs of ipsilateral wings and not those of the contralateral wing. The forewing SR (fSR) makes direct synapses with the depressor MNs which control that forewing in the mesothoracic ganglion, but also with ipsilateral MNs in adjacent segments, the pro- and metathoracic ganglia, whereas the hindwing stretch receptor makes direct connections with ipsilateral depressor MNs in the metathoracic ganglion and also with depressor MNs in the adjacent mesothoracic segment. However, the amplitude of excitatory postsynaptic potentials (EPSPs) in the MNs of adjacent segments is smaller than that of EPSPs in depressor MNs of the same segment. Each wing SR also makes connections with inhibitory interneurons, which contact the elevator MNs of that wing. The excitatory connections with depressor MNs and the inhibitory connection with elevator MNs thus form a simple negative feedback loop that regulates the extent of wing elevation.

Studies on the modulation of neurotransmitter release from the terminals of the forewing SR at an identified synapse with a depressor MN, the first basilar motoneuron (BA1) in *Schistocerca gregaria* (Leitch *et al.*, 1993; Leitch and Pitman 1995) and *Locusta migratoria* (Leitch *et al.*, 1998; Judge and Leitch,

1999), have revealed that release of the neurotransmitter acetylcholine from the central terminals of the fSR is reduced by activation of presynaptic muscarinic receptors (the fSR/BA1 synapse has been shown to be cholinergic, postsynaptic potentials are blocked by α-bungarotoxin and other nicotinic antagonists). When muscarinic antagonists (e.g. scopolamine and atropine) are applied to the synapse, they cause an augmentation in SR evoked EPSP amplitude recorded in BA1 but do not increase the amplitude of responses to ACh applied directly onto the soma of BA1 indicating that central terminals of the fSR possess "muscarinic" autoreceptors that exert a negative feedback control on synaptic transmission. Further studies by Leitch *et al.* (1998) and Judge and Leitch (1999a,b) have revealed that muscarinic receptors are also located on presynaptic GABAergic interneurons which are involved in modulation of acetylcholine release at the fSR/BA1 synapse. ACh released from collateral branches of the fSR neuron excites the inhibitory GABAergic interneurons (via muscarinic receptors on their surface) causing them to release inhibitory neurotransmitter, which in turn depresses ACh release from the fSR terminals. Application of picrotoxin (a GABA antagonist) to the preparation causes a marked increase in the amplitude of EPSPs recorded from BA1 but prevents the augmentation of EPSPs normally caused by muscarinic antagonists, suggesting blockade of GABA receptors on the fSR which normally inhibit ACh release. However it should be noted that the expression of receptors at the somata of insect neurons could differ from those on the neuropilar branches and these pharmacological results should be interpreted with caution.

Electron microscopical (EM) immunocytochemistry has revealed that over 40% of all input to the fSR in *Locusta* are GABAergic supporting the electrophysiological and pharmacological studies. Presynaptic modulation of sensory signals by inhibitory synaptic inputs to the terminals of sensory neurons is common in both vertebrates and invertebrates as a mechanism for changing the effectiveness of a spike in signalling to postsynaptic neurons. EM ICC studies have revealed GABA-immunoreactive (GABA-IR) neurons presynaptic to the terminals of numerous types of locust sensory afferents including campaniform sensilla afferents, Watson and England, 1991; hair plate afferents, Watson *et al.*, 1991; femoral chordotonal organ afferents, Watson *et al.*, 1993; filiform hair afferents, Watson, 1990; Watson and Pflüger, 1994. Likewise, electrophysiological studies have provided evidence of GABA-induced inhibition at these and other sensory terminals (cockroach cercal afferents, Hue and Callec, 1983; locust filiform hair afferents, Boyan, 1988; crayfish primary afferents, El Manira and Clarac, 1991; locust femoral chordotonal organ afferents, Burrows and Laurent, 1993).

Although a large proportion of the presynaptic inputs to the fSR are from GABAergic interneurons, over 50% of the presynaptic inputs are not immunoreactive for GABA. EM ICC studies (Leitch and Richardson, 2004) have revealed neurons presynaptic to the fSR that are immunoreactive for glutamate indicating that glutamatergic neurons may also play a role in presynaptically modulating the fSR terminals. Recent electrophysiological studies have also

shown that the SR/BA synapse is also modulated by biogenic amines (Leitch *et al*, 2000). The amines octopamine, 5-hydroxytryptamine (5-HT, serotonin) and dopamine reversibly decrease the amplitude of EPSPs evoked in BA1 by electrically stimulating the fSR axon, and also reversibly decreased the amplitude of responses to acetylcholine pressure-applied to the soma of BA1. As the muscarinic antagonist scopolamine had no significant effect on the octopamine-induced decrease in ACh responses it appears that these amines potentially could physiologically depress cholinergic transmission between fSR and BA1, at least in part, by altering nicotinic rather than muscarinic cholinergic receptor function. Confocal immunocytochemistry revealed intense octopamine immunoreactivity in the anterior lateral association center, thus confirming the presence of octopamine in neuropil regions containing fSR/BA1 synapses and therefore supporting a role for this amine in the modulation of synaptic transmission between the fSR and BA1. 5-HT-immunoreactivity, conversely, was concentrated within the ventral association centers; very little staining was observed in the dorsal neuropil regions in which fSR/BA1 synapses are located. Dopamine had previously been shown to be present in the dorsolateral neuropil regions. (Watson 1992.)

The principal aims of the present study were: (1) to identify glut-IR processes presynaptic to the terminals of the fSR which could modulate synaptic efficacy at fSR/BA1 synapse and determine their distribution; (2) to analyse the relative proportion of inputs to the fSR which were immunoreactive for either glutamate or GABA and hence assess the relative contribution of each type of

neurotransmitter to modulation at this synapse; and (3) to analyse the proportion of inputs to the fSR that were neither GABAergic or glutamatergic and determine whether any inputs were aminergic. A preliminary account of this work has been given elsewhere in abstract form (Leitch and Richardson 2004).

Materials And Methods

Staining Of The Forewing Stretch Receptor For Electron Microscopy.

The fSR was labelled according to the method of Judge and Leitch (1999). The fSR is retrogradely labelled *in vivo* to preserve the ultrastructure of the mesothoracic ganglion. The wings of the locust were removed with scissors and then the locust was positioned ventral side upper-most on a Sylgard-based petri dish. It was secured by pinning its legs to the Sylgard and the dish was positioned beneath a Zeiss dissecting microscope. A small window of cuticle was cut from the thoracic plate, anterior to the 2nd pair of legs so that the mesothoracic ganglion remained covered by cuticle. The thoracic cavity was perfused with locust saline at 20-22^{O}C throughout the procedure. The fSR bifurcates as it approaches the CNS, (FIG.4.1) sending one branch into prothoracic nerve 6 (N6) and the other into the mesothoracic nerve 1 (N1). Since no other sensory neurons bifurcate in this way (Burrows 1975), the mesothoracic fSR neuron can be selectively backfilled via the distal cut end N6. The nerve was cut as close to the prothoracic ganglion as possible so that

Fig. 4.1. Schematic of a wholemount preparation showing the position of the fSr within the mesothoracic ganglion. The fSr enters the mesothoracic ganglion via nerve 1 (N1) then divides into a medial branch and lateral branch. The lateral branch bifurcates a medio-lateral branch and lateral branch. The levels within the ganglion at which transverse sections were taken and subsequently ultrathin sectioned are indicated by A-D.

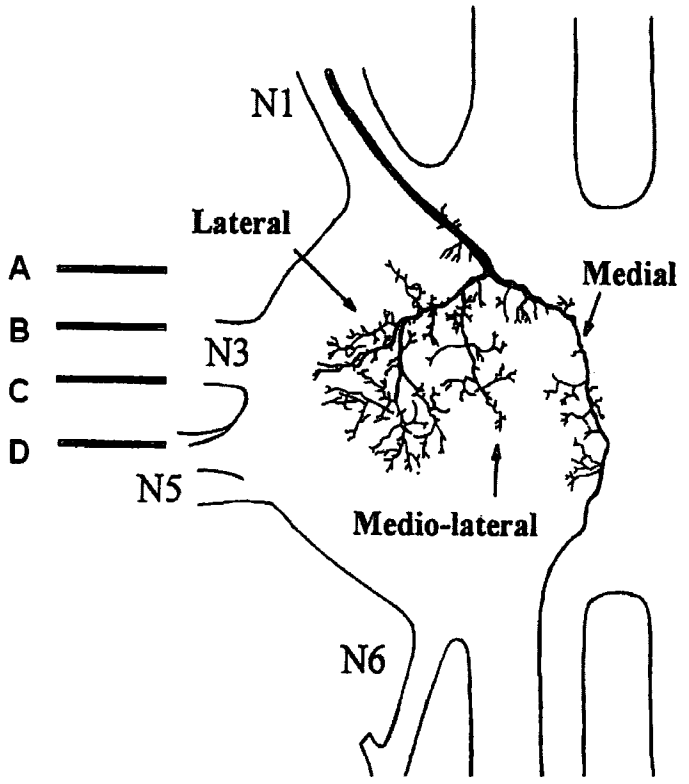

Fig.4.1. Modified from. Modulation of cholinergic synaptic transmission in an identified locust sensory pathway.

Ph.D Thesis S.J.Judge.

a substantial length of prothoracic N6 was left attached to mesothoracic N1, great care was taken to ensure that none of the side branches or other nerves were damaged. This method has been checked repeatedly with cobalt chloride back fills to selectively fill only the fSR (Judge and Leitch, 1999a) and the morphology conforms to that described by Burrows 1975; Altman and Tyrer, 1977; and Peters, Altman and Tyrer, 1985 when filled intracellularly. The connective tissue and air sacs were gently eased to the side to expose mesothoracic N1 and prothoracic N6 on one side of the nerve cord. Prothoracic N6 was cut just distal to the point N6 joins the ganglion so a substantial length of prothoracic N6 was left attached to mesothoracic N1. A Parafilm shield was placed over the thoracic cavity and prothoracic N6 was placed on top of this before the sides of the thoracic cavity were sealed with Vaseline. The distal cut end of prothoracic N6 was placed in a Vaseline well made on the Parafilm shield. The well was filled with 4% horseradish peroxidase, Sigma Type VIA (HRP) made up in 0.2M Tris buffer pH 7.4 (TB) (Appendix 3) (Sigma, Poole, UK.) and sealed with Vaseline. Moist chambers containing the locusts were incubated for 4-5 days at 4°C to allow the HRP to diffuse through the fSR.

Animals were subsequently dissected from the ventral surface and the thoracic ganglion was removed and processed for electron microscopy.

The mesothoracic ganglia containing the HRP-filled fSR were processed for EM according to the method described by and Leitch and Laurent (1993). The

HRP, Vaseline and Parafilm shield were removed and the thoracic cavity was perfused with locust saline. The rest of the thoracic cuticular plate was removed to expose the meso- and metathoracic ganglia before the nerve cord was fixed in situ for 5-10 minutes in 2.5% glutaraldehyde (Agar Scientific, Stansted, U.K.) in 0.1M Sorensen's phosphate buffer pH 7.4 (PB) (Appendix 4) containing 0.2M sucrose. The nerve cord was removed from the thorax and transferred to a vial containing fresh fixative. The posterior-side of each mesothoracic ganglion was dried before quickly mounting on a platform with cyanoacrylate glue. The platform was immediately immersed and secured in the tissue chamber of a Vibroslice 725M tissue slicer (Campden Instruments Ltd, U.K.) filled with fresh fixative. A razor blade was secured in the vibrating arm of the tissue slicer and used to cut the ganglia into serial transverse sections (150-200 (μm thick). The tissue slices were fixed for a further 2 hours in fresh fixative before being washed thoroughly in PB containing 0.2M sucrose, followed by TB. They were then placed in 0.5M cobalt chloride in TB for 10 minutes before being washed in 0.2 M TB followed by PB minus the sucrose. The slices were then transferred to a vial containing 9 ml incubation medium containing diaminobenzidine (DAB) (Appendix 5) and placed in an oven set at 37°C. After 10-15 minutes 20 □l of glucose oxidase (Sigma type V, Poole, U.K.) was added to the medium, which acted on the β-d-glucose to generate hydrogen peroxide. The slices were replaced in the oven but were examined under a dissecting microscope at regular 5 minute intervals to monitor the development of the DAB-HRP reaction product. Washing the slices in PB without sucrose stopped the reaction and at this time the slices

were checked to identify successful fills of the fSR. If the fSR was successfully filled, the slices were incubated in 1% osmium tetroxide (Agar Scientific, Stansted, U.K.) for 1 hour..Following a brief distilled water wash, the tissue slices were dehydrated through and ascending series of ethanol 50%-70%, three 10 minutes rinses in each. The slices were then transferred to a. LR. White Medium grade resin (Agar Scientific, Stanstead , Uk) and 70% ethanol (2:1) mixture for 30 minutes.: slowly add one part of 70% ethanol (drop by drop) to two parts of L.R. White, and shake gently (otherwise the mixture will become milky). The 70 % alcohol should be freshly made from absolute alcohol (Ours is routinely stored over a molecular sieve in a tightly sealed bottle).Two fresh changes of LR White resin were followed by an overnight infiltration. Next morning the slices were placed in a fresh change of LR White resin for 30mins before being positioned in gelatin capsules. The specimen was placed at the bottom of the capsule which was filled up with L.R. White to the brim and then the other half of the capsule was inverted onto it to exclude air. The resin was then polymerised by placing in an oven overnight at 50°C (Newman and Hobot., 2001). Ultrathin sections (70nm) were cut on a Reichert-Ultracut ultra-microtome and mounted on nickel grids coated with Formvar.

After a 1 hr incubation in osmium tetroxide, all material was dehydrated and embedded in L.R.White resin by the protocol employed in Chapter 2. (Agar Scientific, Stansted, U.K.). Unfortunately these experiments were carried our before it had been shown that better ultrastructure and immunogold labelling

could be achieved with Araldite embedding. Ideally, had time permitted, this should have been repeated using the Araldite embedding procedure. The moulds were placed in an oven set at 50-55°C (to help preserve antigenicity) overnight to polymerize the resin. Ultrathin sections for electron microscopy (70 nm) were cut with a diamond knife mounted on a Leica EM UC6 ultramicrotome (Leica Cambridge Ltd, Cambridge, U.K.). The sections were mounted on 200 mesh nickel grids that had been coated with Formvar (Agar Scientific, Stansted, U.K.) and carbon-coated (Edwards model 12E6/1288).

To identify the level at which each slice had been taken through the mesothoracic ganglion, semi-thin sections (1 μm thick) were also cut from the blocks. These were mounted on glass slides and stained with 1% Toluidine blue (Appendix 1) before being examined under an Optiphot compound microscope (Nikon U.K. Ltd, Surrey, U.K.). The level at which each slice had been taken through the ganglion was identified using anatomical guides (Tyrer and Gregory, 1982; Pflüger *et al*, 1988).

GABA And Glutamate Post-Embedding Immunogold Labelling.

Ultrathin sections for ICC were incubated by floating the grids section side down on droplets of the solution placed on clean squares of dental wax. Placing the wax squares onto damp 9cm filter paper in a covered petri dish created moist chambers. This prevented evaporation of the droplets.

Sections for immunocytochemistry were etched for 5 minutes with a saturated solution of sodium metaperiodate (Bendayan and Zollinger, 1983) and then thoroughly washed with distilled water. The grids were then floated face down on droplets of 5% normal goat serum in bovine serum albumin (BSA/TB) (Appendix 2) for 30 minutes to block non- specific staining. Sections were incubated in the primary antibody by floating the grids on droplets of either rabbit anti-glutamate or rabbit anti-GABA antiserum (Sigma, UK) in BSA/TB) for 2-3 hours at room temperature. Following incubation in the primary antibody, sections were washed 5 times in BSA/TB and then once in BSA/Tris buffer (pH 8.2) before being transferred to droplets of 10nm gold-labelled goat anti-rabbit antibody (Biocell, Cardiff, UK) diluted 1:20 in BSA/Tris buffer (pH 8.2) for 1 hour at room temperature. The grids were finally washed in a series of distilled water droplets to remove unbound gold conjugate then stained with 1% uranyl acetate in ethanol followed by Reynolds lead citrate (Reynolds 1963)(5 minutes each). Sections were examined in a Philips EM 400T electron microscope.

Statistics

The significance of the density of gold particles distributed over labelled profiles as against background levels was assessed using a paired Student's t-test (Table 4.1) according to the method of Watson (1988). The paired t-test was used in preference to an unpaired t-test to avoid any effects of differences in labelling density due to variable access of antibody to different parts of a

Table 4.1. Mean density of gold particles (particles /mm^2) over immunoreactive and non-immunoreactive processes after antibody staining of L.R.White sections.

Treatment	Label density (particles/ μm^2)	
Anti-Glutamate		
Labelled profiles	31.66 ± 13.22	$P < 0.001$
Unlabelled profiles	5.23 ± 3.95	
Anti- GABA		
Labelled profiles	21.55 ± 11.33	$P < 0.001$
Unlabelled profiles	1. 87± 1.89	

section (e.g. caused by uneven etching) and differences between grids. Randomly selected labelled profiles were delineated and their areas calculated using the calibrated computer program (ImageJ (Rasband, W. N.I.H. U.S.A. Image J 1.28U. http://rsb.info.nih.gov/ij).

The number of gold particles within each profile was counted and the density of gold particles per μm^2 calculated. This was then compared to the density within the nearest adjacent profile that was not clearly labelled (background levels). A total of 40 pairs of measurements were used for each comparison. To compare the density of gold particles distributed over labelled Golgi interneuron profiles in *stg* and wild-type cerebellar sections an unpaired Student's t-test was used. A total of 40 pairs of measurements for each mouse brain examined, taken from different sections throughout the cerebellum, was used for each comparison.

Octopamine Immunolabelling.

Confocal Microscopy.

Mesothoracic ganglia were processed for confocal immunocytochemistry and immunolabelled with an anti-octopamine antibody, either as whole mounts or as transverse frozen sections.

Whole mount preparations.

Using a modification of the method described by Duch *et al.* 1999, whole mount preparations of mesothoracic and prothoracic ganglion were performed

to assess if known octopamine–immunoreactive neurons were labelled by the antibody. The ganglia to be processed for whole mount preparations were washed overnight in 0.1M Sorensen's phosphate buffer pH 7.4 with 1% triton X (PBT). The major limitation of using whole mounts is that antibody penetration may not be complete in the tissue, resulting in uneven staining or false negative staining. So the detergent Triton X-100 treatment was used to enhance penetration of the antibody (Nassel 1996) and to prevent hydrophobic interactions between antisera and tissue components (Van Leeuwen 1987). Penetration of the antibody is further improved by 10 minute washes each in 50%, 70% ethanol and then 1hr in 90% ethanol, then rehydrated by immersion in 70%, 50% and 30% ethanol for 10 minutes each. (Llewellyn- Smith & Minson, 1992). After a thorough wash in PB any free aldehydes were removed by a 30 min wash with 1% sodium borohydride in PB, this reduces the remaining aldehyde groups and eliminate free reactive groups that may cause non-immunological binding of IgGs and create background labelling and is essential when using glutaraldehyde containing fixatives. (Nässel 1969) After another thorough rinse in PB the ganglia were treated with 0.1% collagenase and 0.1% hyaluronidase in PB for 1hr at 37^{O}C and then washed again in PB. The enzyme digestion helps to the improve permeability of the ganglionic sheath (Stevenson *et al* 1994; Wildman *et al.*2002; Nassel 1996*)*. After incubating for a further 10 minutes in PBT the ganglia were left overnight in PBT, 1%BSA and 5% NGS overnight. Ganglia were then incubated in octopamine antibody (MoBiTec, # 1003GE Germany) diluted 1:200 in PBT, 1%BSA and 5% NGS for 4 days at 4^{O}C then thoroughly

washed with PBT, 1%BSA and 5% NGS. The secondary antibody, Rhodamine Red- labelled goat anti-rabbit (Jackson Labs USA), was diluted 1:200 in PBT, 1%BSA and 5% NGS and sections were incubated for 2 days at 4^{O}c. After thoroughly washing in PBT the ganglia were finally dehydrated through an ethanol series cleared in methyl salicylate and mounted onto cavity slides. Methyl salicylate not only clears the tissue but also has no deleterious affects on fluorescence. Slides were examined with a Zeiss 510 Meta confocal microscope (Carl Zeiss, UK) and imaged using the excitation wavelength 543nm and a long pass 560nm filter. Optical sections were recorded at 5.0-10.0 μm intervals and projected to one plane.

Transverse Frozen Sections.

Transverse frozen sections were used to determine if octopamine was present in the anterior lateral association centre (a LAC), a region of the dorsolateral neuropil known to contain projections of the fSR and dendrites of flight motor neurons, and therefore located where they could potentially modulate the fSR/BA1 synapse.

Mesothoracic ganglia were processed for immunofluorescence to identify if octopamine is present in the neuropil region. The nerve cord was exposed and fixed *in situ* for 5 minutes in 2% paraformaldeyhde and 0.25% glutaraldehyde in PB. After removal, the ganglia were immersion fixed in fresh fixative for a further 1hr at room temperature. The ganglia were then thoroughly washed in PB then cryoprotected overnight in 20% sucrose in PB. After freezing in liquid

nitrogen 50μm cryostat slices were taken and free floated through several changes of PB to remove the sucrose, any free aldehydes were removed by treating for 30 minutes with 1% sodium borohydride in PB and then thoroughly washed again in PB. The slices were left overnight in 0.1M Sorensen's phosphate buffer pH 7.4 with 1% triton X (PBT), 1% BSA and 5% NGS then incubated in octopamine antibody diluted 1:100 in PBT, 1%BSA and 5% NGS for 20hrs at 4^{O}C then thoroughly washed with PBT, 1%BSA and 5% NGS. Primary antibody controls had the octopamine antibody omitted from the incubation medium. Fluorescent labelling was carried out overnight at 4°C by incubating in Rhodamine Red- labelled goat anti-rabbit (Jackson Labs USA) diluted 1:200 in PBT, 1% BSA and 5% NGS. After thoroughly washing in PBT the slices were rinsed in PB and finally mounted on glass slides in 30 % glycerol and stored in the dark at 4^{O}C until they were examined. Slides were examined with a Zeiss 510 Meta confocal microscope (Carl Zeiss, UK) and imaged using the excitation wavelength 543nm and a long pass 560nm filter. Optical sections were recorded at 0.5-1.0 μm intervals and projected to one plane.

Electron Microscopy.

To identify octopamine-IR processes at electron microscope level two different techniques were used. An immunogold cryosectioning method and a pre-embedding immunogold silver intensification technique.

Cryo-Immunolabelling.

The nerve cord was exposed and fixed *in situ* for 5 minutes in 2% paraformaldeyhde and 0.25% glutaraldehyde PB. After removal the mesothoracic ganglia were immersion fixed in fresh fixative for a further 1hr at room temperature, then rinsed with PB. A Vibroslice 725M tissue slicer (Campden Instruments Ltd, U.K.) was used to cut sections of 200μm thickness these were embedded in 10% gelatine and infiltrated overnight in 2.3M sucrose in PB (Geuze and Slot 1980). Ultrathin sections were prepared according to the method of Liou *et al* (1996). Slices were mounted onto pins with the cut face uppermost and plunge frozen in liquid nitrogen. Ultrathin sections (50-100nm) were cut with a cryo immuno diamond knife (Diatome, Switzerland) using a Leica EM UC6 ultramicrotome with EMFC6 attachment. (Leica Microsystems; Vienna Austria). The sections were picked up with 1% methylcellulose 25CP / 1.15M sucrose in PB and placed onto Formvar/carbon coated nickel grids. Immunostaining was carried out according to the method of Posthuma *et al* (1987). Grids were floated in 2% gelatine in PB at 37^{O}C for 20 minutes, thoroughly rinsed in phosphate buffered saline (PBS) with 0.1% glycine to block free aldehyde groups remaining from unreacted the fixative, followed by three 1 minute rinses in PBS with 0.1% BSA. Mesothoracic ganglion sections were then incubated with anti–octopamine (MoBiTec, Germany) at a dilution of 1:100 for 30 minutes at room temperature, rinsed with PBS and then incubated with 10nm protein A gold secondary antibody diluted in PBS with 0.1% BSA (Slot *et al* 1991) for 20minutes. After thorough

washing with PBS the grids were stabilised with 1% glutaraldehyde, rinsed in distilled water and contrasted with 2% aqueous methyl cellulose containing 0.5% aqueous uranyl acetate at 4°C for 5 minutes then embedded in this solution according to the method of Griffiths (1984). The grids are removed individually from the methylcellulose in metal loops; excess methylcellulose is removed and left to dry.

All sections were examined with a Hitachi H7600 transmission electron microscope.

Pre-embedding Immunogold Labelling.

Mesothoracic ganglion that had been fixed in 2% paraformaldeyhde and 0.25% glutaraldehyde in PB were infiltrated overnight in 20 % sucrose in PB. After freezing in liquid nitrogen, 50 μm cryostat sections were free floated through PB to remove the sucrose. Any free aldehydes were removed by treating for 30 minutes with fresh 1% sodium borohydride in PB. The slices were left overnight in 0.1M Sorensen's phosphate buffer pH 7.4 with 1% triton X PBT with 1% BSA and 5% NGS then incubated in Octopamine antibody diluted 1:100 in PBT, 1%BSA and 5% NGS for 20hrs at 4°C. Following the antibody incubation the slices had three washes of PB and were then blocked in PB with 0.2% gelatine and 0.8% BSA for 5 minutes; then incubated in 1nm gold-labelled goat anti-rabbit antibody (Biocell, Uk) diluted 1:50 in PB with 0.1% gelatine and 0.8 % BSA for 2-3hrs. The sections were then washed with PB, fixed with 2% glutaraldehyde in PB for 10 minutes, washed again with PB

and then rinsed with distilled water. The colloidal gold was intensified by silver enhancement with a Biocell kit for 25mins at room temperature followed by a thorough wash in distilled water. Post-fixation was then carried out in 2% aqueous osmium tetroxide for 30 minutes following a water wash the tissue was dehydrated and embedded in L.R.White.

Ultrathin sections (70nm) were cut using a Leica EM UC6 ultramicrotome and mounted on copper grids coated with Formvar, stained for 10mins in 1% aqueous uranyl acetate, rinsed in distilled water and then stained for 10mins and Reynolds Lead citrate (Reynolds 1963). Aqueous uranyl acetate is used to stain L.R. White as ethanolic uranyl acetate softens the resin.

Controls and Specificity Tests

GABA and glutamate antisera

The primary antibodies anti- glutamate (Sigma, UK # G-6642) and anti-GABA antisera (Sigma, UK# A 2052) were obtained from rabbits after immunisation with an antigen-glutaraldehyde-carrier conjugate. Anti-glutamate was developed using purified glutamate conjugated to KLH as the immunogen and was treated to remove lipoproteins. The rabbit anti-glutamate reacted with L-glutamate Glu-KLH, Glu-BSA, and KLH, but not with BSA using a dot blot immunobinding assay. The anti-GABA was developed using GABA-BSA as the immunogen. The antibody was isolated from the antiserum by immunospecific methods of purification (antigen specific affinity isolation removes essentially all rabbit serum proteins, including immunoglobulins

which do not specifically bind to GABA). . Rabbit anti-GABA showed positive binding with GABA, and GABA-KLH in a dot blot assay, and negative binding with BSA (Sigma, UK product information).

The specificity of the anti-GABA antibody was tested by applying it to locust nervous tissue sections and checking for positive staining of known GABA-IR axons, (Leitch and Laurent, 1993). The specificity of the Sigma anti-glutamate was similarly tested and had also been tested in other systems (Pearlstein et al., 1998; Watson et al., 2000). Furthermore, the anti-GABA and anti-glutamate antibodies used had previously been tested on known GABAergic and glutamatergic neurons in mouse cerebellar tissue (Richardson and Leitch, 2005) and also on serial sections from mesothoracic ganglia of locust (Judge. 2000) to check that they were specific and did not label the same population of neurons. Each antibody was tested at doubling dilutions up to 1:32,000; optimal staining was achieved with 1:1000 for the glutamate antibody and 1:500 for GABA antibody.

Preabsorption of the primary antibodies with the immunising peptide eliminated immunoreactivity in agreement with previous studies (Watson.,1988 ; Bicker et al.,1988; Leitch and Laurent, 1993). Preabsorption of the glutamate antiserum with the GABA complex has been shown to not reduce the immunoreactivity (Bicker et al., 1988). Omission controls, in which the respective primary antibodies were replaced with incubating buffer, were also negative.

Octopamine antiserum

The polyclonal octopamine antiserum (MoBiTec, # 1003GE Germany) had been raised in rabbits after immunization with an octopamine-glutaraldehyde-BSA conjugate. The octopamine antibody specificity was determined in an ELISA test by competition experiments. The antibody showed very high cross-reactivity to Octopamine-G-BSA but very little to other amine-G-BSA conjugates or to unconjugated octopamine (Mons and Geffard, 1987). Immunoreactivity was eliminated when the primary antibody was preabsorbed with the octopamine –glutaraldehyde complex (Konings et al., 1988; Stevenson et al., 1992).

Wholemount preparations of locust CNS immunolabelled for octopamine produced similar results to those of Duch et al., (1999). Likewise in transverse and sagittal sections, DUM cell somata were positively stained in agreement with the pattern of staining seen by Stevenson et al., (1992). The antibody was tested at doubling dilutions up to 1:2,000. Sections were incubated overnight in the optimal dilution of 1:100. Omission controls were performed to test the specificity of the secondary antibodies by replacing the primary antibody with incubating buffer; in all cases staining was eliminated.

Results.

Glutamate-IR Contacts On The fSR.

The proportion of synaptic inputs to the fSR that are immunoreactive for glutamate was determined by analysing the number and location of immunogold-labelled and non- labelled contacts on medial and mediolateral/lateral branches of the fSR at each of the four levels indicated in figure 4.1. The levels selected for analysis represent equally spaced transverse sections through the major field of branches of the HRP-filled fSR within the mesothoracic ganglion and correspond to those previously analysed for GABA-IR inputs to the fSR (Judge & Leitch, 1999). A detailed description of the morphology of the fSR branches within the mesothoracic ganglion with respect to the major tracts and neuropil regions has already been published (Judge & Leitch 1999). In brief, the single axon of the fSR runs in towards the CNS in peripheral nerve branch N1D2. As it approaches the CNS it bifurcates sending one branch into prothoracic N6 and the other into mesothoracic N1. On entering the dorsal mesothoracic ganglion it projects medially and posteriorly towards the midline and bifurcates into two main branches, a large medial branch and a smaller lateral branch. The lateral branch subdivides into a medio-lateral and a lateral branch which further divide to form elaborate arborizations in the dorso-lateral neuropil region. The larger medial branch runs parallel and close to the midline throughout the mesothoracic ganglion into the ipsilateral meso-metathoracic connective, and through the

metathoracic ganglion close to the midline, eventually terminating in the fused first three abdominal neuromeres.

For the present study, glutamate-IR inputs and outputs on the main medial branch and side branches of the fSR were analysed separately from those on the mediolateral and lateral field of branches (.2). The mediolateral and lateral field of branches however, were not analysed individually as at level B the two fields of branches are difficult to resolve. The fSR was identified in ultrathin sections by the presence of electron dense DAB-HRP reaction product (Fig. 4.2a.). Synaptic contacts were identified by the presence of a presynaptic bar, presynaptic vesicles and postsynaptic density.

In total 168 synaptic contacts (inputs and outputs) between the fSR and other neurons were identified and analysed for the presence of glutamate-IR in a single mesothoracic ganglion (Table 4.2). Inputs and outputs were intermingled throughout the fields of branches at all levels examined with no evidence of segregation on particular branches, in agreement with a previous report (Leitch & Judge, 1999). The majority of synapses were located on the mediolateral and lateral fields of branches. In total, 63 inputs were identified of which 49 (78%) were located on mediolateral and lateral branches. A similar proportion of inputs were found on these fields of branches by Judge & Leitch (1999); they recorded 16 medial, and 53 mediolateral and lateral inputs representing 76% synaptic inputs to the mediolateral and lateral field of branches.

Fig. 4.2. Electron micrographs showing HRP – filled fSR profiles in the locust mesothoracic ganglion.

A. The profiles of the HRP-filled fSR are uniquely identifiable by the presence of electron dense HRP-DAB reaction product. Scale bar = 500nm.

B. The fSR receives two inputs from (arrow heads) a glutamate immunoreactive process. (identified by the concentrated scattering of gold beads) profile in synaptic contact with the fSR. Scale bar = 500nm.

Fig 4.2. Electron micrographs showing HRP – filled fSR profiles in the locust mesothoracic ganglion.

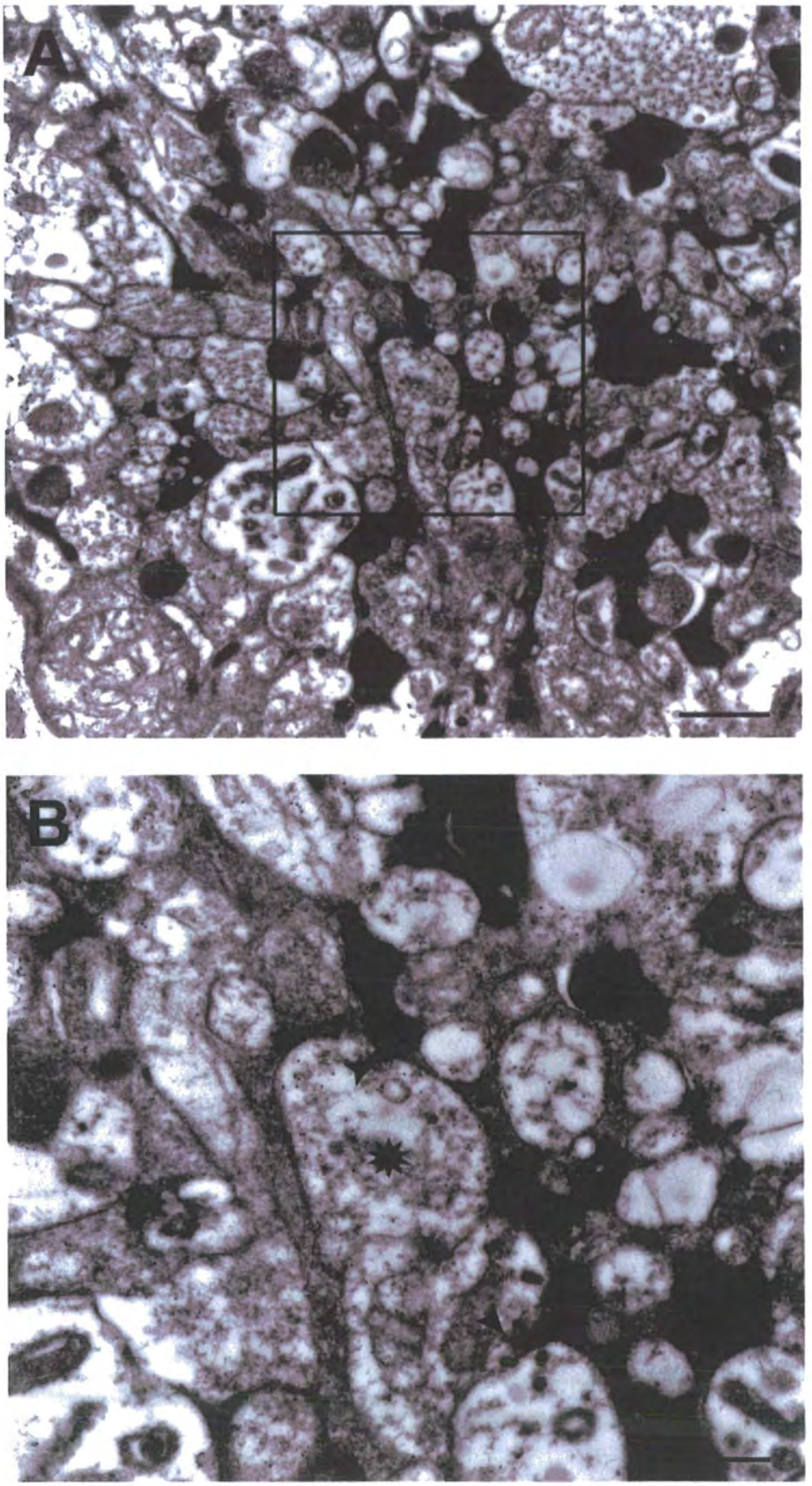

TABLE 4.2. Number and Type of Synaptic Contacts Onto and From the Locust Forewing Stretch Receptor at its Main Field of Branches Analysed in a Single Specimen

SYNAPSE TYPE	LOCATION		
	Medial	Medio-lateral and Lateral	Total
Inputs to the fSR from			
Glutamate-IR	6	29	35
Non-IR	8	20	28
Total inputs	14	49	63
Outputs from the fSR to			
Glutamate-IR	9	39	48
Non-IR	11	46	57
Total outputs	22	85	105
Grand total	34	134	168

Transverse sections through the mesothoracic ganglion labelled with anti-glutamate antibody revealed numerous glutamate-IR (identified by their concentrated scattering of gold beads) profiles in synaptic contact with the fSR. (Fig.4.2b, 4.3). Non-IR inputs had only a very few random scattered gold particles similar to background levels (Fig. 4.4). Glutamate-IR profiles, presynaptic and postsynaptic to the fSR, were randomly distributed on all fields of branches; most, however were located on medio-lateral and lateral branches. Thirty-five out of the 63 identified inputs to the fSR (56%) were immunoreactive for glutamate. Forty-eight of the 105 outputs (46%) from the fSR were made onto profiles immunoreactive for glutamate. A previous study (Judge & Leitch, 1999) had found that approximately (43%) of all inputs to the fSR were GABAergic. This would suggest that the majority of synaptic inputs to the fSR are from either glutamatergic or GABAergic neurons. However, electrophysiological studies have indicated that the synapse between the fSR and the first basilar motoneuron BA1 is modulated by both GABAergic (Judge & Leitch 1999b) and octopaminergic (Leitch *et al.*, 2003) neurons. Taken together the findings from immunolabelling experiments would imply that either very few of the morphologically identifiable synaptic inputs to the fSR are octopaminergic or that octopaminergic neurons do not make structurally recognisable synaptic contacts with the fSR.

Fig. 4.3. The fSR receives a synaptic input from a glutamate immunoreactive process.

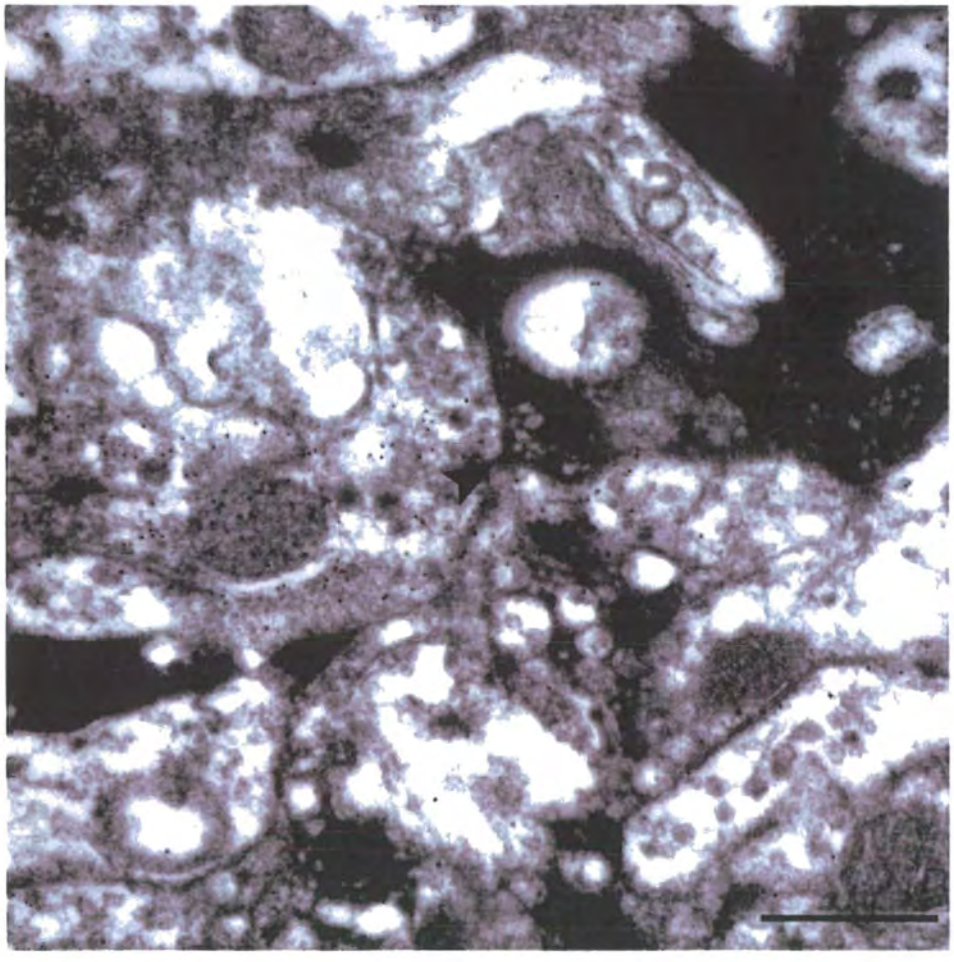

Fig. 4.3. The fSR receives synaptic input (arrow head) from a glutamate immunoreactive process indicated by the high density of gold beads.The glutamate-IR process contains spherical agranular vesicles. Scale bar = 500nm.

Fig. 4.4. The fSR receives synaptic input (arrow head) from a non-glutamate immunoreactive process.

A. Low power electron micrograph showing a dense field of HRP-filled fSR profiles. Scale bar = 2μm

B. Higher power electron micrograph showing the non-glutamate immunoreactive process (arrow head) indicated in **A.** Notice it has only a few randomly scattered gold particles compared to the heavily labelled immunoreactive process (asterix) not making a synaptic contact with the fSR. Scale bar = 500nm.

Fig. 4.4. The fSR receives input from a non-glutamate-immunoreactive process.

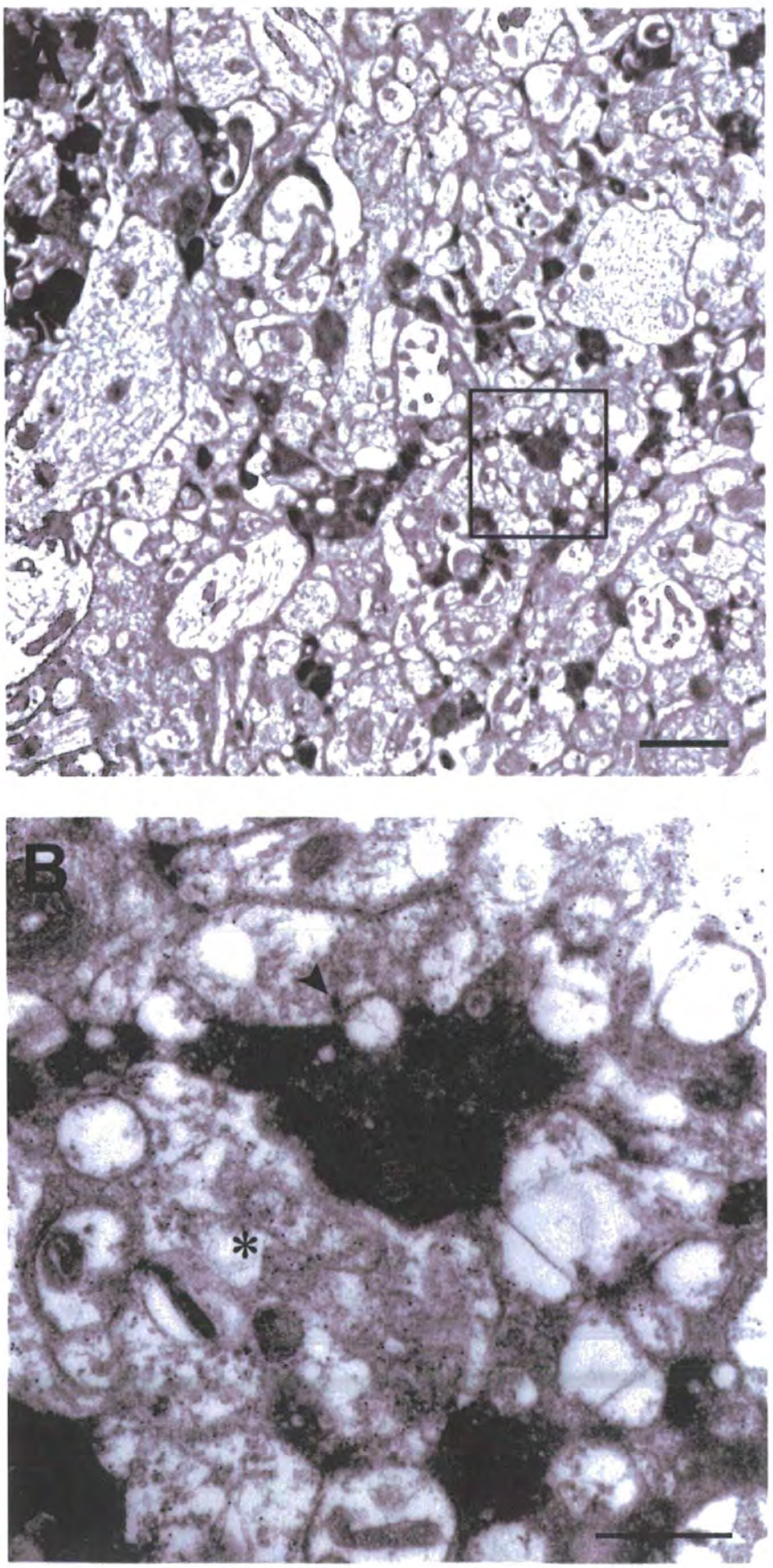

GABA-IR Inputs To The fSR.

To compare the relative proportion of inputs to the fSR that were GABAergic in this study with those reported previously in another locust preparation (Judge & Leitch 1999), a sample of sections were taken from each of the four levels within the same mesothoracic ganglion that had been analysed for glutamatergic inputs. These were immunolabelled with anti-GABA antibody and immunogold labelled to assess the percentage of synaptic inputs that were GABA-IR (Table 4.3) at each of the levels already analysed for glutamate-IR. Approximately 43% of all inputs to the fSR in this study were found to be immunoreactive for GABA (Figs. 4.5 ,4.6). This correlates well with the proportion (43%) of GABA-IR inputs to the fSR reported in the early study (Judge & Leitch 1999) and confirms that over 40% of inputs to the fSR are from GABAergic neurons. Since approximately 55% of inputs in the same preparation were immunoreactive for glutamate, it would appear that most synaptic inputs to the fSR are either glutamatergic or GABAergic.

Identification Of Octopaminergic Neuronal Profiles.

Wholemount preparations immunolabelled for octopamine gave very similar results to those of Duch *et al* 1999. The prothoracic ganglion (Fig.4.7) shows that the antibody is labelling the same population of neurons, two anterior median neurons, two posterior ventral neurons and 10 dorsal unpaired median neurons are clearly labelled. Similarly for the mesothoracic ganglion, a cluster

TABLE 4.3. Number and Type of Synaptic Contacts Onto and From the Locust Forewing Stretch Receptor at its Main Field of Branches Analysed in a Single Specimen

SYNAPSE TYPE	LOCATION		
	Medial	Medio-lateral and Lateral	Total
Inputs to the fSR from			
GABA-IR	1	8	9
Non-GABA-IR	5	7	12
Total inputs	6	16	21
Outputs from the fSR to			
GABA-IR	2	9	11
Non-GABA-IR	6	13	19
Total outputs	8	22	30
Grand total	14	38	51

Fig. 4.5. The fSR receives input (arrow head) from a GABA immunoreactive process, which contains small pleomorphic vesicles. Scale bar = 500nm.

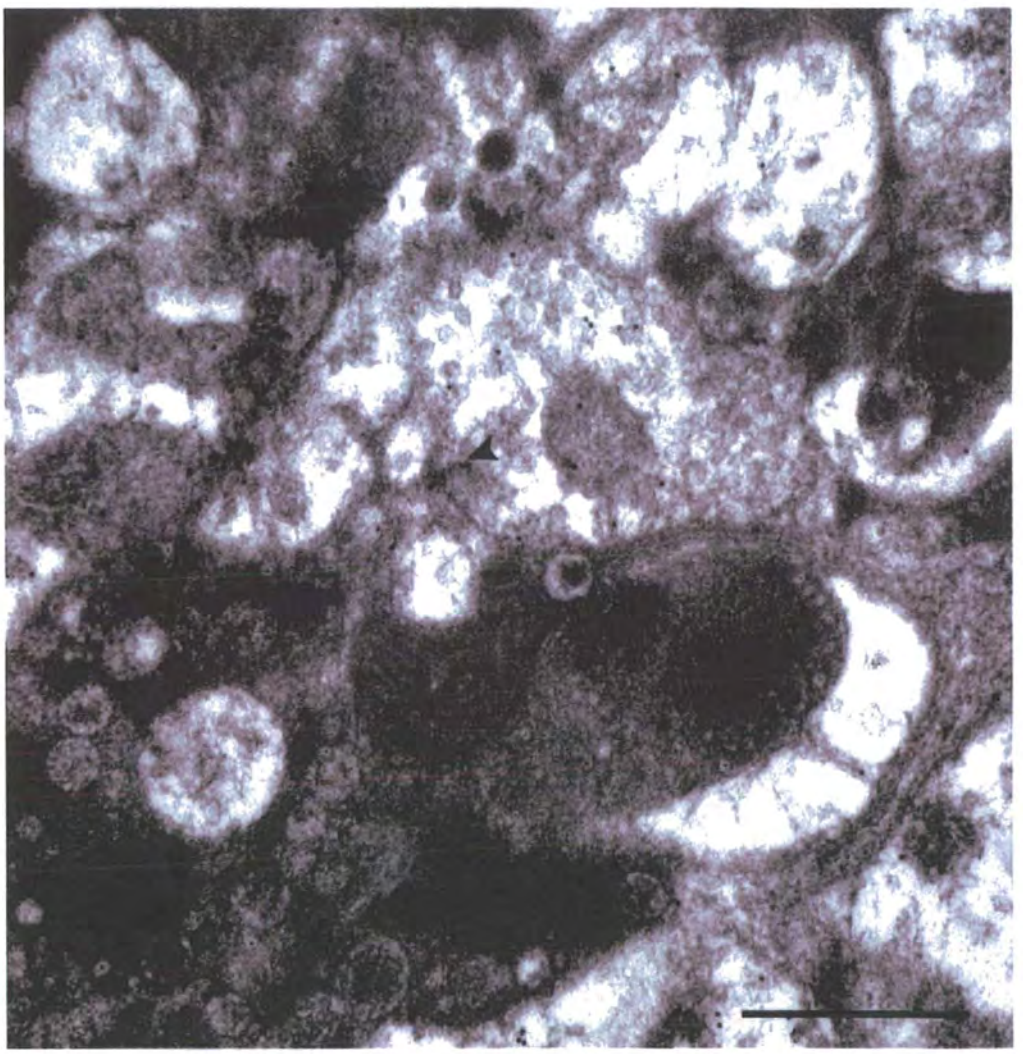

Fig. 4.6. The fSR receives two inputs (arrow heads) from a GABA immunoreactive process, which contains small pleomorphic vesicles.Scale bar = 100nm.

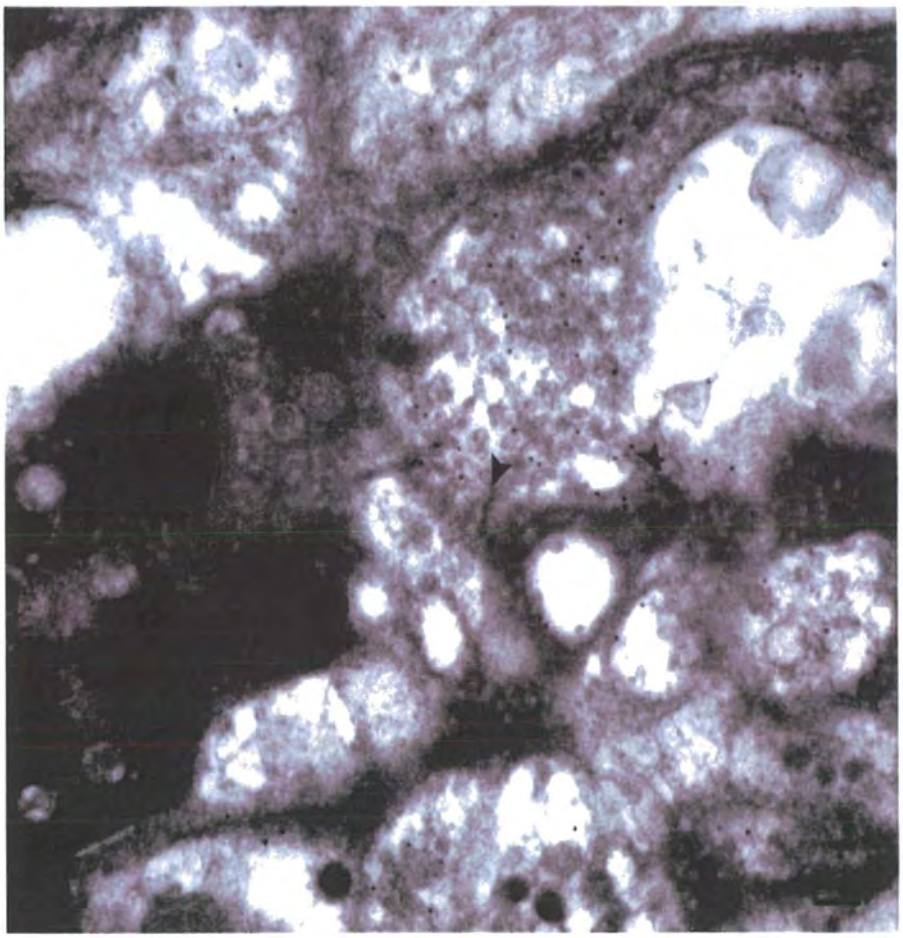

Fig. 4.7. Confocal microscope image from a wholemount of a prothoracic ganglion labelled with anti-octopamine antibody. Showing two anterior median (AM) neurons, two posterior ventral (PV) neurons and 10 pairs of unpaired dorsal neurons. Scale bar = 100μm.

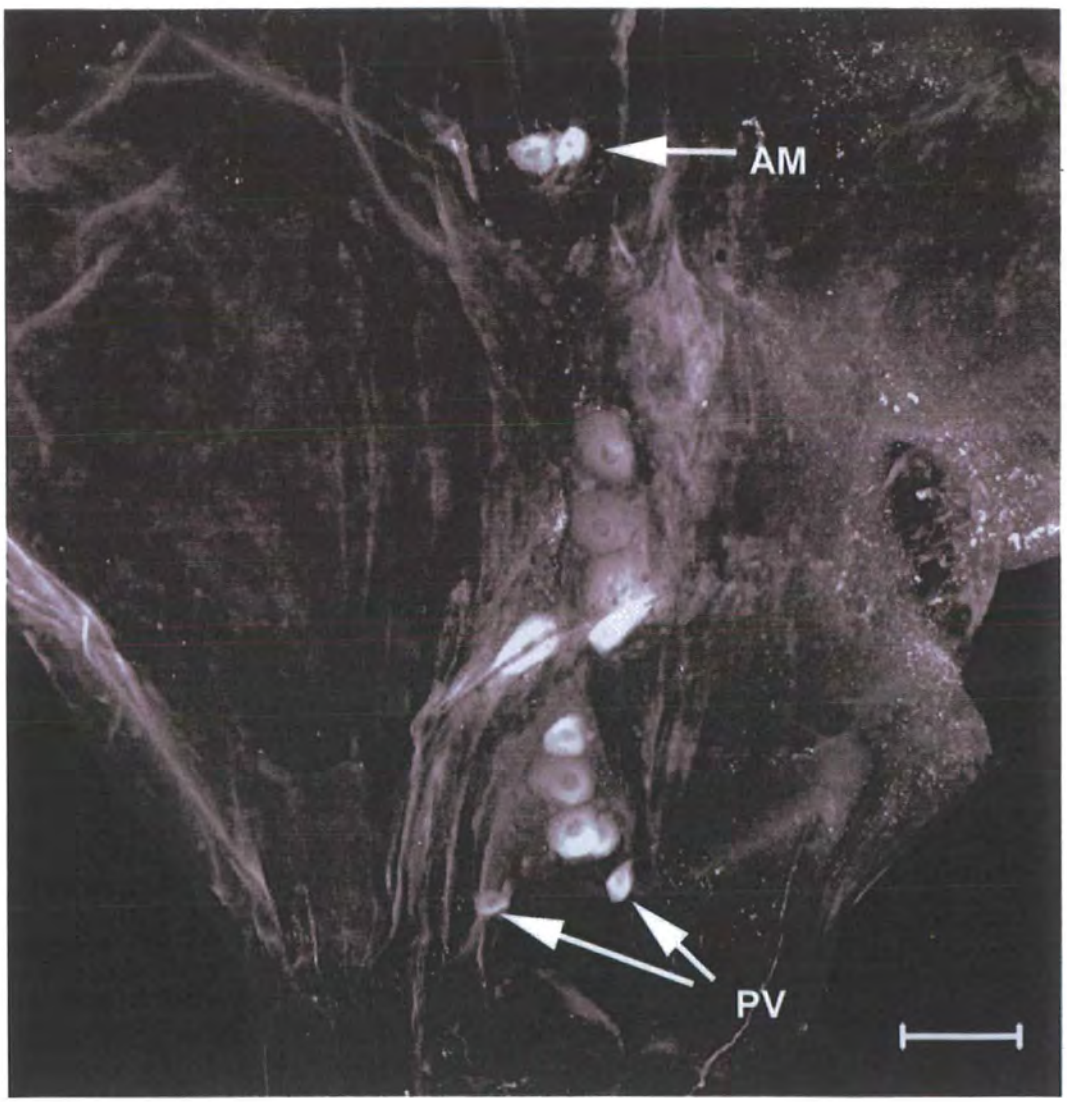

of octopaminergic somata is easily identified (Fig. 4.8). Figure 4.9 A show positively stained DUM cell somata in transverse and sagittal sections agreeing with the pattern of staining seen by Stevenson *et al.*, (1992). The location of immunolabelling with respect to regions of neuropil into which branches of the fSR project were examined (Figs. 4.9 B). Octopamine-IR processes were found within the dorsal and dorsolateral neuropil regions and showed a similar distribution pattern to that previously reported by Stevenson *et al.*, (1992) and Leitch *et al.*, (2003) again confirming the specificity of the antibody labelling. Octopamine-IR was most intense in the dorsal region of each slice coincident with aLAC, the neuropil region into which the dendrites of the fSR and the flight motoneuron project.

To identify octopaminergic neuronal profiles at the EM level, two different methods of gold immunolabelling were used; a pre-embedding labelling technique employing silver intensification of small nanogold particles (Figs. 4.10-4.13) and a cryo-labelling technique using 10nm gold beads (Figs. 4.14-4.16). The post-embedding immunogold labelling technique previously used to identify GABA-IR and glutamate-IR processes in tissue sections in which the fSR had also been processed for HRP-DAB reaction product, could not be employed for identification of potential octopaminergic inputs as the octopamine antibody did not detect octopamine antigen in tissue sections subjected to this processing regime. Instead tissue slices from each of the four levels through the mesothoracic ganglion corresponding to the main field of branches of the fSR were immunolabelled for octopamine-IR using pre-

Fig. 4.8. Confocal microscope image from a wholemount of a mesothoracic ganglion labelled with anti-octopamine antibody.Showing an a cluster of somata at a depth of 100 - 200mm in an extended focus image. (z distance 6μm). Scale bar = 200μm.

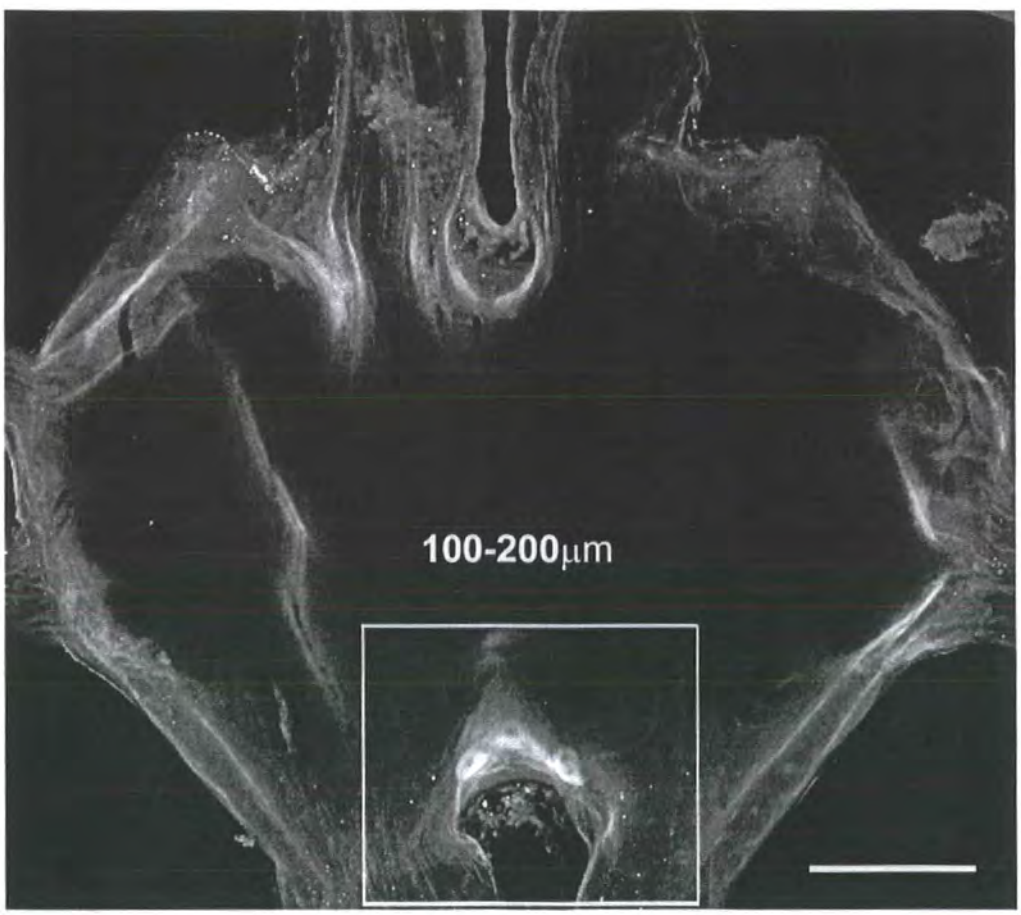

Fig. 4.9. Confocal microscope images from sections of a mesothoracic ganglion labelled with anti- octopamine antibody.

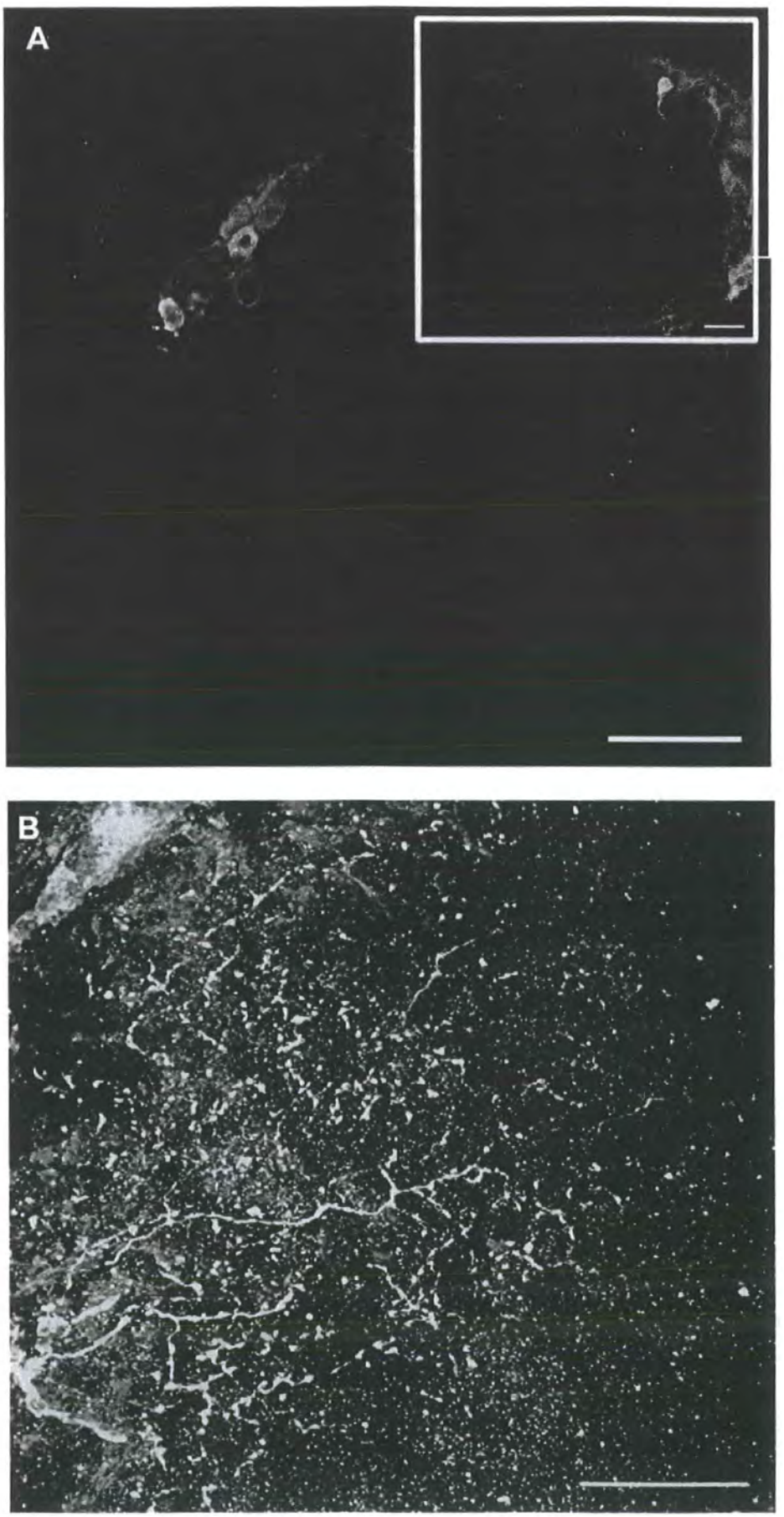

Fig. 4.10. A small profile in the mesothoracic ganglion is labelled with an anti- octopamine antibody. Silver intensified 1nm gold particles are clearly seen in the profile containing the distinct 'elongate' shaped granules. The tissue was immunolabelled using a pre-embedding technique.Scale bar = 500nm

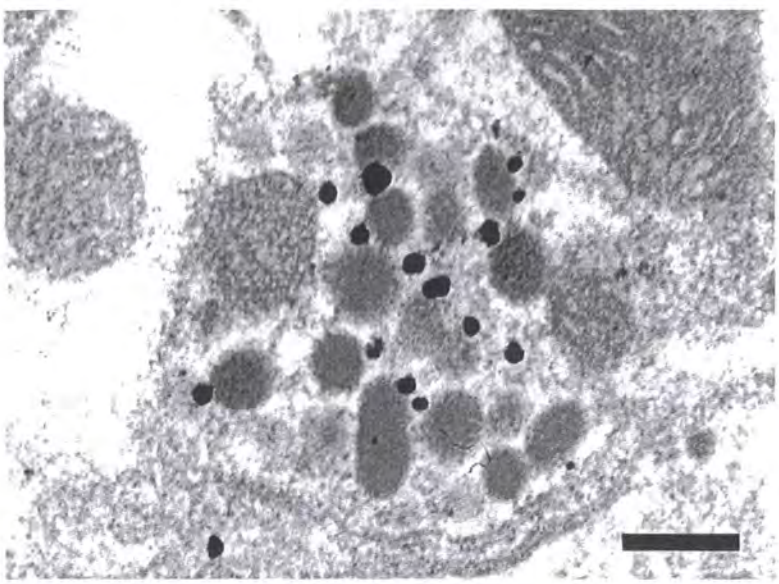

Fig. 4.11. A small profile in the mesothoracic ganglion is labelled with an anti- octopamine antibody. Silver intensified 1nm gold particles are clearly seen in the profile containing distinct 'elongate' shaped granules.The tissue was immunolabelled using a pre-embedding technique.Scale bar = 500nm.

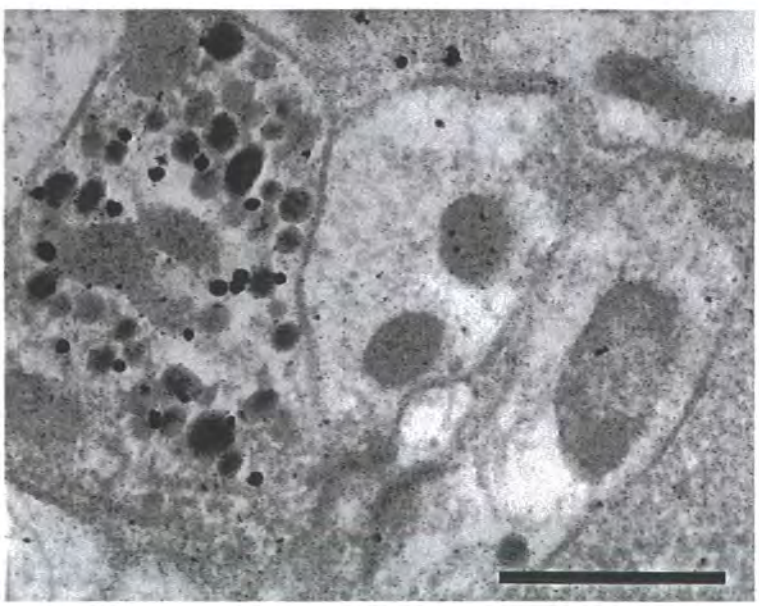

Fig. 4.12. A section from a mesothoracic ganglion labelled with an anti- octopamine antibody and 1nm silver intensified gold particles by a pre-embedding technique.Two distinctly different neuronal profiles are seen. One (white arrow) containing small round granules and another (black arrow) containing larger 'elongated' granules. Only the profile with these distinct shaped granules is labelled. Scale bar = 500nm.

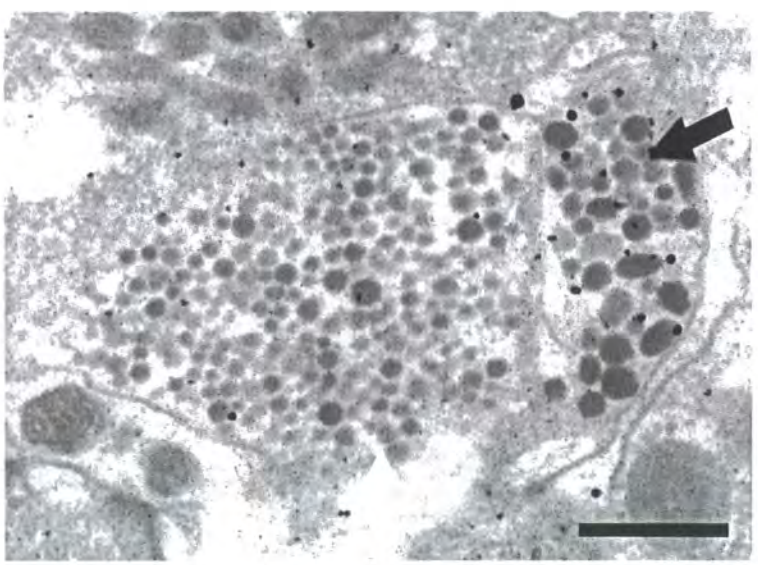

Fig. 4.13. Anti-octopamine labelled profile from a mesothoracic ganglion.

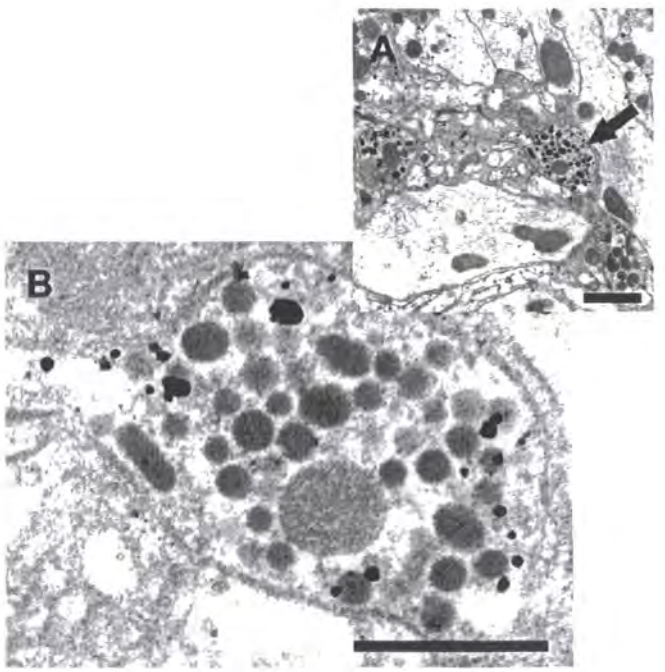

Fig. 4.13. Anti-octopamine labelled profile from a mesothoracic ganglion.

A. A low power electron micrograph showing the location of the profile (black arrow) shown in **B**.

Tissue was prepared using a pre-embedding immunogold silver intensification technique.

Silver intensified 1nm gold particles are clearly seen in the profile with the distinctly shaped granules.

Immunolabelling was carried out using a pre-embedding technique. Scale bars. **A.** =1 um **B.**= 500nm.

Fig. 4.14. Anti-octopamine labelled profile from a mesothoracic ganglion prepared by a cryo-immunogold labelling technique. Note the same 'elongate' shaped granules in the profile. Scale bar = 500nm.

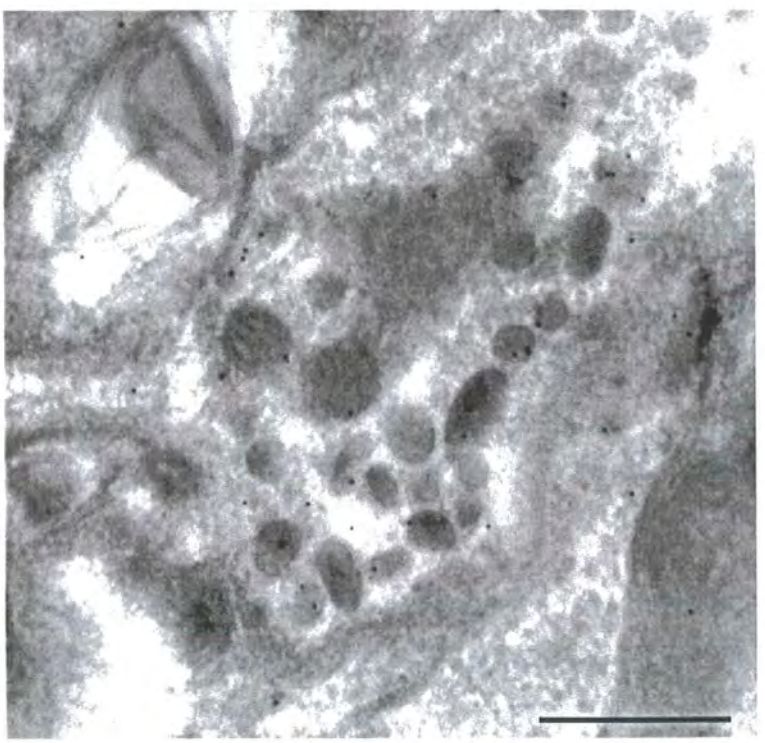

Fig. 4.15. Anti-octopamine labelled profile from a mesothoracic ganglion prepared by a cryo-immunogold labelling technique. Note only profile with the 'elongate' shaped granules is labelled with gold particles. Scale bar = 200nm.

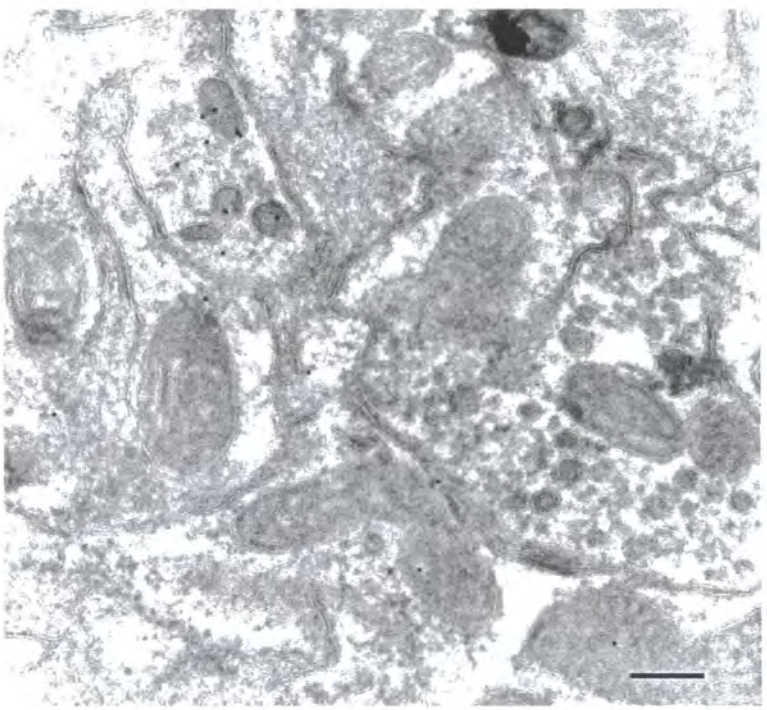

Fig. 4.16. Anti-octopamine labelled profile from a mesothoracic ganglion prepared by a cryo-immunogold labelling technique. Note only profile with the 'elongate' shaped granules is labelled with gold particles. Note that one of the dense cored vesicles (arrow) appears to fusing with the plasma membrane this could be an indication of non-synaptic exocytosis (Volume transmission). Scale bar = 500nm.

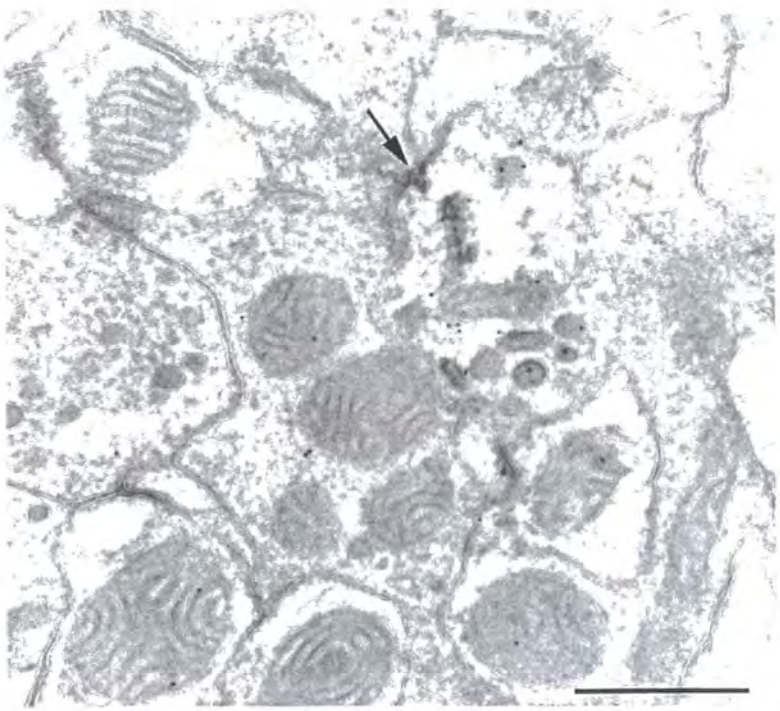

Fig. 4.17. A neuronal profile showing distinctive 'elongate' shaped granules is easily distinguished from other neurons in tissue processed for routine EM without immunolabelling. Scale bar = 500nm.

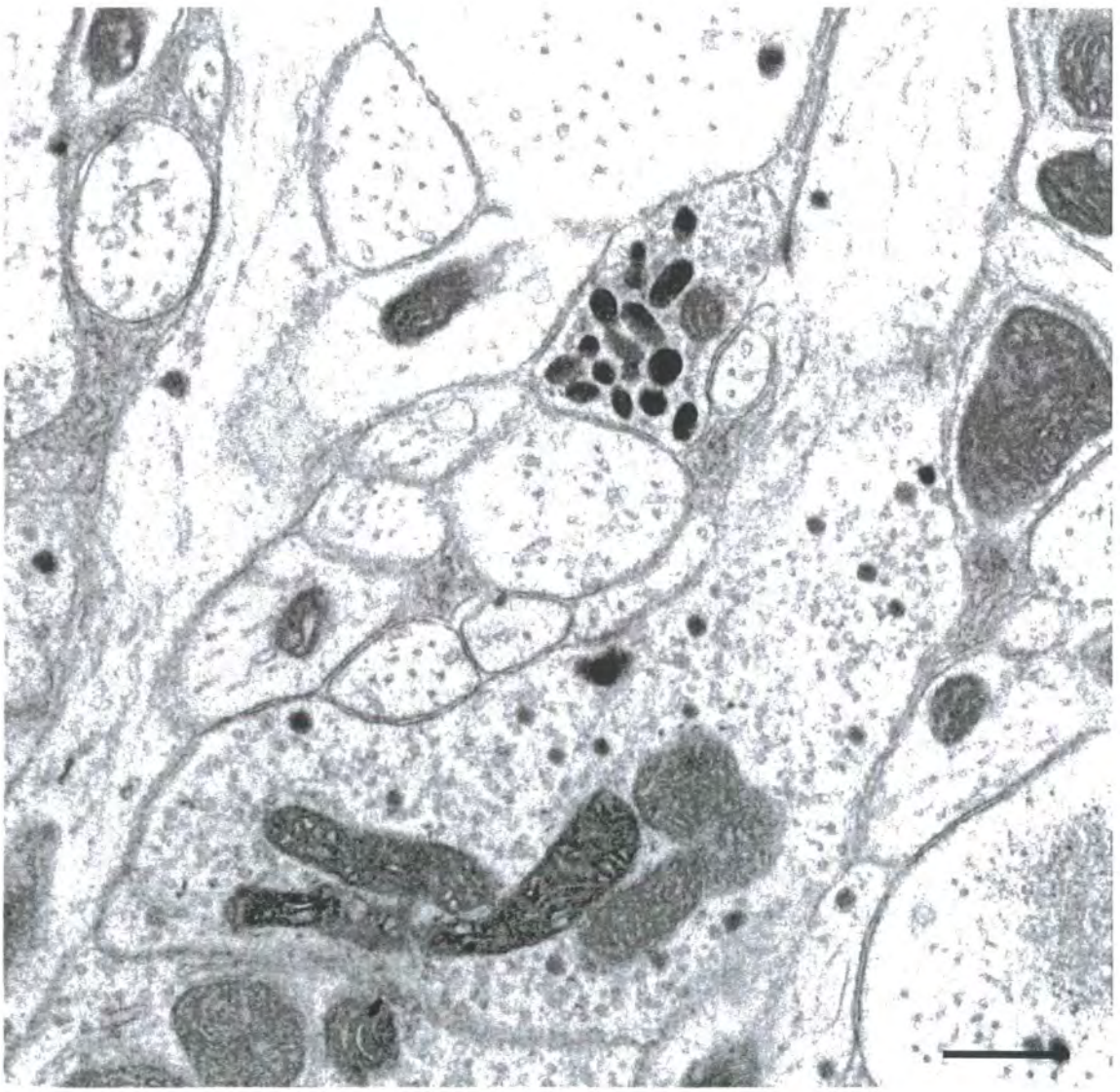

Fig. 4.18. A neuronal profile showing distinctive 'elongate' shaped granules is easily distinguished from other neurons in tissue processed for routine EM without immunolabelling. Scale bar = 500nm.

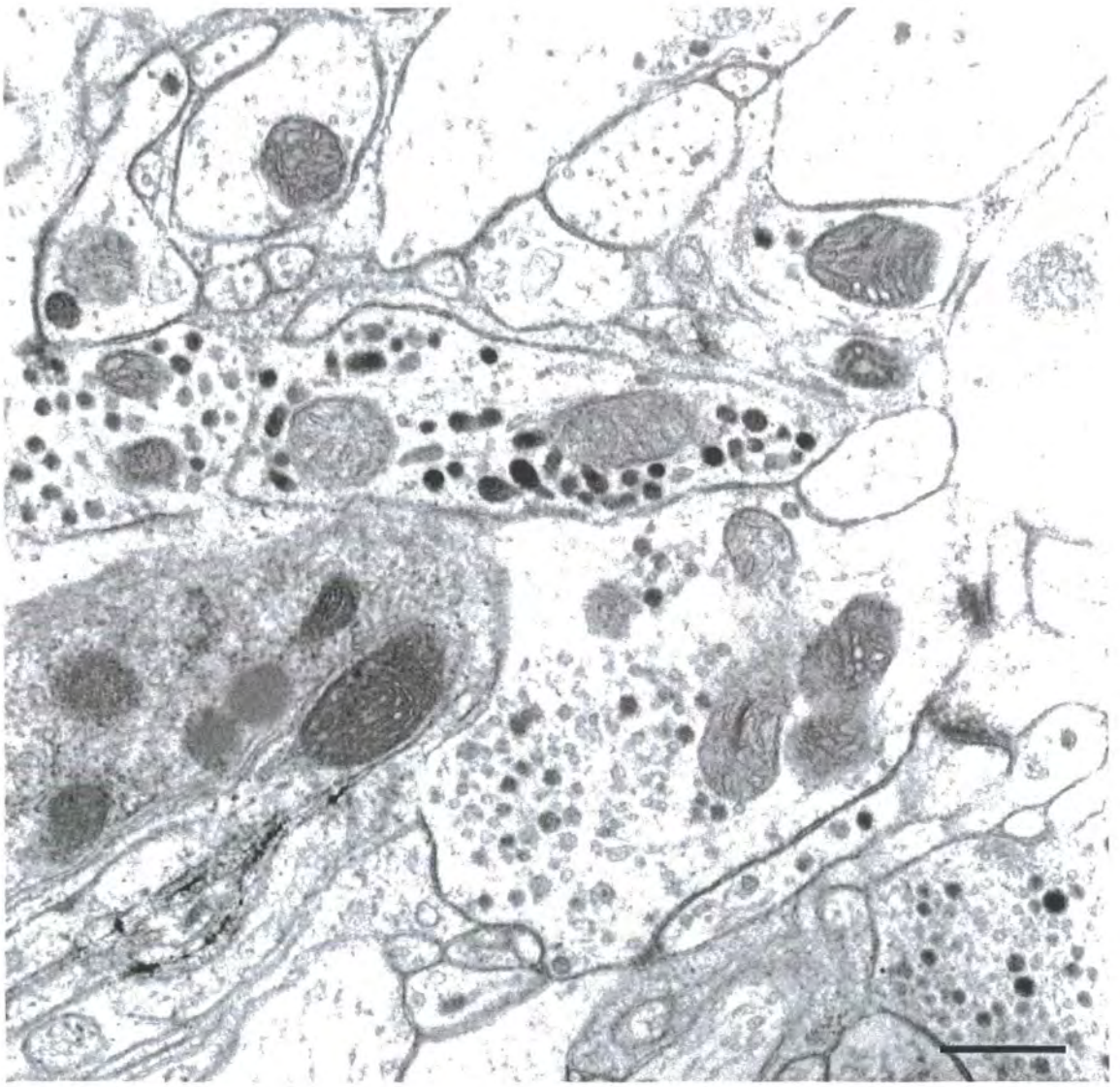

Fig. 4.19. An octopaminergic neuronal profile with two output synapses.

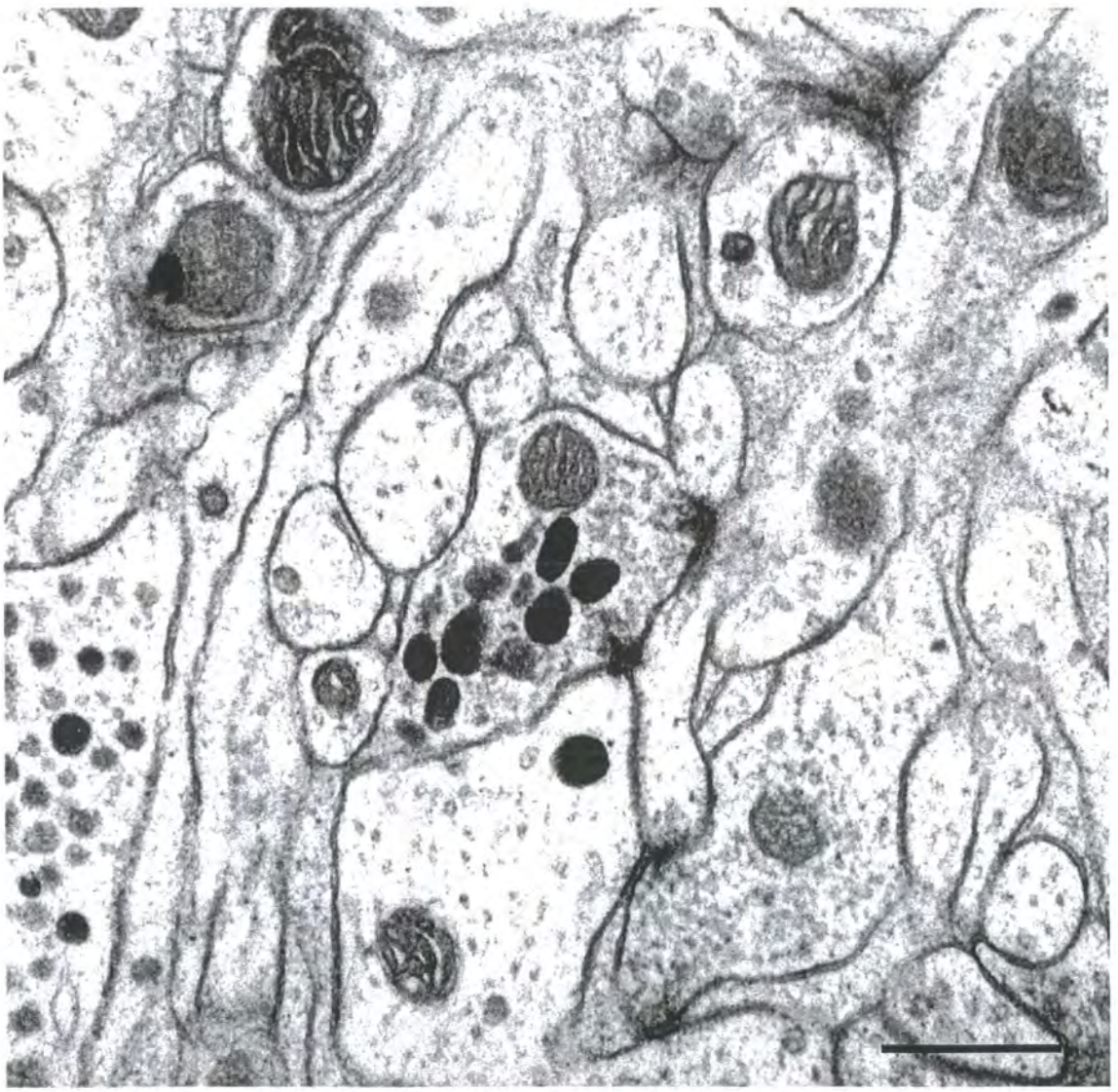

Fig. 4.19. An octopaminergic neuronal profile with two output synapses. Only one profile was found which contained the distinctive electron-dense cylindrical vesicles and also had clearly recognisable output synapses Two output synapses are clearly evident on this profile, each forming classical dyadic contact with two postsynaptic partners. Scale bar =500nm

large dense granules also had small clear elliptical vesicles were also evident in terminals. It was thus possible to identify octopaminergic processes on the basis of the presence of these highly distinctive large electron dense granules in both routinely fixed tissue and also tissue in which the fSR had been labelled with HRP.

Examination of sections, in which the fSR had been filled with HRP-DAB reaction product, revealed nearby profiles with the same distinctive granules (Figs. 4.20-4.21); these processes were therefore considered to be potential octopaminergic neuronal processes. Although neuronal processes containing these distinctive granules were found in several sections closely apposed to HRP-filled fSR profiles, no morphologically recognisable synaptic structure could be discerned. Hence tissue was processed for routine EM, to achieve maximum preservation of synaptic ultrastructure. Sections were sampled and analysed at all levels throughout the mesothoracic ganglion into which the fSR branched to determine if any processes containing these distinctive granules had ultrastructurally recognisable synapses associated with them. Although hundreds of profiles were randomly sampled throughout several mesothoracic ganglion only one profile was found which contained the distinctive electron-dense cylindrical vesicles and also had clearly recognisable output synapses (Fig. 4.19). Two output synapses were clearly evident on this profile, each forming classical dyadic contact with two postsynaptic partners. This would suggest that although profiles, which contain these distinctive granules and are thus potential octopaminergic terminals, have morphologically

Fig. 4.20. A profile with the same distinctive granules lies very close to the fSR filled with HRP-DAB reaction product. No synapses are evident. Scale bar = 500nm.

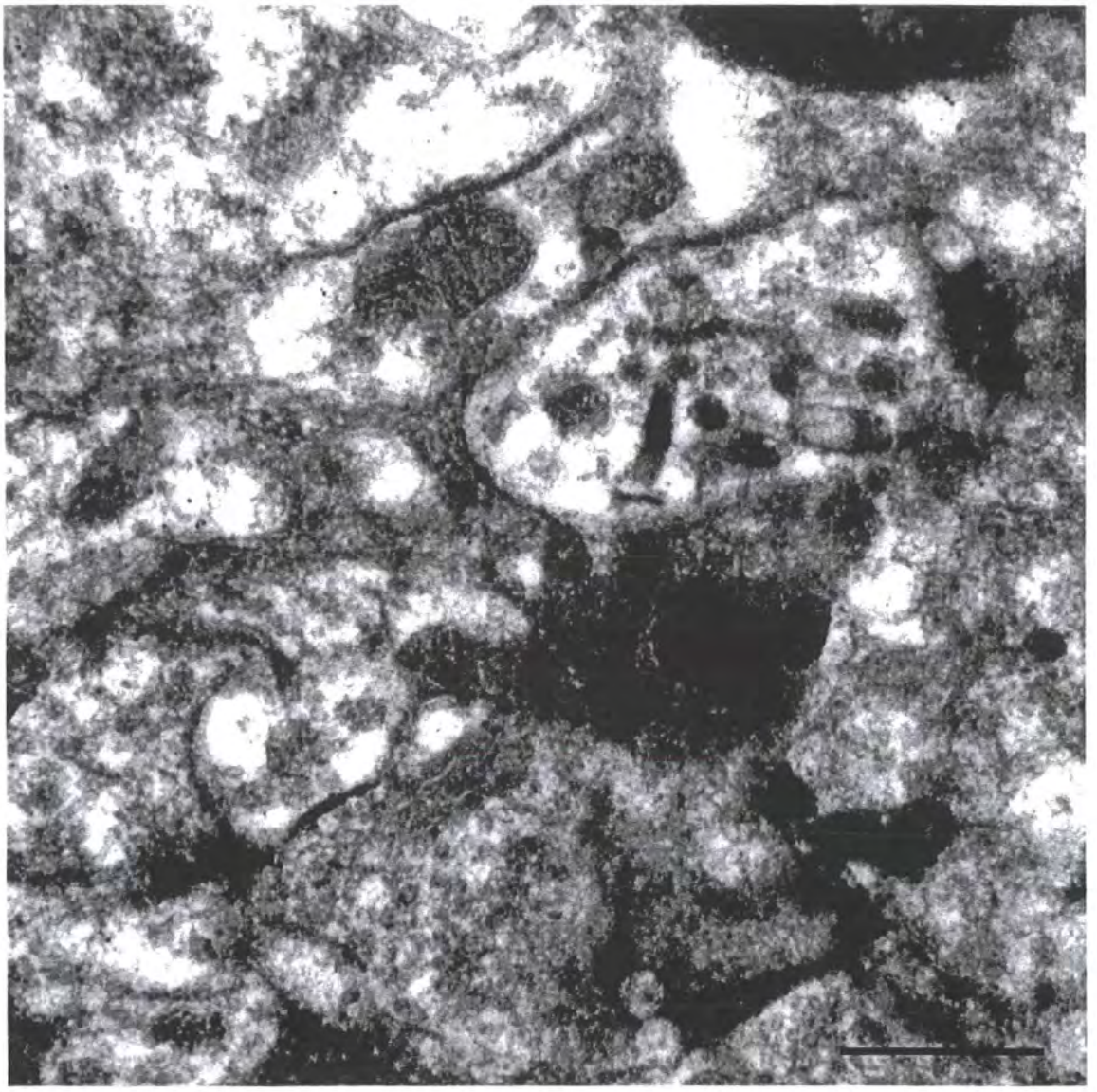

Fig. 4.21. A profile with the same distinctive granules lies very close to the fSR filled with HRP-DAB reaction product. No synapses are evident. Scale bar = 500nm.

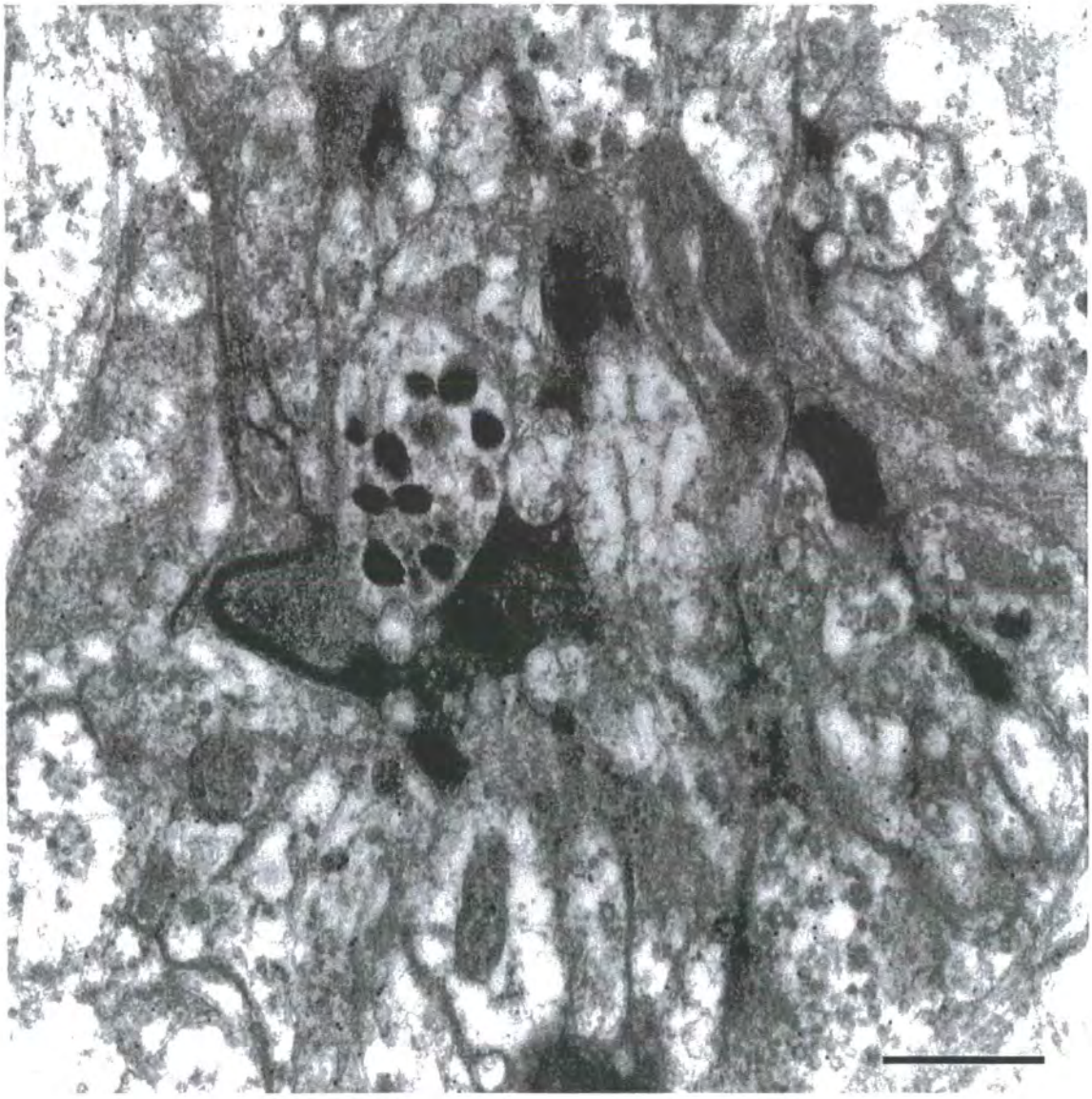

embedding techniques as outlined above and in the methods section. Immunogold labelling was specifically localised over neuronal profiles containing abundant large polymorphic electron-dense granules (Figs. 4.10-14), which had a distinctive morphological appearance similar to the granules identified in octopamine-IR neurons in Limulus (Lee & Wyse, 1991). Profiles containing these large polymorphic granules could be readily distinguished from other profiles containing dense-cored vesicles (Figs. 4.10, 4.15, 4.16) on the basis of the size and appearance of their granules. Dependent on the plane of section the granules appeared as either spherical (cross-section) or sub-cylindrical structures (longitudinal section). They were typically between 80-100nm wide and ranged in length from 100-300 nm. Profiles containing these large distinctive granules were heavily labelled with either silver-intensified gold beads in sections processed for pre-embedded immunocytochemistry (Figs. 4.10- 4.13) or 10nm gold beads in tissue processed for cryo-immunogold labelling (Figs. 4.14- 4.16). Profiles containing smaller dense-cored vesicles were not immunolabelled (Figs. 4.12, 4.15, 4.16). The distinctive size and morphology of the large dense granules allowed octopaminergic terminals and processes to be readily recognised in tissue processed for routine EM (Figs. 4.17- 4.19) without immunolabelling. Such terminals were typically filled with many of these distinctive granules. From routine EM sections it was evident that some of the large dense granules were irregularly cylindrical in shape with a variation in electron-density towards one end and as such were identical to the dense granules reported in octopamine-IR neurons in Limulus CNS (Lee & Wyse, 1991). Terminals containing these

recognisable synapses these are nevertheless relatively rare. No synaptic contacts were ever found in this study between HRP-filled fSR terminals and processes containing these large distinctive granules despite several such processes being found closely apposed to fSR profiles.

Discussion.

Glutamatergic And GABAergic Inputs To The fSR Terminals.

The results from this study show that the majority of synaptic inputs to the fSR terminals in the mesothoracic ganglion of the locust are from either GABAergic or glutamatergic neurons. Glutamatergic neurons were identified by immunolabelling sections with an antibody raised against glutamate that does not label neurons containing GABA, for which glutamate is a precursor. The anti-GABA and anti-glutamate antibodies used had previously been tested on known GABAergic and glutamatergic neurons in mouse cerebellar tissue (Richardson & Leitch 2005) and also on serial sections from mesothoracic ganglia of locust to check that they were specific and did not label the same population of neurons.

In locust mesothoracic ganglia, GABA-IR and glutamate-IR profiles were found presynaptic to HRP-filled fSR terminals at each of the four levels examined through the main fields of branches within the dorsal neuropil. There was no

evidence of segregation of either class of input onto particular branches or at particular levels within the ganglion. They appeared to be randomly intermingled with output synapses made by the fSR and as such are similar to the random distribution pattern exhibited by GABAergic and glutamatergic inputs to other classes of sensory afferents in insects (Watson & Pflüger 1994; Watson *et al.*, 1991).

Approximately 55% of all of synaptic inputs to branches of the fSR within the CNS were immunoreactive for glutamate indicating that glutamatergic neurons potentially could play a key role in presynaptic modulation of the fSR sensory neuron output within the CNS. However, despite the wealth of evidence from numerous ultrastructural ICC studies to implicate glutamate as one of the major neurotransmitters involved in presynaptic modulation of insect afferent neurons, little evidence is available as to its potential role or mechanism of action at CNS synapses. In insects it has been identified as the major neurotransmitter in most excitatory motor neurons (Bicker *et al.*, 1988; Burrows, 1996) and has also been demonstrated in some interneurons (Bicker *et al.*, 1988; Watson, 1988; Watson & Seymour-Laurent 1993). In locusts, a group of thoracic interneurons called group 404, thought to be involved in initiating flight, have been recognised as glutamatergic (Burrows, 1996). However, only a few studies have investigated the effect of glutamate on central synapses in insects. At identified central synapses between antagonistic motor neurons in the locust, glutamatergic transmission has been shown to be excitatory (Sombati & Hoyle, 1984; Burrows *et al.*, 1989; Parker,

1994). Conversely, direct application of glutamate to the desheathed mesothoracic ganglion of the locust or injection into the neuropil has an inhibitory effect on flight motor neurons as recorded in their neuropilar arborisations (Dubas, 1990; 1991). Clearly then glutamate may have either an excitatory or inhibitory effect at central synapses in the locust

In this study, over 40 % of inputs to the fSR were from neuronal profiles immunoreactive for GABA confirming the findings from a previous study by Judge & Leitch (1999a) which reported 43% of all inputs to the fSR terminals within the mesothoracic ganglion were GABAergic. These studies provide morphological support for electrophysiological and pharmacological findings (Judge & Leitch 1999b;) that GABAergic neurons are involved in the presynaptic modulation of the fSR. Several other studies have also provided clear evidence that GABA is the major neurotransmitter mediating presynaptic inhibition in the arthropod nervous system. A study by Watson & Pflüger (1994) found that of the 35 identified inputs to prosternal hair afferent terminals in the locust 18 (51%) were immunoreactive for GABA; 14 (41%) were immunoreactive for glutamate and only 3 were unlabelled. In both this study and ours a high proportion (41% and 55% respectively) of the inputs to sensory afferent terminals were glutamatergic. Interestingly in both studies the sensory afferents under investigation are involved in pathways involving flight motor neurons that control wing position. The sensory afferents that innervate the locust prosternal filiform hairs make strong monosynaptic connections with an identified intersegmental interneuron (A4I1) that is known to contact motor

neurons that supply muscles controlling wing angle during flight. The fSR is a tonic receptor signalling wing position. Presumably GABA and glutamate are both important in modulation of these sensory output signals. Other classes of sensory afferent e.g. those innervating receptors associated with leg joints, have proportionally fewer glutamatergic compared to GABAergic inputs onto their terminal branches. For example, over 90% of processes presynaptic to terminal branches of hair plate afferents on the mesothoracic and metathoracic legs of the locust are GABAergic (Watson *et al.*, 1991). Similarly, 72% of inputs to afferents from campaniform sensilla on the locust leg (Watson and England, 1991) and 78% of inputs to afferents from femoral chordotonal organ a locust leg proprioceptor (Watson *et al.*, 1993) are GABAergic.

Identification Of Octopaminergic Processes Adjacent to the fSR terminals.

Confocal microscopical analysis of a series of tissue sections through the entire mesothoracic ganglion immunolabelled with an anti-octopamine antibody revealed octopamine-IR distributed in a pattern similar to that reported in previous studies (Stevenson *et al.*, 1992; Stevenson and Spörhase -Eichmann, 1995), Octopamine-IR was evident in the anterior lateral association centre (a LAC), a region of the dorsolateral neuropil known to contain projections of the fSR and dendrites of flight motor neurons. The location of these octopamine-positive processes is such that they could mediate modulation of fSR/flight motor neuron synapses.

However, despite electrophysiological and pharmacological evidence (Leitch *et al.*, 2003) that the biogenic amine octopamine modulates synaptic transmission between the fSR and the wing depressor motor neuron BA1, no morphological evidence was found in this study that octopaminergic neurons make ultrastructurally recognisable synaptic inputs onto the fSR. Octopamine-IR processes were clearly identified in ultrathin sections using two independent EM ICC methods (a pre-embedding ICC method and a cryo immunolabelling method on frozen EM sections). In both cases immunolabelled octopaminergic neuronal processes and terminals could be unequivocally identified by the presence of large electron-dense inclusion granules in their cytoplasm. Octopamine-IR was specifically localised over processes and terminals containing these large dense-cored granules measuring 80-100nm wide and 100-300 nm long. These unusual large electron dense granules were similar to the large cylindrical dense-cored granules described in octopaminergic neurons in the CNS of *Limulus* by Lee & Wyse (1991) and Watson and Schürmann 2002) in cricket prothoracic ganglion. Their unique characteristic morphology and presence in all octopamine-IR profiles allowed octopaminergic processes to be identified unequivocally even in tissue slices not immunolabelled with anti-octopamine antibody. Examination of tissue sections containing HRP-filled fSR profiles revealed that although processes containing these characteristic granules, and thus identified as octopaminergic, were located in close proximity to fSR

terminal branches no structural synaptic contacts could be found between them and the fSR.

A potential source of these octopamine-IR processes in the locust are the octopaminergic dorsal unpaired median (DUM) neurons (Watson, 1984). As the processes of the DUM neurons project into the same dorsolateral neuropil region into which the fSR and BA1 project, and in which octopamine-immunoreactivity is present, they are strong candidates as the source of the octopamine, which may potentially modulate transmission across the fSR/BA1 synapse. The peripheral terminals of DUM neurons contain large granular vesicles (60-230nm in diameter) and smaller (28-66nm) agranular vesicles (Hoyle *et al.*, 1980). However, within the central ganglion the primary and lateral neurites, but not the fine neurites, contain scattered granular vesicles 100-180nm in diameter (Watson, 1984). Interestingly, the central neurites of thoracic efferent DUM neurons have only a few sites that might represent output synapses (Watson, 1984). Conventional synaptic structures are not evident at the EM level suggesting that either DUM neurons make very few central output synapses or they release octopamine at sites not ultrastructurally recognised as synapses. In this study the octopaminergic neuronal processes within the central ganglion had no morphologically recognisable synaptic contacts onto the fSR. Recently, Braünig and Burrows (2004) have suggested that one potential source for the modulatory effects of octopamine on central synapses of sensory neuronal projections is the octopaminergic neurons in the sub-oesophageal ganglion. The sub-

oesophageal ganglion contains six descending DUM cells with extensive projections in the pro- and mesothoracic ganglia and all of which are most likely to be octopaminergic (Braünig,1991; Stevenson and Spörhase - Eichmann, 1995). One group (DUM SD 2) projects to dorsal neuropils. Braünig and Burrows (2004) have suggested that the projection patterns of these putatively octopaminergic neurons is such that they could be the source of the octopaminergic modulation of networks underlying sensory processing and motor pattern generation within the thoracic ganglia.

Octopaminergic neurons could potentially release their contents at sites other than identifiable synapses. (Buma and Roubos, 1986; Golding, 1994; Schürmann et al., 1991) By diffusion through intracellular clefts (volume transmission)and modulate the fSR even though it is not in direct contact with it. (Golding 1994). In Fig.4.16 note that one of the dense cored vesicles appears to be fusing with the plasma membrane; this could be an indication of non-synaptic exocytosis (volume transmission).

Chapter 5. Discussion Of Methods.

This study is the first to show the influence that the buffering system can have on antigenicity and clearly demonstrates the improved labelling obtained when using phosphate buffer rather than cacodylate buffer regardless of the embedding resin used. It is not clear why this should be the case, but Coetzee and Van der Merwe (1984), working with bean leaves, found that phosphate buffers lead to less extraction of ions, amino acids and proteins. Conversely, Salema and Brandao (1973) and Kuran and Olszewska (1974) both reported a significant loss of proteins in plant cells and nuclei respectively. However it has been found to redistribute cellular materials along an osmotic gradient and also cause changes in membrane permeability. (Hayat, 2000). Cacodylate is an arsenate based compound and it is thought it may increase the amount of oxygen available for crosslinking reactions by quickly shutting down respiration (Griffith 1993). Increased crosslinking is beneficial for ultrastructural preservation but it is known to be detrimental to antigenicity. It is possible that the reduced antibody binding seen with tissue fixed in cacodylate buffered fixative is at least partially due to increased crosslinking.

The results also show that although the acrylic resin LR White does give higher density immunolabelling for shorter etching times than the epoxy resin Araldite CY212, it does so at the expense of ultrastructure. This seems to be a major limitation of the acrylics (Skepper 2000). The ultrastructural preservation

of the tissue is important in immuno-electron microscopical procedures, and not only the intensity of the immunolabeling (Brorson 1998b);

The problems encountered with the brain tissue embedded in L.R. White in this study may be due to problems with only dehydrating to 70% alcohol or the method of polymerisation used. It is reported that LR White will polymerise with up to 12% by volume of water present and is best in tissue that has not been totally crosslinked by strong fixation (Newman *et al* 2001). The fact that tissue was very strongly crosslinked with aldehyde and osmium fixation may very well be related to the problems encountered. In fact many labs now dehydrate to 100% alcohol, for example, Electron Microscope Facility, San Diego State University, University of Bristol, Veterinary pathology and University of Pittsburgh, Center for Biologic Imaging all have web pages indicating that they use this method. Polymerization carried out under UV light led to better structural preservation of brain tissue than resin cured with heat or catalyst. (Gocht 1992). If a combined study of immunolabelling and ultrastructure is to be performed on precious experimental tissue then an embedding regime that allows for both to be optimised at the same time, in the same piece of tissue, is highly advantageous. Araldite CY212 gives superior ultrastructural preservation and, simply by increasing the time taken to provide adequate levels of antigen unmasking, similar levels of immunolabel density can be achieved without significant loss of ultrastructural detail. The incubation of the Araldite based sections in sodium metaperiodate (Bendayan and Zollinger 1983, Stirling and Graff, 1995) is a gentle way to de-osmicate and

reveal the hidden antigens. Because there is no surface etching of the resin this is not detrimental to ultrastructure. These methods of pre-treatment have been found to be particularly beneficial for secretory proteins, peptides and neurotransmitters (Probert *et al*, 1981; *et al*, 1986; Varndell et al., 1986; Skepper *et al*.,1988; Watson *et al* 2000). And so, as many others have found, (Brorson and Skjørten 1995; 1996c, 2004; Stirling and Graff, 1995), at least for some antigens, the acrylic resins do not have the considerable influence over the efficiency of immunolabelling the literature leads us to believe. (Newman, 1987, 1989; Newman and Hobart, 1987: Skjorten *et al*, 1992, 1996; Rawdon 1997) and with careful by of manipulating the resin before and after embedding it is possible to improve the immunolabeling of resin sections for electron microscopy without degrading ultrastructure.

It is entirely possible, for some antigens, that archival material, post fixed in osmium tetroxide and embedded in an epoxy could yet prove useful for immunolabelling as there are other more vigorous 'etching' regimes for resin removal.

Semi - quantitative immunogold labelling analysis has already been validated for use in examining the relationship between levels of immunoreactivity of transmitter antibodies and actual neurotransmitter concentration. (Somogyi 1986, Ottersen 1989; Bramham et al., 1990.) The results, for both GABA (Fig. 2.7, 2.10) and glutamate (Fig.3 .4) immunoreactivity, show conclusively that only specimens that have undergone fixation, processing, embedding and

immunolabelling in parallel can be compared for meaningful results to be obtained. The differences seen between the experiments carried out at different times on animals that were perfused embedded and immunolabelled on different occasions indicate how important it is to compare like with like.

All of the estimates of density of synapse and mean length of active zones were based exclusively on single sections and this can lead to overestimation of numbers. For example if glutamatergic terminals averaged 2 μm in diameter and then non- glutamatergic terminals 1 μm in diameter. If the EM sections are 100 nm thick (0.1 μm), then each glutamatergic terminal will show up on 20 sections, on average, and each non- glutamatergic terminal in 10 sections. If you count the number of glutamatergic and non- glutamatergic terminals in one section, many sections, or all of the sections, you will always find that the glutamatergic terminals are over-represented in your sample by twofold. It does not make any difference if you count sections that are adjacent, far apart, or even only one section per ganglion. The overcount of glutamatergic synapses is inherent in each an every section because each terminal shows up in twice as many sections as each non- glutamatergic terminal.

It possible to get a more accurate estimate of synapse density by resorting to a method called the physical disector method (Coggeshall and Lekan 1996.) With this method, adjacent thin sections are examined, and only synapses that show up in the first section and not in the second are counted. This means that synapses are counted only once in a series of however many sections

you wish to evaluate (i.e., the first section in which it shows up or the "top" of the synapse), and cannot over count. To go back to the example, glutamatergic terminals show up in an average of 20 sections, but would only be counted as a "top" once and non- glutamatergic terminals show up 10 times, but again are only counted when they are a "top". As a result, when you use the physical disector, only a single pair of sections are needed assuming that the synapses are relatively homogeneously distributed throughout the tissue to get a reasonable estimate of the total.

When only one section is available an assumption based method could have been used (Coggeshall and Lekan, 1996) to correct the synapse numbers by using a correction factor. This is less accurate than a physical disector method, as it makes assumptions that the terminals are roughly spherical, but it will yield at least a reasonable estimate of the actual synapse numbers in the tissue. In this method, synapse counts (n) are multiplied by mean synapse diameter (D) divided by mean synapse diameter plus section thickness (T) to yield neuron numbers (N); $N = (n \times D)/ [D + T)$. The reasoning is sound if the assumptions are met. Some of the assumptions are that synapses are spherical; that one can recognize any fragment of a synapse sectioned by the microtome knife and that the sections are perfectly smooth. But synapses are not true spheres, thin slices of synapses do fade into background, and sections are not perfectly smooth, this method will not estimate cell or synapse numbers accurately and should be used with caution.

ICC specificity relies on the antibody recognizing only the epitope of the protein used as the immunogen (Burry, 2000). In all of the ICC experiments carried out negative controls were used. Omission of the primary antibody will identify if there is any non-specific binding caused by poor blocking or reactive groups. Pre-absorption controls are often used as evidence of antibody specificity. The paratrope sites on the antibody are blocked by mixing the antibody with an excess of the protein or peptide used as the immunogen. However, Swaab *et al,* 1977; Josephsen *et al,* 1999 and Willingham, 1999 have all shown that pre-absorption controls are not a reliable method for determining antibody specificity. "the absorption control determines only the specificity of the antibody for the incubating protein or peptide and does not prove the specificity of the antibody for the protein in the tissue. An antibody can bind to any epitope that has the correct conformation, and this potentially includes the protein used for immunization, as well as any protein with a similar epitope. Therefore, the absorption control does not indicate that the protein to which the antibody binds in tissues is exactly the same protein that was used to generate the antibody" (Burry 2000). Immunoblotting is a much more reliable and sensitive indicator of antibody specificity. Positive controls, with tissues and cells of known specificity for the antibody also help to confirm the specificity of labelling in the test tissue.

The combined HRP labelling of the fSR and subsequent immunogold labelling allowed the neurotransmitter content of synapses onto the retrogradely

labelled neurons to be identified. This showed that most, but not all, of the inputs to the fSR were immunoreactive for either glutamate or GABA. Octopamine has shown to be a possible candidate as another input to the fSR by electrophysiology and immunofluorescent staining, however the octopamine antibody would not label under the same conditions used for GABA and glutamate. Specific immunolabelling was achieved with immunofluorescence (Figs. 4.7 - 4.9), so a pre-embedding immunolabelling technique was then used following the same fixation and antibody labelling conditions used for the immunofluorescent technique. This gave the very specific labeling shown in Figs. 4.10-4.13 and this was absent in the negative controls. A cryo-immunogold technique confirmed that the same neuronal profiles containing abundant large polymorphic electron dense granules were labelled Figs.4.14-4.16.

This highlights the sensitivity of some antigens to the post-embedding treatment (Humbel *et al* 1998), and the limitations of the combination of retrograde labelling with post-embedding immunocytochemistry. (Smith and Bolam.,1992). But it should be possible, maybe with some adjustment to the fixative, to combine the retrograde labelling of the fSR with HRP and pre – embedding labelling for the octopamine antibody. (Smith and Bolam.,1992).

In conclusion then it is possible with careful planning of conditions (Totterdell *et al* 1992; Skepper 2000; Bolam 1992) to produce meaningful semi-quantitative immunogold labelling on tissue that has been prepared to show superior ultrastructural preservation. Retrograde labelling and post embedding

immunogold labelling can, for many antigens, be combined to elucidate synaptic connectivity between identified neurons. But it is also clear that for immunocytochemical analysis it is the nature of the antibody and of the antigen that directs the way in which they can be visualized.

References.

Alsina, B., Vu, T. and Cohen-Cory, S. (2001) Visualizing synapse formation in arborizing optic axons in vivo: dynamics and modulation by BDNF. Nat. Neurosci., 4: 1093-1101.

Aoki, C., Wu, K., Elste, A., Len, G.W., Lin, S.Y., McAuliffe, G. and Black, I.B. (2000) Localization of brain-derived neurotrophic factor and TrkB receptors to postsynaptic densities of adult rat cerebral cortex. J. Neurosci., Res. 59: 454-463.

Axelrod, J., Saavedra, J.M. (1977) Octopamine. Nature., 10; 265(5594):501-4.

Bao, S., Chen, L., Qiao, X. and Thompson, R. F. (1999) Transgenic brain-derived neurotrophic factor modulates a developing cerebellar inhibitory synapse. Learn. Mem., 6: 276 -283.

Baschong, W., Lucocq, J.J. and Roth, J. (1985) Thiocyanate gold: Small (2–3 nm) colloidal gold for affinity cytochemical labelling in electron microscopy. Histochemistry., 83:409–411.

Baschong, W. and Wrigley, N.G. (1990) Small colloidal gold conjugated to Fab fragments or to immunoglobulin G as high-resolution labels for electron microscopy: A technical overview. J. Electron. Microsc.Tech.,14:313–323.

Baude A, Sequier J-M, McKernan RM, Olivier KR, Somogyi P (1993) The metabotropic glutamate receptor (mGluRloc) is concentrated at perisynaptic membrane of neuronal subpopulations as detected by immnogold reaction. Neuron., 11:771-787.

Bauer, H., Gerber, H. & Horisberger, M. (1975) Morphology of colloidal gold, ferritin and anti-ferritin antibody complexes.
Experientia., 31: 1149-1151.

Bendayan, M., Nanci, A., Herbener, G.H., Gregoire, S. & Duhr, M.A. (1986) A review of the study of protein secretion applying the protein A-gold immunocytochemical approach. Am. J. Anat., 175; 379-400.

Bendayan, M. and Zollinger, M. (1983) Ultrastructural localisation of antigenic sites on osmium-fixed tissues applying the protein A-gold technique. J Histochem. Cytochem., 31: 101-109.

Bernhard, W. and Leduc, E.H. (1967) Ultrathin frozen sections. I. Methods and ultrastructural preservation. J. Cell. Biol., 34(3): 757-71.

Bernard, W. and Viron, A. (1971) Improved Techniques for the Preparation of Ultrathin Frozen Sections. J. Cell. Biol., 49, 731-746.

Bicker, G., Schafer, S., Ottersen, O.P. and Storm-Mathisen, J. (1988) Glutamate-like immunoreactivity in identified neuronal populations of insect nervous systems. J. Neurosci., 8, 2108-2122.

Bolam, J.P. (1992) Preparation of central nervous system tissue for light and electron microscopy. Experimental Neuroanatomy; A practical approach. Oxford University Press., Ed 1. p1-29.

Bolton, M.M., Pittman, A.J. and Lo, D.C. (2000) Brain-derived neurotrophic factor differentially regulates excitatory and inhibitory synaptic transmission in hippocampal cultures. J. Neurosci., 20: 3221-3232.

Boyan, G.S. (1988) Presnaptic inhibition of identified wind-sensitive afferents in the cercal system of the locust. J. Neurosci., 8 (8): 2748-2757.

Bramham, C.R., Torp, R., Zhang, N., Storm-mathisen, J. and Ottersen, O.P. (1990) Distribution of glutamate-like immunoreactivity in excitatory hippocampal pathways – A semiquantitative electron-microscopical study in rats. Neurosci., 39: 405-417.

Braunig, P. (1991) Subesophageal Dum Neurons Innervate the Principle Neuropils of the Locust Brain. Philos. T. Roy. Soc. B., 332 (1264): 221-240.

Braunig, P. and Burrows, M. (2004) Projection patterns of posterior dorsal unpaired median neurons of the locust subesophageal ganglion. J. Comp. Neurol., 478 (2): 164-175.

Brorson, S.H. (1996) Improved immunogold labelling of epoxy sections by use of propylene oxide as additional agent in dehydration, infiltration and embedding. Micron., 27 (5): 345 -353.

Brorson, S.H. (1997a) How to examine the antigen-damaging effect of sodium ethoxide on deplasticized epoxy sections. J. Histochem. Cytochem., 45 (1): 143-146.

Brorson, S.H. (1997b) Bovine serum albumin (BSA) as a reagent against non-specific immunogold labeling on LR-White and epoxy resin. Micron., 28(3): 189-195.Brorson, S.H. (1998a) The combination of high-accelerator epoxy resin and antigen retrieval to obtain more intense immunolabeling on epoxy sections than on LR-white sections for large proteins. Micron., 29 (2-3): 89-95.

Brorson, S.H (1998b) Antigen detection on resin sections and methods for improving the immunogold labeling by manipulating the resin. Histol. Histopathol., 13, 275-281.

Brorson, S.H. (2004) A method for measurements of the efficiency of immunogold labelling of epoxy embedded proteins subjected different retrieval techniques. Micron., 35:619–621

Brorson, S.H. and Nguyen, G.H. (2001) Increased level of immunogold labeling of epoxy sections by rising the temperature significantly beyond 100 degrees C in the antigen retrieval medium. Micron., 32 (6): 591-597.

Brorson, S.H., Skjorten, F. (1995) Mechanism for antigen detection on deplasticized epoxy sections. Micron., 26 (4): 301-310 1995

Brorson, S.H., Skjorten, F. (1996a) Improved technique for immunoelectron microscopy. How to prepare epoxy resin to obtain approximately the same immunogold labeling for epoxy sections as for acrylic sections without any etching. Micron., 27 (3-4) 211-217.

Brorson, S.H., Skjorten, F. (1996b) The theoretical relationship of immunogold labeling on acrylic sections and epoxy sections Micron., 27 (3-4) 193-201.

Brorson, S.H., Skjorten, F. (1996c) The theoretical ratio of immunogold labeling of deplasticized epoxy sections and acrylic sections. Micron., 27 (3-4) 203-209.

Buma, P. and Roubos, E.W. (1986) Ultrastructural demonstration ofnonsynaptic release sites in the central nervous system of the snail *Lymnaea stagnalis*, the insect *Periplaneta americana*, and the rat. Neurosci.,17: 867–879.

Burrows, M. (1975) Monosynaptic connexions between wing stretch receptors and flight motor neurons of the locust. J. Exp. Biol., 62:189-219.

Burrows, M. (1996) The neurobiology of an insect brain. New York. Oxford, Oxford University Press.

Burrows, M. and Laurent, G. (1993) Synaptic potentials in the central terminals of locust proprioceptive afferents generated by other afferents from the same sense organ. J. Neurosci., 13:808–819.

Burrows, M., Watson, A.H.D. and Brunn, D.E. (1989) Physiological and ultrastructural characterization of a central synaptic connection between identified motor neurons in the locust. Eur. J. Neurosci., 1:111–126.

Burry, R.W., Vandre, D.D. and Hayes, D.M.(1992) Silver enhancement of gold antibody probes in pre-embedding electron microscopic immunocytochemistry. J.Histochem. Cytochem., 40(12): 1849-1856.

Burry, R.W. (2000) Specificity Controls for Immunocytochemical Methods. J. Histochem. Cytochem., 48(2): 163–165

Caja,I R.S. (1911) Histologie du systerme nerveux de l'homme et des vertgbr6s. Paris: Maloine,vol. 2.

Campistron, G., Buijs, R.M. and Geffard, M. (1986) Glycine neurons in the brain and spinal cord: antibody production and immunocytochemical localization. Brain Res., 376: 400-405.

Carmona, M.A., Martinez. A., Soler. A., Blasi.J., Soriano.E., Aguado. F. (2003) Ca2+-evoked synaptic transmission and neurotransmitter receptor levels are impaired in the forebrain of trkB (-/-) mice. Mol. Cell. Neurosci., 22 (2): 210-226.

Carmona, M.A., Pozas,E., Martinez, A., Espinosa-Parrilla, J.F., Soriano,E., Aguado, F. (2006) Age-dependent spontaneous hyperexcitability and

impairment of GABAergic function in the hippocampus of mice lacking trkB. Cerebral Cortex., 16 (1): 47-63.

Carter, A.R., Chen, C.F., Schwartz, P.M. and Segal, R. (2002) Brain-derived neurotrophic factor modulates cerebellar plasticity and synaptic ultrastructure. J. Neurosci., 22: 1316-1327.

Causton, B.C. (1984) The choice of resins for electron immunocytochemistry. In PolakJM, Varndell IM, eds. Immunolabelling for electron microscopy. Amsterdam, New York, Oxford, Elsevier Science Publishers, 29.

Causing, C.G., Gloster, A., Aloyz, R., Bamji, S.X., Chang, E., Fawcett, J., Kuchel, G. and Miller, F. D. (1997) Synaptic innervation density is regulated by neuron-derived BDNF. Neuron., 18: 257-267.

Ceccarelli, B., Hurlbut, W.P. and Mauro, A. (1973). Turnover of transmitter and synaptic vesicles at the frog neuromuscular junction. J. Cell. Biol., 57: 499-524.

Chan, J., Aoki, C., and Pickel, V.M. (1990) Optimization of differential immunogold silver and peroxidase labeling with maintenance of ultrastructure in brain sections before plastic embedding. J. Neurosci.Methods., 33:113–127.

Chen, L., Chetkovich, D.M., Petralia, R.S., Sweeney, N.T., Kawasaki, Y., Wenthold, R.J., Bredt, D.S. and Nicol,I R.A. (2000) Stargazin regulates synaptic targeting of AMPA receptors by two distinct mechanisms. Nature., 408: 936-943.

Coetzee, J. & Van der Merwe, C.F. (1989) Extraction of carbon 14-labelled compounds during processing for electron microscopy. J. Electron. Microsc. Tech., 11:155-160.

Coggeshall, R. E. and Lekan, H. A. (1996) Methods for Determining Numbers of Cells and Synapses: A Case for More Uniform Standards of Review. J. Comp. Neurol., 364:6-15

Collin, C., Vicario-Abejon, C., Rubio, M.E., Wenthold, R.J., McKay, R.D.G. and Segal M. (2001) Neurotrophins act at presynaptic terminals to activate synapses among cultured hippocampal neurons. Eur. J. Neurosci., 13: 1273-1282.

Colonnier, M. (1968) Synaptic pattern on different cell types in the different laminae of the cat visual cortex. An electron microscope study. Brain Research., 9(2):268-87.

Coons, A.H., Creech, H.J. & Jones, R.N. (1941) Immunological properties of an antibody containing a fluorescent group. Proc. Soc. Exptl. Biol., Med. 47, 200-202.

Craig, S and Goodchild DJ (1982): Post-embedding immunolabeling. Some effects of tissue preparation on the antigenicity of plant proteins. Eur. J. Cell. Biol., 28:251

Dale, H.H. (1935) Walter Ernest Dixon Memorial Lecture, 1934. Pharmacology and nerve endings. Proc. Roy. Soc. Med. (Therap.Sect)., 28, 319.

De Graaf, A., Humbel, B.M., Stuurman, N., van Bergen en Henegouwen, P.M.P., and Verkleij, A.J. (1992) Three-dimensional immunogold labeling of nuclear matrix proteins in permeabilized cells. Cell. Biol. Int. Rep., 16:827–836.

De Valck, V., Renmans,W., Segers, E., Leunissen, J., and DeWaele, M. (1991) Light microscopical detection of leukocyte cell surface antigens with a one-nanometer gold probe. Histochem., 95:483–490.

Descarries, L Gisiger, V., and Steriade, M (1997).Diffuse transmission by acetylcholine in the CNS. Prog. Neurobiol., 53; 603 – 625.

Di Pasquale, E., Keegan, K.D. and Noebels, J.L. (1997) Increased excitability and inward rectification in layer V cortical pyrimidal neurons in the epileptic mutant mouse stargazer. J. Neurophysiol., 77: 621-631.

Dluzen, D.E., Story, G.M., Xu, K., Kucera, J. and Walro, J.M. (1999) Alterations in nigrostriatal dopaminergic function within BDNF mutant mice. Exptl. Neurol., 16:500-507.

Dobrunz, L.E. and Stevens, C.F., (1997) Heterogeneity of release probability, facilitation, and depletion at central synapses. Neuron., 18:995–1008.

Dosemeci, A., Tao-Cheng, J., Vinade, L., Winters, C. A., Pozzo-Miller, L.D. and Reese, T.S. (2001) Glutamate-induced transient modification of the postsynaptic density. Pro. Natl. Acad. Sci., USA, 98:10428-10432.

Dubas, F. (1990) Inhibitory effect of L-Glutamate on the neuropil arborizations of flight motoneurons in locusts. J. Exp. Biol., 148: 501-508.

Dubas, F. (1991) Actions of putative amino-acid neurotransmitters on the neuropil aborizations of locust flight motoneurons. J. Exp. Biol., 155: 337-356.

Duch, C., Mentel, T. and Pflüger H.J. (1999) Distribution and activation of different types of octopaminergic DUM neurons in the locust. J. Comp. Neurol., 403:119-134.

Duch , C. & Pfluger, H.J. (1999) DUM neurones in locust flight: a model system for amine-medicated peripheral adjustments to the requirements of a central motor program. J. Comp. Neurol., 184:489-499.

Dugich-Djordjevic, M.M., Tocco, G., Willoughby, D.A., Najm, I., Pasinetti, G., Thompson, R.F., Baudry, M., Lapchak, P.A. and Hefti, F. (1992) BDNF messenger-RNA expression in the developing rat-brain following kianic acid-induced seizure activity. Neuron., 8: 1127-1138.

Eccles, J. C., M. Ito, and J. Szentagothai. (1967) The Cerebellum as a Neuronal Machine. Springer Publishing Co., Inc., New York.

Eccles, J. C., Llinás, R. and Sasaki, K. (1966) The excitatory synaptic action of climbing fibres on the Purkinje cells of the cerebellum J. Physiol., 82(2): 268–296.

Eckert, M., Rapus, J., Nurnberger, A. and Penzlin, H. (1992) A new specific antibody reveals octopamine-like immunoreactivity in cockroach ventral nerve cord. J. Comp. Neurol., 322:1–15.

Elliot, T.R., 1904. On the action of adrenaline. J. Physiol. (Lond.) 31, XX–XXI.

El Manira, A. and Clarac, F. (1991) GABA-mediated presynaptic inhibition in crayfish primary afferents by non-A, non-B GABA receptors. Eur. J. Neurosci., 3: 1208 –1218.

Evans, P. D. (1981). Multiple receptor types for octopamine in the locust. J. Physiol., Lond. 318: 99–122.

Evans, P.D. (1985) Octopamine. In: Kerkut, G.A., Gilbert, L.I. editors. Comprehensive insect physiology biochemistry and pharmacology. Oxford: Pergamon. 499–530.

Faulk, W.P. and Taylor, G.M. (1971) An immunocolloid method for the electron microscope. Immunochemistry., 8: 1081.

Feldblum, S., Ackermann, R.F. and Tobin, A.J. (1990) Long-term increase of glutamate decarboxylase mRNA in a rat model of temporal lobe epilepsy. Neuron., 5: 361-371.

Fesce, R.,Grohovaz, F., Valtorta, F. and Meldolesi, J. (1994). Neurotransmitter release:fusion or 'kiss-and-run'? Trends in Cell Biology,, 4:1-4.

Gabbott, P.L.A., Somogyi, J., Stewart, M.G. and Himori, J. (1986) GABA-immunoreactive neurons in the rat cerebellum: a light and electron microscope study. J. Comp. Neurol., 251:474.

Geffard, M., Henrich-Rock, AM., Dullac, , J., Seguela, P. (1985) Antisera against small neurotransmitter-like molecules Neurochemistry international., 7(3):403-413.

Geuze, J.J., Slot, J.W. and Tokuyasu, K.T. (1979) Immunocytochemical localization of amylase and chymotrypsinogen in the exocrine pancreatic cell with special attention to the Golgi complex. J. Cell. Biol., 82 :697-707.

Ghez, C., Thach. W.T. (2000) The cerebellum. In: Principles of neural science, Ed 4 (Kandel ER, Schwartz JH, Jessell TM, eds), pp 832-852. New York: McGraw-Hill.

Glauert, A.M. (1975). Fixation, dehydration and embedding of biological specimens. Practical methods in electron microscopy. Amsterdam, North-Holland Publishing Company.

Golding, D.W. (1994) A pattern confirmed and refined- synaptic, nonsynaptic and parasynaptic exocytosis. BioEssays., 16:503–508.

Good, N.E., Winget, G.D., Winter, W., Connolly, T.N., Izawa, S., & Singh, R.M.M. (1966) Hydrogen ion buffers for biological research. Biochemi., 5(2) 467-477.

Gocht, A. (1992). Use of LR white resin for post-embedding immunolabelling of brain tissue. Acta. Anat., (Basel). 145(4):327-39.

Gottschalk, W., Pozzo-Miller, L.D., Figurov, A. and Lu, B. (1998) Presynaptic modulation of synaptic transmission and plasticity by drain-derived neurotrophic factor in the developing hippocampus. J. Neurosci., 18: 6830-6839.

Gray, E.G. (1959) Axo-somatic and axo-dendritic synapses of the cerebral cortex: an electron microscope study. J. Anat. (Lond.), 93:420-433.

Griffiths, G. (1984) Selective contrast for electron microscopy using thawed frozen sections and immunocytochemistry. In: Revel, J. P., T. Barnard, G.H. Harris (eds). Proc. Congr. Specimen Preparation. Traverse City, Michigan, SEM Inc., Chicago., 153-159.

Griffiths, G. (1993) Fine structure immunocytochemistry. Springer. Verlag, Heidelberg.

Griffiths, G. and H. Hoppeler. (1986) Quantitation in immuncytochemistry, correlation of immunogold labelling to absolute numbers of membrane antigens. J.Histochem. Cytochem., 34:1389-1398.

Griffiths, G., Simons, K., Warren, G. and Tokuyasu, K.T. (1983) Immunoelectron microscopy using thin frozen sections: applications to studies of the intracellular transport of Semliki Forest virus spike proteins. Methods Enzymol., 96:466-484.

Gustavson, K.H. (1956). The Chemistry of Tanning Processes. New York: Academic Press.

Hainfeld, J.F. (1987) A small gold-conjugated antibody label: Improved resolution for electron microscopy. Science., 263:450–453.

Hainfeld, J.F. (1988) Gold cluster-labeled antibodies. Nature., 333:281–282.

Hainfeld, J.F., and Furuya, F.R. (1992) A 1.4-nm gold cluster covalently attached to antibodies improves immunolabeling. J. Histochem. Cytochem., 40:177–184.

Hàmori, J., Takàcs, J. & Petruz, P. (1990) Immunogold Electron Microscopic Demonstration of glutamate and GABA in normal and deafferented cerebellar cortex: correlation between transmitter content and synaptic vesicle size. J Histochem. Cytochem., 38 (12): 1767-1777.

Hamori, J. and Szentagothai, J. (1966) Participation of Golgi neuron processes in the cerebellar glomeruli: an electron microscope study. Exp. Brain. Res. 2: 35-48.

Hand, A.R. and Jungmann,R.A. (1989) Localization of cellular regulatory proteins using postembedding immunogold labelling. Am. J. Anat. 185:183-196.

Hanse, E. & Gustafsson, B. (2001a) Vesicle release probability and pre-primed pool at glutamatergic synapses in area CA1 of the rat neonatal hippocampus. J. Physiol. (Lond.) 531: 481–493.

Hanse, E. & Gustafsson, B. (2001b) Paired-pulse plasticity at the single release site level: an experimental and computational study. J. Neurosci. 21:8362–8369.

Hanse, E. & Gustafsson, B. (2002) Release dependence to a paired stimulus at a synaptic release site with a small variable pool of immediately releasable vesicles. J. Neurosci. 22: 4381–4387.

Hardy, P.M., Nicholls, A.C., Rydon, H.N. (1976)The nature of the cross-linking of proteins by glutaraldehyde. Part I. Interaction of glutaraldehyde with amino-groups of 6-aminohexanoic acid and of alpha-N-acetyl-lysine. J. Chem. Soc. (Perkin I) 1:958.

Harris, J. R., Bhella, D. and Adrian,M. (2006) Recent Developments in Negative Staining for Transmission Electron Microscopy. Microscopy and Analysis 20(3):17-21 (UK).

Hashimoto, K., Fukaya, M., Qiao, X., Sakimura, K., Watanabe, M. and Kano, M. (1999) Impairment of AMPA receptor function in cerebellar granule cells of the ataxic mouse stargazer. J. Neurosci., 19: 6027-6036.

Hayashi, T., Umemori, H., Mishina, M. and Yamamoto, T. (1999) The AMPA receptor interacts with and signals through the protein tyrosine kinase Lyn. Nature., 397: 72-76.

Hayat, M. A. (1989) Rinsing, dehydration and embedding. In:Principles and Techniques of Electron Microscopy. The Macmillan Press Ltd, p. 88.

Hayat, M. A. (1970.) Polymerization. In: Principles and Techniques of Electron Microscopy. Vol. I. Van Nostrand Reinhold Company,p. 140.

Hayat, M.A. (2000) Principles and Techniques of Electron Microscopy, Biological Applications. 4th Edition. Cambridge, Cambridge University Press.

Hayat, M.A. (2002) Antigens and antibodies. In: Microscopy, Immunohistochemistry, and antigen retrieval methods for light and electron microscopy, ed. Hayat MA, pp 31-51, Kluwer Academic, New York, NY.

Helenius, A., and Simons, K. (1975) Solubilization of membranes by detergents. Biochim. Biophys. Acta, 415:29–79.

Heuser, J.E. (1981) Comparing several detergents commenly used to visualise the cytoskeleton. J. Cell. Biol., 91:302a.

Heuser ,J.E. (1989) Review of electron microscopic evidence favouring vesicle exocytosis as the structural basis for quantal release during synaptic transmission. Q. J.Exp. Physiol., 74(7):1051-69.

Heuser, J.E. and Reese, T.S. (1973). Evidence for recycling of synaptic vesicle membrane during transmitter release at the frog neuromuscular junction. J. Cell. Biol., 57: 315-344.

Holm, R., Nesland, J.M., Attramadal, A., Johannessen, J.V. (1988) Double-staining methods at the ultrastructural level applying colloidal gold conjugates. Ultrastruct. Pathol., 12:279-290.

Horisberger, M. (1981) Colloidal gold a cytochemical marker for light and fluorescent microscopy and for transmission and scanning electron microscopy. Scanning Microsc., 2: 9-31.

Howell, K.E., Reuter-Carlson, U., Devaney, E., Luzio, J.P. and Fuller, S.D. (1987) One antigen, one gold ? A Quantitative-analysis of immunogold labelling of plasma-membrane 5'-nucleotidas in frozen thin-sections. Eur. J. Cell. Biol., 44 (2): 318-327.

Hoyle, G., Colquhoun, W. and Williams, M. (1980) Fine structure of an octopaminergic neuron and its terminals. J. Neurobiol., 11:103 – 126.

Hu, B.R., Park, M., Martone, M.E., Fischer, W.H., Ellisman, M.H. and Zivin, J.A. (1998) Assembly of proteins to postsynaptic densities after transient cerebral ischemia. J. Neurosci., 18: 625-633.

Huang, E.J. and Reichardt, L.F. (2001) Neurotrophins: Roles in neuronal development and function. Ann. Rev. Neurosci., 24: 677-736.

Huang, Z.J., Kirkwood, A., Pizzorusso, T., Porciatti, V., Morales, B., Bear, M.F., Maffei, L. and Tonegawa, S. (1999) BDNF regulates the maturation of inhibition and the critical period of plasticity in mouse visual cortex. Cell., 98: 739-755.

Hue, B. and Callec, J.J. (1983) Presynaptic inhibition in the cercal-afferent giant-interneurone synapses of the cockroach, (*Periplaneta Americana)*. J.Insect. Physiol., 291:741–748.

Humbel, B.M., Sibon, O.C., Stierhof,Y.D., Schwarz, H. (1995) Ultra-small gold particles and silver enhancement as a detection system in immunolabeling and in situ hybridization experiments. J. Histochem. Cytochem., 43(7):735-7.

Humbel, M.B., de Jong, M.D.M., Müller, W.H. and Verkleij, A.J. (1998) Pre-embedding immunolabeling for electron microscopy: An evaluation of permeabilization methods and markers. Micros. Res.Tech.., 42:43–58.

Hulstaert, C.E., & Blaauw, E.H. (1986) Cellular contrast depending on buffer and period of rinsing after glutaraldehyde fixation. Ultramicroscopy., 19: 97.
Isackson, P.J., Huntsman, M.M., Murray, K.D. and Gall, C.M. (1991) BDNF messenger-RNA expression is increased in adult- rat forebrain after limbic seizures-temporal patterns of induction distinct from NGF. Neuron., 6: 937-948.

Ingham C.A.(1992) Immunocytochemistry II: Post embedding staining Experimental Neuroanatomy; A practical approach. Oxford University Press.Ed 1. p129-151.

Itami, C., Kimura, F., Kohno, T., Matsuoka, M., Ichikawa, M., Tsumoto, T. and Nakamura, S. (2003) Brain-derived neurotrophic factor-dependent unmasking of "silent" synapses in the developing mouse barrel cortex. Proc. Natl. Acad. Sci. USA., 100:13069-13074.

Ito, H., Nomoto, H., Furukawa, Y. and Furukawa, S. (2003) Neurotrophins facilitate synthesis of choline acetyltransferase and tyrosine hydroxylase in cultured mouse neural stem cells independently of their neuronal differentiation. Neurosci. Lett., 339: 231-234

Itoh. K., Konishi. A., Nomura. S., Mizuno. N., Nakamura. Y and Sugimoto T. (1979). Application of coupled oxidation reaction to electron microscopic demonstration of horseradish peroxidase: cobalt-glucose oxidase method. Brain Res 175:34.

JI, Z., Aas J-E., Laake, A, J., Walberg, F. and Ottersen, O. P. (1991) An electron microscopic, immunogold analysis of glutamate and glutamine in terminals of rat spinocerebellar fibers .J. Comp. Neurol. 307:296-310

Johnson, T.J.A (1985) Aldehyde fixatives: Quantification of acid-producing reactions. J .Electron. Microsc. Tech. 2: 129-138.

Johnson TJA (1987): Glutaraldehyde fixation chemistry: oxygen-consuming reactions. Eur.J. Cell. Biol., 45:160

Josephsen, K., Smith, C.E. and Nanci, A. (1999) Selective but nonspecific immunolabeling of enamel protein-associated compartments by a monoclonal antibody against vimentin. Histochem. Cytochem., 47:1237–1246.

Jourdi, H., Iwakura, Y., Narisawa-Saito, M., Ibaraki, K., Xiong, H.B., Watanabe, M., Hayashi, Y., Takei, N. and Nawa, H. (2003) Brain-derived neurotrophic factor signal enhances and maintains the expression of AMPA receptor-associated PDZ proteins in developing cortical neurons. Dev. Biol., 263: 216-230.

Judge, S.J. (2000) Modulation of cholinergic synaptic transmission in an identified locust sensory pathway. Ph.D Thesis. Department of Biological Science, University of Durham.

Judge, S. and Leitch, B. (1999a) GABA immunoreactivity in processes presynaptic to the locust wing stretch receptor neuron. J. Comp. Neurol., 407:103-114.

Judge, S. and Leitch, B. (1999b) Modulation of transmitter release from the locust forewing stretch receptor neuron by GABAergic interneurons activated via muscarinic receptors. J, Neurobiol., 40:420-431.

Kann, M. -L and. Fouquet, J. –P. (1989) Comparison of LR white resin, lowicryl K4M and Epon postembedding procedures for immunogold staining of actin in the testis. Histochem. Cell. Biol., 91 (3): 221-226.

Karnovsky, M. J. (1956) A formaldehyde-glutaraldehyde fixative of high osmolality for use in electron microscopy. J. Cell. Biol., 27 :137 A.

Katz, P.S. and Frost, W.N. (1966) Intrinsic neuromodulation: altering neuronal circuits from within. Trends. Neurosci., 2:54-61.

Keller, G.A., Tokuyasu, K.T., Dutton, A.H., et al. (1984) An Improved Procedure for Immunoelectron Microscopy: Ultrathin Plastic Embedding of Immunolabeled Ultrathin Frozen Sections. Proc. Natl .Acad. Sci. USA-Biological Sciences., 81 (18): 5744-5747.

Kellenberger, E., Durrenberger, M., Villiger, W., Carlemalm, E. and Wurtz, M. (1987) The efficiency of immunogold label on Lowicryl sections compared to the theoretical predictions. J.Chem.Histochem., 35 (9): 959-969.

Kellenberger, E. and Hayat, M.A. (1991) Colloidal Gold: principles, methods and application. 3. London, Harcourt Publishers Ltd.

Kellenberger, E., Villiger, W. and Carlemalm,E. (1986) The influence of thin sections of embedded, unstained biological- material on image quality. Micron and Microscopica Acta., 17(4) ; 331-348.

Kerwien P, and Schürmann FW. 1990. Nichtsynaptische Exocytose im Hirn und in den Corpora cardiaca von *Gryllus bimaculatus*: Eine Tannin-Studie. In: Elsner N, Roth G, editors. Brain-perceptioncognition. Proc 18th Go¨ttingen Neurobiology Conf. Stuttgart: Thieme, p 312.

Kiernan, J.A. (2000) Formaldehyde, formalin, paraformaldehyde and glutaraldehyde: What they are and what they do. Microscopy Today. 00-1, 8-12.

Kobberta, C., Apps, R., Bechmannc,I., Lanciegod,J.L., Meye, J. and Thanosa,S. (2000) Current concepts in neuroanatomical tracing. Prog. Neurobiol., 62: 327-351.

Köhler,G. and Milstein, C.(1976) Derivation of specific antibody-producing tissue culture and tumor lines by cell fusion. Eur. J. Immunol., 6:511-519.

Konings, P.N.M., Vullings, H.G.B., Geffard, M., Buijs, R.M., Diederen, J.H.B. and Jansen, W.F. (1988) Immunocytochemical demonstration of octopamine-immunoreactive cells in the nervous system of Locusta migratoria and Shistocerca gregaria. Cell. Tissue. Res., 251:371-379.

Kristensson, K. and Olsson, Y. (1971) Retrograde axonal transport of a protein. Brain Research., 29 363-365.

Kohara, K., Kitamura, A., Adachi, N., Nishida, M., Itami, C., Nakamura, S. and Tsumoto, T. (2003) Inhibitory but not excitatory cortical neurons require presynaptic brain-derived neurotrophic factor for dendritic development, as revealed by chimera cell culture. J. Neurosci., 23:6123–6131.

Kuran, H. and Olszewska, M.J. (1974) Effect of some buffers on ultrastructure, dry mass content and radioactivity of nuclei of haemanthus-katharinae.Folia Histochemica et Cytochemica,. 12 (2): 173.

Langanger, G., De Mey, J., Moeremans, M., Daneels, G., De Brabander, M., and Small, J.V. (1984) Ultrastuctural localization of a-actinin and filamin in cultured cells with the immunogold staining (IGS) method. J. Cell Biol., 99:1324–1334.

Larkfors, L., Lindsey, R.M. and Alderson, R.F. (1996) Characterisation of the responses of Purkinje cells to neurotrophin treatment. J. Neuro. Chem., 66: 1362-1373.

La Vail, J.H. and La Vail, M.H. (1972) Retrograde axonal transport in the central nervous system. Science., 176 1416.

Leduc, E.H., Bernhard, W., Holt, S.J. and Tranzer, J.P. (1967) Ultrathin frozen sections II. Demonstration of enzymic activity. J. Cell .Biol., 34:773–86.

Lee, H. M. and Wyse, G. A. (1991) Immunocytochemical localization of octopamine in the central nervous system of *Limulus polyphemus*: a light and electron microscopic study. J. Comp. Neurol., 307, 683-694.

Leitch, B. and Richardson, A.C. (2004) Identification of the neurotransmitters involved in modulation of transmitter release from the central terminals of the locust wing hinge stretch receptor. Washington, DC: Society for Neuroscience., 2004.

Leitch, B., Judge, S. and Pitman, R.M. (1998) Modulation of an identified sensory pathway by muscarinic receptors. Soc. Neurosci. Abstr., 24: 624.10.

Leitch, B., Judge, S. and Pitman, R.M. (2003) Octopaminergic modulation of synaptic transmission between an identified sensory afferent and flight motoneuron in the locust. J. Comp. Neurol., 462: 55-70.

Leitch, B. and Laurent, G. (1993) Distribution of GABAergic synaptic terminals on the dendrites of locust spiking local interneurones. J. Comp. Neurol., 337: 461-470.

Leitch, B. and Pitman, R.M. (1995) Modulation of transmitter release from the terminals of the locust wing- stretch receptor neuron by muscarinic antagonists. J. Neurobiol., 28:455-464.

Leitch, B. and Richardson, A.C. (2004) Identification of the neurotransmitters involved in modulation of transmitter release from the central terminals of the locust wing hinge stretch receptor. Washington, DC: Society for Neuroscience., 2004.

Leitch, B., Watkins, B.L. and Burrows, M.(1993) Distribution of Acetylcholine-receptors in the central nervous system of adult locusts. J. Comp. Neurol.,1: 47-58.

Lessmann, V, Gottmann, K. and Malcangio, M. (2003) Neurotrophin secretion: current facts and future prospects. Prog .Neurobiol., 69:341-374.

Lessmann, V. and Heumann, R. (1998) Modulation of unitary glutamatergic synapses by neurotrophin-4/5 or brain-derived neurotrophic factor in hippocampal microcultures: Presynaptic enhancement depends on pre-established paired-pulse facilitation. Neurosci., 86:399-413.

Letts, V.A., Felix, R., Biddlecome, G.H., Arikkath, J., Mahaffey, C.L., Valenzuela, A., Bartlett, F.S., Mori, Y., Campbell, K.P. and Frankel, W.N. (1998) The mouse stargazer gene encodes a neuronal Ca^{2+} channel gamma subunit. Nature Genetics., 19:340-347.

Li, J. and Schwarz, T.L. (1999) Genetic evidence for an equilibrium between docked and undocked vesicles. Philos. T. Roy. Soc. B., 354:299-306.

Light, K.E., Brown, D.P., Newton, B.W., Belcher, S.M. and Kane, C.J.M. (2002) Ethanol-induced alterations of neurotrophin receptor expression on Purkinje cells in the neonatal rat cerebellum. Brain Res., 924:71-81.

Light, K.E., Ge, Y. and Belcher, S.M. (2001) Early postnatal ethanol exposure selectively decreases BDNF and truncated TrkB-T2 receptor mRNA expression in the rat cerebellum. Mol.Brain.Res., 93:46 -55.

Linke, R.P., Huhn, D., Casanova, S. and Donini, U. (1989) Immunoelectron microscopic identification of human AA-type amyloid- Exploration of various monoclonal AA-antibodies, methods of fixation, embedding and other

parameters for the protein –A gold method. Laboratory Investigation., 61 (6): 691-697.

Liou, W., Geuze, H.J. and Slot, J.W. (1996) Improved structural integrity of cryosections for immunogold labeling. Histochem. Cell. Biology., 106:41–58.

Llewellyn-Smith, I.J. and Minson, J.B. (1992) Complete penetration of antibodies into vibratome sections after glutaraldehyde fixation and ethanol treatment: light and electron microscopy for neuropeptides. J. Histochem. Cytochem., 40(11):1741-9.

Llewellyn- Smith, I.J, Pilowsky, P. and Minson, J.B. (1992) Retrograde tracers for light and electron microscopy. Experimental Neuroanatomy; A practical approach., p.31-59.

Loewi O (1921) Über humorale Übertragbarkeit der Herznervenwirkung. Pflügers. Arch. 189: 239-242

Lu, B. (2001) Neurotrophic regulation of synapse development and plasticity. Prog. Nat. Sci., 11: 1-5.

Lu, B. and Gottschalk, W. (2000) Modulation of hippocampal synaptic transmission and plasticity by neurotrophins. Prog. Brain. Res., 128: 231-241.

Lucocq, J. (1992) Quantitation of gold labelling and estimation of labelling efficiency with a stereological counting method. J. Histochem. Cytochem., 40 (12): 1929-1936.

Macville, M.V.E., Wiesmeijer, K.C., Dirks, R.W., Fransen, J.A.M., and Raap, A.K. (1995) Saponin pre-treatment in pre-embedding electron microscopic in situ hybridization for the detection of specific RNA sequences in cultured cells: A methodological study. J. Histochem. Cytochem., 43:1005–1018.

Mayhew,T. M., Lucocq, J. M., Griffiths, G. (2002) Relative labelling index: a novel stereological approach to test for non-random immunogold labelling of organelles and membranes on transmission electron microscopy thin sections J. Microsc. 205 (2):153–164.

Mark, H. F., Bikales, N. M., Overberger, C. G. and Menges, G.(1986). Encyclopaedia of Polymer Sciences and Engineering Vol. 6.Kroschwitz, J. I. (ed.). John Wiley and Sons, 335-400.

Marlier, L., Sandillon, F., Poulat, P., Rajaofetra, N., Geffard, M., and Privat, A. (1991): Serotonergic innervation of the dorsal horn of rat spinal cord: light and electron microscopic immunocytochemical study. J. Neurocytol., 2 0:310-322.

Marmigere, F., Rage, F. and Tapia-Arancibia, L. (2003) GABA-glutamate interaction in the control of BDNF expression in hypothalamic neurons. Neurochem. Int., 42: 353-358.

Martinez, A., Alcantara, S., Borrell, V., Del Rio, J.A., Blasi, J., Otal, R., Campos, N., Boronat, A., Barbacid, M., Silos-Santiago, I. and Soriano. E. (1998) TrkB and TrkC signalling are required for maturation and synaptogenesis of the hippocampal connections. J. Neurosci., 18: 7336-7350.

Martinez, H.J., Drefuss, C.F., Jonakait, G.M. and Black, I.B. (1987) Nerve growth-factor selectively increases cholinergic markers but not neuropeptides in rat basal forebrain in culture. Brain Res., 412: 295-301.

Marty, S., Berzaghi, M.P. and Berninger, B. (1997) Neurotrophins and activity-dependant plasticity of cortical interneurons. Trends in Neurosci., 20: 198–202.

Marty, S., Carroll, P., Cellerino, A., Castren, E., Staiger, V., Thoenen, H. and Lindholm, D. (1996) Brain-derived neurotrophic factor promotes the differentiation of various hippocampal nonpyramidal neurons, including Cajal-Retzius cells, in organotypic slice cultures. J. Neurosci., 16: 675 –687.

Martone, M.E., Pollock, J.A., Jones, Y.Z., and Ellisman, M.H. (1996) Ultrastructural localization of dendritic messenger RNAin adult rat hippocampus. J. Neurosci., 16:7437–7446.

Marty, S., Wehrle, R. and Sotelo, C. (2000) Neuronal activity and brain-derived neurotrophic factor regulate the density of inhibitory synapses in organotypic slice cultures of postnatal hippocampus. J. Neurosci., 20: 8087-8095.

Matsumoto, T., Numakawa, T., Adachi, N., Yokomaku, D., Yamagishi, S., Takei, N. and Hatanaka, H. (2001) Brain-derived neurotrophic factor enhances depolarization-evoked glutamate release in cultured cortical neurons. J. Neurochem., 79: 522-530.

Matsuno, A., Ohsugi, Y., Utsunomiya, H., Takekoshi, S., Osamura, R.Y., Watanabe, K., Teramoto, A. and Kirino, T. (1994) Ultrastructural distribution of growth hormone and prolactin mRNAs in normal rat pituitary cells: A comparison between pre-embedding and postembedding methods. Histochem., 102:265–270.

McAllister, A.K. (2001) Neurotrophins and neuronal differentiation in the central nervous system. Cell. Mol. Life. Sci., 58 (8): 1054-1060.

McAllister, A.K., Katz, L.C. and Lo, D.C. (1999) Neurotrophins and synaptic plasticity. Ann. Rev. Neurosci., 22: 295-318.

Mertz, K., Koscheck, T. and Schilling, K. (2000) Brain-derived neurotrophic factor modulates dendritic morphology of cerebellar basket and stellate cells: an in vitro study. Neurosci., 97: 303-310.

Mighell, AJ., Hume, WJ. and Robinson, PA. (1998). An overview of the complexities and subtleties of immunohistochemistry. Oral Dis., 4:217-223,

Mizuno, K., Carnahan, J. and Nawa, H. (1994) Brain-derived neurotrophic factor promotes differentiation of striatal GABAergic neurons. Dev. Biology., 165: 243-256.

Mobley, W. C., Rutkowski, J.L., Tennekoon, G. I., Buchanan, K. and Johnston, M.V. (1985) Choline acetyltransferase activity in striatum of neonatal rats increased by nerve growth factor. Science., 229: 284 -287.

Moeremans, M., Daneels, G., Van Dijck, A., Langanger, G. and De Mey, J. (1984): Sensitive visualization of antigen-antibody reactions in dot and blot immune overlay assays with immunogold and immunogold/silver staining. J. Imm. Meth. 74:353

Monsan, .P, Puzo, G.and Mazarguil, H. (1975) Mechanism of glutaraldehyde-protein bond formation. Biochimie., 57:1281

Mons, N. and Geffard, M. (1987) Specific antisera against the catecholamines : L-3,4- dihydroxyphenylalanine, octopamine tested by and enzyme-linked immunosorbent assay. J. Neurochem., 48: 1826-1833.

Murthy, V.N., Schikorski, T., Stevens, C.F. and Zhu, Y. (2001) Inactivity produces increases in neurotransmitter release and synapse size. Neuron., 32: 673–682.

Naisbitt , S., Kim, E., Weinberg, R. J., Rao, A., Yang, F., Craig, A. M.and Sheng, M. (1997) Characterization of Guanylate Kinase-Associated Protein, a postsynaptic density protein at excitatory synapses that interacts directly with postsynaptic density-95/synapse-associated protein 90. J. Neurosci., 17(15): 5687-5696.

Narisawa-Saito, M., Iwakura, Y., Kawamura, M., Araki, K., Kozaki, S., Takei, N. and Nawa, H. (2002) Brain-derived neurotrophic factor regulates surface expression of alpha-amino-3-hydroxy-5-methyl-4-isoxazoleproprionic acid receptors by enhancing the N-ethylmaleimide-sensitive factor/GluR2 interaction in developing neocortical neurons. J. Biol. Chem., 277: 40901-40910.

Nässel, R. R. (1996) Advances in the immunocytochemical localization of neuroactive substances in the insect nervous system. J. Neurosci. Methods., 69: 3–23.

Nelson, P.N., Reynolds, G.M., Waldron, E.E., Ward, E., Giannopoulus, K. and Murray, P.G .(2000) Monoclonal antibodies. J. Clin.Pathol. Mol. Pathol. **53**:111-117.

Newman, G. R. (1987) Use and abuse of LR White. J.Histochem., 19:118-120.

Newman, G. R. and Hobot, J. A. (1987) Modern acrylics for post-embedding immunostaining techniques. J. Histochem.Cytochem., 35:971-981.

Newman, G. R. and Hobot, J. A. (1989) Role of tissue processing in colloidal gold methods. In ; Hayat, M.A (ed) Colloidal gold: principles, methods, and applications, Vol.2. Academic Press, San Diego, 33-45.

Newman, G. R. and Hobot, J. A. (2001) Resin microscopy and on-section immunocytochemistry. Berlin, Germany: Springer-Verlag KG.

Nyíri, G., Freund, T.F. and Somogyi, P. (2001), Input-dependent synaptic targeting of a_2-subunit-containing $GABA_A$ receptors in synapses of hippocampal pyramidal cells of the rat. Eur. J. Neurosci. 13 (3):428-442.

Noebels, J.L., Qiao, X., Bronson, R.T., Spencer, C. and Davisson, M.T. (1990) Stargazer: a new neurological mutant on chromosome 15 in the mouse with prolonged cortical seizures. Epilepsy. Res., 7: 129-135.

O'Dell, D.A. and Watkins, B.L. (1988) The development of GABA-like immunoreactivity in the thoracic ganglia of the locust *Schistocerca-gregaria*. Cell Tissue. Res., 254 (3): 635-646.

Nusser, Z., Sieghart, W., Benke, D., Fritschy, J-M, and Somogi,P. (1996) Differential synaptic localization of two major g-aminobutyric acid type A receptor a subunits on hippocampal pyramidal cells. Neurobiolog Proc. Natl. Acad. Sci. USA 93:11939–11944.

Orchard, I., Ramirez,J-M. and Lange, A.B. (1993) A multifunctional role for octopamine in locust flight. Annu. Rev. Entomol., 38:227–249.

Ottersen, O.P. (1989) Postembedding immunogold labelling of fixed glutamate—an electron-microscopic analysis of the relationship between gold particle density and antigen concentration. J. Chem. Neuroanat., 2:57–66.

Ottersen, O.P., Laake, J.H. and Storm-Mathisen, J. (1990) Demonstration of a releasable pool of glutamate in cerebellar mossy and parallel fibre terminals by means of light and electron microscopic immunocytochemistry. Arch. Ital. Biol., 128(2-4):111-25.

Ottersen,O.P. and Laake, J.H. (1992) Light and electron microscopic observations of putative Neurotransmitter amino acids in the cerebellum with some observations on the distribution of glutamine. The cerebellum revisited. Ed.Sotelo R.L.C. Springer-Verlag. NewYork. P.116-134.

Ottersen, O. P., Madsen, S., Storm-Mathisen, J., Somogyi, P., Scopsi, L. and Larsson, L.I. (1988) Immunocytochemical evidence suggests that taurine is colocalized with GABA in the Purkinje cell terminals, but that the stellate cell terminals predominantly contain GABA: a light- and electronmicroscopic study of the rat cerebellum. Exptl. Brain. Res., 72 (2): 1432-1106.

Ottersen, O. P. and Storm-Mathisen, J. (1984) Glutamate-containing and GABA-containing neurons in the mouse and rat-brain, as demonstrated with a new immunocytochemical technique. J. Comp. Neurol., 229 :374-392.

Ottersen, O. P. and Storm-Mathisen, J. (1987) Localization of amino acid neurotransmitters by immunocytochemistry. Trends. Neuroscie.,10(6): 250-254.

Ottersen, O.P., Storm-Mathisen, J. and Somogyi, P. (1988) Colocalisation of glycine-like and GABA-like immunoreactivities in Golgi cell terminals in the rat cerebellum- A postembedding light and electron microscope study. Brain Res., 450 (1-2): 342-353.

Ottersen, O.P & Storm-Mathisen, J. (2004) Glutamate- and GABA-containing neurons in the mouse and rat brain, as demonstrated with a new immunocytochemical technique. J. Comp. Neurol., 229 (3): 374-392.

Ottersen, O.P., Zhang, N. and Walberg, F. (1992) Metatabolic compartmentation of glutamate and glutamine: morphological evidence obtained by quantitative immunocytochemistry in rat cerebellum. Neurosci., 46(3):519-34.

Parker, D. (1994) Glutamatergic transmission between antagonistic motor neurons in the locust. J. Comp. Physiol. [A]., 119:267–283.

Pearson, K.G., Reye, D.N. and Robertson, R.M. (1983) Phase-dependent influences of wing stretch receptors on flight rhythm in the locust. J.Neurophysiol., 49:1168-1181.

Pearlstein, E., Watson, A.H., Bevengut, M. and Cattaert, D. (1998) Inhibitory connections between antagonistic motor neurones of the crayfish walking legs. J. Comp. Neurol., 399:241–254.

Pfau, H.K., Kock, U.T. and Möhl, B. (1989). Temperature dependence and response characteristics of the isolated wing hinge stretch receptor in the locust. J. Comp. Physiol., 165A: 247-252.

Pflüger, H.J. and Watson, A.H.D. (1995) GABA and glutamate-like immunoreactivity at synapses received by dorsal unpaired median neurons in the abdominal nerve cord of the locust. Cell. Tissue. Res., 280:325–333.

Posthuma, G., Slot. W. and Geuze, H. (1987) Usefulness of the immunogold technique in quantitation of a soluble protein in ultra-thin sections. Histochem. Cytochem., 35:405.

Poo, M.M. (2001) Neurotrophins as synaptic modulators. Nat. Rev. Neurosci., 2: 24-32.

Porter, R.R. (1959) The hydrolysis of rabbit y-globulin and antibodies with crystalline papain. Biochem. J. 73:119-127.

Pozzo-Miller, L.D., Gottschalk, W., Zhang, L., McDermott, K., Du, J., Gopalakrishnan, R., Oho, C., Sheng, Z.H. and Lu, B. (1999) Impairments in high-frequency transmission, synaptic vesicle docking, and synaptic protein distribution in the hippocampus of BDNF knockout mice. J. Neurosci., 19: 4972-4983.

Probert, L., De Mey, J. & Polak, J. (1981) Distinct subpopulations of enteric p-type neurones contain substance P and vasoactiveintestinal protein. Nature., 294;470-471.

Qiao, X., Chen, L., Gao, H., Bao, S., Hefti, F., Thompson, R.F. and Knusel, B. (1998) Cerebellar brain-derived neurotrophic factor- TrkB defect associated with impairment of eye-blink conditioning in stargazer mutant mice. J. Neurosci., 18: 6990-6999.

Qiao, X., Hefti, F., Knusel, B. and Noebels, J.L. (1996) Selective failure of brain-derived neurotrophic factor mRNA expression in the cerebellum of stargazer, a mutant mouse with the ataxia. J. Neurosci., 16: 640 -648.

Ramirez, J.M. and Orchard, I. (1990) Octopaminergic modulation of the forewing stretch receptor in the locust, *Locusta migratoria*. J. Exp. Biol. 149:255–279.

Ramirez. J-M., Büschges. A., Kittman. R. (1993) Octopaminergic modulation of the femoral chordotonal organ in the stick insect. J. Comp. Physiol. A. 173: 209-219.

Rasband, W. N.I.H. U.S.A. Image J 1.28U. http://rsb.info.nih.gov/ij.

Rawdon, B.B. (1997). Fixatives and embedding media for immunocytochemistry. Trans. Roy. Soc. South Africa., 52:405-425.

Reibel, S., Benmaamar, R., Le, B.T., Larmet, Y., Kalra, S.P., Marescaux, C. and Depaulis, A. (2003) Neuropeptide Y delays hippocampal kindling in the rat. Hippocampus., 13: 557-560.

Reith, A., Kraemer, M., and Vassey, J. (1984) The influence of mode of fixation, type of fixation and vehicles on the same rat liver: a morphometric/ stereologic study by light and electron microscopy. Scanning. Electron.Microsc., 2: 645.

Renno, W. M. (2001) Post-embedding double-gold labeling immunoelectron microscopic co-localization of neurotransmitters in the rat brain. Basic Research: Med. Sci. Monit., 7(2): 188-200

Reye, D.N. and Pearson, K.G. (1988) Entrainment of the locust central flight oscillator by wing stretch receptor stimulation. J. Comp. Physiol. A., 162:77-89.
Reynolds, E.S. (1963) The use of lead citrate of high pH as an electron-opaque stain in electron microscopy. J. Cell. Biol., 17 :208.

Richardson, A.C. and Leitch, B. (2002) Cerebellar Golgi, Purkinje, and basket cells have reduced gamma-aminobutyric acid immunoreactivity in stargazer mutant mice. J. Comp. Neurol., 453: 85-99.

Richardson, C.A. and Leitch, B.(2004)Identification of the neurotransmitters involved in modulation of transmitter release from the central terminals of the locust wing hinge stretch receptor. Program No. 870.15. 2004 Abstract Viewer/Itinerary Planner. Washington, DC: Society for Neuroscience.

Richardson, A.C. and Leitch, B. (2005) Phenotype of cerebellar glutamatergic neurons is altered in stargazer mutant mice lacking brain-derived neurotrophic factor mRNA Expression. J. Comp. Neurol., 481:145–159.

Ridet,J-L.,and Privat,A.(2000)Volume transmission. Trends in Neurosci. 23(2):58-9.

Ridet J.-L., Rajaofetra J. R., Teilhac M., Geffard M. and Privat A. (1993) Evidence for nonsynaptic serotonergic and noradrenergic innervation of the rat dorsal horn and possible involvement of neuron-glia interactions. Neurosci. 52: 143-157.

Robinson, J.M., Takizawa, T., Vandré, D.D. and Burry, R.W. (1998) Ultrasmall immunogold particles: Important probes for immunocytochemistry. Micro.Res. Tech., 42: 113-23.

Rico, B., Xu, B.J. and Reichardt, L.F. (2002) TrkB receptor signaling is required for establishment of GABAergic synapses in the cerebellum. Nat. Neurosci., 5: 225-233.

Rocken, C. and Roessner, A. (1999) An evaluation of antigen retrieval procedures for immunoelectron microscopic classification of amyloid deposits. J.Histochem. Cytochem., 47 (11): 1385-1394.

Roeder, T. (1999) Octopamine in invertebrates. Prog. Neurobiol., 59 (5): 533-561.

Romano, E.L., Stolinski, C. and Hughes-Jones, N.C. (1974) An antiglobulin reagent labelled with colloidal gold for use in electron microscopy. Immunochemistry., 11: 521-522.

Roos, A. and Boron, W.F. (1983) Intracellular pH. Physiol. Rev., 61: 296–434.

Rutherford, L.C., DeWan, A., Lauer, H.M. and Turrigiano, G.G. (1997) Brain - derived neurotrophic factor mediates the activity dependant regulation of inhibition in neocortical cultures. J. Neurosci., 17: 4527-4535.

Sabatini, D.D., Bensch, K. and Barrnett, R.J. (1963) Cytochemistry and electron microscopy. The preservation of cellular ultrastructure and enzymatic activity by aldehyde fixation. J. Cell. Biol., 17:19-58.

Salmea, R. and Brandao, I. (1973) Use of pipes buffer in fixation of plant-cells for electron-microscopy. J.Submicro. Cytol. Pathol., 5 (2): 79-96.

Sato, T., Wilson, T.S., Hughes, L.F., Konrad, H.R., Nakayama, M. and Helfert, R.H. (2001) Age-related changes in the levels of tyrosine kinase B receptor and fibroblast growth factor receptor 2 in the rat inferior colliculus: Implications for the neural senescence. Neurosci., 103: 695–702.

Satijn, D.P., Gunster. M.J., van der Vlag, J., Hamer, K.M., Schul, W., Alkema, M.J., Saurin, A.J., Freemont, P.S., van Driel, R. and Otte, A.P. (1997) RING1 is associated with the polycomb group protein complex and acts as a transcriptional repressor. Mol. Cell. Biol.,17:4105–4113.

Schäfer, S. and Bicker, G. (1986) Distribution of GABA-like immunoreactivity in the brain of the honeybee. J. Comp. Neurol., 246 (3): 287-300.

Schikorski, T. and Stevens, C.F. (2001) Morphological correlates of functionally defined synaptic vesicle populations. Nature. Neurosci., 4 (4):391-395.

Schinder, A.F. and Poo, M.M. (2000) The neurotrophin hypothesis for synaptic plasticity. Trends. Neurosci., 23: 639-645.

Shupliakov, O., Brodin, L., Cullheim., Ottersen, O.P. and Storm-Mathisen, J. (1992) Immunogold quantification of glutamate in two types of excitatory synapse with different firing patterns. J. Neurosci., 12; 3789-3803

Schürmann, F.W., Hörner, M. and Spörhase-Eichmann, U. (1995) The diverse layout of amine-containing systems in the ventral cord of an insect. Acta. Biol. Hung., 46:485–490.

Schürmann, F.W., Sandeman, R. and Sandeman, D. (1991) Dense core vesicles and non-synaptic exocytosis in the central body of the crayfish brain. Cell. Tissue.Res., 265:493–501.

Schwartz, P.M., Borghesani, P.R., Levy, R.L., Pomeroy, S.L. and Segal, R.A. (1997) Abnormal cerebellar development and foliation in BDNF -/- mice reveals a role for neurotrophins in CNS patterning. Neuron., 19: 269–281.

Seguela, P., Gamrani, H., Geffard, M., Calas, A., and Le Moal, M. (1985) Ultrastructural immunocytochemistry of γ-aminobutyrate in the cerebral and cerebellar cortex of the rat. Neurosci., 14(4): 865-874.

Seguela, P., Geffard, M., Buijs, R.M. and Lemoal, M. (1984) Antibodies against gamma-aminobutyric acid: specificity studies andimmunocytochemical results. Proc. Natl. Acad. Sci. USA., 81: 3888-3892.

Seil, F.J. (1999) BDNF and NT-4, but not NT-3, promote development of inhibitory synapses in the absence of neuronal activity. Brain. Res., 818: 561-564.

Seil, F.J. and Drake-Baumann, R. (2000) TrkB receptor ligands promote activity-dependent inhibitory synaptogenesis. J. Neurosci., 20: 5367-5373.

Seil, F.J., Drake-Baumann, R., Leiman, A.L., Herndon, R.M. and Tiekotter, K.L. (1994) Morphological correlates of altered neuronal activity organotypic cerebellar cultures chronically exposed to anti-GABA agents. Dev. Brain. Res., 77: 123-132.

Shimada, A., Mason, C.A. and Morrison, M.E. (1998) TrkB signalling modulates spine density and morphology independent of dendrite structure in cultured neonatal Purkinje cells. J. Neurosci.,18: 8559–8570.

Shepherd, G.M. (1994) Neurobiology. 3rd ed. Oxford, Oxford University press.

Sinakevitch, I.G., Geffard, M., Pelhate, M. and Lapied, B. (1994) Octopamine-like immunoreactivity in the dorsal innervating the accessory gland of the male cockroach, *Periplaneta americana*. Cell.Tissue. Res., 276 (1): 15-21.

Sinakevitch, I.G., Geffard, M., Pelhate, M. and Lapied, B. (1995) Octopaminergic dorsal unpaired median (DUM) glands of the female cockroach, *Periplaneta americana*. J. Exptl. Biol., 198: 1539-1544.

Skepper, J.N., Woodward, J.M. & Navaratnam, V. (1988)Immunocytochemical localisation of natriuretic peptide sequences in the human right auricle. J. Mol. Cell. Cardiol. 20, 343-353.

Skepper, J.N. (2000) Immunocytochemical strategies for electron microscopy: choice or compromise. J.Micros., 199(1): 1-36.

Slot, J.W., and Geuze, H.J. (1985) A new method of preparing gold probes for multiple-labeling cytochemistry. Eur. J. Cell Biol., 38: 87–93.

Smith, Y. and Bolam, J.P. (1992.) Combined approaches to experimental Neuroanatomy: combined tracing and immunocytochemical techniques for the study of neuronal microcircuits. Experimental Neuroanatomy; A practical approach. 239- 266.

Sombati, S. and Hoyle, G (1984a) Central nervous sensitization and dishabituation of reflex action in an insect by the neuromodulator octopamine. J. Neurobiol., 15:455-480.

Sombati, S. and Hoyle, G. (1984b) Generation of specific behaviors in a locust by local release into neuropil of the natural neuromodulator octopamine. J. Neurobiol., 15: 481-506.

Sombati, S. and Hoyle, G. (1984c) Glutamatergic central nervous transmission in locusts. J. Neurobiol., 15:507–516.

Somogyi P, Halasy K, Somogyi J, Storm-Mathisen J, Ottersen OP. (1986). Quantification of immunogold labelling reveals an enrichment of glutamate in mossy and parallel fibre terminals in cat cerebellum. Neurosci., 19:1045-1050.

Somogyi, P., Hodgson, A.J., Chubb, W., Penke, B. and Erdei, A. (1985) Antisera to gamma-aminobutyric acid. II. Immunocytochemical application to the central nervous system. J. Histochem. Cytochem., 33: 240- 248.

Somogyi, P. and Llewellyn-Smith I. J. (2001) Patterns of colocalization of GABA, glutamate and glycine immunoreactivities in terminals that synapse on dendrites of noradrenergic neurons in rat *locus coeruleus*. Eur.J. Neurosci., 14: 219.

Sterling, P.and Matthews,G.(2005) Structure and function of ribbon Synapses. Trends in Neurosci., 28(1) 20:29.

Stevenson, P.A., Pfluger, H.J., Eckert, M., et al. (1992) Octopamine immunoreactive cell-populations in the locust thoracic-abdominal nervous-system. J. Comp. Neurol., 315 (4): 382-397.

Stevenson, P.A., Pflüger, H.J., Eckert, M. and Rapus, J. (1994) Octopamine-like immunoreactive neurones in locust genital abdominal ganglia. Cell. Tissue. Res., 275: 299–308.

Stevenson, P.A. and Spörhase-Eichmann, U. (1995) Localization of octopaminergic neurones in insects. Comp. Biochem. Physiol., 110A: 203–215.

Stierhof, Y.-D., Schwarz, H., and Frank, H. (1986) Transverse sectioning of plastic-embedded immunolabeled cryosections: Morphology and permeability to protein A-colloidal gold complexes. J. Ultrastruct. Mol. Struct. Res., 97:187–196.

Stirling, J.W. (1990) Immuno and Affinity Probes for Electron Microscopy: A Review of Labeling and Preparation Techniques. J. Histochem.Cytochem., 38(2): 145-157.

Stirling, J.W. and Graff, P.S. (1995) Antigen unmasking for immunoelectron microscopy: labeling is improved by treating with sodium ethoxide or sodium metaperiodate, then heating on retrieval medium. J. Histochem. Cytochem., 43: 115–123.

Storm-Mathisen, J., Leknes, A. K., Bore, A. T., Vaaland, J. L., Edminson, P., Haug, F-M. S. and Ottersen, O.P. (1983) First Visualization of glutamate and GABA in neurons by immunocytochrmistry. Nature., 301: 517-520.

Stratech Scientific Ltd (2007) http://www.stratech.co.uk.

Swaab, D.F., Pool, C.W. and Van Leeuwen, F.W. (1977) Can specificity ever be proven in immunocytochemical staining? J. Histochem. Cytochem., 25: 388–390.

Tanner, V.A., Ploug, T., and Tao Cheng, J.H. (1996) Subcellular localisation of SV2 and other secretory vesicle components in PC12 cells by an efficient method of pre-embedding EM immunocytochemistry for cell cultures. J. Histochem. Cytochem., 44:1481–1488.

Tartaglia, N., Du, J., Tyle, W.J., Neale, E., Pozzo-Miller, L.D. and Lu, B. (2001) Protein synthesis-dependent and -independent regulation of hippocampal synapses by brain-derived neurotrophic factor. J.Biol. Chem., 276: 37585-37593.

Tisdale, A.D. and Nakajima, Y. (1976) Fine-structure of synaptic vesicles in 2 types of nerve-terminals in crayfish stretch receptor organs – influence of fixation methods. J. Comp. Neurol., 165 (3): 369-386.

Thompson, C.L., Tehrani, M.H.J., Barnes Jr, E.M. and Stephenson, A.F. (1998) Decreased expression of $GABA_A$ receptor $\alpha 6$ and $\beta 3$ subunits in stargazer mutant mice: a possible role for brain- derived neurotrophic a factor in the regulation of cerebellar $GABA_A$ receptor expression? Mol. Brain. Res., 60: 282-290.

Tokuysu, K. T. (1973) A technique for ultracryotomy of cell suspensions and tissues. J. Cell. Biol., 57: 551-565.

Tokuysu, K. T. (1976) Membranes as observed in frozen sections. J. Ultrastruct. Res., 55: 281-287.

Tokuysu, K. T. (1986) Application of cryoultramicrotomy to immunocytochemistry. J. Microsc., 143:139-149.

Tokuyasu, K. T. and J. S. Singer. (1976) Improved procedures for immunoferritin labelling of ultrathin frozen sections. J. Cell. Biol., 71: 894-906.

Tömböl, T., Davies, D. C., A. Németh., Alpár A., Sebestény. T. (2000) A Golgi and a combined Golgi/GABA immunogold study of local circuit neurons in the homing pigeon hippocampus. Anatomy and Embryology 201:3181-196

Totterdell, S., Ingham, C.A. and Bolam, J.P. (1992) Immunocytochemistry 1: Pre-embedding staining. Experimental Neuroanatomy; A practical approach.103-128.

Tyler, W.J., and V N. Murthy (2004) Synaptic vesicles. Current Biology., 14,(8): R294-R297.
Tyler, W.J., Perrett, P. and Pozzo-Miller, L.D. (2002) The role of neurotrophins in neurotransmitter release. Neuroscientist., 8: 524-531.

Tyler, W.J. and Pozzo-Miller, L.D. (2001) BDNF enhances quantal neurotransmitter release and increases the number of docked vesicles at the active zones of hippocampal excitatory synapses. J. Neurosci., 21: 4249-4258.

Tyler, W.J. and Pozzo-Miller, L.D. (2003) Miniature synaptic transmission and BDNF modulate dendritic spine growth and form in rat CA1 neurones. J, Physiol-London., 553: 497-509.

Tyrer, N.M. and Altman, J.S. (1976) Spatial distribution of synapses onto thoracic motor neurones in locusts. Cell. Tissue. Res., 166:389–398.

Van de Plas, P., and Leunissen, J.L.M. (1993) Ultrasmall gold probes: Characteristics and use in immuno(cyto)chemical studies. Methods. Cell. Biol., 37: 241–257.

Van Leeuwen, F. 987. Immunocytochemical techniques in peptide localization. Possibilities and pitfalls. In A.A. Boulton, G.B. Baker and Q.G. Pittman_Eds.., Neuromethods 6, Peptides, Humana Press, Clifton, NJ. 73–111.

Van Lookeren Campagne, M., Dotti, C.G., Jap Tjoen San, E.R.A.,Verkleij, A.J., Gispen, W.H., and Oestreicher, A.B. (1992) B-50/GAP43 localization in polarized hippocampal neurons *in vitro*: An ultrastructural quantitative study. Neurosci., 50:35–52.

Varndell, I.M., Sikri, K.L., Hennessy, R.J., Kalina, M., Goodman,R.H., Benoit, R., Diani, A.R. & Polak, J.M. (1986) Somatostatin containing D cells exhibit immunoreactivity for rat somatostatin cryptic peptide in six mammalian species: An electron-microscopical study. Cell. Tissue. Res., 246; 197-204.

Vaughn, J.E. (1989) Fine-structure of synaptogenesis in the vertebrate central nervous system. Synapse., 3: 255-285.

Ventimiglia, R., Mather, P.E., Jones, B.E. and Lindsay, R.M. (1995) The neurotrophins BDNF, NT-3 and NT-4/5 promote survival and morphological and biochemical differentiation of the striatal neurons in vitro. Eur. J. Neurosci., 7: 213-222.

Vicario-Abejón, C., Collin, C., McKay, R.D.G. and Segal, M. (1998) Neurotrophins induce formation of functional excitatory and inhibitory synapses between cultured hippocampal neurons. J. Neurosci., 18: 7256-7271.

Vicario-Abejon, C., Owen, D., McKay, R. and Segal, M. (2002) Role of neurotrophins in central synapse formation and stabilization. Nat .Rev. Neurosci., 3: 965-974.

Watson, A.H.D. (1984) The dorsal unpaired median neurons of the locust metathoracic ganglion: neuronal structure and diversity, and synapse distribution. J. Neurocytol., 13:303–327.

Watson, A.H.D. (1988) Antibodies against GABA and glutamate label neurons with morphologically distinct synaptic vesicles in the locust central nervous system. Neurosci., 26: 33–44.

Watson, A.H.D. (1990) Ultrastructural evidence for GABAergic input onto cercal afferents in the locust (*Locusta migratoria*). J. Exptl. Biol., 148:509–515.

Watson, A.H.D. (1992) The distribution of dopamine-like immunoreactivity in the thoracic and abdominal ganglia of the locust (*Schistocerca gregaria*). Cell Tissue Res., 270:113-124.

Watson, A.H.D. and Bazzaz, A.A.(2001) GABA and glycine-like immunoreactivity at axoaxonic synapses on 1a muscle afferent terminals in the spinal cord of the rat. J. Comp. Neurol. 433 :335 - 348

Watson, A.H.D. and Bazzaz, A.A.(2003) GABA- and glycine-like immunoreactivity in axons and dendrites contacting the central terminals of rapidly adapting glabrous skin afferents in rat spinal cord. J. Comp. Neurol., 464:497 - 510

Watson AHD, Bevengut M, Pearlstein E, Cattert D. (2000) GABA and glutamate-like immunoreactivity at synapses on depressor motorneurones of the leg of the crayfish, *Procambarus clarkia*. J.Comp.Neurol., 422:510-520.

Watson, A.H.D. and Burrows, M. (1982) The ultrastructure of identified locust motor neurons and their synaptic relationships. J. Comp. Neurol., 205: 383–397.

Watson, A.H.D., Burrows, M. and. Leitch, B (1993) GABA- immunoreactivivity in processes presynaptic to the terminals of afferents from a locust leg proprioceptor. J. Neurocytol., 22 (7): 547-557.

Watson, A.H.D. and England, R.C.D. (1991) The distribution of and interactions between GABA-immunoreactive and non-immunoreactive processes presynaptic to afferents from campaniform sensilla on the trochanter of the locust leg. Cell. Tissue. Res., 266:331–341.

Watson, A.H.D. & Schürmann, F.W. (2002) Synaptic structure, distribution, and circuitry in the central nervous system of the locust and related insects. Micro. Res. Tech., 56: 210–226.

Watson, A.H.D., Seymour-Laurent K.J. (1993) The distribution of glutamate-like immunoreactivity in the thoracic and abdominal ganglion of the locust (*Schistocerca gregaria*). Cell. Tissue. Res., 273: 557–570.

Watson, A.H.D., Storm-Mathisen, J. and Ottersen, O.P. (1991) GABA and glutamate-like immunoreactivity in processes presynaptic to afferents from hair plates on the proximal joints of the locust leg. J. Neurocytol., 20: 796–809.

Watson, A.H.D., Pflüger, H.J. (1994) Distribution of input synapses from processes exhibiting GABA- or glutamate-like immunoreactivity onto terminals of prosternal filiform afferents in the locust. J. Comp. Neurol., 343: 617–629.

Widmer, H.R. and Hefti, F. (1994) Neurotrophin-4/5 promotes survival and differentiation of rat striatal neurons developing in culture. Eur. J. Neurosci., 6:1669-1679.

Wildman, M., Ott, S.R. and Burrows, M. (2002) GABA-like immunoreactivity in nonspiking interneurons of the locust metathoracic ganglion. J. Exptl. Biol., 205: 3651-3659.

Willingham, M.C. (1999) Conditional epitopes: is your antibody always specific? J. Histochem. Cytochem., 47: 1233–1236.

Wood, M.R., Pfenninger, K.H. and Cohen, M.J. (1977) Two types of presynaptic configurations in insect central synapses: an ultrastructural analysis. Brain Res., 130: 25–45.

Yan, Q., Radeke, M.J., Matheson, C.R., Talvenheimo, J., Welcher, A.A. and Feinstein, S.C. (1997) Immunocytochemical localisation of TrkB in the central nervous system of the adult rat. J. Comp. Neurol., 382: 546-547.

Yazama, F., Esaki, M., and Sawada, H. (1997) Immunocytochemistry of extracellular matrix components in the rat seminiferous tubule: Electron microscopic localization with improved methodology. Anat.Rec., 248:51–62.

Yokota, S. (1988) Effect of particle-size on labeling density for catalase in protein A-Gold Immunocytochemistry. J. Histochem. Cytochem., 36 (1): 107-109.

Yokota, S. and Okada, Y. (1997) Quantitative evaluation of preparation procedures affecting immunogold staining in post-embedding immunocytochemistry. Acta. Histochem. Cytochem., 30: 497-504.

Young, H.M., and Furness, J.B. (1995) Ultrastructural examination of the targets of serotonin-immunoreactive descending interneurons in the guinea pig small intestine. J. Comp. Neurol., 356:101–114.

Zafra, F., Castren, E., Thoenen, H. and Lindholm, D. (1991) Interplay between glutamate and γ-aminobutyric acid transmitter systems in the physiological regulation of brain - derived neurotrophic factor and nerve growth factor synthesis in hippocampal neurons. Proc. Natl. Acad. Sci. USA., 88: 10037-10041.

Zhang ,N., Walberg,F., Laake,J.H., Meldrum B.S. and Ottersen,O.P. (1990) Aspartate-like and glutamate-like immunoreactivities in the inferior olive and climbing fibre system: A light microscopic and semiquantitative electron microscopic study in rat and baboon (*Papio anubis*). Neurosci., 38 (1): 61-80.

Appendices.

Appendix 1. **Toluidine Blue Stain**

Sodium tetraborate. = 0.8g.

Distilled water. = 100ml.

Toluidine blue. = 0.8g.

Pyronine Y. = 0.2g.

Dissolve the borax in the distilled water before adding the two dyes.

Filter.

Appendix 2. **Bovine serum albumin/Tris buffer**

1. Dissolve 0.9gm of NaCl, 0.1gm bovine serum albumin and 0.242g Tris in a final volume of 100ml of distilled

2. Adjust pH to 8.2 .

3. Adjust the remaining 50 ml to pH 7.4.

4. Add 0.5ml tween 20 to each 50 ml.

Appendix 3. **0.2M Tris buffer pH 7.4**

Add 24.2gm of Tris to a final volume of 100ml-distilled water.

Adjust pH to 7.4 with 0.1M HCl.

Appendix 4. **Sorenson's Sodium Phosphate Buffer**

A. Preparation of Phosphate Buffer at pH 7.2-7.4 pH

1. Stock solutions:

a. Stock A: 0.2 M solution of $NaH_2PO_4 \cdot H_2O$

Add 27.6 g of $NaH_2PO_4 \cdot H_2O$ to 900 ml of distilled water and bring the final volume to 1 L

b. Stock B: 0.2 M solution of Na_2HPO_4 (anhydrous)

Add 28.4 g of Na_2HPO_4 (anhydrous) to 900 ml of distilled water and bring the final volume to 1 L

2. Preparation of Mixing Buffer (0.2 M buffer) for mixing with fixatives:

Mix 23 ml of stock A and 77 ml of stock B

The pH of the final solution should be 7.2-7.4, but it should be checked.

Appendix 5. 0.2M Sodium cacodylate buffer

Sodium Cacodylate 4.28 grams
Distilled water 100 mls

For pH 7.2 add 8.4 mls of 0.2N Hydrochloric Acid to 100 mls of the Sodium cacodylate buffer.

For pH 7.4 add 5.6 mls of 0.2N Hydrochloric Acid to 100 mls of the Sodium cacodylate buffer

Note : addition of acid produces Arsenic gas, handle in fume cupboard.

Appendix 6. DAB incubation medium

1. Dissolve 20mg ammonium chloride and 100mg B- D- glucose in 50ml 0.1M Sorensons phopshate buffer pH 7.4

2. Add 5mg diaminobenzidine (1ml 0.5% solution) to 9ml incubation medium.

Appendix 7. Modified Karnovsky Fixative.

Makes 100ml 2% PFA, 2.5% glut in 0.1M buffer pH 7.4:

25ml 8% PFA in H_2O
10ml 25% glutaraldehyde
50ml 0.2M phosphate buffer

Make up to 100ml with distilled H_2O